U.S. Department
of Transportation

Federal Highway
Administration

Asphalt Behavior at Low Service Temperatures

Research, Development, and Technology
Turner-Fairbank Highway Research Center
6300 Georgetown Pike
McLean, Virginia 22101-2296

Publication No. FHWA-RD-89-070
March 1990

FOREWORD

thermal cracking of asphalt cement concrete (ACC) pavements, including both low temperature shrinkage cracking and thermal fatigue cracking, continues to be a problem in many parts of the United States. Current test procedures and specifications do not protect against its occurrence. In 1985, an FHWA administrative contract research study with the Pennsylvania Transportation Institute, the Pennsylvania State University, was begun to (1) investigate the relationship between various experimental measures related to low temperature cracking, and (2) to develop a cost-effective instrument for the measurement of low temperature stiffness of asphalt cement.

The results are presented in this FHWA Research Report No. FHWA-RD-89-052, "Asphalt Behavior at Low Service Temperatures." A bending beam test for the direct measurement of the low temperature stiffness of asphalt cement developed under this contract is being further refined under Contract A-002 of the Strategic Highway Research Program (SHRP).

Additional copies of the report are available from the National Technical Information Service (NTIS), U.S. Department of Commerce, Springfield, Virginia 22161.

Thomas J. Pasko, Jr., P.E.
Director, Office of Engineering and Highway
Operations Research and Development

NOTICE

This document is disseminated under the sponsorship of the Department of Transportation in the interest of information exchange. The United States Government assumes no liability for its contents or use thereof. The contents of this report reflect the views of the contractor, who is responsible for the accuracy of the data presented herein. The contents do not necessarily reflect the official policy of the Department of Transportation. This report does not constitute a standard, specification, or regulation.

The United States Government does not endorse products or manufacturers. Trade or manufacturers' names appear herein only because they are considered essential to the object of this document.

GENERAL DISCLAIMER

This document may have problems that one or more of the following disclaimer statements refer to:

- This document has been reproduced from the best copy furnished by the sponsoring agency. It is being released in the interest of making available as much information as possible.

- This document may contain data which exceeds the sheet parameters. It was furnished in this condition by the sponsoring agency and is the best copy available.

- This document may contain tone-on-tone or color graphs, charts and/or pictures which have been reproduced in black and white.

- The document is paginated as submitted by the original source.

- Portions of this document are not fully legible due to the historical nature of some of the material. However, it is the best reproduction available from the original submission.

TECHNICAL REPORT STANDARD TITLE PAGE

1. Report No.	2. Government Accession No.	3. Recipient's Catalog No.
FHWA-RD-88-078		

4. Title and Subtitle	5. Report Date
ASPHALT BEHAVIOR AT LOW SERVICE TEMPERATURES	March 1990
	6. Performing Organization Code

7. Author(s)	8. Performing Organization Report No.
D. A. ANDERSON, D. W. CHRISTENSEN, R. DONGRE, M. G. SHARMA, J. RUNT, and P. JORDHAL	PTI 8802

9. Performing Organization Name and Address	10. Work Unit No.
The Pennsylvania Transportation Institute The Pennsylvania State University Research Building B University Park, PA 16802	3E1a4041
	11. Contract or Grant No. DTFH61-85-C-00111
	13. Type of Report and Period Covered Final Report Oct. 1985-Sept. 1988
12. Sponsoring Agency Name and Address Office of Engineering and Highway Operations R&D Federal Highway Administration 6300 Georgetown Pike McLean, VA 22101-2296	14. Sponsoring Agency Code

15. Supplementary Notes

FHWA Contract Manager (COTR): Dr. Ernest J. Bastian, Jr. (HNR-30)

16. Abstract

A general review of methods for measuring the stiffness properties of asphalt at temperatures below 77°F (25°C) is presented. Methods used traditionally for asphalt cement as well as those used in other technologies, such as polymer science, are reviewed. A method that is simple to conduct, suitable for specification use, and suitable for the entire range of stiffness below room temperature was not identified.

Models available for predicting low temperature cracking were reviewed and all were considered as requiring further development. Two models were selected for use in the study: Program TC-1 and Lytton's fracture mechanics model. The fracture mechanics model requires considerable work to make it operational, but it shows the most promise; TC-1 provides reasonable answers for most asphalts.

Correlations between various parameters related at low temperature cracking indicated that direct measurements such as Fraass brittle point, asphalt stiffness, mix stiffness and strength and DMA data correlate best with cracking potential. A bending beam test for the direct measurement of the low temperature stiffness of asphalt cement is proposed along with the protocol for a field verification trial.

17. Key Words	18. Distribution Statement
Asphalt, rheology, thermal cracking, fracture mechanics, temperature susceptibility, tensile strength, limiting stiffness, Fraass, mechanical properties	No restrictions. This document is available to the public through the National Technical Information Service, Springfield, VA 22161

19. Security Classif. (of this report)	20. Security Classif. (of this page)	21. No. of Pages	22. Price
UNCLASSIFIED	UNCLASSIFIED	337	

Form DOT F 1700.7 (8-69)

SI* (MODERN METRIC) CONVERSION FACTORS

APPROXIMATE CONVERSIONS TO SI UNITS

Symbol	When You Know	Multiply By	To Find	Symbol
LENGTH				
in	inches	25.4	millimetres	mm
ft	feet	0.305	metres	m
yd	yards	0.914	metres	m
mi	miles	1.61	kilometres	km
AREA				
in^2	square inches	645.2	millimetres squared	mm^2
ft^2	square feet	0.093	metres squared	m^2
yd^2	square yards	0.836	metres squared	m^2
ac	acres	0.405	hectares	ha
mi^2	square miles	2.59	kilometres squared	km^2
VOLUME				
fl oz	fluid ounces	29.57	millilitres	mL
gal	gallons	3.785	litres	L
ft^3	cubic feet	0.028	metres cubed	m^3
yd^3	cubic yards	0.765	metres cubed	m^3

NOTE: Volumes greater than 1000 L shall be shown in m^3.

MASS				
oz	ounces	28.35	grams	g
lb	pounds	0.454	kilograms	kg
T	short tons (2000 lb)	0.907	megagrams	Mg
TEMPERATURE (exact)				
°F	Fahrenheit temperature	5(F-32)/9	Celcius temperature	°C

APPROXIMATE CONVERSIONS FROM SI UNITS

Symbol	When You Know	Multiply By	To Find	Symbol
LENGTH				
mm	millimetres	0.039	inches	in
m	metres	3.28	feet	ft
m	metres	1.09	yards	yd
km	kilometres	0.621	miles	mi
AREA				
mm^2	millimetres squared	0.0016	square inches	in^2
m^2	metres squared	10.764	square feet	ft^2
ha	hectares	2.47	acres	ac
km^2	kilometres squared	0.386	square miles	mi^2
VOLUME				
mL	millilitres	0.034	fluid ounces	fl oz
L	litres	0.264	gallons	gal
m^3	metres cubed	35.315	cubic feet	ft^3
m^3	metres cubed	1.308	cubic yards	yd^3
MASS				
g	grams	0.035	ounces	oz
kg	kilograms	2.205	pounds	lb
Mg	megagrams	1.102	short tons (2000 lb)	T
TEMPERATURE (exact)				
°C	Celcius temperature	1.8C + 32	Fahrenheit temperature	°F

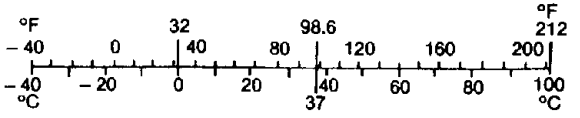

* SI is the symbol for the International System of Measurement

(Revised April 1989)

TABLE OF CONTENTS

TABLE OF CONTENTS (Continued)

LIST OF FIGURES

LIST OF TABLES

NOMENCLATURE

δ	phase angle, rad
δ	deformation or deflection, in (mm)
δ_t	displacement of sample in sample tube, in (mm)
ΔK	change in stress intensity factor at the crack tip during one load (thermal) cycle, $lb/in^2\text{-}\sqrt{in}$ ($Pa\text{-}\sqrt{m}$)
ΔT	ring and ball softening point temperature minus T_{Pen800}, °C
η	constant dependent upon geometry, fracture mechanics
η	coefficient of viscosity, $lb\text{-}s/in^2$ (Pa-s)
η_{275}	coefficient of viscosity at 275 °F (135 °C), cSt
η_{140}	coefficient of viscosity at 140 °F (60 °C), P
$\eta"_{275}$	log [coefficient of viscosity at 275 °F (135 °C)/13,000], coefficient of viscosity expressed in poises
$\eta"_{140}$	log [coefficient of viscosity at 140 °F (60 °F)/13,000], coefficient of viscosity expressed in poises
$\eta_{1,1}$	coefficient of viscosity at the initial pressure and initial shear rate, (P)
$\eta_{i,j}$	coefficient of viscosity at the ith pressure and jth shear rate, (P)
$\dot{\gamma}'$	apparent shear strain rate, in/in/s (mm/mm/s)
γ'	apparent shear strain, in/in (mm/mm)
$\dot{\gamma}_{1,1}$	initial shear strain rate at initial pressure, in/in/s (mm/mm/s)
γ_e	elastic surface energy per unit area, $lb\text{-}in/in^2$ (J/m^2)
$\dot{\gamma}_{i,j}$	jth shear strain rate of ith pressure, in/in/s (mm/mm/s)
γ_p	plastic surface energy per unit area, $lb\text{-}in/in^2$ (J/m^2)
$\gamma(T,t)$	shear strain at temperature T and time t, in/in (mm/mm)
$\gamma(\omega)$	peak to peak shear strain in dynamic shear, in/in (mm/mm)
γ	shear strain, in/in (mm/mm)

$\dot{\gamma}$	shear strain rate, in/in/s (mm/mm/s)
Φ	cone angle, degrees
ν	Poisson's ratio
ω	angular frequency, rad/s
σ	stress, lb/in^2 (Pa)
σ_c	remote critical stress, lb/in^2 (Pa)
σ_t	tensile strength, lb/in^2 (Pa)
τ	shear stress, lb/in^2 (Pa)
τ'	apparent shear stress, lb/in^2 (Pa)
$\tau(T,t)$	shear stress at temperature T and time t, lb/in^2 (Pa)
$\tau(\omega)$	peak to peak shear stress in dynamic shear, lb/in^2 (Pa)
a	crack (notch) length, in (mm)
A	area, in^2 (mm^2)
A	fatigue crack propagation parameter
A	pavement age, years
A	absolute value of slope of plot on Shell BTDC, penetration branch, °C
A_F	absolute value of slope of plot of log-penetration versus temperature, °F
A'	absolute value of slope of plot on Shell BTDC, viscosity branch, °C
A'	age of pavement/10, years
a_1	empirical coefficient used in the calculation of K_{1c}
a_c	critical crack length, in (mm)
a_o	initial crack length, in (mm)
a(T)	shift factor, °F (°C)
b	width, in (mm)

b	$d(\ln\eta)/dp$, or 2.303 times the slope of a plot of log-viscosity versus pressure
B	parameter used in calculating penetration indices
B	uncracked ligament length, in (mm)
b_1	empirical coefficient used in the calculation of K_c
BTDC	Bitumen Test Data Chart, after Heukelom [22]
c	degree of complex flow, defined as slope of log shear strain rate versus log shear stress
C	parameter used in calculating penetration indices
C	cummulative damage index
C.I.	asphalt class index
C_k	Barenblatt's correction factor
c_v	volumetric concentration of the aggregate
COD	Crack Opening Displacement (method)
COLD	low temperature pavement cracking model [39]
d	depth of beam, in (mm)
D	indicator variable for subgrade type, Hajek-Haas model, unitless
D	diameter, in (mm)
D2S	precision based on maximum expected difference between two independent observations
D_c	capillary diameter, in (mm)
D_F	intercept of plot of log-penetration versus temperature, °F
DMA	dynamic mechanical analysis
DSC	differential scanning calorimetry (calorimeter)
D_t	sample tube diameter, in (mm)
e	base for naperian logarithm
exp	indicates that the expression that follows is an exponent

E	elastic modulus, lb/in^2 (Pa)
$f(a_o/d)$	dimensionless variable that depends on the geometry of the specimen and crack length
G	shear modulus, lb/in^2 (Pa)
G''	shear loss modulus, lb/in^2 (Pa)
G'	shear storage modulus, lb/in^2 (Pa)
$\|G^*\|$	absolute value of complex shear modulus, lb/in^2 (Pa)
$\|G^*(\omega)\|$	absolute value of complex shear modulus as a function of angular frequency, lb/in^2 (Pa)
G_{1c}	linear elastic strain energy release rate for plane strain, $lb\text{-}in/in^2$ (Pa-m)
GPC	gel permeation chromatography
HP-GPC	high pressure gel permeation chromatography
I	cracking index, number of transverse cracks per 500 ft (152 m) of roadway
J_{1c}	critical value of J integral in plane strain, $lb\text{-}in/in^2$ (Pa-m)
K	stress intensity factor, $lb/in^2\text{-}\sqrt{in}$ (Pa-$\sqrt{m}$)
K_1	stress intensity factor for plane strain, $lb/in^2\text{-}\sqrt{in}$ (Pa-$\sqrt{m}$)
K_{1c}	plane strain fracture toughness, $lb/in^2\text{-}\sqrt{in}$ (Pa-$\sqrt{m}$)
K_{1c}	critical stress intensity factor for plane strain, $lb/in^2\text{-}\sqrt{in}$ (Pa-$\sqrt{m}$)
K_c	critical stress intensity factor for plane stress, $lb/in^2\text{-}\sqrt{in}$ (Pa-$\sqrt{m}$)
K_g	geometric correction factor for a forced flow capillary viscometer, unitless
$K_{\dot{\gamma}}$	geometric constant for forced flow capillary viscometer, in^{-1} (mm^{-1}), used to calculate apparent shear strain rate
K_R	Rabinowitch correction factor, unitless
K_τ	geometric constant for forced capillary flow, in^{-2} (mm^{-2}), used to calculate apparent shear stress

L	length, in (mm)
L_c	capillary length, in (mm)
LEFM	linear elastic fracture mechanics
LMS	large molecular size
L_t	sample tube length, in (mm)
LVDT	Linear Variable Differential Transformer
m	slope of the relaxation master curve at the base temperature 77 °F (25 °C)
M	winter design temperature in program COLD, °F
$m_1..m_4$	regression coefficients used in the prediction of fracture coefficients a_1 and b_1
MMS	medium molecular size
MT'	(minimum monthly air temperature + 20)/5.7, °F
$\bar{M}_n$	number average molecular weight
$\bar{M}_w$	weight average molecular weight
n	fatigue crack propagation parameter
N	number of load (thermal) cycles
N_f	number of cycles to failure
P	load, lb (kg) or lb (N)
P	viscosity, P
p	absolute pressure, atm
PDI	Polydispersity Index
Pen_{77}	penetration 0.1 mm, 77 °F (25 °C), 100 g, 5 s
$Pen_{77}(t)$	penetration at some pavement age, t years, 0.1 mm, 77 °F (25 °C), 100 g, 5 s
$Pen_{77}(0)$	original penetration, 0.1 mm, 77 °F (25 °C), 100 g, 5 s
PI	penetration index calculated using penetration at 77 °F (25 °C) and ring and ball softening point temperature

PI′	0.25(PI + 2)
$PI_{log\text{-}pen}$	penetration index calculated using log-penetration versus temperature data
PI_{Fraass}	penetration index calculated using penetration at 77 °F (25 °C) and Fraass brittle point temperature
P_{RTFOT}	ratio found by dividing penetration measured at 77 °F (25 °C) after RTFOT by original penetration
PVN	penetration-viscosity number
PVN_{140}	penetration-viscosity number, calculated using penetration at 77 °F (25 °C) and viscosity at 140 °F (60 °C)
PVN_{275}	penetration-viscosity number, calculated using penetration at 77 °F (25 °C) and viscosity at 275 °F (135 °C)
R	correlation coefficient
°R	degrees, Rankine scale
R^2	coefficient of determination
R_η	viscosity ratio calculated by dividing viscosity at 140 °F (60 °C) by viscosity at 275 °F (135 °C), consistent units
RI	refractive index
RTFOT	Rolling Thin-Film Oven Test, ASTM D 2872 "Effect of Heat and Air on a Moving Film of Asphalt (Rotating Thin-Film Oven Test)"
RVDT	Rotary Variable Differential Transformer
s	seconds
s	standard deviation
SA′	average annual amplitude of solar radiation/240, langleys/day
S_B	stiffness of bitumen (asphalt), lb/in^2 (Pa)
S_B'	stiffness of bitumen at 20,000 s loading time and winter design temperature, kg/m^2
$S_B(0)$	stiffness of the original asphalt at 20,000 s loading time and at the winter design temperature, kg/m^2

$S_B(T,t)$	stiffness of bitumen (asphalt) at temperature T and time t, lb/in^2 (Pa)
$S_m(T,t)$	stiffness of hot-mix asphalt concrete at temperature T and time t, lb/in^2 (Pa)
SMS	small molecular size
SP'	ring and ball softening point temperature/125.6, °F
t	time, s
t	thickness of asphalt concrete surface layer, in (mm)
t	thickness of asphalt concrete/8, in
T	temperature, °F (°C)
T	torque, in-lb (kg-m)
T_B	base temperature, derived from penetration at 77 °F (25 °C) and penetration-viscosity number found using penetration at 77 °F (25 °C) and viscosity at 140 °F (60 °C); determined using a nomograph, and used in conjunction with McCleod's modification of Heukelom and Klomp's version of Van der Poel's nomograph
T_g	glass transition temperature,°F (°C)
T_H	Hills' cracking temperature, °F (°C)
T_{Fraass}	Fraass brittle point temperature, °F (°C)
$T_{Pen1.2}$	estimated temperature at which penetration equals 1.2, °F (°C)
T_{Pen800}	estimated temperature at which penetration equals 800, °F (°C)
$T_{Pen800F}$	temperature, °F, at a penetration of 800, extrapolated from plot of Fraass brittle point temperature and penetration at 77 °F (25 °C)
T_0	any arbitrarily selected reference temperature, °F (°C)
T_r	difference between the air temperature and the stress-free mix temperature, °F (°C)
$T_{R\&B}$	ring and ball softening point temperature, °F (°C)
$T_{R\&B}(O)$	ring and ball softening point temperature of original asphalt, °F (°C)

$T_{R\&B}(t)$	ring and ball softening point temperature at some pavement age, t, °F (°C)
T_s	an asphalt-specific characteristic reference temperature, used in the WLF equation, °F (°C)
T_{vis4GP}	temperature at which coefficient of viscosity is 4 GP, °F (°C)
TC-1	Shahin-McCullough pavement cracking model
TFOT	Thin Film Oven Test, ASTM D 1754 "Effect of Heat and Air on Asphaltic Materials (Thin-Film Oven Test)"
THERM	computer program to model thermal cracking in flexible pavements, Lytton.
T_{1GPa}	temperature, °F (°C), at which estimated stiffness is 1.0 GPa at a loading time of 30 min
U_e	elastic strain energy to failure, lb-in (J)
U_e^{nc}	stored elastic strain energy in a beam with no crack, lb-in (J)
U_T	total strain energy to failure, lb-in (J)
uv	ultraviolet
V	velocity, in/s (mm/s)
$V_{AV}(0)$	initial volume percentage of air voids, preferably after placement and initial compaction
vis	abbreviation for viscosity
VPO	Vapor Pressure Osmometry
VTS	viscosity temperature susceptibility, slope of log-log viscosity versus log absolute temperature, coefficient of viscosity in centistokes and temperature in degrees kelvin or rankine
z	distance between crack tip and the first node of the finite element mesh in the crack-tip region, in (mm)

1. INTRODUCTION

Thermal cracking of hot-mix asphalt pavements continues to be a problem in many parts of the United States. Current specifications and test procedures do not adequately ensure against the occurrence of thermal cracking. Although thermal cracking of hot-mix asphalt pavements was first studied by those concerned with low-temperature shrinkage cracking in Canada and the northern United States, thermal fatigue cracking is now recognized as a problem in more temperate climates.

1.1 BACKGROUND

Several different procedures and techniques have been developed to predict thermal cracking and to characterize the susceptibility of asphalt cements to thermal cracking. Temperature susceptibility parameters, such as penetration index (PI) and penetration-viscosity number (PVN), have been used in conjunction with stiffness nomographs to predict a limiting stiffness or temperature, below which thermal cracking is expected to occur. Such techniques fail to account for thermal fatigue and are of questionable accuracy with regard to predicting the shrinkage cracking that will occur in the field under actual service conditions.

Numerous computer-based models have been developed to predict thermal cracking. The earlier models are based upon empirical or statistical relationships that relate cracking to various asphalt specification data and environmental parameters. More recently, fracture mechanics theory was used to develop a computer-based model that can be applied to the thermal cracking problem. During the development of this model, it was necessary to resort to statistical regression equations to predict fracture properties, rather than to incorporate fundamental asphalt or mixture fracture properties into the model. Thus, neither the statistically based models nor the more recently developed fracture mechanics model is a completely mechanistic approach for relating fundamental asphalt or mixture properties to the incidence of thermal cracking.

Past studies have shown that asphalt cement stiffness is clearly the primary material variable that accounts for thermal cracking. Yet there is currently no acceptable test method for the direct measurement of asphalt stiffness at temperatures below 77 °F (25 °C), the range in which both thermal fatigue and thermal shrinkage cracking occur. An acceptable specification test method must provide test data in fundamental engineering units, be simple and rapid to perform, and require neither highly sophisticated operators nor expensive equipment.

1.2 PROJECT OBJECTIVES

Given the plethora of temperature susceptibility parameters that exists in the literature, and the recent claims for the accuracy of high performance-gel permeation chromatography, HP-GPC, in predicting thermal cracking, a study of the interrelationships among these parameters is clearly needed. The results from such a study would permit user agencies to select the most reliable of the parameters that are currently available and to discard those that are less reliable.

To develop a rational method for predicting thermal cracking and to provide an accurate and precise test method for specification purposes, an improved method for determining asphalt stiffness is required. A direct measure of stiffness at low temperatures is preferable to the various nomographs that currently represent the only practical procedure for obtaining low-temperature stiffness. Therefore, the following two objectives were established for this project:

1. Provide correlations between selected engineering and physicochemical tests that are currently used or have been proposed for use in assessing the susceptibility to thermal cracking of mixtures made with different asphalt cements.

2. Investigate the feasibility of developing a procedure for measuring the stiffness, expressed in fundamental engineering units, of asphalt cement at low temperatures. Only those procedures that are uncomplicated and suitable for routine use in asphalt cement specifications will be considered.

1.3 SCOPE

This study encompasses a review and laboratory evaluation of a number of procedures that are readily available for assessing the low-temperature cracking susceptibility of asphalt cement. The procedures studied varied from relatively simple ones, such as the calculation of penetration index from penetration and softening point, to such complex procedures as the calculation of crack propagation energy using fracture mechanics. Statistical procedures were used to identify correlations between the various test results and to assess their utility in predicting actual performance.

In addition, the feasibility of developing a routine test for measuring asphalt stiffness that can be expressed in fundamental units was explored. A recommended test procedure and an experimental plan for its verification were developed.

1.4 RESEARCH APPROACH

The research plan followed is shown graphically in figure 1. The first step was to review the existing literature related to temperature susceptibility parameters and to review methods for measuring the stiffness of asphalt at temperatures less than 77 °F (25 °C). The literature search was expanded to include rheological measurement techniques for other materials that display viscoelastic behavior. The literature review formed the basis for selecting the tests that were performed on the asphalt cements and for developing a new test procedure for the direct measurement of low-temperature stiffness.

Seventeen asphalts were selected for study. These asphalts were tested in the laboratory to characterize their physical properties. Mixes were made with 12 of the 17 asphalts, and specimens were tested for modulus, strength, and fracture properties. A single mixture design was used.

A review of the models that are currently available for predicting the thermal cracking of pavements was completed, and two models were selected for further study. These models were used with the test data obtained from the

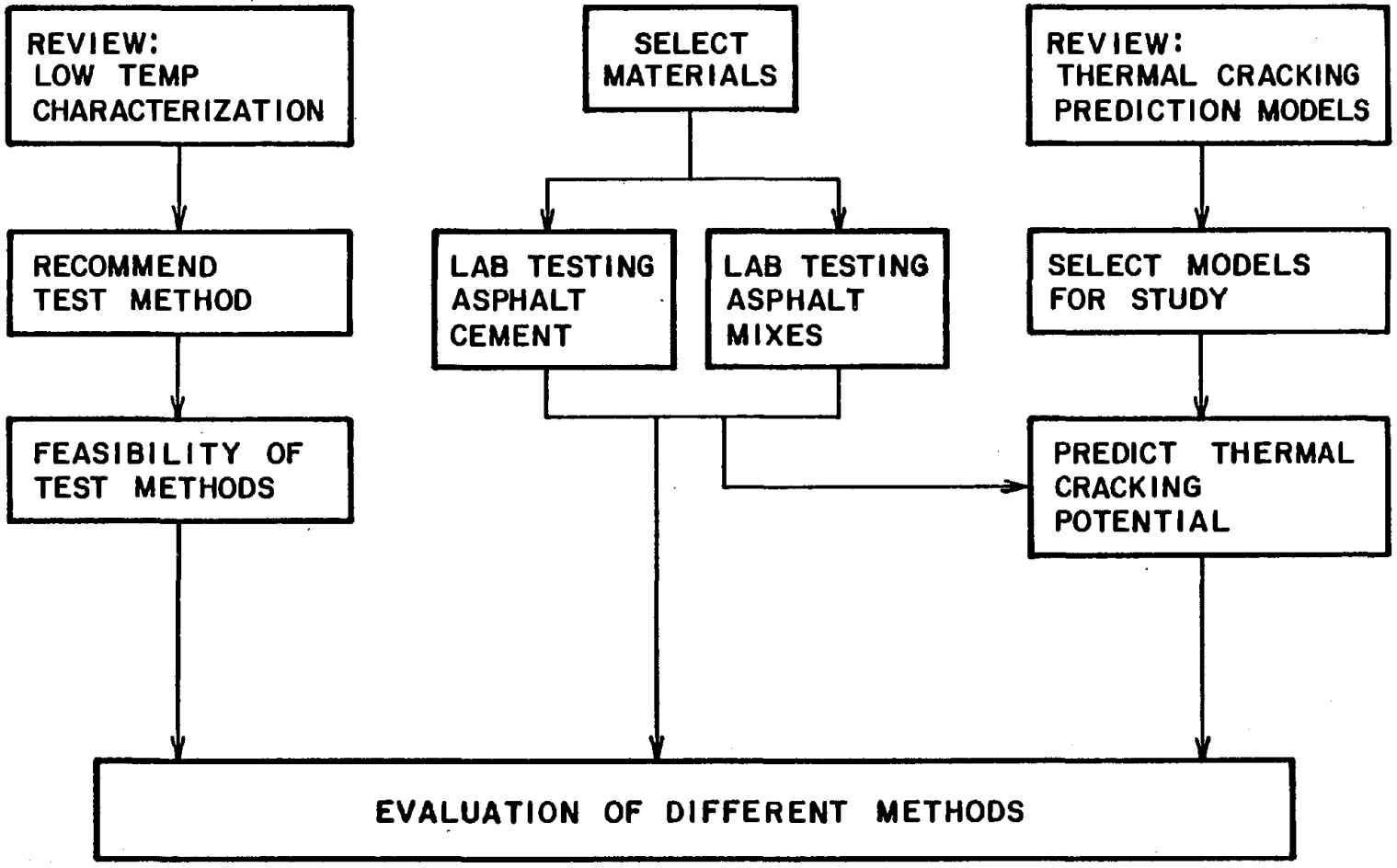

Figure 1. Flow chart illustrating the research plan.

laboratory to predict the incidence of thermal cracking that could be expected in five different climatic regions of the United States. These results were compared with the various temperature susceptibility and thermal cracking parameters calculated for the neat asphalt and for the asphalt concrete.

Based upon the literature review and the testing of the asphalt cements, a bending beam test was recommended for further study as a potential specification test. A recommendation for a field study to verify the validity of the recommended test procedures was also developed.

Details regarding the various phases of the study are presented in the following chapters.

2. REVIEW OF TEST METHODS FOR THE MEASURE OF ASPHALT STIFFNESS AT LOW TEMPERATURES

At present, there is no specification test method suitable for routinely measuring the low-temperature stiffness of asphalt cement. The recommendation of a prototype test method for making such measurements was one of the main tasks in this project. As part of this task, a review of the literature was completed to identify promising techniques and to evaluate the development work accomplished by others. The general characterization of the low-temperature stiffness or rheological properties was considered rather than the more limited problem of the characterization of low-temperature viscosity.

Rheology can be broadly defined as the study of the flow of matter. The flow of asphalt cement at low temperatures is more complicated than in the Newtonian flow region, which occurs, for most paving asphalts, at temperatures of approximately 140 °F (60 °C). The Newtonian flow region, however, is defined by temperature and loading rate, and as the rate of loading decreases, the minimum temperature at which Newtonian flow is retained also decreases. At small strains and temperatures below approximately 140 °F (60 °C), asphalt cements behave as a linear-viscoelastic material, which is defined as follows:

- The strain at any given time is directly proportional to the applied stress.
- The effect of an applied stress is additive; i.e., the Boltzman Superposition Principle is valid.
- Time/temperature superposition is valid.

The literature review is summarized in the following sections. The review is in turn followed by a recommendation for a prototype device that can be used to measure the stiffness of asphalt cement at low temperatures.

2.1 INTRODUCTION

Some investigators have described the consistency of asphalt cement at temperatures less than 77 °F (25 °C) in terms of viscosity alone. Since it is accepted that at such temperatures the flow of asphalt cement deviates greatly

from Newtonian behavior, the simple Newtonian characterization is invalid. Thus, it is necessary to invoke the concept of stiffness in measuring consistencies at these temperatures. This concept allows the inclusion of the elastic and delayed elastic response.

Stiffness measurement systems can be categorized according to loading time or loading frequency and the geometry of the test fixture. Geometry refers to the nature of both the stresses and strains applied to the specimen, as well as the specimen shape and the configuration of the loading device. Transient tests performed by applying a constant strain to a specimen are called stress relaxation tests whereas transient tests performed by applying a constant load are called creep tests. Dynamic testing involves the application of cyclically varying stresses (or strains) and the measurement of the magnitude and phase lag of the resulting strain (or stress). The main advantages of transient tests are that they are simple to perform and analyze and that they give information on asphalt stiffness at long loading times. Dynamic tests typically require complicated and expensive equipment for their execution and sophisticated computer systems for the data analysis. However, such tests can be performed much more rapidly than transient tests; can provide accurate data at very short loading times; and, through the use of time/temperature superposition, can be used to estimate the flow properties at very long loading times.

Since asphalt cement may be fairly soft at room temperature and above, 77 °F (25 °C) to 140 °F (60 °C), and may flow under its own weight, most methods of measuring stiffness embody geometries which restrain the sample during testing. Generally such geometries involve the application of shear stress to a specimen and the measurement of the resulting shear strain, shown schematically in figure 2. The stiffness can then be calculated by dividing the applied shear stress, τ, by the observed shear strain, γ, which is a function of time and temperature:

$$S_B(T,t) = \tau/\gamma(T,t) \qquad (1)$$

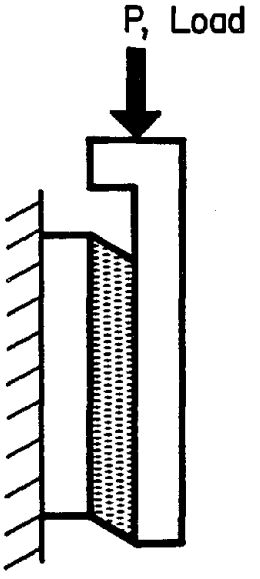

Figure 2. Schematic illustration of idealized shear test.

where

$S_B(T,t)$ = stiffness of bitumen (asphalt) at temperature T and time t, lb/in^2 (Pa)

τ = shear stress, lb/in^2 (Pa)

$\gamma(T,t)$ = shear strain at temperature T and time t, in/in (mm/mm)

T = temperature, °F (°C)

t = time, s

Asphalt stiffness may be measured in tension or in shear. Asphalt is generally considered an incompressible material in the viscous region and, therefore, in this region, Poisson's ratio is equal to 0.50. In this case the tensile stiffness is equal to three times the shear stiffness.[1] For simplicity's sake, and to easily compare various techniques for measuring asphalt stiffness, all stiffness values in this report are given as uniaxial tensile stiffness, unless otherwise stated.

The tensile stiffness of asphalt cement reaches a limiting value of about 380,000 lb/in^2 (2.6 GPa) at low temperatures and short loading times.[2] The ability to measure stiffnesses of this magnitude is of major importance when considering various methods for measuring low temperature stiffness.

Most devices and techniques suitable for measuring the stiffness of asphalt cement at room temperature or above are unsuitable for very low temperatures because the displacements at low temperatures are too small to be measured accurately with these devices. Therefore, one of the major considerations during the literature review and in the selection of an appropriate test device was the upper limit of stiffness that can be measured by each device.

The fact that the magnitude of the asphalt cement stiffness changes dramatically over the range of service temperatures presents several measurement problems. The test device must permit measurements within the range of linear behavior. At temperatures above 77 °F (25 °C), even extremely small stresses may result in excessive strains, at which point the behavior of the asphalt is no longer linear. Conversely, asphalt cement becomes very

stiff at low temperatures, below 32 °F (0 °C), necessitating the application of large stresses in order to obtain measureable strains or deflections.

Establishing levels of stress and strain that ensure linear behavior during the measurement of stiffness is not straightforward because these levels depend upon the test temperature and test time or frequency. Viscosity tests performed at intermediate temperatures, 77 °F (25 °C) to 140 °F (60 °C), exhibit nonlinear behavior at shear stresses greater than approximately 4.8 lb/in^2 (33 kPa).[3] Within this range of test temperatures, nonlinear behavior may not be observed until the shear strains are as large as 100 percent.[1] At lower temperatures, below 32 °F (0 °C), at which the asphalt cement is much stiffer, the shear strain should be limited to 0.1 percent to ensure linear behavior.[4]

When calculating the range of stiffnesses that can be measured with a particular device, in addition to applying the limiting stress and strain criteria described above, it is necessary to consider the minimum deflection that can be accurately measured and the minimum load that can be reliably applied to a test fixture under actual test conditions. For example, linear variable differential transformers (LVDTs) are highly accurate devices for determining displacements, and they possess theoretically infinite resolution. However, in practice, the resolution of an LVDT is limited by the conditioning, amplification, and recording equipment used.

Experience of the research team has shown that sensitivities of 100 µin/V (2.5 µm/V) are readily attainable with small LVDTs and commercially available signal conditioners. To keep electronic and mechanical noise to an acceptable level, the smallest displacement that can be reliably measured with this equipment is typically 10 µin (250 nm), corresponding to an output voltage of 0.1 V. With special cabling and conditioners, this limit may be extended to 1 µin (25 nm) or less. The minimum resolution for a rotary variable differential transformer (RVDT), which is typically linear over an 80-degree range of rotation, is approximately 0.008 degrees. Load may be applied to a rheometer by means of dead weights or some mechanical loading system. Although transducers capable of measuring loads much less than 1 g are

commercially available, a minimum load of 100 g appears appropriate for routine test devices.

Schweyer compiled an excellent summary of the techniques that have been used for measuring viscosity and stiffness over a wide range of temperatures and loading times.[5] Numerous geometries have been used to measure asphalt stiffness: sliding plate, rotating concentric cylinders, cone and plate, torsion bar, falling concentric cylinder, rotating parallel plate, and rotating eccentric plates. Most of these geometries have been used both in the creep mode and in the dynamic mode although some geometries are more suited to particular testing modes. These testing geometries are discussed in detail below.

In summary, the following requirements must be met in a device that will be used to measure the low temperature stiffness of asphalt cement within the context of specification testing:

- At low temperature, accurately measure stiffnesses as large as 380,000 lb/in^2 (2.6 GPa).
- At moderate temperatures and above, limit shear stresses to less than 4.8 lb/in^2 (33 kPa).
- Be sufficiently sensitive to measure very small strains (0.1 percent) at low temperatures and limit the strain at high temperatures to less than 100 percent.
- Be simple and easy to operate so that it may be used by typical testing personnel.
- Be cost effective.
- Use specimens that can be easily stored, to allow measurement of steric hardening effects.
- Use relatively small quantities of asphalt, so that TFOT or RTFOT residue can be economically tested.

2.2 THE SLIDING PLATE MICROVISCOMETER

The sliding plate microviscometer, as described by Griffin and others, was developed in the mid-1950's.[6] This device was developed so that the

effect of aging on the viscosity of thin films of asphalt could be studied. A schematic of the most commonly used sliding plate configuration (dual plates) is shown in figure 2. In this test method, a 0.0004 to 0.0040-in (10 to 100-μm) thick layer of asphalt is sheared between two 0.79-in by 1.22-in (20-mm by 30-mm) glass plates. One of these plates is fixed, while a load is applied to the other plate through a lever system upon which various weights are suspended. The subsequent displacement of the moving plate over time is then monitored using a complicated servo-controlled system.

The sliding plate microviscometer was designed to measure the steady state coefficient of viscosity, not the stiffness of asphalt cement. The shear strains developed in the test specimen are very large, generally exceeding 100 to 1,000 percent, well beyond the linear range of behavior. Consequently, the sliding plate microviscometer does not warrant further consideration in this study.

2.3 THE SLIDING PLATE RHEOMETER

In the early 1970's, the sliding plate rheometer was developed to permit the testing of much thicker asphalt films.[1,7,8] The thickness of the asphalt layers used in the sliding plate rheometer are 0.08 to 0.4 in (2 to 10 mm), which permits measurement of strains as small as 5×10^{-5}. At the maximum load of 4.4 lb (2.0 kg), this corresponds to a maximum measurable stiffness of 290,000 lb/in^2 (2.0 GPa), which approaches the maximum observed stiffness of asphalt at low temperatures. The minimum measurable stiffness for this device, using the limitations established earlier, is 0.71 lb/in^2 (4,900 Pa). The sliding plate geometry is shown in figures 2 and 3. The geometry shown in figure 3 minimizes the effect of loading eccentricity and has also been used for testing asphalt cements.[9]

As with the sliding plate microviscometer, the loading time can be varied from about 1 s to a practical maximum of approximately 2 h. The test is normally performed in a controlled temperature bath so that tests can be performed at temperatures as low as -40 °F (-40 °C). Test specimens are fairly easy to prepare and can be stored after preparation for evaluation of steric hardening.

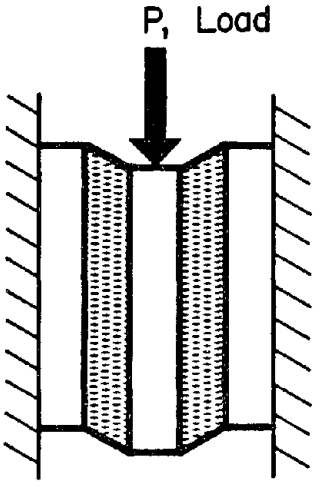

Figure 3. Schematic of double sliding plate geometry.

Potential sources of error in the sliding plate rheometer include moments caused by slight eccentricities in loading, perturbations resulting from the application of the load, errors in measured deflections caused by thermal contraction or expansion of supports, and loose mountings and linkages. Fenijn has reported the repeatability of the sliding plate rheometer to be 15 to 18 percent (maximum difference between 9 replicates).[7] Gaw later modified this device by adding an improved method for clamping the test plates and by improving the instrumentation.[1]

The sliding plate rheometer is capable of accurately measuring asphalt stiffnesses approaching the limiting value of 380,000 lb/in^2 (2.6 GPa). The sliding plate geometry is best suited for stiffness measurements in the intermediate range. Since it is a creep test, the stiffnesses measured can, in turn, be resolved into viscous and elastic components. However, the time required to run the test can be quite long, and several days of testing may be required to obtain a master curve. Gaw indicated that the price of the sliding plate rheometer was several thousand dollars in 1977.[1] The current price of the sliding plate rheometer is approximately $10,000; and the Shell design is protected by patents. Of the currently available methods, the sliding plate rheometer is probably the most promising for measuring asphalt stiffness at low temperatures.

2.4 THE CONE AND PLATE VISCOMETER

In the early 1960's, the static cone and plate viscometer was applied to the testing of asphalt cements; an early prototype was described by Sisko.[10] In this device, as constructed by the Cannon Instrument Company, the asphalt sample is sheared between a rotating cone and a fixed plate in the creep mode. However, the cone and plate geometry has been used widely in other modes, for example, in the Rheometrics rheometer (Rheometrics mechanical spectrometer). The Cannon cone and plate viscometer is designed so that the shear stresses during loading are equal throughout the test specimen. Loading is accomplished by hanging a selected weight on a string which, through a system of pulleys, transmits a torque to the vertical cone shaft. A diagram of the cone and plate geometry is shown in figure 4.

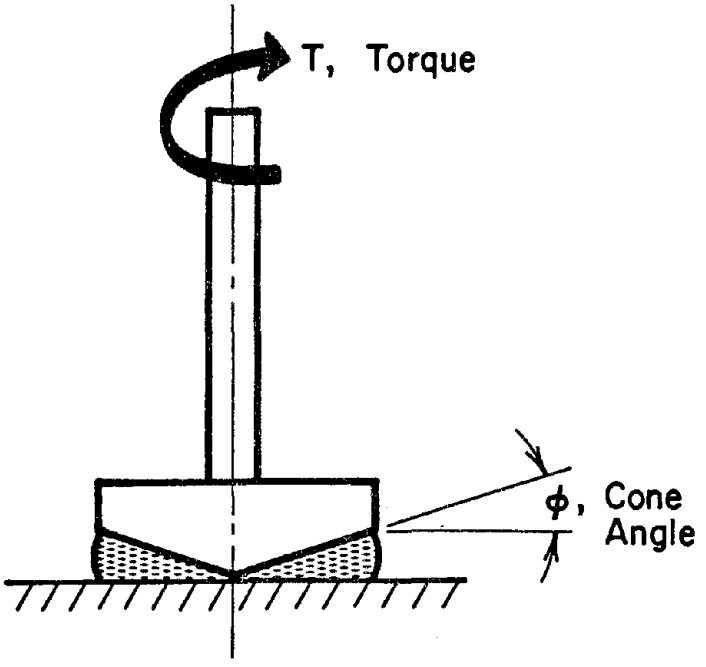

Figure 4. Schematic of cone and plate rheometer.

In the original Cannon design, rotational displacements are measured visually, using an optical magnifying scope and a scale divided into degrees. The device has been modified by adding an RVDT to measure angular rotation, a convenient and accurate means of measuring this movement.[11] The maximum practical load for the Canon cone and plate viscometer is approximately 22 lb (10 kg), corresponding to a stress of 290 lb/in^2 (2.0 MPa). If the minimum rotational displacement measurable with an RVDT is assumed to be 0.008 degree, corresponding to a shear strain of 0.016, then the maximum measurable stiffness using the cone and plate viscometer will be 54,000 lb/in^2 (370 MPa), which is less than the desirable limit of 380,000 lb/in^2 (2.6 GPa). With the addition of the RVDT, the cone and plate device can be used to generate a stiffness master curve, and the strains can be limited to 10 percent or less. An ASTM standard for using the cone and plate viscometer can be found under ASTM D 3205.[12] The principal disadvantage of this device is its poor productivity. Test specimens can be prepared only as they are tested, slowing productivity and preventing determinations of steric hardening effects. The cone and plate viscometer is therefore unacceptable for the routine measurement of asphalt stiffness at low temperature.

2.5 THE SCHWEYER RHEOMETER

Schweyer has reported the use of a forced capillary flow viscometer to measure asphalt cement viscosity and stiffness at temperatures as low as 23 °F (-5 °C).[13-15] In this technique, asphalt from a reservoir is forced through a capillary tube of known diameter. The shear stress is calculated from the applied load, and the shear rate is calculated from the velocity of flow in the tube. A schematic of the Schweyer rheometer is shown in figure 5.

The theory of operation of this device is somewhat complex. The apparent shear rate, $\dot{\gamma}'$, is calculated using the following equation:

$$\dot{\gamma}' = (8(D_t^2/D_c^3))V = K_{\dot{\gamma}}V \qquad (2)$$

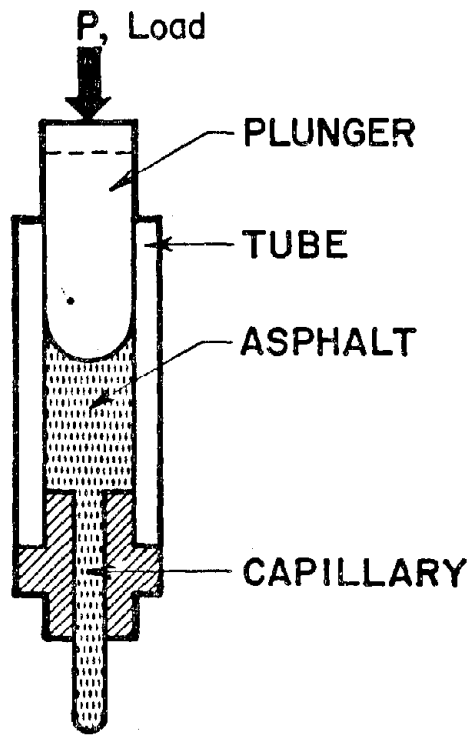

Figure 5. Schematic of Schweyer capillary rheometer.

where

$\dot{\gamma}'$ = apparent shear strain rate, in/in/s (mm/mm/s)

D_t = sample tube diameter, in (mm)

D_c = capillary diameter, in (mm)

V = velocity, in/s (mm/s)

$K_{\dot{\gamma}}$ = geometric constant for a forced flow capillary viscometer, in^{-1} (mm^{-1})

The shear rate, $\dot{\gamma}$, is then calculated from the apparent shear rate by application of the Rabinowitsch correction factor, K_R, to account for non-Newtonian flow:

$$\dot{\gamma} = K_R \dot{\gamma}' \tag{3}$$

where

$K_R = (0.75 + 0.25/c)$

c = degree of complex flow, defined as slope of log shear strain rate versus log shear stress

The apparent shear stress, τ', is calculated by a similar equation:

$$\tau' = (D_c/L_c D_t^2)\ P = K_\tau P \tag{4}$$

where

τ' = apparent shear stress, lb/in^2 (Pa)

D_c = capillary diameter, in (mm)

L_c = capillary length, in (mm)

D_t = sample tube diameter, in (mm)

P = load, lb (kg)

K_τ = geometric constant for forced capillary flow, in^{-2} (mm^{-2})

A geometric correction factor, K_g, is applied to the apparent shear stress to calculate the actual value:

$$\tau = K_g \tau' \tag{5}$$

where

τ = shear stress, lb/in^2 (Pa)

K_g = geometric correction factor for a forced flow capillary viscometer, unitless

τ' = apparent shear stress, lb/in^2 (Pa)

and

$$K_g = ((L_t/L_c)(D_c/D_t)^{3c+1}+1)^{-1} \quad (6)$$

where

K_g = geometric correction factor for a forced flow capillary viscometer, unitless

L_t = sample tube length, in (mm)

L_c = capillary length, in (mm)

D_c = capillary diameter, in (mm)

D_t = sample tube diameter, in (mm)

c = degree of complex flow

The coefficient of viscosity can then be calculated by dividing the shear stress by the shear rate:

$$\eta = \tau/\dot{\gamma} \quad (7)$$

where

η = coefficient of viscosity, $lb\text{-}s/in^2$ (Pa-s)

τ = shear stress, lb/in^2 (Pa)

$\dot{\gamma}$ = shear strain rate, in/in/s (mm/mm/s)

As an alternative, equation 3 can be stated in terms of shear strain:

$$\gamma' = (8(D_t^2/D_c^3))\delta_t = K_{\dot{\gamma}}\delta_t \quad (8)$$

where

γ' = apparent shear strain, in/in (mm/mm)

D_t = sample tube diameter, in (mm)

D_c = capillary diameter, in (mm)

δ_t = displacement of sample in sample tube, in (mm)

$K_{\dot{\gamma}}$ = geometric constant for a forced flow capillary viscometer, in^{-1} (mm-1)

This equation permits the calculation of asphalt stiffness and related parameters.

Because pressures as large as 10,000 lb/in^2 (70 MPa) may be generated in the asphalt sample during this test, a correction for increased viscosity due to pressure effects should be applied as follows:[13]

$$\eta_{i,j} = \eta_{1,1}[e^{b(p-1)}][(\dot{\gamma}_{i,j}/\dot{\gamma}_{1,1})^{c-1}] \quad (9)$$

where

$\eta_{i,j}$ = coefficient of viscosity at ith pressure and jth shear rate, P

$\eta_{1,1}$ = coefficient of viscosity at the initial pressure and initial shear rate, P

e = base for naperian logarithm

b = $d(\ln\eta)/dp$, or 2.303 times the slope of a plot of log viscosity versus pressure

p = absolute pressure, atm

$\dot{\gamma}_{i,j}$ = jth shear strain rate of ith pressure, in/in/s (mm/mm/s)

$\dot{\gamma}_{1,1}$ = initial shear strain rate at initial pressure, in/in/s (mm/mm/s)

c = degree of complex flow

In Schweyer's earlier work, his testing was conducted at a constant rate of strain.[14] Subsequently, a constant stress mode was developed to allow for more rapid testing.[13] Schweyer attempted to account for the large pressures generated with the Schweyer capillary rheometer by assuming that the log of the shear rate is a linear function of the log of the shear stress.

The Schweyer rheometer can result in extremely large shear rates and extremely large shear stresses and strains. This may be acceptable in some applications but is questionable at the low temperatures and large stiffnesses

encountered when evaluating low-temperature cracking. In addition, it is questionable whether rheological data at the very large shear rates developed in this device are applicable to low-temperature cracking. The combined effect of these factors probably explains why Schweyer found a significant incidence of dilatant flow (i.e., increasing viscosity with increasing shear rate), whereas most other researchers have found asphalt to be pseudoplastic (i.e., decreasing viscosity with increasing shear rate) at low temperatures. When the measurement criteria presented earlier (section 2.1) are applied, the shear strains produced in the Schweyer rheometer are so large that linear behavior cannot be achieved throughout most of the temperature range of interest.

The useful temperature range of the Schweyer rheometer extends to only about 23 °F (-5 °C), which does not fully cover the temperature range experienced in cold-weather regions, where thermal cracking of asphalt concrete pavements is common. Schweyer has reported stiffnesses of up to 440,000 lb/in^2 (3.0 GPa) using the capillary rheometer.[14] However, because of the large shear stresses and strains that are produced, the researchers eliminated the Schweyer device from further consideration.

2.6 FALLING COAXIAL CYLINDER VISCOMETER

A device briefly mentioned by Schweyer and reported by others is the falling coaxial cylinder viscometer or rheometer.[5,16] A schematic of this apparatus appears in figure 6.

Although similar in principle to the sliding plate rheometer, the falling coaxial cylinder has several advantages. Because of the symmetry of the geometry, eccentric loading is minimized. Test specimens can be prepared simply by pouring the asphalt into the annulus between the cylinders. However, some additional factors must be considered when this configuration is used for materials that are essentially solids. When undergoing shear, such materials also deform in the direction perpendicular to the applied load. This deformation, the result of Poisson's effect, introduces normal stresses which can make this test geometry very complicated to analyze. A further disadvantage is the relatively large amount of asphalt required to prepare a

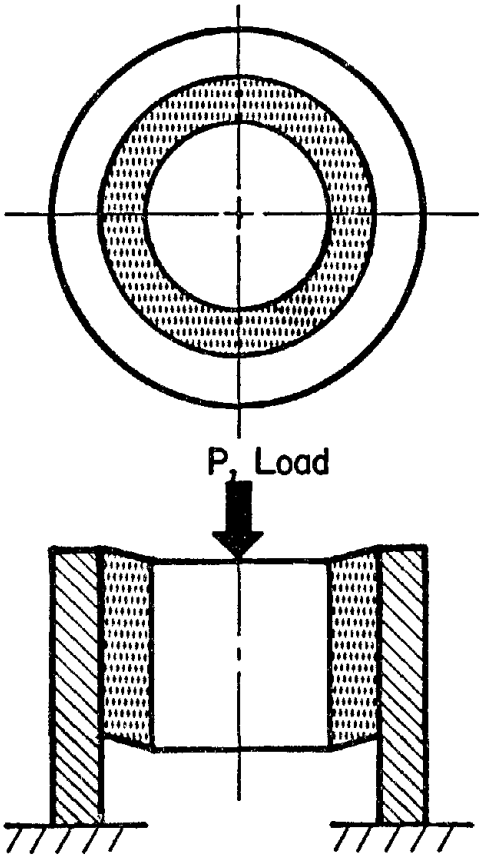

Figure 6. Schematic of falling coaxial cylinder geometry.

test specimen. In summary, this device is similar to the sliding plate rheometer; it requires a large quantity of asphalt to prepare a test specimen, offers no significant advantages, and is suspect with regard to Poisson's effect. It was therefore not considered for further study.

2.7 RHEOMETRICS MECHANICAL SPECTROMETER

The Rheometrics mechanical spectrometer was originally developed for testing polymers. As described by Macosko and Starita, the device consists of an electronically controlled torque motor which applies a cyclical strain to the test specimen through various geometries and an arrangement of transducers to measure the resulting stress.[17] It is possible to program the rotation of the motor to produce oscillatory motion, constant speed rotation, or various other strain cycles. The transducers are highly sensitive silicon strain gauges, which allow precise measurement of load without excessive deflections.

The mechanical spectrometer can employ various geometries, thereby permitting rheological characterization over a wide range of consistencies. For measuring the viscosity of fluids, rotating disks (figure 7), cone and plate viscometers, rotating hemispheres, or concentric cylinders (figure 8) may be used. For viscoelastic materials, in addition to the cone-and-plate, eccentric rotating disks (figure 9) and eccentric rotating hemispheres can be used. For evaluating the rheological properties of solids, a torsion bar (figure 10) is frequently used.[17]

The analysis of data from the mechanical spectrometer generally involves the determination of the amplitude and phase lag of the response (stress) compared with the input (strain). The complex modulus, $|G^*(\omega)|$, is analogous to stiffness:

$$|G^*(\omega)| = \tau/\gamma(\omega) \qquad (10)$$

where

$|G^*(\omega)|$ = absolute value of complex shear modulus, lb/in^2 (Pa)

τ = peak to peak shear stress in dynamic shear, lb/in^2 (Pa)

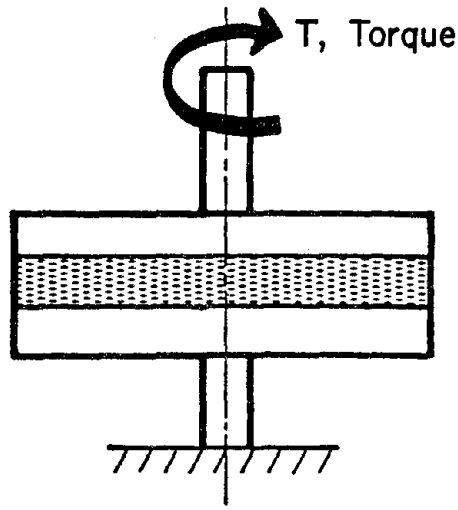

Figure 7. Schematic of parallel rotating disk geometry.

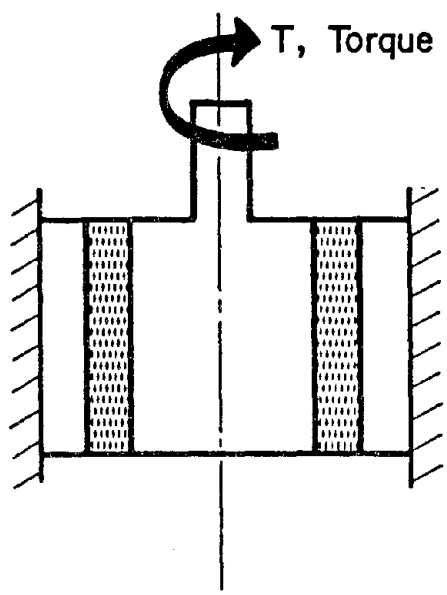

Figure 8. Schematic of rotating concentric cylinder geometry.

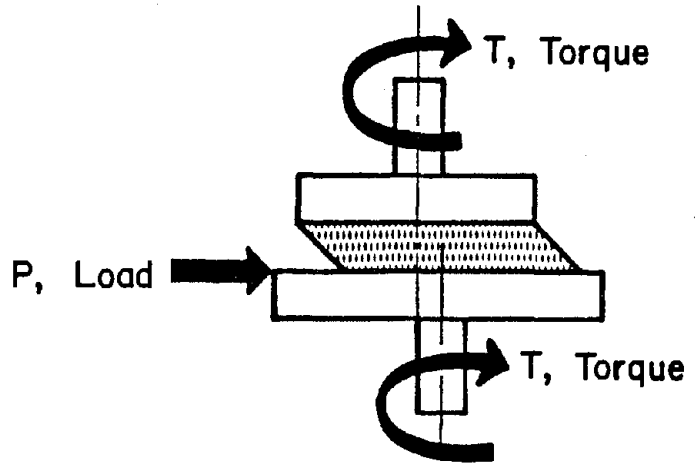

Figure 9. Schematic of rotating eccentric geometry.

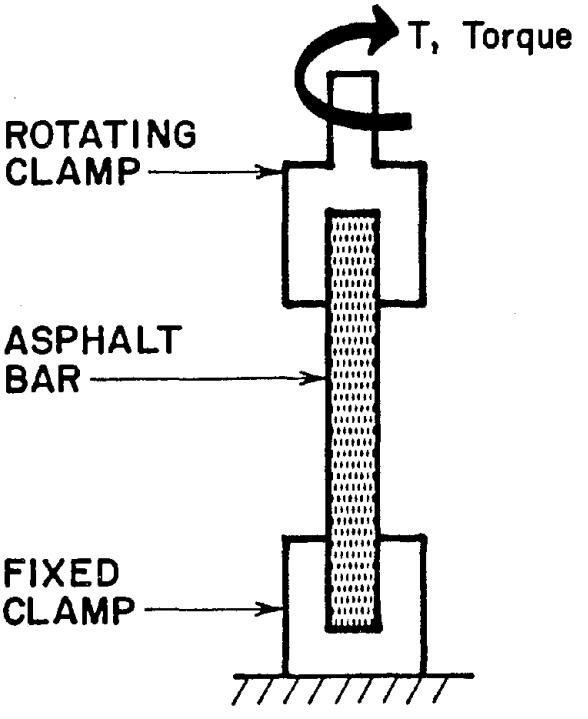

Figure 10. Schematic of torsion bar.

$\gamma(\omega)$ = peak to peak shear strain in dynamic shear, in/in (mm/mm)

ω = angular frequency, rad/s

The complex modulus is composed of an elastic component, G', and a viscous component, G''. The viscous and elastic components of the complex modulus are calculated automatically with a microcomputer and sophisticated software. The phase angle, δ, represents the lag between the strain applied to the specimen and the resulting stress. The tangent of the phase angle, tan delta, is calculated by dividing the loss modulus by the storage modulus. Tan delta decreases as the elastic component of modulus increases; a tan delta value of zero indicates completely elastic behavior. With liquid nitrogen, test temperatures well below -40 °F (-40 °C) can be attained.[4] The relationship between the different complex or dynamic components is discussed in more detail later in chapter 4, section 4.4.

Pink and associates used the Rheometrics mechanical spectrometer to characterize the stiffness of asphalt cements.[4] They used a parallel rotating disk geometry (figure 7) at intermediate temperatures and a torsion bar geometry (figure 10) at low temperatures where the asphalt behaves essentially as a solid. They found reasonably close agreement between their results and the results from a sliding plate rheometer, which indicates that a repeatability of about $\pm$10 percent was possible with the Rheometrics mechanical spectrometer.

The mechanical spectrometer can be used to measure asphalt stiffnesses from 0.15 to 150,000 lb/in^2 (1.0 kPa to 1.0 GPa) at shear rates ranging from 0.001 to 250 s^{-1}. The shear magnitude of the stress applied during testing depends on the stiffness of the sample and the geometry used in testing. The available temperature range is from -315 °F (-193 °C) to 621 °F (327 °C).[18]

Although the mechanical spectrometer can be used to rapidly and accurately determine stiffness over a wide range of temperatures and loading rates, it has several distinct disadvantages for routine use in asphalt cement characterization. The cost of the device is approximately $300,000, placing it well beyond the budgets of most testing and pavement research laboratories, and a skilled operator is needed to operate the device. Therefore, further

consideration of this device for use in specification or acceptance testing was rejected.

2.8 OTHER DYNAMIC TEST METHODS

Other test devices which use dynamic loading are available, and most have been used, at least to a limited extent, to measure asphalt cement stiffness. The rheogoniometer is based upon an oscillating cone-and-plate geometry; the balance rheometer, eccentric rotating hemispheres; and the rheovibron, oscillating parallel plates. These devices are generally similar to the mechanical spectrometer and have the same advantages and disadvantages, although they are not as flexible since they normally use a single, fixed geometry.[5,18]

In recent years, a new generation of low cost ($50,000 to $100,000) dynamic mechanical analyzers (DMAs) has been developed. An example is the DuPont Series 9000 instrument. This device can be used to measure the loss and storage modulus and the phase angle of a material subjected to dynamic loading. Several sample geometries are possible with this device, but small bars, 0.25 in by 0.50 in by 1.0 in (6.4 mm by 12.7 mm by 25 mm), appear to be the most convenient geometry for testing asphalt cement at low temperatures. The test frequency is the resonant frequency of the bar. With the asphalts tested as part of this project, the resonant frequency ranged from 10 to 40 Hz over the temperature range -40 °F (-40 °C) to 86 °F (30 °C). The resonant frequency decreases monotonically over this temperature range. Other manufacturers, including DuPont, offer variable-frequency devices that can accommodate beams, sliding plates, rotating cylinders, and a variety of other geometries.

Testing performed in conjunction with this project indicates that the DuPont Series 9000 device, even in the variable-frequency configuration, can be used for measuring asphalt stiffness. It is particularly useful for determining the mechanical glass transition temperature, which is indicated by a distinct and very repeatable peak in the loss modulus. This type of transition measurement is probably more significant to the pavement engineer than are calorimetrically determined transitions, since it represents a change

in mechanical response rather than a change in heat capacity. Although the mechanical and calorimetric transitions are related in simple linear polymers, the relationship is quite complex in asphalt cement. Transitions seen in the loss modulus curves generated with the DMA are singular and clearly defined, whereas calorimetric transitions (differential scanning calorimeter) in asphalt cement are frequently multiple, diffuse, and as a result, difficult to interpret.

The less expensive mechanical spectrometers, such as those offered by DuPont, Perkin-Elmer, and others, are not cost prohibitive, but considerable expertise is required to operate them and to analyze the data. Although these devices can provide usable test data, the researchers have concluded that they are unsuitable as routine specification test devices in their present form because of their complexity.

2.9 TENSILE STRENGTH TESTS FOR ASPHALT CEMENT

The Fraass test consists of flexing a thin steel plate coated with a thin layer of asphalt. The temperature of the plate is reduced at a constant rate, while the steel plate is flexed once every minute. The temperature at which a crack is first observed in the asphalt coating is recorded as the Fraass brittle point temperature. A detailed description of the test and apparatus is found in The Institute of Petroleum specification IP 80/53.[19]

Several investigators have attempted to correlate the Fraass brittle point temperature with direct or extrapolated results of other tests. Rigden and Lee found that the Fraass brittle point temperature is an equiviscous temperature, at which the viscosity of the asphalt is approximately 58,000 lb-s/in^2 (400 MPa-s).[20] Van der Poel supported this conclusion and stated that, at the brittle point temperature, the stiffness of the asphalt as determined from his nomograph is about 16,000 lb/in^2 (110 MPa).[21] Heukelom similarly suggested that the stiffness of asphalt cement at the Fraass brittle point temperature ranges from 12,000 to 29,000 lb/in^2 (83 to 200 MPa).[2] On Heukelom's Bitumen Test Data Chart, the Fraass temperature corresponds to the temperature at which the penetration of the asphalt is 1.25.[22]

More recent work by Thenoux, Lees, and Bell found that the stiffness of asphalt cement at the Fraass brittle point temperature was about 290,000 lb/in^2 (2.0 GPa), which is much larger than values suggested earlier.[23] Thenoux and his associates determined asphalt stiffnesses at the brittle point by experimental techniques, rather than by use of a nomograph. They also found that the temperature of the asphalt layer on the plate is generally about 9.9 °F (5.5 °C) less than the temperature indicated by the mercury thermometer used in the test. Apparently the thermal mass of the mercury-in-glass thermometer is greater than for the steel plate, explaining why the temperature of the thermometer was greater than that of the plate.

Since the Fraass test is one of the few standard tests which can directly characterize the mechanical behavior of asphalt when it is in a more or less brittle state, it should prove a valuable tool for predicting the asphalt properties at low temperatures. Unfortunately, the Fraass test has not been widely used in the United States and Canada, and little or no data exist that can be used to establish a relationship between the Fraass brittle point temperature and asphalt properties or pavement performance. Thenoux, Lees, and Bell indicated that the precision of the test is inadequate when the specified sample preparation procedures are used.[19] However, the precision of the test can be significantly improved by changing the sample preparation technique.[23]

The standard ductility test has been used for many years as a measure of the tensile properties of asphalt cement. A number of States use a 60 °F (16 °C) ductility test in their specifications, but, in its current configuration, it is inappropriate for testing at temperatures below approximately 60 °F (16 °C). Several investigators have tried to improve the basic test procedure through a variety of modifications, including a modified specimen shape, provisions for measuring the force required to rupture the specimen, and provisions for measuring the strain that occurs in the specimen.[24-26]

In its modified form, the force ductility test has been applied predominantly to asphalt rubber and polymer-modified asphalts by researchers who wanted to emphasize the large amount of extension exhibited by these

materials at low temperatures.[24-26] The major drawback with this test is that it is very difficult to obtain reliable strain measurements for the specimen. Merely measuring specimen elongation is inadequate because of the end effects which cannot be separated from the strain that occurs in the midportion of the specimen. In its modified form, a midsection with a uniform cross section is generally employed. However, obtaining direct strain measurements from this section is impossible without adopting some very sophisticated instrumentation. Consequently, further development of the ductility test and its derivatives was not considered in this study.

2.10 TEST METHODS USED FOR PLASTICS

Various publications on the properties and testing of polymers were reviewed, including ASTM standard test methods for measuring the stiffness and fracture properties of plastics. Many of the techniques encountered are intended for measuring the viscosity of polymer melts, or the viscosity of polymer-solvent solutions, and are not useful for measuring asphalt stiffness at low temperatures. Examples of such devices include the Brookfield viscometer; ASTM D 1823 and D 1824, which is a rotating concentric cylinder viscometer; and various capillary viscometers similar or identical to the viscometers used in standard testing of asphalt cement at high temperatures.[27-30] These devices are all intended for measuring the viscosity of polymer melts at large strains and are unsuitable for measuring asphalt stiffnesses at low temperatures.

A capillary rheometer for use with polymers is described in ASTM Standard D 3835-79 and is nearly identical to the Schweyer rheometer in theory, design, and analysis.[30] It is significant that this standard states that "...The shear stress and shear rate applied should also closely approximate those observed in the actual processing...." This rheometer, like the extrusion devices, is intended for characterizing the behavior of polymer melts during extrusion processing. Consequently, the forced capillary flow rheometers are characterized by the same limitations as the Schweyer rheometer, which was discussed earlier.

A torsion bar test for measuring the stiffness of polymers is also described in ASTM D 1043-84.[31] The geometry of the test is similar to that shown in figure 10. In practice, the load is applied by a series of pulleys similar to those used with the cone and plate viscometer. A reasonably sized specimen for such a test would be 0.40 in by 0.80 in by 3.50 in (10 mm by 20 mm by 90 mm). Angular deflections as small as 0.008 degree can be measured with an RVDT corresponding to a shear strain of 0.000029 for the assumed sample size. At the maximum practical shear stress of 110 lb/in^2 (760 kPa) and by using an RVDT to measure rotational displacement, measurements of stiffnesses as large as 2.2×10^7 lb/in^2 (150 GPa) can be obtained. For a 0.40 in by 0.80 in by 3.50 in (10 mm by 20 mm by 90 mm) bar with a moment arm of 0.8 in (20 mm), a 0.22-lb (100-g) weight will produce a maximum shear stress of 5.6 lb/in^2 (39 kPa), which is too large for use with asphalts having stiffnesses less than 17,000 lb/in^2 (120 MPa). The use of an unconfined sample and end clamps also indicates that this technique would be useful only for very stiff materials.

Two other techniques of interest found in the ASTM standards are bending beam tests described in ASTM D 747-84a and ASTM D 790-84a.[32,33] The former is based on a cantilever beam tested in the creep mode, while the latter standard is based on either three-point or four-point bending and a constant rate of strain. For the cantilever test, if the sample size is 0.40 in by 0.80 in by 6.0 in (10 mm by 20 mm by 150 mm), a weight of 0.22 lb (100 g) at the beam end will produce stresses of 64 lb/in^2 (440 kPa) at the outer surface. Thus, this test could be used only to measure stiffnesses larger than 64,000 lb/in^2 (440 MPa). The test is consequently unacceptable for measuring asphalt stiffnesses. A schematic of the cantilever beam test appears in figure 11.

The bending beam test, figure 12, described in ASTM D 790 is quite different from the other tests described in this paper in that it is performed at a constant rate of strain rather than at a constant stress.[33] Although a viscoelastic analysis of data gathered in this fashion is very complicated, the usual techniques of data analysis simply involve the calculation of an initial tangent modulus, ultimate flexural strength, strain at failure, and the secant modulus at specified points.[33] Such data would be difficult to

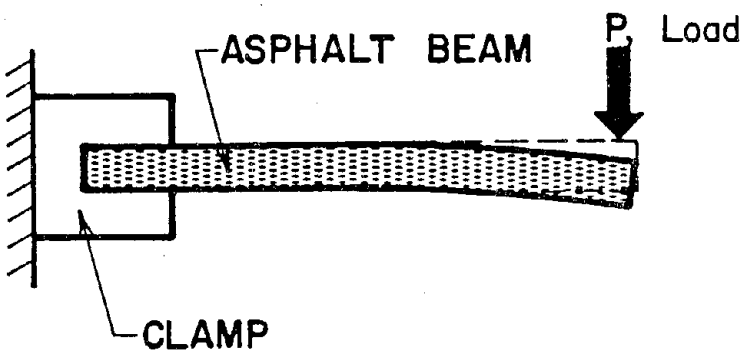

Figure 11. Schematic of cantilever beam geometry.

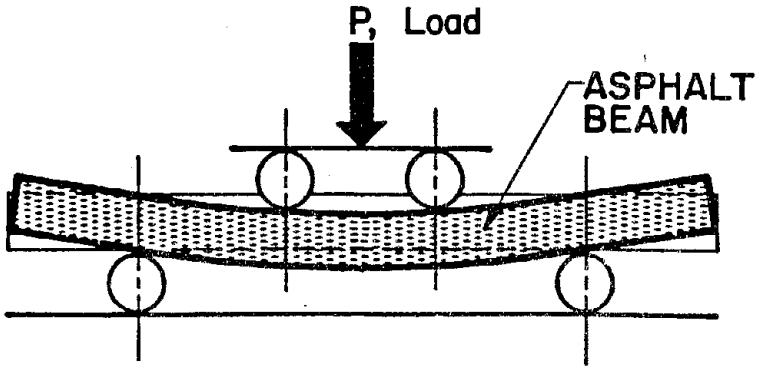

Figure 12. Schematic of four-point bending beam geometry.

correlate with creep data without extensive testing. A further disadvantage of this test, except at the beginning of testing, is that the stresses are much larger than the limits established earlier in this chapter.

The bending beam test was recognized by the research team as having the greatest potential for generating reliable low-temperature stiffness data with simple, low-cost equipment. Although Heukelom included data from such tests in one of his papers, a detailed description of this work was not given, and apparently has never been published.[2]

The most straightforward application of the bending beam test is in the creep mode. Assuming four-point loading is used and the asphalt specimen is 0.25 in by 0.50 in by 5.00 in (6.4 mm by 12.7 mm by 127 mm)--the standard dimension indicated by ASTM D 790--a 0.22-lb (100-g) load would produce stresses of about 17 lb/in^2 (120,000 Pa). It is assumed that the nature of this test precludes its use on asphalts having stiffnesses less than 1500 lb/in^2 (10 MPa) because the test specimens would deform excessively during handling. By applying the maximum tensile stress and measuring the resulting midpoint deflection of the beam, stiffnesses as large as 4.9×10^6 lb/in^2 (34 GPa) can be measured--about 10 times the observed maximum stiffness of asphalt cement. Because the bending beam test in the creep mode is easy to conduct, the ranges of measurable stiffnesses are in the desired range (i.e., much greater than 380,000 lb/in^2 (2.6 GPa)), and the interpretation of the data is relatively straightforward, the bending beam test was selected by the research team for further development.

2.11 SUMMARY OF LITERATURE REVIEW AND RECOMMENDATIONS FOR FURTHER DEVELOPMENT

The literature review and the judgment and experience of the researchers support a number of findings:

- Nomographic methods of predicting asphalt cement stiffness are sometimes inaccurate, particularly for asphalts produced from waxy crude sources.
- Current methods for the experimental determination of asphalt cement stiffness at intermediate to low temperatures are, in general, not suitable for routine use in asphalt specifications; some are

inappropriate for accurately measuring low-temperature stiffness, some are very tedious to operate, and others are too expensive.

- An ideal instrument for measuring asphalt stiffness at intermediate to low temperatures would be operable at temperatures from 77 °F to -40 °F (25 °C to -40 °C); it would be capable of measuring stiffnesses as large as 380,000 lb/in^2 (2.6 GPa); it would not apply shear stresses greater than 4.8 lb/in^2 (33 kPa) while measuring stiffnesses less than 13,000 lb/in^2 (90 MPa) and would not apply strains over 0.1 percent in measuring asphalts with larger stiffnesses; repeatability should be less than approximately 7 percent, and reproducibility, less than approximately 15 percent; and cost should be reasonable.

- A primary constraint on the productivity of stiffness-measurement techniques is the time required for the sample to reach equilibrium when changing the test temperature. For optimum performance, the temperature control device should be integrally designed for use with the instrument to provide rapid temperature change and precise control at $\pm$1 °F ($\pm$0.5 °C)

- Instruments currently used for measuring asphalt stiffness use either transient tests (creep tests) or dynamic tests (rapid cyclic loading of the sample). Research indicates that low-temperature cracking is best predicted by using loading times of about 1/2 h; traffic loading times are in the range of 0.1 s. It is believed that short-term creep tests of about 1,000 s duration represent the best compromise between the need for reasonable productivity in performing tests and the duplication of loading rates experienced in the field.

The various testing techniques, several of which can be easily eliminated, are summarized in table 1. The sliding plate microviscometer and the cone and plate viscometer, as previously discussed, cannot be used to measure stiffnesses as large as 380,000 lb/in^2 (2.6 GPa) and are thus unsuitable for use on asphalt cements at very low temperatures. The Schweyer rheometer and other forced capillary flow devices generate unacceptably large shear strains, generate normal stresses when the flow is non-Newtonian, and require unreasonably large stresses and, therefore, must also be eliminated from further consideration. The cantilever beam test, although attractively simple, results in unacceptably high tensile stresses in the test specimen. The Rheometrics mechanical spectrometer, the DuPont dynamic mechanical analyzer, and similar dynamic mechanical testing systems are considered too complex for routine specification use by most highway departments, although the rapidity with which tests can be conducted with these devices may ultimately justify their cost. More important, experienced personnel are

Table 1. Summary of test methods for measuring low-temperature rheology of asphalt cements.

Test Method	Test Mode	Stiffness Data	Viscosity Data	Strength Data	Fracture Parameters	Practical Loading Time, s	Useful Temperature Range, F	lb/in2 (Pa) Minimum	lb/in2 (Pa) Maximum	Unit Cost, $
Glass Capillary Viscometer ASTM D 2170	Viscous Shear Flow	No	Yes	No	No	NA	275	NA	NA	90
Glass Capillary Viscometer ASTM D 2171	Viscous Shear Flow	No	Yes	No	No	NA	140	NA	NA	90
Sliding Plate Microviscometer ASTM D 3570	Viscous Shear Flow	No	Yes	No	No	NA	77 to 140	NA	NA	No longer made
Gaw Sliding Plate Rheometer	Creep, Shear	Yes	No	No	No	1 to 7,200	-40 to 77	0.71 (4.9 KPa)	290,000 (2 GPa)	16,000
Cone and Plate Viscometer ASTM D 3205	Rotational Shear Flow	Yes	Yes	No	No	1 to 7,200	-40 to 140	0.13 (930 Pa)	54,000 (370 MPa)	
Falling Coaxial	Creep, Shear	Yes	Yes	No	No	1 to 7,200	-40 to 77	1 (7 KPa)	300,000 (2 GPa)	1,000
Rheometrics Mechanical Spectrometer	Varies	Yes	Yes	Possible	No	0.001 to 250 s-1	-315 to 621	0.15 (1 KPa)	150,000 (1 GPa)	300,000
DuPont Series 9000 DMA and Other Suppliers	Varies	Yes	Yes	No	No	0.0040 to 0.016 s-1	-200 to 200	7,300 (50 MPa)	3.0 x 107 (200 GPa)	50,000 to 100,000
Fraass Brittle Point Temperature	Fractrure	No	No	No	Limited	NA	-20 to 30	NA	NA	10,000
Ductility ASTM D 113	Ductility	No	No	No	No	0 to 1,200	32 to 77	NA	NA	
Force Ductility	Ductility	No	No	Limited	No	1 to 1,200	32 to 77	NA	NA	
Torsion Bar	Creep, Torsion	Yes	No	Possible	No	1 to 7,200	-40 to 77	17,000 (120 MPa)	2.2 x 107 (150 GPa)	2,000
Cantilever Beam	Creep, Bending	Yes	No	Possible	No	1 to 7,200	-40 to 77	64,000 440 MPa	--	1,000
Bending Beam	Creep, Bending	Yes	No	Possible	No	1 to 7,200	-40 to 77	17,000 (120 MPa)	4.9 x 106 (34 GPa)	1,000

required to operate and interpret the data from these devices, which precludes a positive recommendation for them.

This elimination process leaves four devices for further consideration: the sliding plate rheometer; the torsion bar test; the bending beam test, using either a constant rate of strain, stress relaxation, or constant-stress loading; and the falling coaxial cylinder.

A rating system was devised for each of the four devices to facilitate their comparison. These ratings of 1 (very poor) to 5 (excellent) for each device are shown in table 2. When the ratings were summed, the bending beam in the constant stress (creep) mode emerged as the preferred device, mainly because of the ease with which very low temperature stiffnesses can be measured. Theoretically, the bending beam poses some analytical questions for smaller stiffness values where viscoelastic or viscous behavior predominates. In the region of interest, however, the bending beam is simple in its analysis and is easy for the operator or specification writer to envision.

Although the bending beam device would be unsatisfactory for the higher temperatures where viscous deformation predominates, it is an excellent device for measuring stiffnesses at low temperatures. Although the test as used for plastics is a constant rate-of-strain test, using it in a creep mode on asphalt cement to measure bending stiffness as a function of time provides rheologic characteristics in a more straightforward fashion. The device itself is inexpensive, and sample preparation and testing are not complicated.

For the purposes of this study, it was necessary to measure stiffness at a variety of temperatures. However, when the bending beam test is used as a specification test, the researchers envision measurements made at a single, critical temperature appropriate for the particular agency and the environmental region within that agency. In other words, the test would be employed on a go/no-go basis where, to be acceptable, an asphalt cement must have a stiffness below some maximum value at the specified temperature. The test temperature would be adjusted according to the environmental region within the agency's jurisdiction.

Table 2. Device ratings.

	Device			
Device	Sliding Plate	Torsion Bar	Falling Coaxial Cylinder	Bending Beam (constant stress)
Stiffness Range	3	4	3	3
Fracture Properties	0	0	0	0
Time Range	1	3	1	3
Device Complexity	3	3	4	4
Analysis Complexity	5	3	4	4
Sample Preparation	3	4	4	4
Ease of Use	4	3	5	5
Cost	4	4	4	4
Probability of Successful Development	3	2	3	5
Total Points	26	26	28	32

Rating: 0 = not obtainable; 1 = very poor; 5 = excellent

3. METHODS FOR PREDICTING THERMALLY INDUCED CRACKING

Two distinct mechanisms are now recognized as causing thermal cracking. The first mechanism that was recognized by researchers is typified by a single low-temperature excursion that causes the pavement to shrink to the extent that the thermal shrinkage stresses exceed the tensile strength of the asphalt concrete. The second mechanism to be recognized is called thermal fatigue and results from the accumulated damage caused by stresses associated with repeated thermal cycling. In reality, most thermal cracking is probably caused by a combination of the two mechanisms.

A number of researchers have studied low-temperature shrinkage cracking and have developed analytical and predictive models. Thermal fatigue cracking has received less attention from researchers; however, several models have been developed that account for both types of cracking. The models may be classified according to the analytical approach taken by their developers:

- Concept of limiting stiffness.
- Calculation of limiting stresses or strains.
- Development of statistical regression models.
- Crack development based on fracture mechanics principles.

Thermal cracking models that have been reported in the literature were reviewed to identify the characteristics of each model and their predictive accuracy. The models that were reviewed are described in table 3. Two of the models were to be chosen to predict the cracking potential of the asphalt cements studied as part of this project. This chapter presents a summary of the models and the rationale for using them in the subsequent work.

3.1 LIMITING STIFFNESS

By far the most commonly used approach for predicting thermal cracking in bituminous pavements, and among the first to be used by researchers, is limiting stiffness. This approach is based on the relationship between mixture or asphalt cement stiffness at the minimum service temperature and the incidence of low-temperature cracking. Although this approach may at first

Table 3. Summary of input and output data for low-temperature cracking models.

Properties	Hajek-Haas	TC-1	COLD	THERM	Ruth	Hills
INPUTS:						
Stiffness of Original Asphalt vs. Temperature (Loading Time = 20,000 s using McLeod's version of Van der Poel's nomograph)	X					
Asphalt Stiffness vs. Temperature, Van der Poel's nomograph as modified by Heukelom and Klomp						
Loading Time = 20,000 s		X				
Loading Time = 7,200 s		X	X			
Static Compression Modulus of Mixture vs. Mix Viscosity					X	
Asphalt Specific Gravity		X			X	
Original Penetration at 77 °F (25 °C)	X	X	X	X		X
Original Penetration at 41 °F (25 °C)						X
Original Softening Point of the Asphalt, °F		X		X		
Thin Film Oven Test, Weight Loss and Retained Penetration		X				
Volumetric Concentration of the Aggregate	X	X		X		
Penetration Index: Penetration at 77 °F (25 °C) and Kinematic Viscosity at 275 °F (135 °C)	X	X		X		
Absolute Viscosity vs. Temperature (Schweyer rheometer)					X	
Indirect Tensile Strength vs. Temperature (0.01 in/min) (0.25 mm/min)		X	X			
Linear Thermal Coefficient of Expansion/Contraction			X		X	
Thermal Coefficient of Expansion/ Contraction vs. Temperature		X				

Table 3. Summary of input and output data for low-temperature cracking models (continued).

Properties	Hajek-Haas	TC-1	COLD	THERM	Ruth	Hills
Thermal Fatigue Constants		X				
Surface Absorptivity		X	X	X		
Mix Conductivity		X	X	X		
Mix Specific Heat		X	X	X		
Mix Density		X	X	X		
Emissivity			X			
Connection Coefficient			X			
Age	X	X		X		
Thickness	X	X	X	X	X	
Winter Design Temperature	X					
Moisture Content			X			
Wind Velocity		X		X		
Average Temperature		X		X		
Yearly Temperature Range		X		X		
Daily Temperature Range (Cooling Rate)		X		X	X	
Solar Radiation		X	X	X		
Subgrade Type	X					
OUTPUTS:						
Cracking Index with Time	X			X		
Area Cracking with Time		X				
Critical Temperature at which Cracking Occurs			X		X	X

appear to be largely empirical, the demonstrated relationship between asphalt cement stiffness and tensile strength suggests a theoretical basis for the concept of limiting stiffness.[2] In practice, the method of limiting stiffness involves several steps:

- Determination of the minimum, or critical, pavement service temperature.
- Determination of the binder or pavement stiffness at that temperature, either by experimental methods or by estimating mixture stiffness with a method such as that of Bonnaure and others.[34]
- Comparison of the measured or estimated stiffness with a critical or limiting value, which, if exceeded, will cause pavement cracking.

Gaw and others suggested a limiting mixture stiffness of 2.6×10^6 lb/in^2 (18 GPa) at 30 min loading time.[35] Suggested values for the limiting stiffness of asphalt cement range from 20,000 lb/in^2 (140 MPa) at a loading time of 2.8 h to 145,000 lb/in^2 (1 GPa) at 30 min.[36,37] The latter value is suggested by the Asphalt Institute in a comprehensive report on designing asphalt concrete pavements to resist low-temperature cracking.[37]

The limiting stiffness approach may be applied to the asphalt cement, in which case the mix variables such as voids, percent asphalt content, and maximum aggregate size are neglected. When the limiting stiffness approach is applied to the asphalt mixture, the values of stiffness are generally not measured but predicted from a procedure such as that of Bonnaure.[34] The limiting stiffness method predicts the minimum temperature below which cracking can be expected. It does not predict the extent of cracking or the time to cracking, which are needed to estimate the serviceability of a pavement.

3.2 INCREMENTAL STRESS/STRAIN CALCULATION

Various computer models use the calculation of incremental stress or strain to predict thermal cracking in asphalt concrete pavements. These include the Shahin-McCullough model (Program TC-1), Program COLD, and the Ruth model.[38,39,40] Although the primary feature of these programs is the

incremental calculation of stress or strain in the pavement, all include various submodels for predicting pavement temperature, fatigue effects, extent of cracking, and so forth.

Hills and Brien Model

Hills and Brien proposed that low-temperature cracking can be predicted through the incremental calculation of thermal shrinkage stresses in the pavement.[41] In this method, the pavement is assumed to be free of thermal stresses above 32 °F (0 °C); the stiffness of the asphalt cement at this temperature is estimated from Van der Poel's nomograph; and a cooling rate of 18 °F (10 °C) per hour is generally assumed. The thermal strain in the asphalt cement is calculated, for each temperature increment, by multiplying an assumed linear coefficient of thermal expansion of 1.1×10^{-4}/°F (2×10^{-4}/°C) by the change in temperature, which is generally 9 °F (5 °C). The stress in the asphalt cement at this temperature level can then be calculated by multiplying the asphalt stiffness by the thermal strain. This stress is compared with typical tensile strength-stiffness data for asphalt cement, such as that presented by Heukelom.[2] The stresses are summed for each temperature increment, and the calculation proceeds to successively lower temperatures until the stress calculated exceeds the tensile strength. According to this method, failure by thermal cracking is probable at this temperature. This method of calculation assumes that asphalt concrete behaves elastically--a major shortcoming of this type of analysis because, although at very low temperatures this assumption may be reasonable, at intermediate temperatures, asphalt cement and asphalt concrete behave viscoelastically.

In the Hills and Brien procedure, measurements of the penetration of the asphalt cement made at 41 °F (5 °C) and 77 °F (25 °C) are used to calculate a penetration index (PI) for the asphalt cement and, by extrapolation, the temperature at which the penetration would be 800. Therefore, the critical temperature found by the incremental stress calculations can be expressed as a singular function of penetration at the two test temperatures. A nomograph can thus be constructed for predicting the critical temperature of asphalt cement from the penetration at these two test temperatures.[37] This procedure neglects the stress relaxation which occurs during the cooling

cycle; assumes that the behavior of the asphalt cement is linear-elastic; and assumes that the strain in the asphalt cement is the same as in the hot-mix asphalt concrete. The method is suspect because of these assumptions; however, it provides a rapid method for estimating the probability of thermal cracking. Another, serious disadvantage of this method is that it predicts only a critical cracking stiffness; it does not predict the extent of cracking or the time to cracking.

Shahin-McCullough Model, TC-1

The Shahin-McCullough model, TC-1, is based on a probabilistic empirical/mechanistic computer program that computes the extent of thermal cracking as a function of time.[38] The main program contains four submodels that are described briefly below.

The pavement temperature model, an improved version of the model developed by Barber, is used to predict an hourly pavement temperature as a function of air temperature, wind velocity, solar radiation, asphalt concrete thermal properties, and depth below the pavement surface.[42]

The thermal stress model is used to calculate the thermal stresses and strains in the asphalt mixture as a function of its stiffness and changes in pavement temperature. This model, in turn, consists of four interacting submodels for predicting aging asphalt, asphalt stiffness, asphalt concrete stiffness, and thermal stresses and strains.

The low-temperature cracking model is used to predict the percentage of the pavement surface that is cracked at any time, t. Probabilistic methods are used to predict whether the thermal stresses exceed the mixture strength. Both the thermal stress and mixture strength are assumed to be random variables and are defined in terms of their means and standard deviations.

The thermal fatigue cracking model adds the effect of thermal fatigue caused by daily temperature cycling to the effect of low-temperature cracking. The model grew out of the realization that thermal cracking of asphalt

concrete pavements occurs in the milder climatic zones of the United States as well as in the northern zones having much lower temperatures.

For calculating thermal stresses and strains, the bitumen and asphalt concrete mixture stiffnesses are determined using the relationship developed by Van der Poel and later modified by Heukelom and Klomp.[21,43] The model assumes that the surface layer is fully restrained; the surface behaves as an infinite beam; the thermal stresses, at the end of each daily temperature cycle, are negligible; and the maximum thermal stress occurs at the minimum daily pavement temperature. Thermal stresses, calculated over the range of temperatures used as input to the program, are then compared with a tensile strength versus temperature relationship that is input to the program. However, no test procedure for measuring this tensile strength is recommended in the TC-1 documentation.

To account for the variability of the properties of the hot-mix asphalt concrete, it is assumed that both the stress and tensile strength are normally distributed random variables. The probability of an occurrence of thermal cracking is defined as the probability that the thermal stress will exceed the tensile strength at any point in the mixture.

As stated above, the primary program incorporates aging equations (one for penetration and the other for the softening point) in an attempt to predict the aging characteristics of asphalt cement. These equations were obtained by applying stepwise regression to data collected in California, Delaware, Utah, and Pennsylvania. They predict the penetration, and softening point, as a function of service time and have a coefficient of determination, R^2, of 0.85 and 0.87, respectively. These equations are given below:

$$\begin{aligned} Pen_{77}(t) = {} & -48.3 - 2.56\sqrt{t} + 0.144\ Pen_{77}(0) \\ & - (8.47\ V_{AV}(0))(1/t+1) + 1.36\ P_{TFOT} \\ & + 0.923\ V_{AV}(0)\ (1/t+1) \end{aligned} \tag{11}$$

and

$$T_{R\&B}(t) = -4.63 + 3.16\sqrt{t} + 1.59\ T_{R\&B}\ (0) - 0.93\ P_{TFOT}$$

where

$Pen_{77}(t)$ = penetration at some pavement age, t, 0.1 mm, 77 °F (25 °C), 100 g, 5 s

t = pavement age, years

$Pen_{77}(0)$ = original penetration, 0.1 mm, 77 °F (25 °C), 100 g, 5 s

$V_{AV}(0)$ = initial volume percentage air voids, preferably after placement and initial compaction

P_{TFOT} = ratio formed by dividing penetration measured at 77 °F (25 °C) after TFOT exposure by original penetration

$T_{R\&B}(t)$ = ring and ball softening point temperature at some pavement age, t, °F

$T_{R\&B}(0)$ = ring and ball softening point temperature of original asphalt, °F

These equations were based on asphalt extracted from cores recovered from pavements that varied in age from 1 to 100 months.

In observations made in the field and reported in the literature, the spacing between transverse cracks varied from 5 ft (1.5 m) to several hundred feet (more than 30 m). Using these observations, it was assumed that, when the spacing decreases to 5 ft (1.5 m), the pavement is no longer restrained and is insensitive to further cracking. Therefore, Shahin assumed that a 5-ft (1.5-m) spacing of transverse cracks was equal to 100-percent cracking, which corresponds to a cracking index of 100 cracks per 500 ft (152 m).[38] Considering only full transverse cracks, figure 13 compares four methods of reporting cracking data:

- Cracking length, ft/1000 ft (m/1000 m).
- Cracking index, I, number of full-width transverse cracks per 500 ft (152 m) of roadway.
- Spacing of full-width cracks, ft (m).
- Percentage of area cracked, percent.

The TC-1 program was used to predict low-temperature cracking observed on the Ontario and Saint Anne test roads in Canada.[38] Initial comparisons of predicted to observed data indicated that the models gave a reasonable

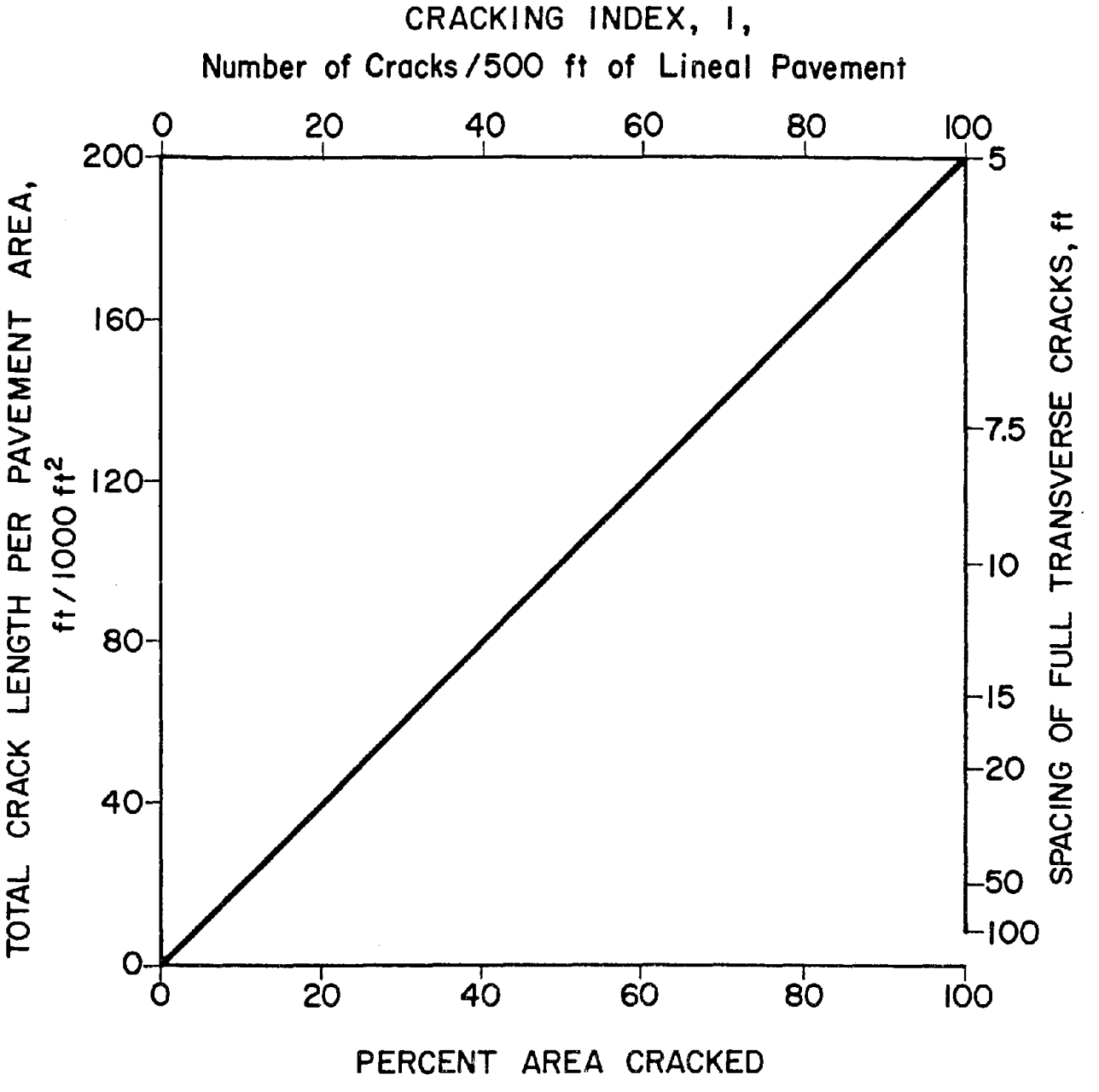

Figure 13. Relationship between different methods of defining pavement cracking.

prediction. Correlations to observed data were also made in the Cost Allocation Study, and results from this study are shown in table 4.[44] The correlation between the observed and predicted cracking indices, I, are poor. In particular, the model grossly overpredicted the cracking index in seven of the pavements, where six of the predicted indices were 60 or larger and the observed indices ranged from 0.0 to 1.9. Linear regression of the predicted cracking on the observed cracking gave an R^2 of 0.0, verifying the lack of agreement between observed and predicted cracking. This overprediction illustrates the need for reliable material and temperature data and the danger of extrapolating a model from the conditions for which it was developed to a new set of conditions.

Program COLD

Program COLD is a sophisticated model that estimates the temperature and resulting thermal stresses in the pavement and the time at which low-temperature cracking is likely to occur.[39] The first part of the program is used to calculate temperatures in the pavement at 1/8-h increments for each day. The model is based on thermodynamic principles that account for the rate of heat transfer through a solid medium. The second part of the model calculates the thermal stresses caused by temperature differentials calculated from the first part of the program. The thermally induced stresses are calculated using a pseudoelastic beam analysis similar to the one used in the Shahin-McCullough TC-1 program. A strength/temperature relationship for the hot-mix asphalt is a required input to the program and is compared with the thermally induced stresses at 2-h intervals. The program predicts the expected time at which low-temperature cracking will occur, but does not directly compute a cracking index or the amount of cracking, as does the TC-1 program.

The materials inputs for the COLD program include the absorptivity, emissivity, and convection coefficient of the surface; thermal conductivity of the asphalt mixtures (both unfrozen and frozen); dry density and moisture content of the asphalt mixtures; thicknesses of the layers; and both creep modulus and tensile strength of the asphalt mixture as functions of temperature. The creep modulus versus temperature relationship can be

Table 4. Comparison of predicted versus observed cracking, TC-1 model, Michigan data.[44]

Site Number	Pavement Age, years	Cracking Index, Number of Cracks per 500 ft (152 m) of Pavement Length	
		Observed	Calculated
1	5	0.7	7.4
2	6	3.3	12.6
3	4	0.0	0.4
4	4	0.1	1.2
7	3	0.0	6.8
8	6	0.1	32.8
9	4	1.0	0.2
10	6	0.3	2.6
11	2	0.0	0.0
12	1	0.0	0.0
13	6	0.4	0.0
14	4	3.4	4.1
15	9	1.0	85.7
16	5	0.0	3.6
17	8	0.0	84.6
18	5	0.0	3.6
19	2	0.0	0.1
20	8	1.9	82.0
21	9	0.0	92.2
22	9	0.0	90.4
29	9	0.2	63.9

estimated using Van der Poel's nomograph as modified by Heukelom and Klomp.[43] Although any time of loading can be used with the nomograph, 7,200 s was recommended by the authors.[39] The tensile strength can be obtained with either the diametral tension or the uniaxial tension test. The loading rate suggested in the program documentation is 0.01 in/min (4.23 μm/s).[39] Unlike the Shahin-McCullough TC-1 model, the thermal coefficient of expansion used in COLD is assumed independent of temperature or stiffness.

The results predicted by the COLD program were compared with field observations made in Canada, including those from the Saint Anne Test Road and a test road in Edmonton. Efforts in a previous study to verify the COLD subsystems were unsuccessful because of a lack of materials and environmental information for the test sections. The same lack of information was a problem when attempts were made to verify the TC-1 program.[44]

Ruth Model

Based on work conducted in Florida, Ruth and associates developed procedures for predicting thermally and load-induced pavement cracking.[45] Low-temperature asphalt viscosity measurements are used in Ruth's model to estimate various strength and failure parameters for the asphalt concrete mixtures. These parameters are then used to compute thermal and load-induced stresses and strains, which are then used to predict relative cracking potential.

Either the temperature/viscosity relationship developed from constant-power asphalt viscosity data for three or more temperatures or the actual temperature/viscosity measurements can be used as input to the program. A pavement cooling rate curve and a minimum pavement temperature typical of the temperatures at the site are calculated. Incremental creep strains are then computed at 15- to 30-min increments using the stress and calculated viscosity of the mix. The absolute viscosity of the asphalt cement is measured with the Cannon constant stress rheometer (Schweyer rheometer). The incremental strain values are accumulated to obtain the total creep strain. Total elastic strain is computed by a summation of incremental elastic

strains, which are calculated from incremental contraction and incremental creep strains.

The computer program output lists all of the computed parameters, including stresses and strains, according to time and temperature. Failure criteria are applied to the appropriate output parameters to identify the failure (critical) temperature or the maximum stress, strain, or strain energy attained. Subroutines are included in the thermal analysis program to calculate the critical temperature and limiting stiffness criteria. The stiffness values at a loading time of 20,000 s obtained for the materials at the Saint Anne Test Road were used by Ruth in the development of the model.[45]

This model is unique in that the viscosity and complex flow measured by the Schweyer rheometer are used to determine the stiffness of the asphalt mix. Application of the model has been confined to its development, and its validity has not been examined by others. Because it does not account for thermal fatigue and it was not possible to verify the model, it was not used in this study.

3.3 STATISTICAL MODELS

Statistical models also have been developed as predictors of the occurrence and extent of thermal cracking. Both studies discussed below were completed in the early 1970's using observations of pavements in Ontario, Canada, as a database.

The Hajek and Haas statistical model requires values of asphalt stiffness (predicted from a nomograph), pavement thickness, pavement age, subgrade type, and a winter design temperature.[46,47] Thirty-two observations were used by Hajek and Haas to develop their regression model, including seven observations used to verify the model. The reported coefficient of determination, R^2, for the regression equation was 0.82 in the following prediction of the cracking index, I:[46]

$$I = 30.3974 - 2.1516D + 1.24958M + (6.7966 - 0.8740t + 1.3388A) \log S_B(0) + .06026\, S_B(0) \log D \quad (12)$$

where

I = cracking index, number of transverse cracks per 500 ft (152 m) of roadway

D = indicator variable for subgrade type, unitless: clay, D = 2; loam, D = 3; sand, D = 5

M = winter design temperature, °C, defined as the temperature below which only 1 percent of the hourly temperatures occur during the coldest January for a 10-year period

A = age of pavement, years

t = thickness of asphalt concrete surface layer, in

$S_B(0)$= stiffness of the original bitumen at 20,000 s loading time and at the winter design temperature, kg/m^2

The bitumen stiffness used in this model is calculated using McLeod's suggested modification of Heukelom and Klomp's version of Van Der Poel's nomograph.[48,43] To use the nomograph, the penetration at 77 °F (25 °C) and kinematic viscosity at 275 °F (135 °C) (or penetration at 77 °F (25 °C) and ring and ball softening point temperature) must be measured for each asphalt cement.

The Hajek-Haas model was used to predict the cracking index for 32 sections of pavement in Michigan.[44] The observed and predicted cracking indices, I, are shown in table 5. Linear regression of the predicted versus the observed cracking gave an R^2 of 0.31. This agreement between the observed and predicted values is poor, demonstrating the same problem shown with the TC-1 model--the models are inaccurate when they are used for conditions other than those for which they were developed. Data collected from six sites in Texas were also used with the Hajek-Haas model, and these results are shown in table 6. Once again, the predicted values showed poor agreement with the observed values, explainable, in part, because the primary mode of thermal cracking in West Texas is thermal fatigue, whereas the primary mode of

Table 5. Comparison of predicted versus observed cracking, Hajek-Haas model, Michigan data.[44]

Site Number	Stiffness of Bitumen, kg/m^2	Winter Design Temp., °C	Pavement Thickness, in	Pavement Age, Years	Subgrade Variable	Cracking Index, I, Number/500 ft	
						Observed	Calculated
1	40.0	-20.0	2.1	5.0	5.0	0.7	3.3
2	35.0	-20.0	2.5	6.0	5.0	3.3	3.0
3	27.0	-20.0	2.5	4.0	5.0	0.0	0.0
4	27.0	-20.0	2.5	4.0	5.0	0.1	0.1
7	5.0	-22.0	3.3	3.0	5.0	0.0	0.0
8	50.0	-25.0	2.5	6.0	5.0	0.1	0.0
9	8.0	-25.0	2.5	4.0	5.0	1.0	0.0
10	5.0	-25.0	2.5	6.0	5.0	0.3	0.0
11	45.0	-30.0	2.5	2.0	5.0	0.0	0.0
12	30.0	-25.0	2.5	1.0	5.0	0.0	0.0
13	25.0	-30.0	2.5	6.0	5.0	0.4	0.0
14	45.0	-25.0	2.8	4.0	5.0	3.4	0.0
15	60.0	-25.0	3.3	9.0	5.0	1.0	3.3
16	3.0	-22.0	2.5	5.0	5.0	0.0	0.0
17	30.0	-22.0	2.5	5.0	5.0	0.0	0.7
18	3.0	-22.0	2.5	5.0	5.0	0.0	0.0
19	10.0	-22.0	2.5	2.0	5.0	0.0	0.0
20	40.0	-22.0	2.5	8.0	5.0	1.9	3.1
21	10.0	-22.0	2.5	9.0	5.0	0.0	0.0
22	7.0	-22.0	2.5	9.0	5.0	0.0	0.0
23	200.0	-22.0	4.5	11.0	5.0	2.6	23.5
24	300.0	-22.0	4.5	12.0	5.0	5.4	32.7
25	100.0	-20.0	4.5	11.0	5.0	1.0	16.5
26	100.0	-20.0	4.5	11.0	5.0	3.1	16.5
27	100.0	-20.0	4.5	12.0	5.0	1.5	17.8
28	100.0	-20.0	4.5	12.0	5.0	10.7	17.8
29	75.0	-20.0	4.5	9.0	5.0	0.2	10.9
30	160.0	-22.0	4.5	12.0	5.0	10.4	21.7
31	120.0	-22.0	4.5	12.0	5.0	21.2	17.6
32	120.0	-22.0	4.5	12.0	5.0	20.3	17.6
33	120.0	-22.0	4.5	12.0	5.0	12.5	17.6
34	110.0	-22.0	4.5	11.0	5.0	0.2	15.1

Table 6. Comparison of predicted versus observed cracking, Hajek-Haas model, Texas data.[44]

Site Number	Stiffness of Bitumen, kg/m^2	Winter Design Temp., °C	Pavement Thickness, in	Pavement Age, years	Subgrade Variable	Cracking Index, I, Number/500 ft	
						Observed	Calculated
26	9.0	-10.0	1.1	6.5	2.0	50.0	13.19
28	4.0	-10.0	2.0	7.0	2.0	0.0	7.9
36	22.0	-17.0	1.5	6.5	5.0	23.5	4.3
38	75.0	-26.0	1.7	10.0	3.0	0.0	10.0
40	7.5	-14.0	2.4	9.0	2.0	35.0	6.6
41	2.0	-10.0	1.5	9.0	2.0	0.0	1.4

cracking in the northern United States and Canada is the result of shrinkage stresses associated with a single low-temperature excursion.

Fromm and Phang also developed a statistical model to predict low-temperature cracking using 33 observations of Ontario roads as a database.[49] They used a stepwise regression procedure to develop several different models applicable to different climatic regions in Ontario. Thirty-two parameters were used as possible predictors in this stepwise procedure, with the final general model resulting in nine predictor variables, the most significant of which were freezing index, viscosity ratio, critical temperature, and pavement voids. The freezing index is the cumulative number of degree-days below 32 °F (0 °C). The viscosity ratio is the viscosity at 140 °F (60 °C) divided by the viscosity at 275 °F (135 °C). The critical temperature was defined as that at which the viscous flow observed in the asphalt concrete under a 44-lb/in^2 (310-kPa) tensile stress equals the shrinkage during a 10.0 °F (5.5 °C) drop in temperature. Viscous flow was measured by loading a 1.5-in by 1.5-in by 8-in (38-mm by 38-mm by 220-mm) asphalt concrete beam in direct tension under a 100-lb (440-N) load. The coefficient of thermal expansion was also measured experimentally on 2-in by 2-in by 11.3-in (51-mm by 51-mm by 287-mm) asphalt concrete beams. The value of R^2 for this model was 0.64, suggesting a need for improvements, before the model can be used for design purposes.

3.4 FRACTURE MECHANICS MODELS

None of the models discussed previously in this chapter provided an acceptable prediction of low-temperature shrinkage cracking or thermal fatigue cracking. Either these models must be improved or alternative models must be developed. One of the more promising, from a theoretical standpoint, is the fracture mechanics model. A short review of fracture mechanics is warranted before this model is presented.

Fracture mechanics theory provides a rational explanation for the strength of a wide range of materials. In this theory, the strength of a material is related to the existence of flaws and the stress concentration at the tips of these flaws. As the load applied to a material containing flaws increases, the stresses around the flaws reach a limiting value, and fracture

becomes possible. The fracture mechanics approach to failure analysis leads to the determination of fracture toughness, a fundamental, or characteristic, material property.

Linear elastic fracture mechanics (LEFM) is based on the Griffith failure hypothesis and is applicable to brittle materials. According to Griffith, brittle materials have microscopic flaws (or cracks) that are distributed randomly throughout their volume. Griffith's theory further states that the most critical crack (the flaw with the greatest stress concentration at its tip) will grow only when the elastic energy that is released during crack growth exceeds the energy of the newly created surface area, figure 14. Therefore, crack growth will occur when:[50]

$$\sigma_c \sqrt{a_c} = (2E\gamma_e/\pi)^{1/2} \tag{13}$$

where

σ_c = remote critical stress, lb/in^2 (Pa)

a_c = critical crack length, in (mm)

E = elastic modulus, lb/in^2 (Pa)

γ_e = elastic surface energy per unit area, $lb\text{-}in/in^2$ (J/m^2)

Equation 13 indicates that a crack extension in brittle materials occurs when the product on either side of equation 13 attains a critical value. This equation was modified by Irwin for a material displaying plastic deformation:[51]

$$\sigma_c \sqrt{a_c} = [2E (\gamma_e + \gamma_p)/\pi]^{1/2} \tag{14}$$

where

σ_c = remote critical stress, lb/in^2 (Pa)

a_c = critical crack length, in (mm)

E = elastic modulus, lb/in^2 (Pa)

γ_e = elastic surface energy per unit area, $lb\text{-}in/in^2$ (J/m^2)

γ_p = plastic surface energy per unit area, $lb\text{-}in/in^2$ (J/m^2)

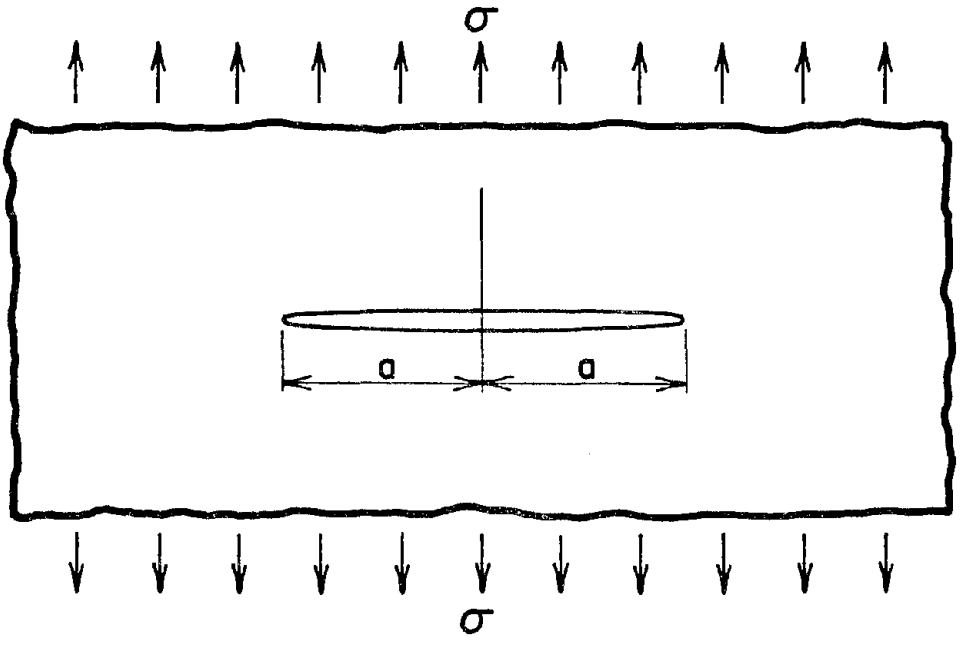

Figure 14. Illustration of flow or crack according to Griffith theory.

According to fracture mechanics theory, the variable that governs fracture is the critical stress intensity factor, K_c, given by:

$$K_c = \sigma_c \sqrt{\pi a_c} \cdot f\ (a_o/d) \qquad (15)$$

where

K_c = critical stress intensity factor for plane stress, $lb/in^2\text{-}\sqrt{in}$ (Pa-$\sqrt{m}$)

σ_c = remote critical stress, lb/in^2 (Pa)

a_c = critical crack length, in (mm)

$f(a_o/d)$ = dimensionless variable that depends on the geometry of the specimen and crack length

a_o = initial crack length, in (mm)

d = depth of beam, in (mm)

K_c is the maximum allowable stress intensity factor; it cannot be exceeded, and when it is equaled, catastropic failure will occur. The remote stress, σ_c, is the stress in the body at a distance removed from the crack equal to 10 times the size of the crack.

The maximum constraint of the crack occurs with plane strain. For the special conditions where plane strain exists and the opening mode of crack extension is present, K_c becomes, by definition, K_{1c}.

The value of K_{1c} at a particular temperature depends on specimen thickness and constraint. With increasing specimen thickness, the value of K_c approaches K_{1c}. Therefore, K_{1c} is a fundamental material property characterizing crack resistance and is therefore called the plane strain fracture toughness. Thus, in principle, the same value of K_{1c} should be found by testing specimens with different geometries and with different critical combinations of crack size and shape.

The fracture toughness for a material that is brittle in nature and has very little crack-tip plasticity is obtained by using linear elastic fracture

mechanics (LEFM) theory and a test procedure such as the compliance method, crack opening displacement (COD) method, or R-curve method.[52,53,54]

During the last 2 decades, attempts were made to characterize the fracture properties of asphalt systems by applying fracture mechanics principles. Some of the research studies on this topic were conducted by Moavenzadeh, Herrin and Bahgat, and Majidzadeh and others.[55-58] Lytton applied fracture mechanics concepts to develop a computer model for predicting thermal crack initiation.[59]

3.5 DEVELOPMENT OF THE LYTTON MODEL

Lytton's model, called THERM, predicts the amount of cracking, as well as the time of crack initiation.[59] Non-load-associated pavement cracking is assumed to result from the thermal fatigue mode of failure, rather than low-temperature tensile strength failure. A total of 576 runs of the computer model for four sites in Michigan and four sites in northern Texas provided data for the development of the necessary regression equations in the model. A pavement design procedure was also developed on the basis of the model.

Thermal fatigue is defined in the THERM program as fatigue caused by thermal cycling occurring below 75 °F (25 °C), which was assumed by Lytton to be a general lower bound for the stress-free temperature (a temperature at which the residual stresses resulting from thermal shrinkage are minimal or nonexistent). Shahin and McCullough's revisions of Barber's equations were used to compute pavement temperatures using the air temperature, wind speed, and solar radiation.[38,42] The temperatures thus determined were used in a fracture mechanics-based model for predicting the thermal fatigue cracking frequency. The thermal fatigue cracking model assumes that:

- Asphalt concrete is a linear, elastic, and homogenous material.
- The Paris-Erdogan fatigue law developed to explain metal fatigue also holds for asphalt concrete fatigue.[60]
- The pavement is assumed to have failed when the crack depth equals the thickness of the pavement.

- Asphalt concrete reaches a glassy state whenever the modulus of elasticity is greater than 100,000 lb/in^2 (690 MPa). This assumption may be in error given the delayed elastic response exhibited by most asphalt concrete specimens with stiffness values in this range.

The Paris-Erdogan fatigue law is given as:[60]

$$\frac{da}{dN} = A(\Delta K)^n \tag{16}$$

where

da = change in crack length, in (mm)

dN = change in number of load (thermal) cycles

A,n = fatigue crack propagation parameters

ΔK = change in stress intensity factor at the crack tip during one (thermal) cycle, lb/in^2-$\sqrt{\text{in}}$ (Pa $\sqrt{\text{m}}$)

An integrated form of equation 16 can be related theoretically to the number of thermal cycles required to cause failure:

$$N_f = \int_{a_o}^{a_c} \frac{da}{A(\Delta K)^n} \tag{17}$$

N_f = number of cycles to failure

a_o = initial crack length, in (mm)

a_c = critical crack length, in (mm)

da = change in crack length, in (mm)

A,n = fatigue crack propagation parameters

In equation 16, if A, ΔK, and n are known, then da can be found by rewriting equation 16:

$$da = A(\Delta K)^n dN \tag{18}$$

To apply equations 16 through 18, the stress intensity factor, K, and the fatigue parameters, A and n, must be determined experimentally. In equations 16 through 18, ΔK is the difference between two values of K computed at the

maximum and minimum stress levels. The stress levels may be imposed by mechanical or thermal loading.

The stress intensity factor at the crack tip for plane strain, K_1, has been expressed by Lytton through the empirical expression:

$$K_1 = a_1(a)^{b_1} \tag{19}$$

where a_1 and b_1 are empirically derived parameters and a is the crack length. The coefficients a_1 and b_1 can be empirically derived as a function of:[59]

- Stiffness of the asphalt concrete mix, $S_m(T,t)$, lb/in^2 (Pa).
- T_r, the difference between the air temperature and the stress-free mix temperature, 75 °F (24 °C).
- Thickness, t, of asphalt concrete, in (mm).

To determine K_1, a finite element computer program was developed by Chang, Lytton, and Carpenter.[61] With this program, K_1 can be computed at the crack tip using equation 19. As represented in figure 15, the crack is assumed to be in a transverse direction. The spacing of these transverse cracks usually ranges from 5 ft to several hundreds of feet.[38] To eliminate boundary effects, the influence of the crack was assumed to be within 45 in (1.14 m) of the crack in either direction. K_1 values were determined for 10,000 lb/in^2 (69 MPa) and 100,000 lb/in^2 (690 MPa) and T_r values of 50, 100, and 150 °F (10, 38, and 66 °C). Corrected values of K_1 were then calculated by Lytton by multiplying the values of K_1 obtained from equation 19 by Barenblatt's correction factor, C_k:[62]

$$C_k = (8/\pi)^{1/2} \sigma_t (z)^{1/2} \tag{20}$$

where

C_k = Barenblatt's correction factor

σ_t = tensile strength, lb/in^2 (Pa)

z = distance between crack tip and the first node of the finite element mesh in the crack-tip region[62]

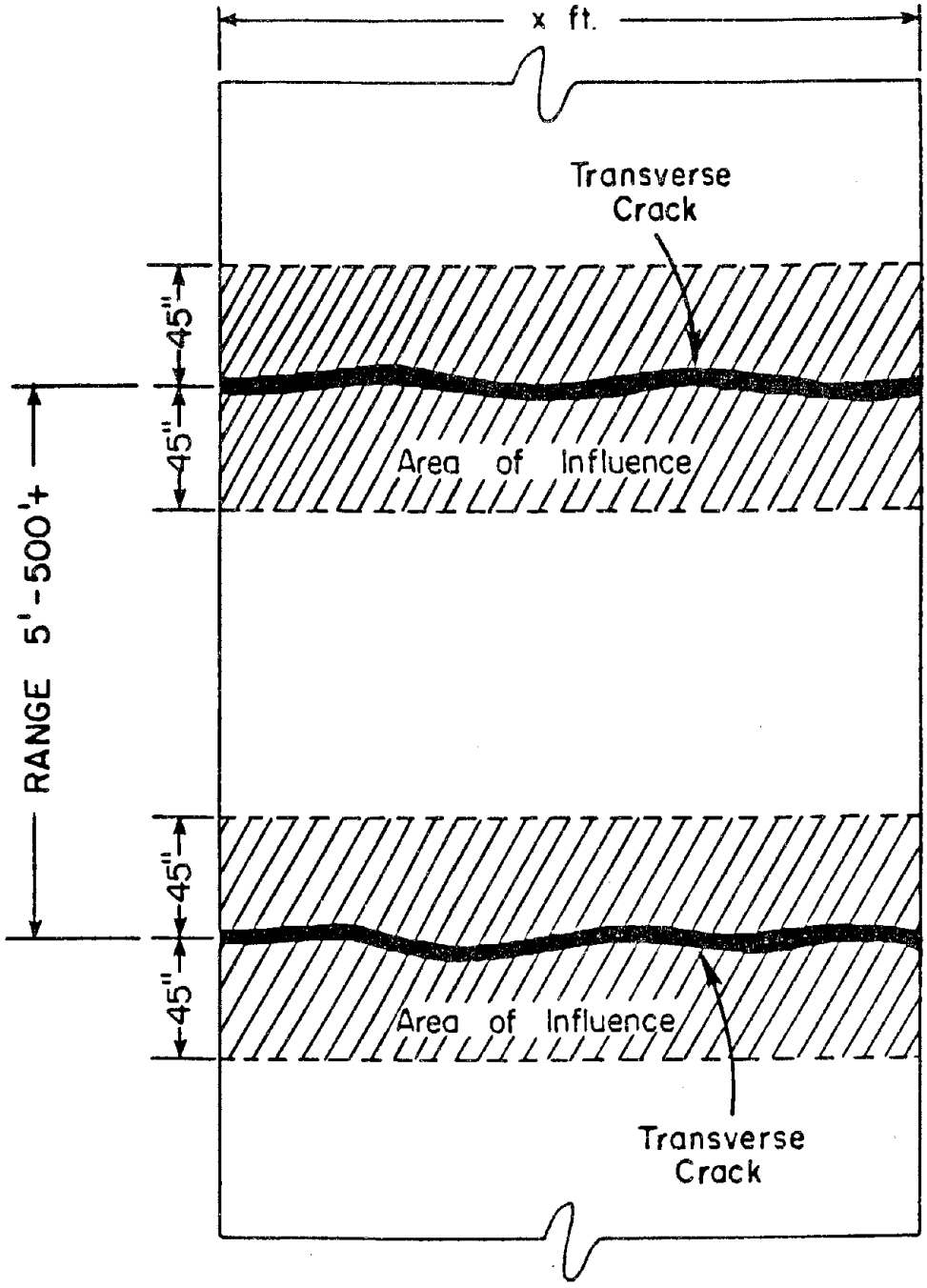

Figure 15. Plan view of pavement illustrating area of influence of transverse cracks.

To determine the constants a_1 and b_1, in equation 19, K_c values for the critical case at particular values of $S_m(T,t)$, T_r, and pavement thickness, t, were plotted against critical crack length, a_c, on log-log graph paper. From these plots, values of a_1 and b_1 were obtained by linear regression analysis. It was found that a_1 and b_1 varied with T_r, the difference between the daily air temperature range and the stress-free temperature. Therefore, a_1 and b_1 were plotted versus T_r and the following relationships were determined:

$$a_1 = (T_r - m_1)\, m_2 \tag{21}$$

and

$$b_1 = m_3 + m_4 T_r \tag{22}$$

where m_1, m_2, m_3, and m_4 are regression coefficients. These values were found to change with the modulus of elasticity, E, and pavement thickness, t; i.e.:

$$m_1,\ m_2,\ m_3,\ m_4 = f(E,\ t) \tag{23}$$

The following relationships, determined through regression analysis, were reported by Lytton:[59]

$$m_1 = 8.8988 + (29.1063 - t)(1.3573 - 0.01357(E/1000))$$
$$10{,}000 < E < 100{,}000 \text{ psi}$$
$$0.0 < t < 29.1063 \text{ in}$$

$$m_2 = 2.0599 - (129.3215 - t)(0.01687 - 0.000169(E/1000))$$
$$10{,}000 < E < 100{,}000 \text{ psi}$$
$$0.0 < t < 129.3215 \text{ in}$$

$$m_3 = 0.8481 + (2.7811 - t)(0.002738(E/1000))$$
$$10{,}000 < E < 100{,}000 \text{ psi}$$
$$0.0 < t < 4.0 \text{ in}$$

$$m_3 = 0.8481 - (6.5835 - t)(0.12912 - 0.0012919(E/1000))$$
$$t > 4.0 \text{ inches}$$

$$m_4 = -0.00157 + (5.0472 - t)(0.001129 - 0.00001129(E/1000))$$

In brief, the equation for the critical thermal stress intensity factor for particular values of E and t is (equation 19 from the critical condition):

$$K_c = a_1(a_c)^{b_1} \tag{24}$$

and

$$a_1 = (T_r - m_1)m_2 \tag{25}$$

$$b_1 = m_3 + m_4T_r \tag{26}$$

Therefore,

$$K_c = (T_r - m_1)m_2(a_c)^{(m_3 + m_4T_r)} \tag{27}$$

where the parameters and variables are as defined above.

The fatigue crack propagation parameters A and n in equation 16 were calculated based on work by Schapery and by Germann and Lytton.[63,64] Although these parameters can be determined experimentally, such experimental data are generally not available to the designer. Therefore, no attempt was made to accommodate measured values of these parameters in the program. Instead, the values of A and n in the model were determined as follows:

1. The asphalt stiffness was calculated using Van der Poel's nomograph as computerized by de Bats.[21,65]

2. Given the stiffness of the asphalt cement, the stiffness of the asphalt mix was calculated for various loading times, producing a relaxation modulus curve.

3. Schapery has shown that the slope, m, of the relaxation master curve plotted versus the $\log_{10}$ time and with a reference temperature of 77 °F (25 °C) can be related to n as follows:[63]

$$n = 2(1 + 1/m) \tag{28}$$

where n is the fatigue parameter of equation 16, which Germann and Lytton used in an attempt to verify Schapery's equation in the laboratory.[64] They found that the values of n calculated from Schapery's equation must be divided by 2.5 in order for the calculated values to agree with laboratory observations; therefore:

$$n = 0.8\ (1 + 1/m) \tag{29}$$

4. The value of the fatigue parameter, A, in equation 16, was found by substituting into the following relationship:

$$n = -0.69 - 0.511\ \log_{10}A \tag{30}$$

which is a relationship obtained experimentally by studying the crack propagation of asphalt concrete.[64]

3.6 DESCRIPTION OF PROGRAM THERM

Program THERM, which is the main part of Lytton's thermal cracking model, assumes that the asphalt concrete is a viscoelastic material and the stiffness of the asphalt concrete is calculated using de Bats' program.[65] In addition, the thickness of the asphalt layer, daily maximum and minimum temperatures, initial crack length, and the volumetric concentration of aggregate must be entered into the program. The THERM program computes, for each day, the maximum and minimum temperatures of the asphalt concrete layers, the change in the stress intensity factor, the number of cycles required to extend a transverse crack through the asphalt concrete layer, and three cumulative damage functions used in the empirical verification of the model. The crack is assumed to start at the bottom of the asphalt layer and propagate upward.

Temperatures are calculated hourly from U.S. Weather Bureau records at three depths within the asphalt using the Shahin and McCullough version of Barber's equation.[38] These temperatures are used to compute time- and temperature-dependent stresses and the effective tensile modulus of the asphalt concrete, which, in turn, are used to compute the stress intensity factor at the tip of the crack and the number of such temperature cycles, N_f, required to drive a crack through the pavement thickness. The computer printout gives the day on which the first thermal crack appears in the pavement and the current cumulative damage index, C.

The stress intensity factors are calculated for each day with a finite element analysis program which uses a hybrid crack-tip element. This

program, developed by Chang, Lytton, and Carpenter, assumes the material to be linear elastic.[61] A full factorial set of computations produces an equation for the stress intensity factor as a function of crack length, mix stiffness, temperature change below the stress-free temperature of asphalt (about 75 °F (24° C)), and asphalt thickness. This procedure is time-consuming, since it uses results from a finite element subprogram at each stage of its iteration. Therefore, Lytton generated a second regression equation from a large factorial of solutions for conditions encountered in Michigan and Texas, and this solution was modified for general use.

A full factorial set of computations was made using detailed climatic data from four locations in Michigan and four in Texas for a variety of pavement thicknesses, volumetric concentrations of aggregates, and bitumen properties. Regression analysis was then used by Lytton to develop the following empirical/mechanistic equation for the cumulative damage index, C:

$$C = 0.519\ (PI')^{-0.257}\ (SP')^{0.122}\ (c_v)^{24.5}\ (t)^{-0.410}\ (A')^{1.66}\ (SA')^{1.97}\ (MT')^{-7.43} \quad (31)$$

where:

PI' = 0.25(PI + 2)
SP' = ring and ball softening point temperature/125.6, °F
c_v = volumetric concentration of the aggregate
t = thickness of the asphalt concrete/8, in
A' = age of the pavement/10, years
SA' = average annual amplitude of solar radiation/240, langleys/day
MT' = (minimum monthly temperature + 20)/5.7, °F

A total of 576 computed values of cumulative damage index were used in developing the above empirical equation, and a coefficient of determination (R^2) of 0.74 was achieved with the equation. This equation considers both low-temperature and thermal fatigue cracking and was developed from a wide range of data from totally different climatic regions (Michigan and Texas).

The THERM program does not compute the cracking index, I, directly, but instead the cracking index is computed from the cumulative damage index, C. The following linear regression equation was obtained for the Michigan data:

$$I = -4.23 + 3.23\ C \qquad (32)$$

where the coefficient of determination R^2 was 0.30 and the standard error was 5.3. Cracking indices calculated from equation 32 for 32 sites in Michigan are shown in table 7 along with observed cracking indices. The agreement between the predicted and observed cracking indices is not good: linear regression of the predicted versus the observed cracking indices gives an R^2 of 0.34. While this R^2 value is not indicative of a reliable relationship between the predictive and observed cracking, the correlation is as good as the empirical Hajek-Haas model and much better than the TC-1 model. It should be pointed out that the THERM model was developed on the basis of the Michigan data, whereas the other models were extrapolated to the Michigan data. The discussion of the THERM model concludes this chapter. The selection of models that warrant further study is discussed in chapter 5.

Table 7. Comparison of predicted versus observed cracking, THERM model, Michigan data.[44]

Site Number	Cracking Index, Number of Cracks per 500 ft (152 m) of Pavement Length	
	Observed	Calculated
1	0.7	0.0
2	3.3	0.0
3	0.0	0.0
4	0.1	0.0
7	0.0	0.0
8	0.1	3.3
9	1.0	0.0
10	0.3	0.2
11	0.0	0.0
12	0.0	0.0
13	0.4	0.0
14	3.4	1.1
15	1.0	6.3
16	0.0	0.0
17	0.0	5.9
18	0.0	0.0
19	0.0	0.0
20	1.9	5.2
21	0.0	4.6
22	0.0	4.2
23	2.6	7.9
24	5.4	9.2
25	1.0	3.3
26	3.1	2.9
27	1.5	3.7
28	10.7	3.7
29	0.2	1.8
30	10.4	8.5
31	21.2	8.2
32	20.3	8.2
33	12.5	8.2
34	0.2	7.4

4. LABORATORY TESTING AND TEST RESULTS

Laboratory testing was required in order to characterize asphalt cement specimens, calculate temperature susceptibility parameters, and conduct strength, stiffness, and fracture studies on hot-mix asphalt concrete specimens. Residue from the Rolling Thin-Film Oven Test (ASTM D 2972) was used to characterize the temperature susceptibility of the asphalt cement and to conduct nonstandard testing, e.g., gel permeation chromatography, differential scanning calorimetry, and Fraass brittle point temperature tests. The research team believes that the Rolling Thin-Film Oven Test (RTFOT) residue is more representative of the asphalt cement in the pavement than the as-supplied asphalt cement, and therefore, the characterization of the asphalt cement focused on the RTFOT residue. Asphalt concrete mixtures were characterized mechanically by several methods, including indirect tensile modulus and strength tests and an evaluation of the fracture properties of notched asphalt concrete beams. The laboratory testing and the test results are presented in this chapter.

4.1 MATERIALS USED IN THE STUDY

Seventeen asphalt cements chosen from nine sources were used in the study. The asphalt cements were chosen from asphalt cements used in different parts of the country and include those known to be good and poor performers with regard to thermal cracking. Three of the sources selected were represented by three grades: AC-5, AC-10, and AC-20. A source producing a waxy asphalt and a blown asphalt was included. The source and grade of each asphalt are given in table 8. A wide range of physical and physicochemical properties was sought; therefore, the asphalts were chosen with regard to their known performance in the field as well as their temperature-susceptibility parameters and aging index. The range in properties is shown in figure 16, where the data for each asphalt are shown on a plot of temperature susceptibility versus aging index. The figure illustrates the range of properties exhibited by the samples selected for study.[66]

A single mixture design and aggregate source was used in the study, as shown in table 9. The coarse and fine aggregates in the mix were a local

Table 8. Description of asphalt cements used in study.

Number	Source Designation	Grade	Crude Source	Comments
1	A	85/100	Montana	
2	B	AC-5	Venezuela	
3	B	AC-10	Venezuela	
4	B	AC-20	Venezuela	
5	C	AC-5	Texas	
6	C	AC-10	Texas	
7	C	AC-20	Texas	
8	D	AR-4000	California	
9	E	AC-5	Oklahoma	
10	E	AC-10	Oklahoma	
11	E	AC-20	Oklahoma	
12	F	AR-4000	California	
13	G	200/300	Canada	
14	G	150/200	Canada	
15	H	85/100	Montana	
16	I	85/100	Canada	Waxy, Vacuum
17	I	85/100	Canada	Waxy, Oxidized

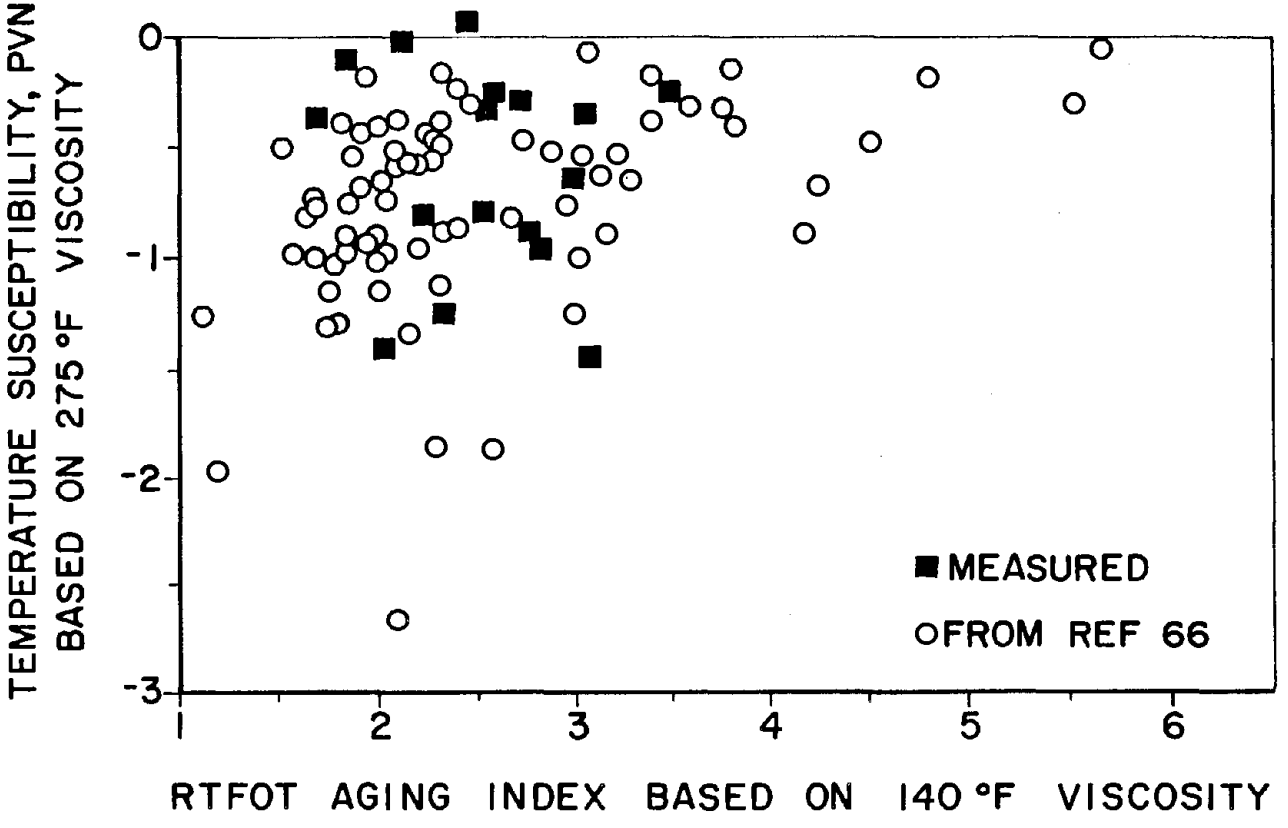

Figure 16. Temperature susceptibility and aging index for study asphalts compared to fingerprint data set.

Table 9. Mix design parameters.

Sieve Size	Aggregate Gradation, % Passing
1/2 in	100
3/8 in	95
No. 4	59
No. 8	38
No. 16	21
No. 30	13
No. 50	9
No. 100	6
No. 200	5
Asphalt content, by total mix weight, percent	6.0
Air voids, percent	3-5

crushed limestone and a manufactured sand crushed from the same parent stone. The mix is used locally and has been used extensively at the Pavement Durability Research Facility at Penn State.[67] The mix is dense-graded with 100 percent passing the 3/8-in (9.15 mm) sieve and is typical of wearing course mixtures used in Pennsylvania.

4.2 ROUTINE TESTS ON ASPHALT CEMENTS

The standard ASTM specification tests (ASTM D 3381) were conducted with the as-supplied asphalt cements to characterize the asphalts and to provide data needed for calculating other parameters or for use in the thermal cracking models:

- ASTM D 5 Test for Penetration of Bituminous Materials.
- ASTM D 36 Test for Softening Point of Bitumen (Ring and Ball Apparatus).
- ASTM D 2170 Test for Kinematic Viscosity of Asphalts (Bitumens).
- ASTM D 2171 Test for Viscosity of Asphalts by Vacuum Capillary Viscometer.
- ASTM D 2972 Test for Effect of Heat and Air on a Moving Film of Asphalt (Rolling Thin-Film Oven Test).

The results of these tests appear in table 10.

The same series of standard tests listed above was also performed on the RTFOT residue for all 17 asphalts. This was done because the data were required for calculating the temperature susceptibility parameters and as input for the cracking models. However, penetration determinations on the RTFOT residue were made at three temperatures: 77 °F (25 °C), 59 °F (15 °C), and 41 °F (5 °C) or 95 °F (35 °C), depending on the stiffness of the asphalt. Three temperatures are needed to calculate the version of the penetration index that is based on penetration. Results for the RTFOT residue are in table 11.

Table 10. Summary of test results for unaged asphalts.

No.	Source	Grade	Penetration at 77 °F, 1/10 mm	Ring and Ball Softening Point, °F	Absolute Viscosity at 140 °F, poises	Kinematic Viscosity at 275 °F, cSt	RTFOT[1] Loss, Weight %
1	A	85/100	90	114	1130	268	-0.01
2	B	AC-5	189	102	650	239	0.75
3	B	AC-10	121	111	1370	333	0.67
4	B	AC-20	71	121	3100	480	0.54
5	C	AC-5	144	108	540	204	0.19
6	C	AC-10	98	114	1020	264	0.09
7	C	AC-20	60	120	1790	336	0.17
8	D	AR-4000	52	119	2230	267	0.27
9	E	AC-5	182	104	560	348	-.13
10	E	AC-10	108	112	1100	479	-.13
11	E	AC-20	68	120	1900	637	-.14
12	F	AR-4000	134	107	1320	318	1.50
13	G	200/300	241	95	610	202	1.28
14	G	150/200	155	104	860	267	.76
15	H	85/100	86	114	1670	331	-.16
16	I	85/100	98	116	770	210	-.33
17	I	85/100	87	119	750	205	-.14

[1]Positive number indicates loss in weight during RTFOT exposure

Table 11. Summary of test results, RTFOT residue.

No.	Source	Grade	Pen (0.1 mm) 100 g, 5 s				Ring and Ball Softening Point, °F	Absolute Viscosity at 140 °F, poises	Kinematic Viscosity at 275 °F, cSt	Fraass Temp., °F	Percent Retained Penetration
			41 °F	59 °F	77 °F	95 °F					
1	A	85/100	-	17	50	152	124	3170	393	13	56
2	B	AC-5	12.0	29	96	-	115	1640	377	4	51
3	B	AC-10	-	22	66	180	125	3520	524	0	55
4	B	AC-20	-	15	41	114	132	8150	797	7	58
5	C	AC-5	7.7	23	76	-	116	1320	292	0	53
6	C	AC-10	-	17	51	163	121	2220	374	7	52
7	C	AC-20	-	11	34	92	130	5170	545	22	57
8	D	AR-4000	-	11	36	110	127	4430	383	24	69
9	E	AC-5	12.0	34	117	-	112	917	452	-6	64
10	E	AC-10	-	23	72	213	120	1940	623	1	67
11	E	AC-20	-	16	45	142	128	4400	894	5	66
12	F	AR-4000	-	28	67	162	124	4350	589	8	50
13	G	200/300	17.0	44	125	-	108	1310	322	-6	52
14	G	150/200	9.0	26	77	-	119	2500	427	0	50
15	H	85/100	-	18	49	121	127	4850	530	6	57
16	I[1]	85/100	-	15	56	171	124	1740	274	10	57
17	I[2]	85/100	-	24	55	137	127	2350	294	3	63

[1]Waxy asphalt, vacuum distilled
[2]Same source as asphalt No. 16, air blown

4.3 FRAASS BRITTLE TEMPERATURE

The Fraass brittle point temperature was obtained for the RTFOT residue. Although this test is not commonly used in the United States, it was included so it could be compared with other variables related to temperature susceptibility and low-temperature brittleness. In the Fraass procedure, a steel plate coated with a thin film of asphalt is slowly flexed at successively lower temperatures until a crack is observed in the asphalt. The temperature at which the crack forms is the brittle point temperature.

The Institute of Petroleum Specification IP 80/53 procedure was followed, with the exceptions noted below.[19] The plates used were a standard size--0.006 in thick by 0.8 in wide by 1.6 in long (0.15 mm by 20 mm by 40 mm). The thickness of the asphalt coating was also standard--0.002 in (0.05 mm). During the test, the temperature was reduced 1.8 °F/min (1.0 °C/min) while the plate was flexed once each minute, figure 17. The sample was cooled by placing it in a flask surrounded by an acetone/dry ice mixture; additional dry ice was added at a controlled rate to achieve the desired cooling rate, shown in figure 18. An automated version of the test device was used; the time required to bend and relax the plate was kept constant at 22 s. The temperature at which a crack first became visible in the asphalt coating was recorded. The procedure was then repeated with a freshly prepared specimen until two measurements agreed to within 3.6 °F (2 °C), as specified in the standard.

The major differences between the procedures described in IP 80/53 and the one used in this project involved the manner in which the samples were prepared. In the standard method of sample preparation, 0.40 g of asphalt are weighed on a test plate, which is then heated on a hot plate until the asphalt becomes fluid and flows over the plate. After a dissecting needle is used to spread the coating evenly, the surface of the asphalt is heated with a small flame to remove air bubbles. The research team was concerned that this localized heating would overheat the surface of the asphalt film. The crack is initiated at the surface of the film, and any hardening of the surface could affect the brittle temperature.

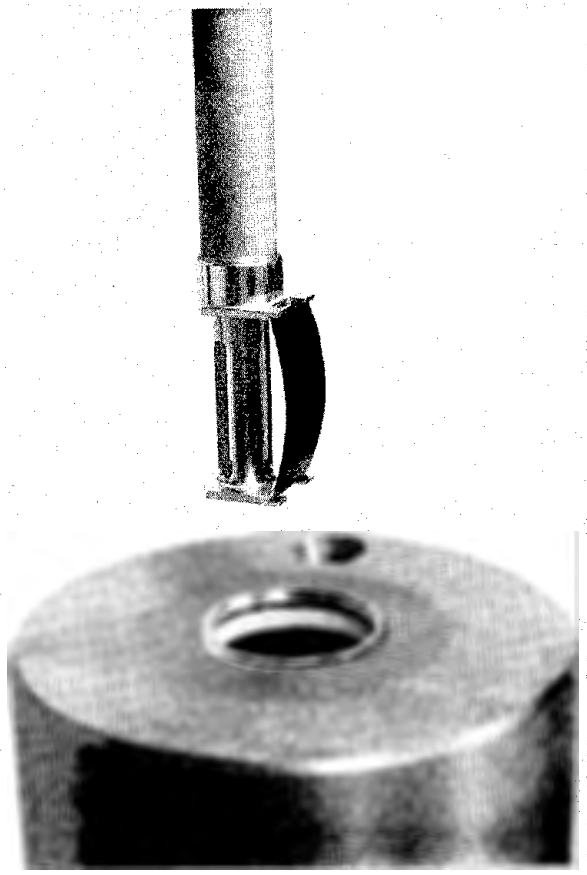

Figure 17. Photograph of the flexible steel plate coated with asphalt and mounted in the Fraass apparatus.

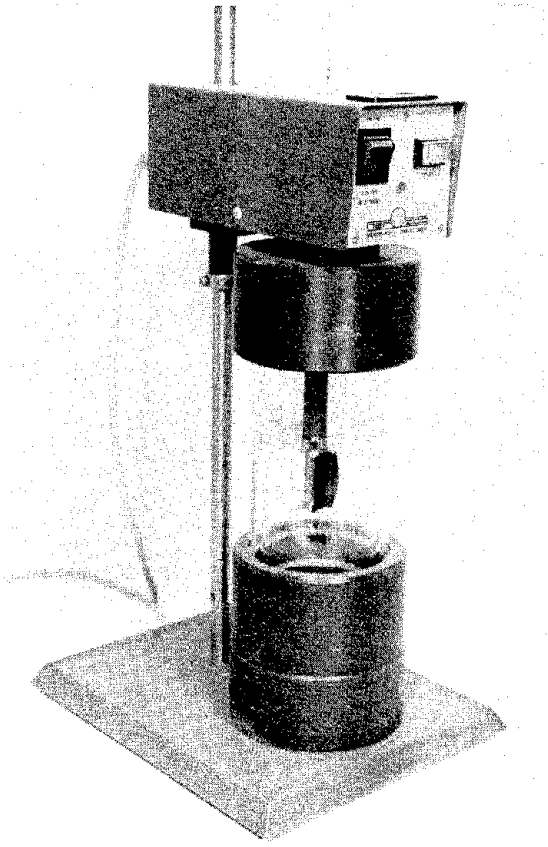

Figure 18. Photograph illustrating Fraass brittle point apparatus.

Given this concern for surface hardening, the test specimens for this study were prepared using a press, which is normally used only for materials having a softening point greater than 212 °F (100 °C). In this procedure, a small amount of asphalt is placed on a test plate resting on the lower block of the press. The upper block is then lowered, pressing the specimen to the specified thickness. During pressing, the blocks are heated to approximately the softening point of the asphalt. Before the specimens were removed, they were cooled by water circulating through the blocks. In the procedure followed by the research team, very thin films of plastic supplied with the device were used to prevent the asphalt from sticking to the blocks during pressing. After the test plates were removed from the press, the thin plastic film was removed and the excess asphalt was trimmed from around the edges of the steel plate with a razor blade. To remove air bubbles, the steel plates were placed on a steel block in a sand bath heated to approximately 275 °F (135 °C). The plates were heated until the asphalt was fluid, kept heated for about 10 min, and then removed from the block. During the heating, the asphalt film was stirred with a pointed glass rod in a slow swirling motion to help remove air bubbles. As in the standard procedure, specimens were tested within 4 h of preparation. The Fraass brittle point temperatures for the 17 project asphalts are given in table 11.

4.4 DYNAMIC MECHANICAL ANALYSIS OF ASPHALT CEMENTS

The dynamic mechanical analyzer offers a means of obtaining stiffness data over a wide range of test frequencies. These data can be generated in a much shorter period of time than creep data, and a mechanical transition temperature, analogous to a volumetric glass transition temperature, can be obtained easily. Beams measuring 1/4 in thick by 1/2 in wide by 2 in long (6.4 mm by 12.7 mm by 51 mm) were formed from the RTFOT residue and then tested in dynamic flexure using a Series 9000 DuPont mechanical analyzer (DMA).

The relationships between the applied strain; response (stress); absolute value of the complex shear modulus, $|G^*|$; storage modulus, G'; loss modulus, G''; and phase angle, δ, are shown in figure 19. If the material being tested is a linear viscoelastic material and the applied strain (or stress) is a sinusoidal function of time, ω, expressed as radians per second, then the

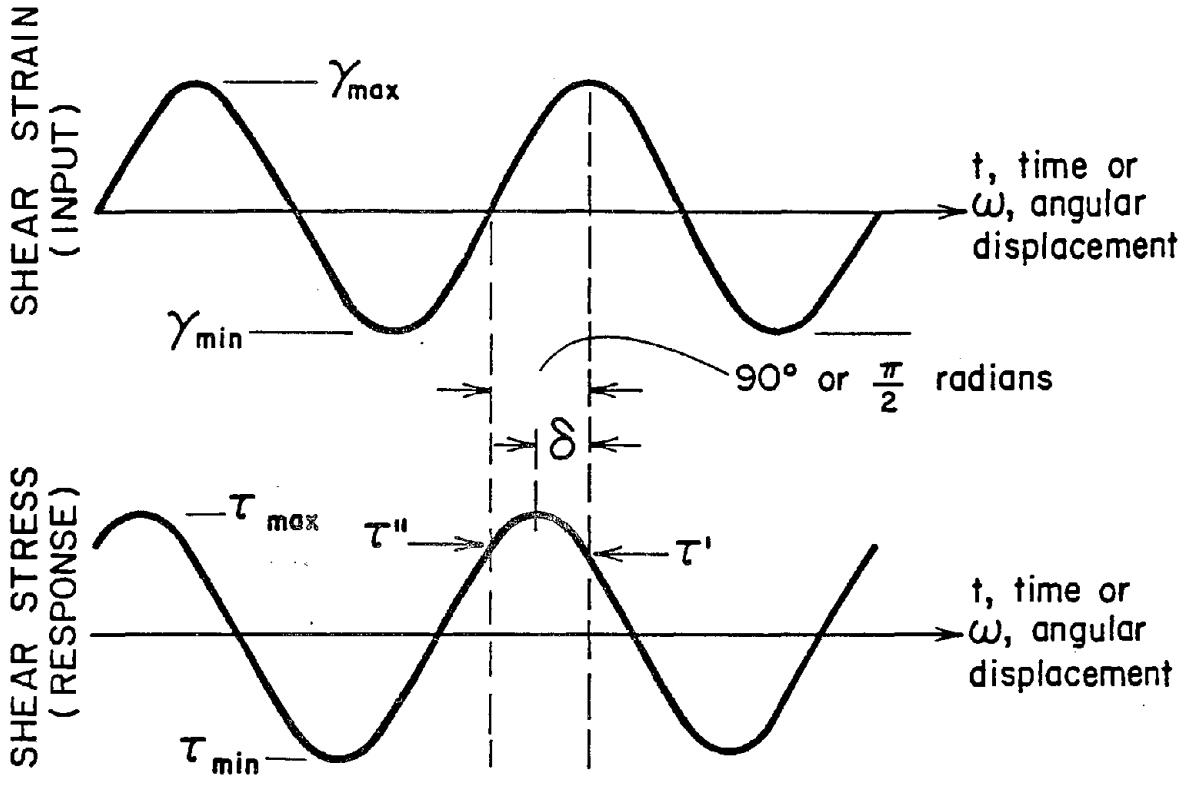

$$|G^*| = \frac{\tau_{max} - \tau_{min}}{\gamma_{max} - \gamma_{min}} = |G' + iG''|$$

$$G' = \frac{\tau'}{\gamma_{max} - \gamma_{min}} = |G^*| \cos\delta$$

$$G'' = \frac{\tau''}{\tau_{max} - \tau_{min}} = |G^*| \sin\delta$$

$$\tan\delta = \frac{G''}{G'}$$

Figure 19. Definition of complex modulus.

response stress (or strain) will also be a sinusoidal function. However, the response stress (or strain) will lag the applied strain (or stress) by an amount δ, which is the phase angle, expressed in radians. The absolute value of the complex modulus is defined as the absolute value of the peak to peak stress divided by the peak to peak strain. The storage modulus represents the in-phase component of the modulus and can be found using the following equation:

$$G' = |G^*| \cos \delta \tag{33}$$

where

G' = shear storage modulus, lb/in^2 (Pa)

$|G^*|$ = absolute value of shear complex modulus, lb/in^2 (Pa)

δ = phase angle, degrees or radians

The loss modulus represents that portion of the material response which is 90° out of phase with the mechanical input:

$$G'' = |G^*| \sin \delta \tag{34}$$

where

G'' = shear loss modulus, lb/in^2 (Pa)

$|G^*|$ = absolute value of the shear complex modulus, lb/in^2 (Pa)

δ = phase angle, degrees or radians

Frequently, the phase lag is representd by tan δ, rather than δ. Tan δ is simply the loss modulus divided by the storage modulus and can be thought of as the fraction of the material response that is viscous in nature. A completely elastic material would have a tan δ value of zero, whereas a completely viscous material would have a tan δ value of infinity.

A photograph of the testing device is given in figure 20 and a schematic of the loading system is shown in figure 21. The frequency of the strain applied by the DMA is equal to the resonant frequency of the beam, which in this case ranged from approximately 40 Hz at low temperatures, -40 °F (-40 °C), to 10 Hz at room temperature.

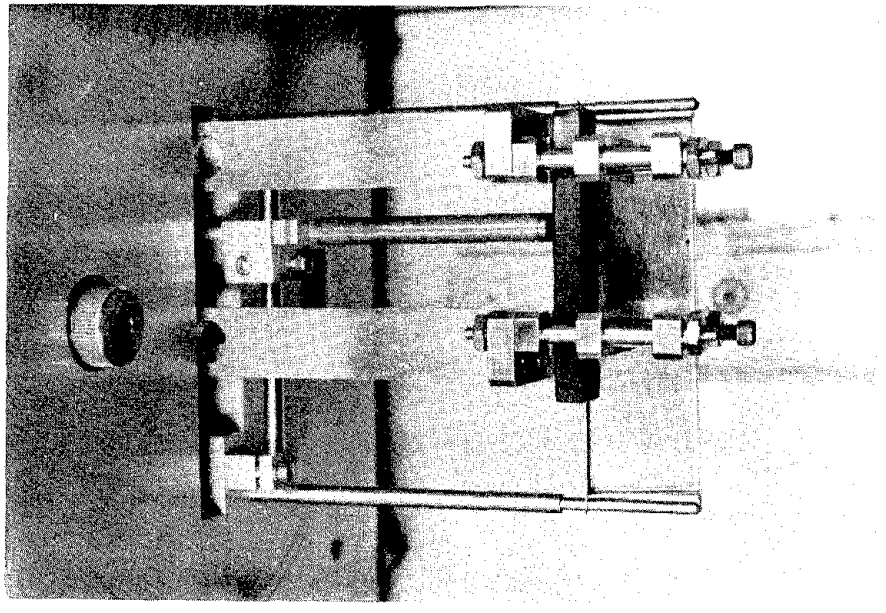

Figure 20. Photograph of test beam clamped in dynamic mechanical analyzer.

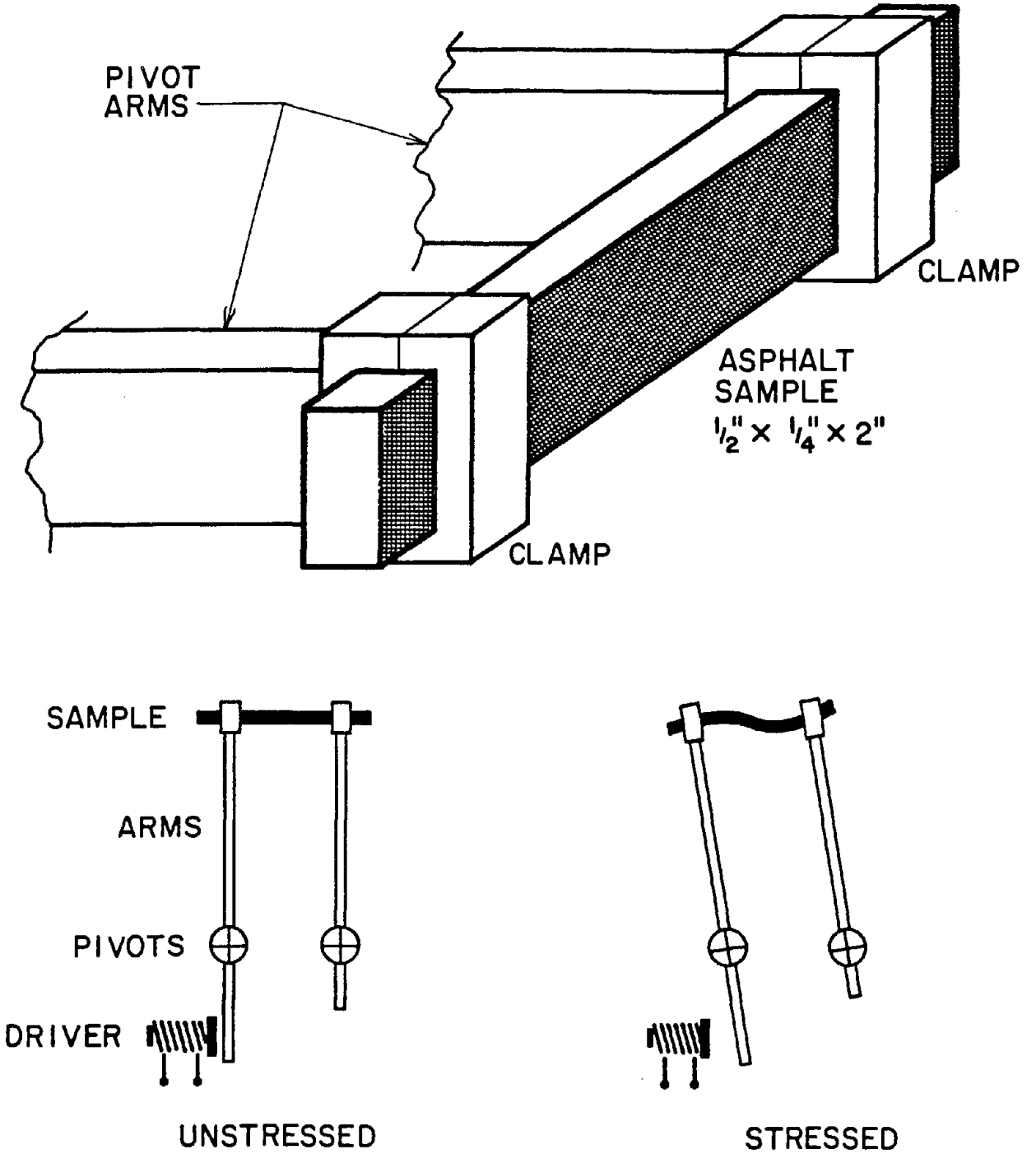

Figure 21. Schematic of bending mode in dynamic mechanical analyzer.

A microcomputer and plotter included with the DMA system automatically reduced and plotted the data. In this case, the storage modulus, loss modulus, and tan δ were calculated and plotted versus the test temperature, which ranged from approximately -40 °F (-40 °C) to 70 °F (21 °C). A typical set of curves generated for a single test or temperature sweep is shown in figure 22, a direct reproduction of the plot prepared with the DuPont device, where "Log (Flex. Stor. (GPa))" represents the log of the storage modulus, G', and "Log (Flex. Loss (GPa))" represents the log of the loss modulus, G''. Of particular interest is the temperature at which the peak in the loss modulus is observed, since it represents a mechanical glass transition temperature and a transition from a leathery to a brittle or glassy state under dynamic loading. In figure 22 the loss modulus attains a maximum value at 48.3 °F (10.32 °C) indicating a glass transition at that temperature. Measured glass transition temperatures are reported in table 12. These temperatures are considerably higher than those measured with the differential scanning calorimeter (DSC). This difference is discussed in the next section in conjunction with the DSC test results. A complete set of DMA curves is given in appendix A.

4.5 DIFFERENTIAL SCANNING CALORIMETRY

From a molecular viewpoint, the glass transition temperature, T_g, represents the point at which all molecular translation and bond rotation cease. T_g can also be explained as the minimum temperature above which the volume between molecules is large enough to permit molecular translation and bond rotation. As the temperature increases above T_g, the volume between molecules, called free volume, increases, permitting molecular motion and vibration to occur. In fluids, the free volume is very large, and thus, there is very little restraint on molecular translation and vibration.[68]

Factors affecting T_g include molecular weight, stiffness and complexity of molecular architecture, and the presence of polar groups, such as amine and carbonyl. Generally, T_g will increase with increases in molecular weight; molecular stiffness; and complexity, concentration, and strength of polar functional groups.[68] The practical importance of the glass transition

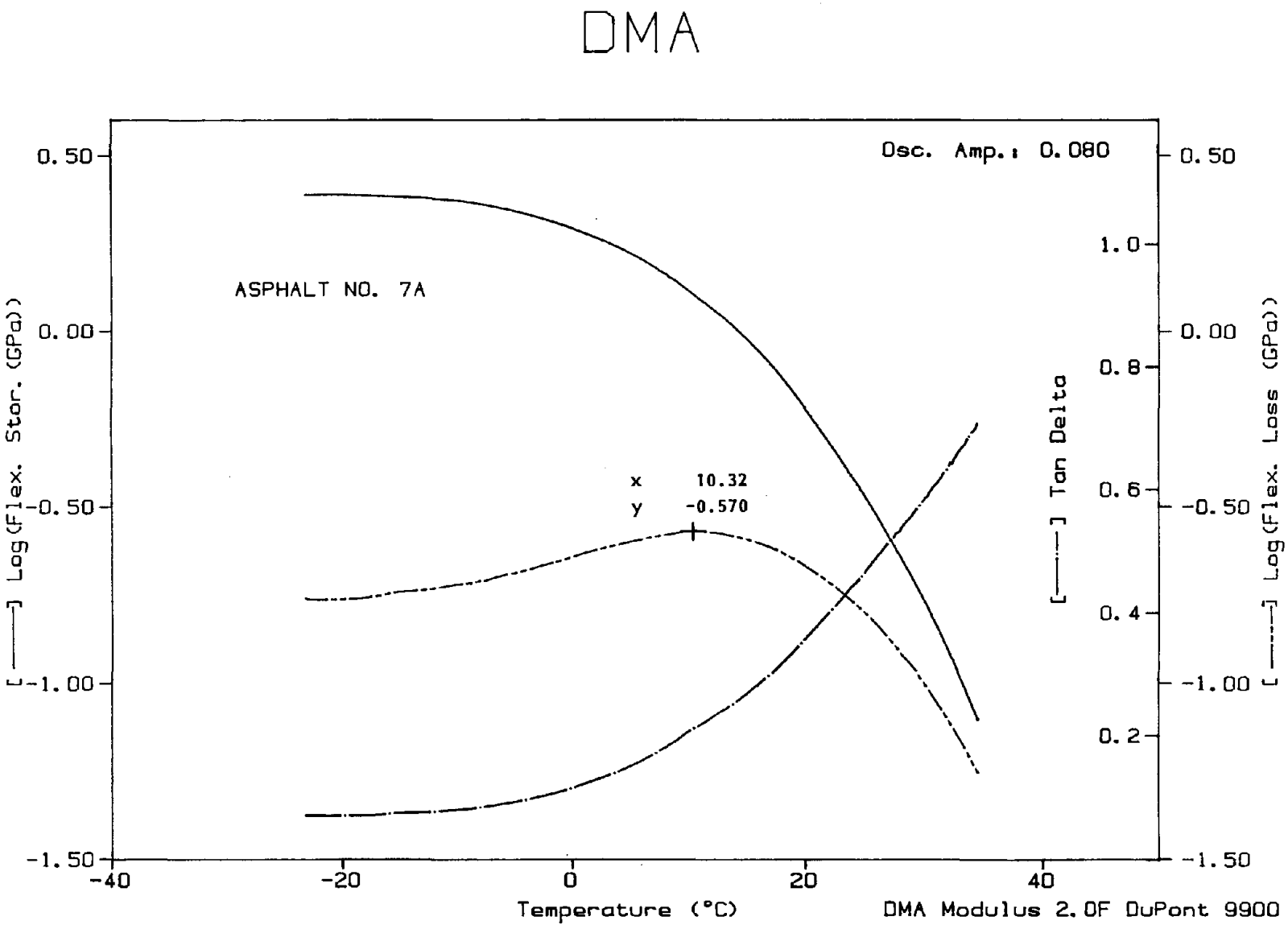

Figure 22. Typical output from dynamic mechanical analyzer.

Table 12. Dynamic and DSC transition temperatures, RTFOT residue.

Asphalt Source Number	DMA Glass Transition Temperature, °F	DSC Glass Transition Temperature, °F
1	55.4	-27
2	42.4	-18
3	47.1	-18
4	46.0	-27
5	50.6	-34
6	50.6	-30
7	48.3	-25
8	68.3	+18
9	43.9	-38
10	43.3	-28
11	44.7	-28
12	42.3	-27
13	42.0	-17
14	42.3	-25
15	42.6	-27
16	55.0	-13
17	37.9	-40

temperature is in the identification of brittle behavior and the identification of phase changes, such as wax crystallization, within the asphalt.

Various techniques exist for the identification of the glass transition temperature. The glass transition temperature is generally identified with change in coefficient of thermal expansion and may be measured dilatometrically.[68] Differential scanning calorimetry is another technique; T_g is identified by a change in the specific heat of the sample, which is characteristic of a change in molecular state. Glass transition temperatures can also be determined through dynamic mechanical testing, where the glass transition is associated with a peak in the loss modulus, or damping, of the material. Regardless of the method to identify the glass transition temperature, it is usually dependent on the thermal history of the material: heating rate, cooling rate, quenching, etc. In the case of dynamic mechanical testing, the frequency of testing would also affect the observed glass transition temperature.[68]

The glass transition temperatures of asphalt cements have been measured dilatometrically by Schmidt and Santucci, who found that the glass transition temperature ranged from -31 °F (-34 °C) to +5 °F (-15 °C) for a group of 52 asphalts, and by Anderson and Goetz.[69,70] Thenoux and associates used differential scanning calorimetry to identify the glass transition temperatures of three asphalt cements, finding diffuse, multiple transitions.[23] They associated the glass transition with the lowest transition temperature, which ranged from -6 °F (-21 °C) to 19 °F (-7 °C).

For this research project, glass transition temperatures were identified using two techniques. As described above in section 4.4, glass transitions were identified through dynamic mechanical analysis as the temperature at the observed peak in the loss modulus. Differential scanning calorimetry was also used to determine the glass transition temperatures of the test asphalts. The procedure and results of these tests are described below.

The residue from the RTFOT test was stored in completely filled, small aluminum canisters that were sealed from the atmosphere. To obtain small

quantities of the residue, a spatula was warmed in the flame of a Bunsen burner, then plunged into the sample to a depth of approximately 1 in and pulled toward the side of the container to open a "hole." A small amount of asphalt from the opened area was transferred to the spatula; the stem of the spatula was again heated to obtain sufficient fluidity in the asphalt so that it could be placed in the appropriate sample cup. The asphalt was not heated directly in the flame, but by conduction of heat along the shaft of the spatula.

A Perkin-Elmer 7 series differential scanning calorimeter (DSC) was used in these studies. Sample weights varied between 10 and 20 mg, and all test specimens were cooled initially and then the thermograms were obtained while heating from -58 °F (-50 °C) to 266 °F (130 °C) at 18 °F/min (10 °C/min). After the initial thermogram was obtained, the specimen was rapidly cooled to -58 °F (-50 °C) to quench it, and a second thermogram was obtained. The thermograms were calibrated by measuring the endothermal areas and transition temperatures for pure indium. The thermograms for the asphalt cements were very complicated and did not indicate a single transition temperature. Because of the complexity of the thermograms, the use of DSC data cannot be recommended as a specification test. The thermograms are further complicated because sample conditioning greatly affects the shape of the thermogram. The authors believe that further study of the DSC procedure is warranted, but further, in-depth research will be required to relate test results to the low-temperature behavior of asphalt cement.

The precise interpretation of the transitional behavior and the identification of transition temperatures was often difficult. This research team defined the glass transition temperature as the midpoint of heat capacity change, as seen from figure 23. A more detailed description of the procedure used to determine the glass transition temperature is given in appendix B. In some cases, two or more transitions were apparent. In these cases, the lowest transition temperature observed on the thermogram was recorded as the DSC glass transition temperature, T_g. These data are shown in table 12, along with the DMA glass transition temperatures. The DMA temperatures are considerably higher than the DSC temperatures. A complete set of thermograms is given in appendix B.

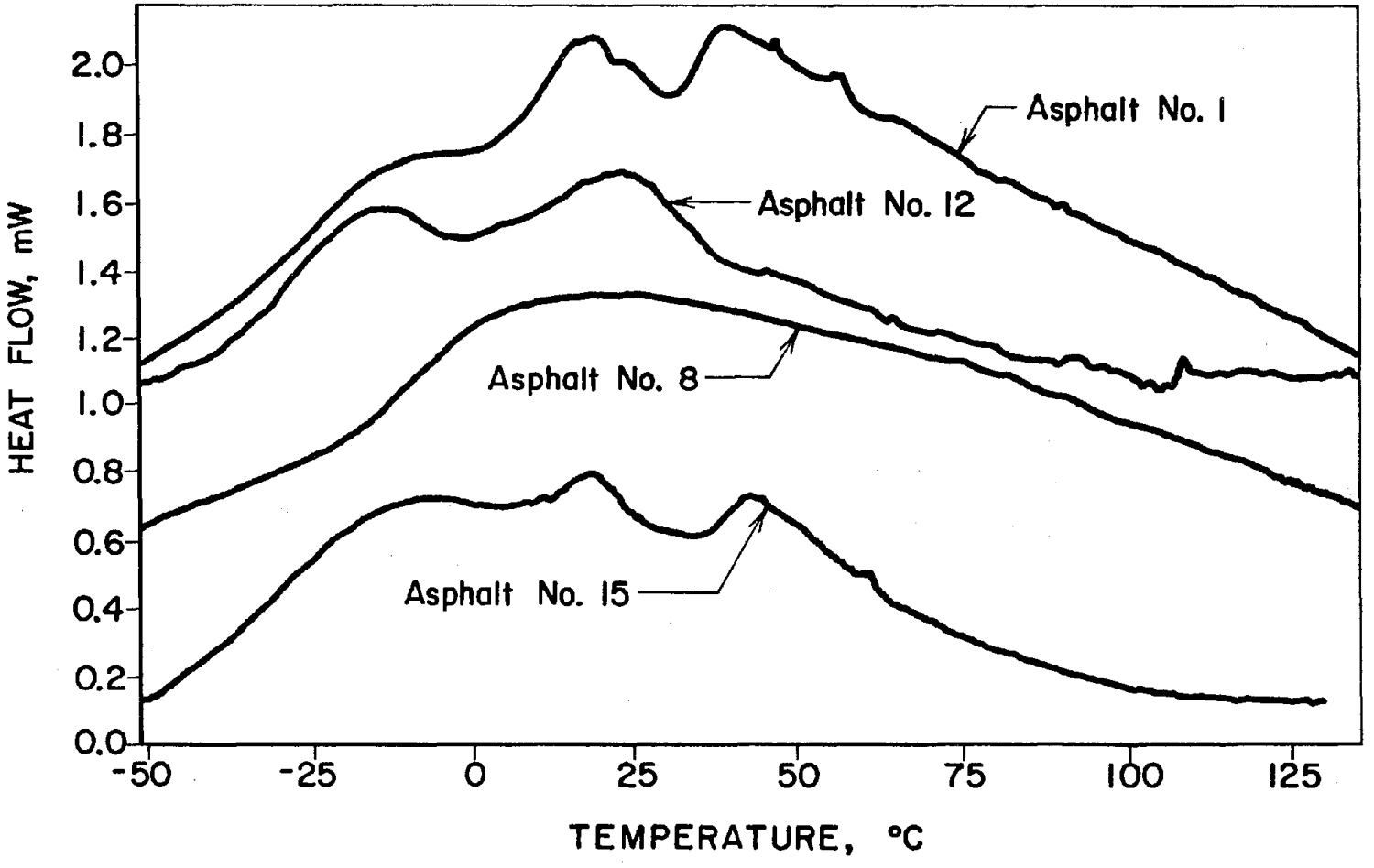

Figure 23. Example of a thermogram from differential scanning calorimeter.

Differences between the DMA and DSC T_g data were expected because of the difference in testing procedures. The DMA glass transition temperatures were determined at 10 to 30 Hz, whereas the effective loading rate for the DSC measurements is much lower, approaching static conditions. Mechanical transition temperatures are known to be affected by the rate or time of testing, which explains why the transition temperatures from the DMA are much higher than for the DSC.[68] A plot of the DSC versus the DMA glass transition temperatures is shown in figure 24. No strong relationship between the two measurements is observed and certainly they are not acceptable surrogates for each other.

4.6 GEL PERMEATION CHROMATOGRAPHY

Various analytical techniques for characterizing asphalts have been used in order to understand the relationship between asphalt structure and physical properties. Gel permeation chromatography (GPC), a molecular separation technique, distinguishes molecules by their hydrodynamic volume (the volume that a molecule possesses in a given solvent). This technique, which was developed within the polymer industry, is relatively straightforward. A given sample contains a distribution of molecular weights. If the sample is dispersed in a solvent and passed through a column containing porous glass or cross-linked polymer beads, the smaller molecular species (which have a smaller hydrodynamic volume) pass slowly through the column. Because their volume is small, they travel through many of the pores in the column. Larger species that cannot easily fit into the pores pass through the column more quickly. By using monodisperse standards, it is possible to correlate the elution time (the time it takes a given fraction to pass through the column) with an apparent weight average molecular weight, $\bar{M}_w$, and an apparent number average molecular weight, $\bar{M}_n$.

GPC has been used to characterize asphalts for more than 30 years.[71-81] Because of the nature of the asphalt structure, the technique is, in most cases, only qualitative. By reviewing several aspects such as methodology, fractionation experiments, and molecular weight calibration, the inherent

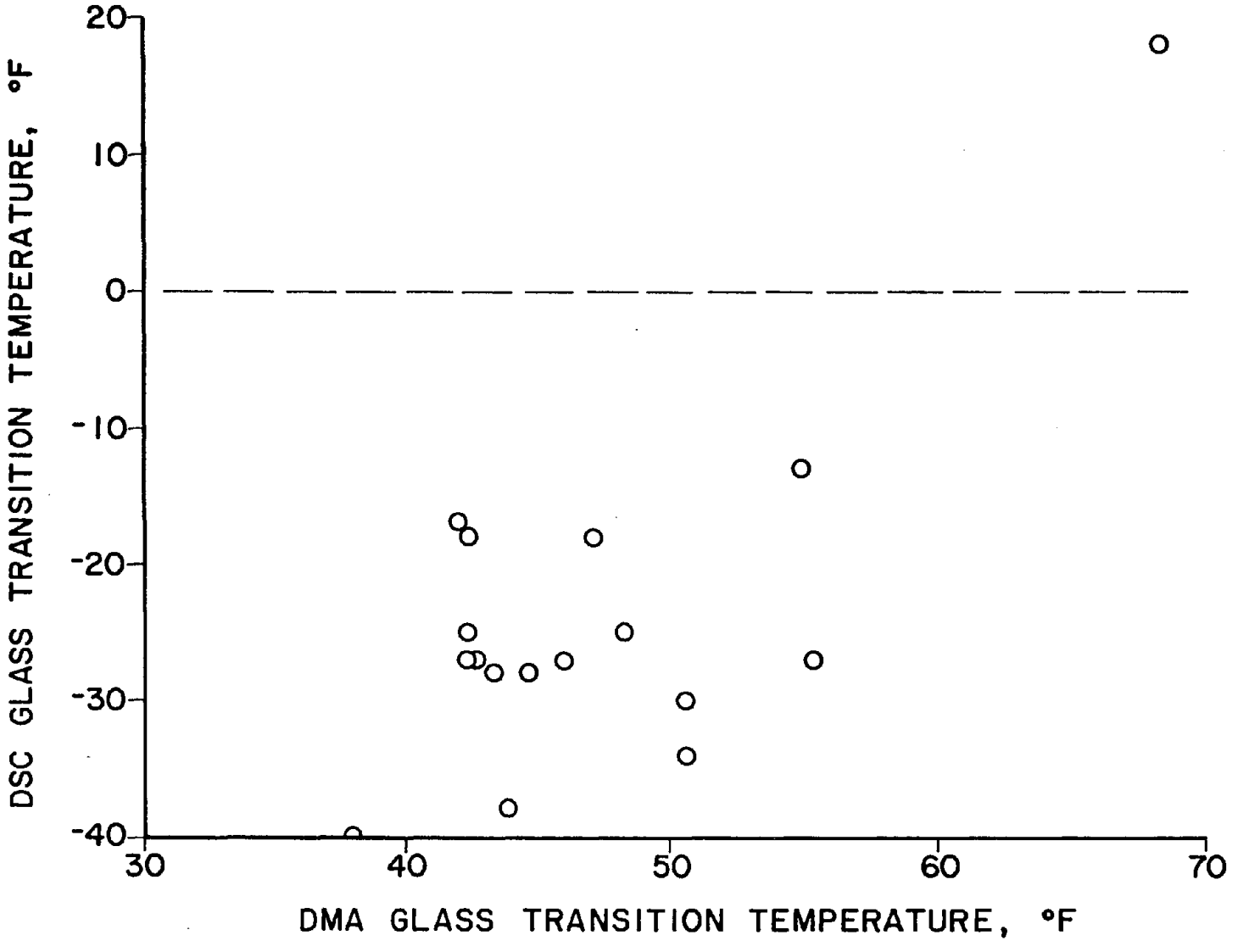

Figure 24. Comparison of glass transition temperatures from differential scanning calorimeter and dynamic mechanical analyzer.

problems in obtaining quantitative molecular weights for asphalt-like materials will become apparent.

Several factors, including the type, size, and number of columns to be used, must be considered before experimentation with GPC is attempted. Of the three types of columns available (glass or silica packed, lightly cross-linked polymer, and heavily cross-linked polymer), the heavily cross-linked polymer columns appear to be most suitable for use with asphalts.[71] Their packing is more stable and separation is faster than with the lightly cross-linked polymer columns. Porous glass columns should not be used because asphaltenes and polar species will adsorb on the polar sites on the surface of the glass.[71] Table 13 shows that the Waters Ultra and Micro Styragel columns are used almost exclusively for GPC analysis of asphalt cement. The size of the columns and their number generally depend on whether analytical or preparatory experiments will be performed. When preparatory work is done, two or more columns (10^3 and 10^4 Å pore size) may be used.[73,77,78,79,81] The number and size distribution of columns used by different researchers varies greatly for analytical experiments.[72,75,76,80]

As one would expect, the solvent (or mobile phase) utilized plays an important role in the separation process. The solvent chosen must completely dissolve the asphalt and promote the advancement of the asphalt through the column. Under some conditions, it has been reported that certain constituents of the asphalt can become adsorbed on the columns. Altgelt recommends two solvent systems to combat this problem, chloroform with 5-percent methanol and benzene with 5-percent methanol.[71] He also mentions that, while pyridine and trichlorobenzene are preferable for discouraging adsorption, they are difficult to remove from collected fractions because of their high boiling points. In the literature, the most frequently reported solvent was tetrahydrofuran (THF) although the chloroform and benzene systems are reported by several researchers, table 13.

In addition to the aforementioned variables, several other factors deserve attention. One is the type of detector. Generally, two types of detectors are used. The first is a differential refractometer, which measures the difference in refractive index, RI, between the solvent and the

Table 13. Review of HP-GPC test procedures for asphalt cement.

Instrument	Column Material and Pore size, Angstroms	Type of Solvent	Flow Rate ml/min	Detector, Wave Length nm	Sample Size, Concentration	Ref No.	Analytical or Preparatory
Waters 200x	Ultrastyragel: 100, 250, 800, 1,000, 10,000	THF	1	RI	2 ml, 0.5 mg/l	72	Analytical
Waters 101	Microstyragel: 1,000, 10,000	Chloroform	20	Not Given	100 ml, 1.0%	73	Preparatory
Not Given	Ultrastyragel: 1,000, 2,500	THF	1	RI, uv: 340, 220, 500, 254, 510	10-20 ml, 0.5%	75	Analytical
Waters 244	Microstyragel: 1,000, 10,000	THF	3.5	RI, uv: 350	15 ul, 2%	76	Analytical
Waters 244	Microstyragel: 1,000, 10,000	THF	3.5	RI, uv: 254, 350	Not Given, 0.5%	78	Preparatory
Not Given	Microstyragel: 1,000, 10,000	Benzene 5% MeOH	2	Not Given	Not Given	77	Preparatory
Not Given	Styragel: 100, 250, 1,000, 10,000	Chloroform 5% MeOH	2	uv: 370	9 g, 20 g/l	79	Preparatory
Waters 200	Not Given: 60, 100, 1,000, 5,000, 100,000	THF	1	Not Given	Not Given, 1%	80	Analytical
Not Given	Not Given 100,000	Benzene 5% MeOH	0.25	Not Given	300 g, 1.5%	81	Preparatory

asphalt-solvent mixture that passes through the detector. The RI detector is also temperature sensitive. The other type is the ultraviolet light, uv, detector. Both are excellent for detecting aromatic compounds and relatively poor for detecting aliphatic hydrocarbons. Pumping rate and sample size are also important. For preparative experiments, the sample size and rate are larger (100 mℓ at 20 mℓ/min) than for analytical experiments, which typically are performed at a rate between 1 and 3 mℓ/min with sample sizes on the scale of microliters. Details of the procedures used in previous GPC studies of asphalts can be found in table 13.

Because of the complicated nature of asphalts, preparative GPC is frequently used to separate individual components (i.e., malthenes, oils, resins, asphaltenes, etc.).[73,78,79,81] Once separated, more quantitative studies can be conducted on the nature and structure of the components. Several studies have been conducted on asphaltenes (defined as the asphalt component that is insoluble in pentane).[75,78] In a study that illustrates the type of analysis that can be performed, vapor pressure osmometry and ultracentrafugation were performed to determine molecular weights, and infrared spectroscopy was performed for structural chemical analysis. In other studies, fractionation has served as an intermediate step for custom blending of asphalt samples.[82] In this case, preparatory GPC was used to separate an asphalt into 30 fractions, which were then further fractionated. Next, the components were recombined in different ratios to assess the effects on the properties of each blend. Other papers have been published on the topic of fractionation and GPC analysis of asphalts, but they are somewhat outside the scope of this project, which focuses primarily on the rheology of asphalt cement.

To obtain molecular weights of polymers, the raw data (elution volume versus time) is normally converted to molecular weight via a universal calibration curve. As a consequence of the inherent distribution of molecular species as well as molecular sizes, from a strictly theoretical standpoint, this technique is not applicable to heterogeneous materials such as asphalts.[71] Several efforts to obtain calibration curves by other, more complex methods have included passing the asphalt through a preparatory GPC in order to fractionate it into as many as 30 fractions.[71,72,73,79] The

molecular weight averages for each of these fractions are then determined by a technique such as ultracentrifugation or vapor pressure osmometry (VPO) which provides a number average molecular weight. The molecular weights thus obtained are plotted versus their GPC elution volume.

Jennings attempted to correlate results from GPC testing with the frequency of thermal cracking.[83] To provide a quantitative variable that he could correlate with cracking, he empirically divided the elution curve into three different regions which he associated with large, medium, or small molecular size (LMS, MMS, and SMS, respectively). Calibration of the apparatus was accomplished with a standard or reference asphalt against which other asphalts were compared. Jennings gave the most attention to large molecular size and found that the LMS correlated reasonably well with the cracking observed in a limited number of pavements. However, when extended to a larger population, the correlations were weak.

High-performance (or pressure) gel permeation chromatography (HP-GPC) testing was conducted by the authors as well as by Jennings and Pribanic.[84] The asphalt samples were oven-hardened in an RTFOT oven in the authors' laboratory, and samples of the same residue were used by the authors and Jennings and Pribanic. All of the testing was done using the RTFOT residue and appendix C as a guide. A Waters model 150 GPC was used by both Jennings and the authors. Tetrahydrofuran was used as the mobile phase and the flow rate was 1 mℓ/min for all runs. Four columns packed with 10-μm ultrastyragel beads with pore sizes 10^3, 10^4, 10^5, and 10^6 Å were used in all tests completed by the research team; the columns used by Jennings and Pribanic are listed in appendix C. The uv and the RI detectors were used by Jennings and Pribanic although they used only the uv chromatograms in their analysis; the authors used a refractive index detector exclusively.

Jennings and Pribanic reduced their data to give the percentage of small, medium, and large molecular size (SMS, MMS, and LMS, respectively), as described in appendix C. Because the standard asphalt, used by Jennings and Pribanic (see appendix D), was not available to the authors, this research team took a slightly different approach: the number average molecular weight

($\bar{M}_n$) and weight average molecular weight ($\bar{M}_w$) were calculated for each asphalt:

$$\bar{M}_n = \frac{\sum n_x m_x}{\sum n_x} \tag{35}$$

where

n_x = number of moles of x mer units

m_x = molecular weight of the x mer unit

and

$$\bar{M}_w = \frac{\sum n_x m_x^2}{\sum n_x m_x} \tag{36}$$

or, in other words, $\bar{M}_n$ is the first moment of the distribution of mer units about the mean while $\bar{M}_w$ corresponds to the second moment about the mean. No attempt was made to curve resolve the various peaks on the chromatogram because Jennings' standard asphalt was unavailable to the research team and because the research team believes the standard asphalt approach is not a reproducible method that can be used by multiple laboratories.

A typical chromatogram obtained by the research team is shown in figure 25. A complete set of chromatograms and a description of the test conditions are given in appendix D. Information derived from the chromatograms is presented in table 14, which also contains the polydispersity indices calculated for each asphalt. The polydispersity index, PDI, is defined as the weight average molecular weight divided by the number average molecular weight. A typical chromatogram obtained by Jennings and Pribanic is shown in figure 26, and the percentages of SMS, MMS, and LMS are given in table 15. A complete set of their chromatograms and their test conditions are presented in appendix D. Correlations between these and other data will be discussed in chapter 6. Details regarding the determinations of SMS, MMS, and LMS are given in appendix D.

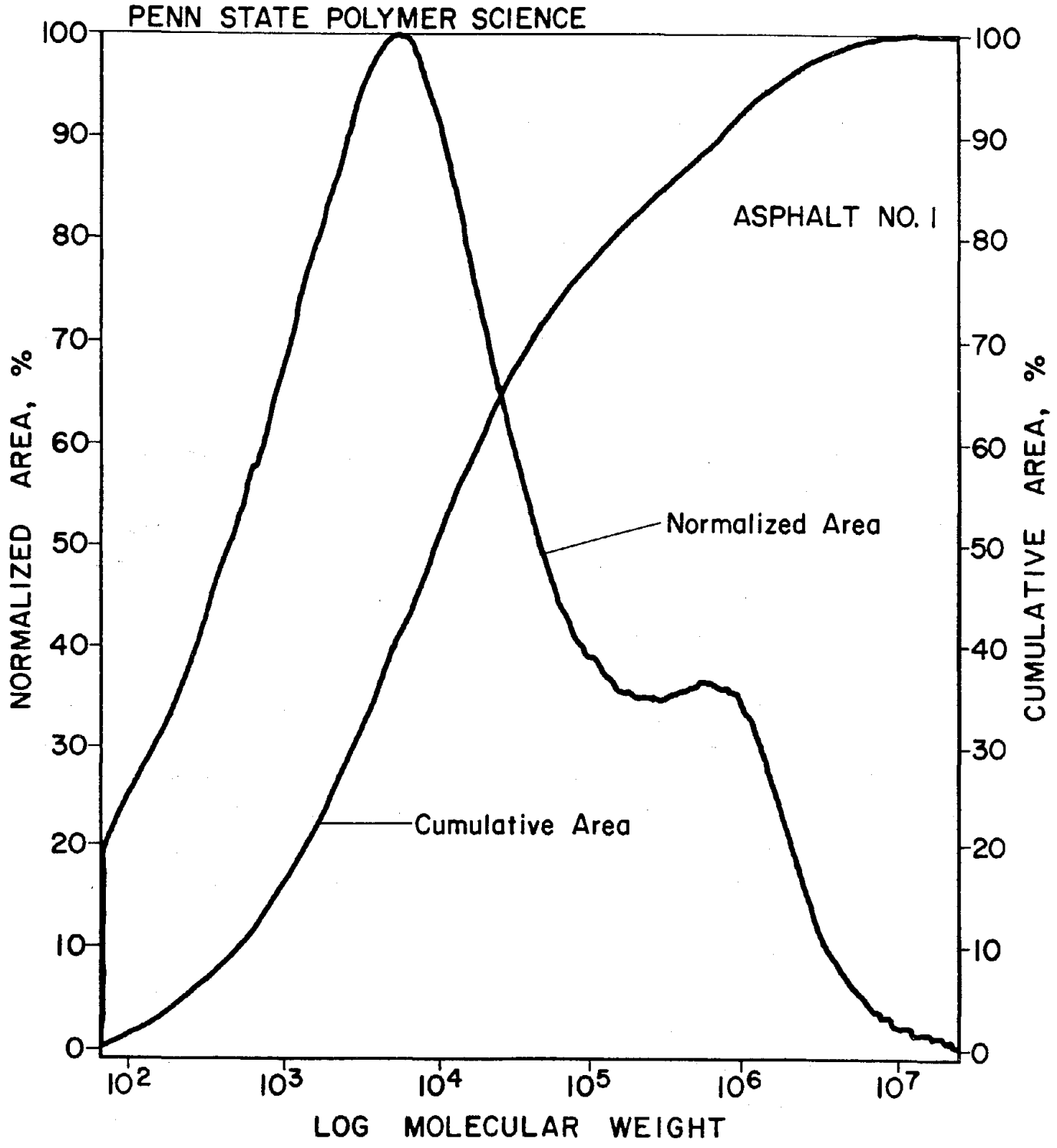

Figure 25. Typical HP-GPC chromatogram obtained by authors.

Table 14. HP-GPC test results obtained by authors.

Asphalt Source Number	Number Average Molecular Weight, g/mol	Weight Average Molecular Weight, g/mol	Polydispersity Index, $\overline{M}_w/\overline{M}_n$
1	1290	2750	2.14
2	1320	4590	3.47
3	1350	5290	3.92
4	1470	5300	3.54
5	1540	8460	5.49
6	1570	2700	1.73
7	1410	8210	5.83
8	1230	2850	2.31
9	2360	8260	3.51
10	1970	7840	3.99
11	1860	7500	4.03
12	1260	8530	6.77
13	1060	3800	3.57
14	1190	4410	3.69
15	1160	2430	2.09
16	1310	3920	3.00
17	1360	2940	2.16

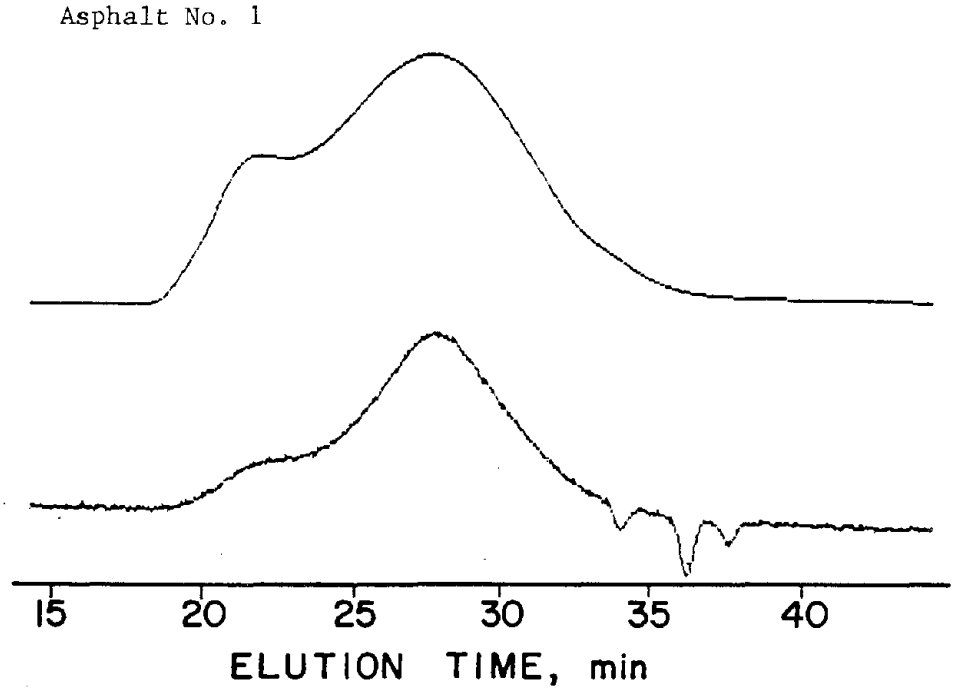

Figure 26. Typical HP-GPC chromatogram obtained by Jennings and Pribanic.

Table 15. HP-GPC test results obtained by Jennings and Pribanic.

Asphalt Number	Large Molecular Size Fraction, weight %	Medium Molecular Size Fraction, weight %	Small Molecular Size Fraction, weight %
1	20.4	43.2	36.4
2	31.0	39.9	29.1
3	30.4	40.8	28.8
4	32.4	41.6	26.0
5	20.2	51.7	28.1
6	20.5	51.6	27.9
7	21.5	51.2	27.3
8	20.6	47.8	31.6
9	36.6	44.7	18.7
10	36.9	44.3	18.8
11	37.0	44.0	19.0
12	41.1	35.6	23.3
13	35.6	37.7	26.7
14	34.5	39.8	25.7
15	25.8	41.6	32.6
16	17.7	49.3	33.0
17	37.2	37.7	25.1

4.7 ROUTINE TESTS ON ASPHALT CONCRETE MIXES

Tensile strength and modulus data were required for the asphalt concrete mixes. For this purpose, standard 75-blow Marshall specimens were prepared using the mix design shown in table 9. In this phase of the project, 12 of the 17 project asphalts were used to prepare mixes.

The tensile modulus and strength were determined with the indirect tension test. The specimens were loaded using a crosshead speed of 0.1 in/min (2.54 mm/min) in order to provide meaningful data over the entire temperature range. This speed was chosen after testing a series of specimens at speeds varying from 0.01 in/min (250 μm/min) to 1.0 in/min (25.4 mm/min). The faster testing speeds did not give reliable test results at lower temperatures because the specimens fractured explosively. At higher temperatures, test speeds less than 0.1 in/min (2.54 mm/min) were too slow, permitting excessive creep deformation. If data at different temperatures are sought, it is imperative that equal test speeds be used, and 0.1 in/min (2.54 mm/min) appears to be the best compromise. The static moduli were obtained from the linear portion of the load-deformation curve and, as such, might be called tangent moduli.

The strength and modulus tests were performed at four temperatures: 10 °F (-12 °C), 40 °F (4.4 °C), 60 °F (16 °C), and 77 °F (25 °C). In all cases, three replicates were tested, and the averages were reported. The static tensile modulus data are summarized in table 16, and the tensile strength data, in table 17.

When the data for tensile strength were plotted versus temperature, each mix produced a curve of similar shape except that the individual curves were shifted along the temperature axis by an amount that was asphalt specific. It was hypothesized that the position of the individual curves relative to each other on the temperature axis could be used as a measure of the susceptibility of each asphalt to thermal cracking. With this hypothesis, an asphalt concrete with its strength/temperature plot displaced toward higher temperatures would be more susceptible to thermal cracking than an asphalt concrete with its curve displaced toward lower temperatures. In other words,

Table 16. Summary of test results, static diametral tensile modulus.

Asphalt Number	Source	Static Diametral Tensile Modulus, 1000 lb/in^2				Static Modulus Temperature Shift, °F
		10 °F	40 °F	60 °F	77 °F	
1	A	830	1150	56.0	14.3	14
2	B	1050	117	18.7	6.1	-18
4	B	2500	720	71.0	19.3	8
5	C	2600	530	23.0	5.0	5
7	C	1200	2500	121.0	41.7	18
8	D	740	1280	77.0	11.0	14
11	E	1030	1040	106.0	30.0	13
12	F	1280	189	20.3	5.1	-9
13	G	460	53	11.7	3.2	-26
14	G	1530	270	19.3	3.5	-4
16	I	2100	270	65.0	14.3	11
17	I	1950	1080	91.0	13.1	-3

Table 17. Summary of test results, static diametral tensile strength.

Asphalt Number	Source	Static Diametral Tensile Strength, lb/in^2				Tensile Strength Temperature Shift, °F
		10 °F	40 °F	60 °F	77 °F	
1	A	420	300	85	40	12
2	B	430	150	47	25	-4
4	B	450	270	95	49	8
5	C	410	210	60	27	0
7	C	460	370	126	68	15
8	D	460	460	125	46	19
11	E	450	240	100	49	4
12	F	440	200	57	28	0
13	G	320	80	35	26	-14
14	G	460	220	53	27	1
16	I	460	240	90	35	5
17	I	450	180	66	33	-1

the asphalt concrete with a curve displaced toward the higher temperature would assume low-temperature behavior at a higher temperature than an asphalt concrete with its curve displaced toward lower temperatures.

A quantitative measure of the relative position of each mix on the temperature axis was developed for each asphalt by plotting the tensile strength data versus temperature, drawing a smooth curve through the data, and shifting the data along the temperature axis until it was coincident with a reference point. The reference point, 300 lb/in^2 (2.1 MPa) and 32 °F (0 °C), was chosen somewhat arbitrarily so that it would fall within the middle portion of the data range. The procedure that was followed is shown schematically in figure 27.

Similar trends were observed in the modulus versus temperature data and the same rationale was applied to the modulus data, using a reference point of 730,000 lb/in^2 (5 GPa) and 32 °F (0°C). The amount of temperature shift for modulus and tensile strength was reported as the temperature shift. These values, along with the moduli and tensile strength data, are reported in tables 16 and 17, respectively.

Composite plots of tensile strength and modulus, figures 28 and 29 respectively, were prepared by applying the asphalt specific temperature shifts to each test temperature (the absolute values of negative shifts were subtracted from the test temperatures and the positive values were added). The results of these plots are shown in figures 28 and 29, where the plots assume the appearance of a master curve. In essence, the different asphalts have the effect of shifting the behavior of the modulus and tensile strength with respect to temperature.

4.8 FRACTURE MECHANICS TESTS ON ASPHALT CONCRETE MIXES

A primary objective of this study was to evaluate the applicability of linear elastic fracture mechanics to hot-mix asphalt concrete. J-integral is used to characterize the fracture properties of materials in elastic-plastic fracture analyses.[85] J-integral is defined as a path-independent contour integral representing the energy obtained by integrating over the

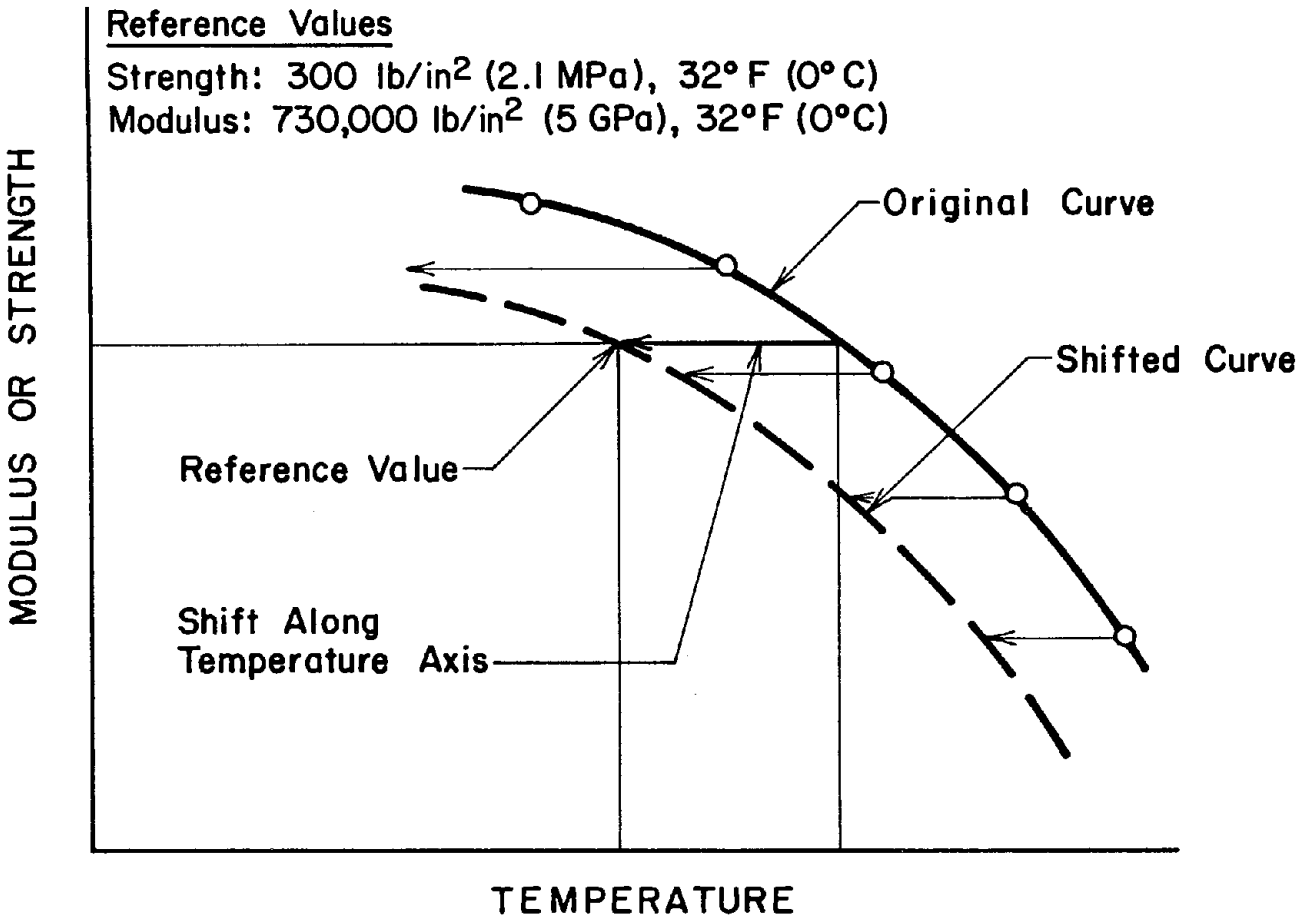

Figure 27. Schematic illustrating technique for determining mixture tensile strength and modulus master curves.

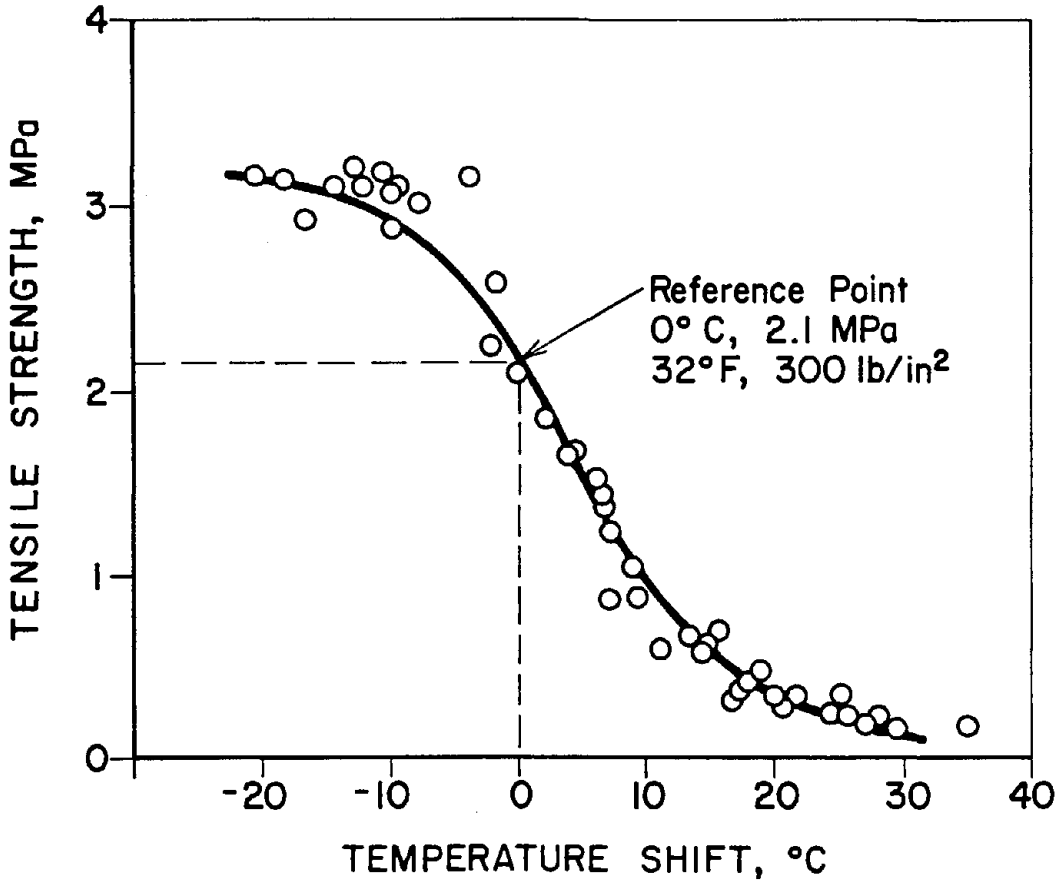

Figure 28. Composite plot of static diametral tensile strength versus temperature shift.

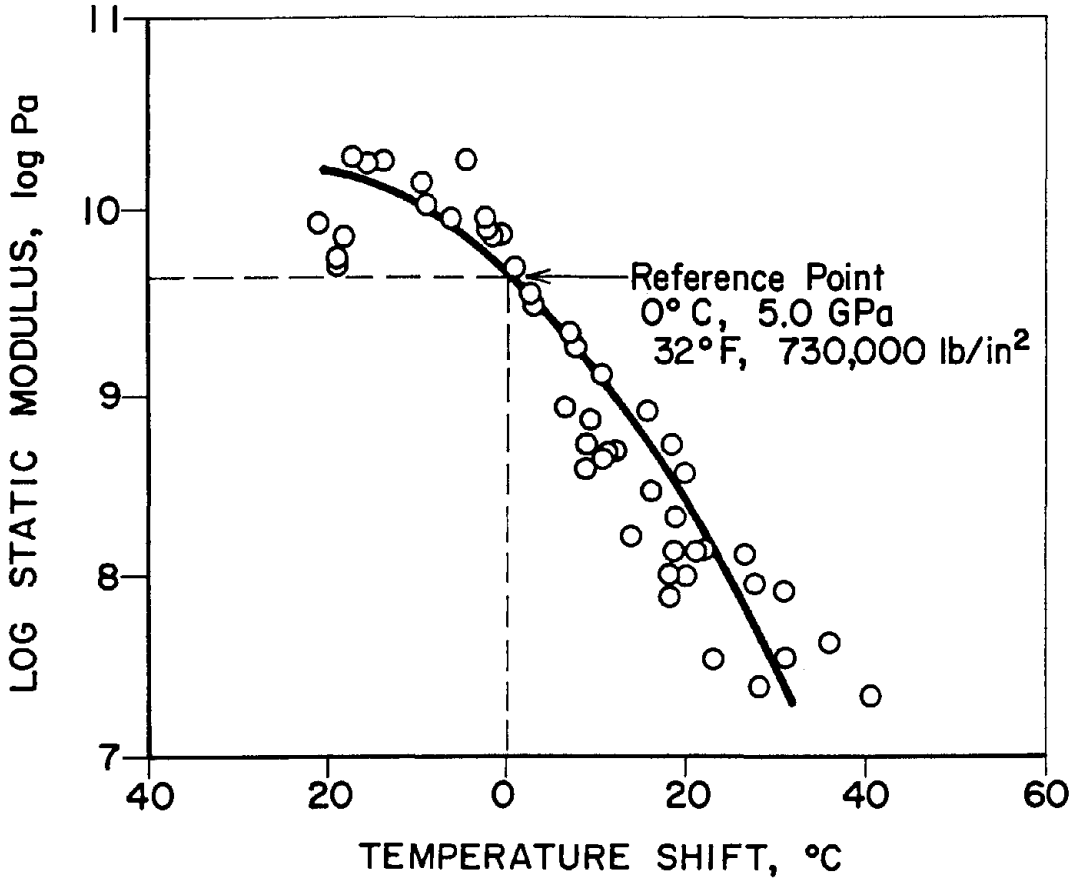

Figure 29. Composite plot of static diametral tensile modulus versus temperature shift.

stress-strain field in the vicinity of a crack tip. The critical value of J-integral in plane strain, J_{1c}, can be expressed as:

$$J_{1c} = -\frac{1}{b}\frac{dU_T}{da} \tag{37}$$

where

J_{1c} = critical value of J-integral in plane strain, lb-in/in^2 (Pa-m)

b = beam width, in (mm)

U_T = total strain energy to failure, lb-in (J)

a = crack (notch) length, in (mm)

In the laboratory, J_{1c} can be determined by testing, to failure, a series of notched beams in three-point bending.[85] A monotonically increasing load is used to fail the beam, and the load and midpoint deflection of the beam is recorded (figure 30). Failure is defined as the point when the load on the beam is at a maximum, figure 31. This testing necessitates the preparation of a series of notched beams for mixtures made with selected asphalts.

The critical value of J-integral, J_{1c}, is obtained when the load on the beam is just sufficient to cause the crack initiation at the root of the notch. When the testing is done in plane strain (lateral strain in beam equal to zero), maximum restraint to the propagation of the crack is developed. This condition (plane strain) is denoted by the subscript 1 (one) and J_c becomes J_{1c}.

Laboratory beam specimens, 3 in by 3 in by 16 in (76 mm by 76 mm by 406 mm), were compacted with a Cox model CS-1000 kneading compactor. The compaction procedure followed ASTM D3202-83 and ASTM D1561 except that the kneading pressure and the number of tamping blows were modified to obtain densities such that the air voids were between 4 and 6 percent for all specimens. The compaction sequence that was used is shown in table 18. This procedure gave air void percentages that were uniform throughout the height of the beam.

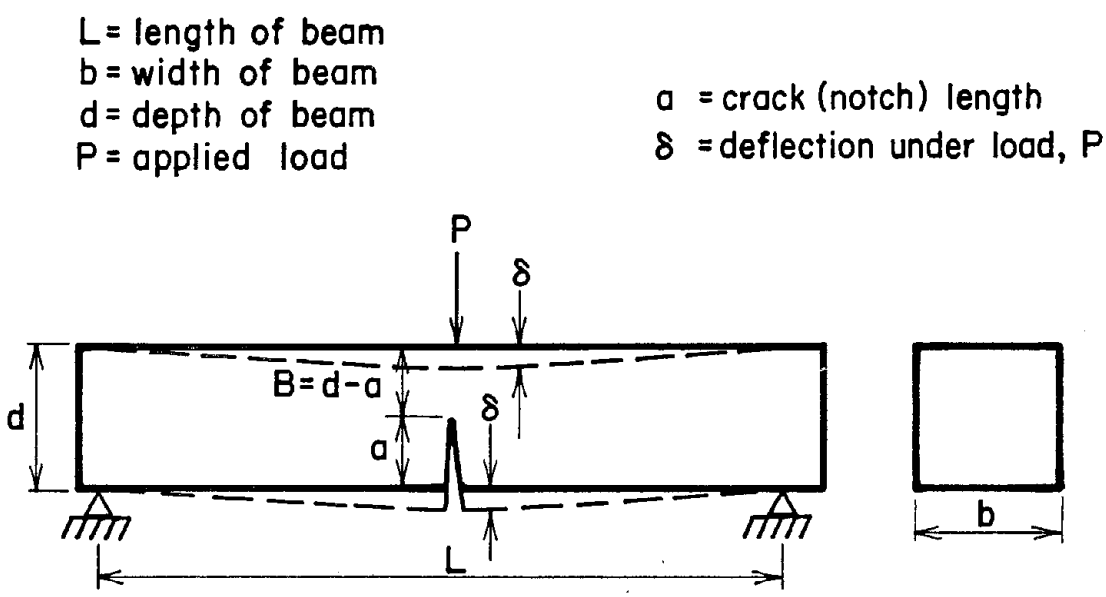

Figure 30. Schematic of beam used for fracture mechanics testing.

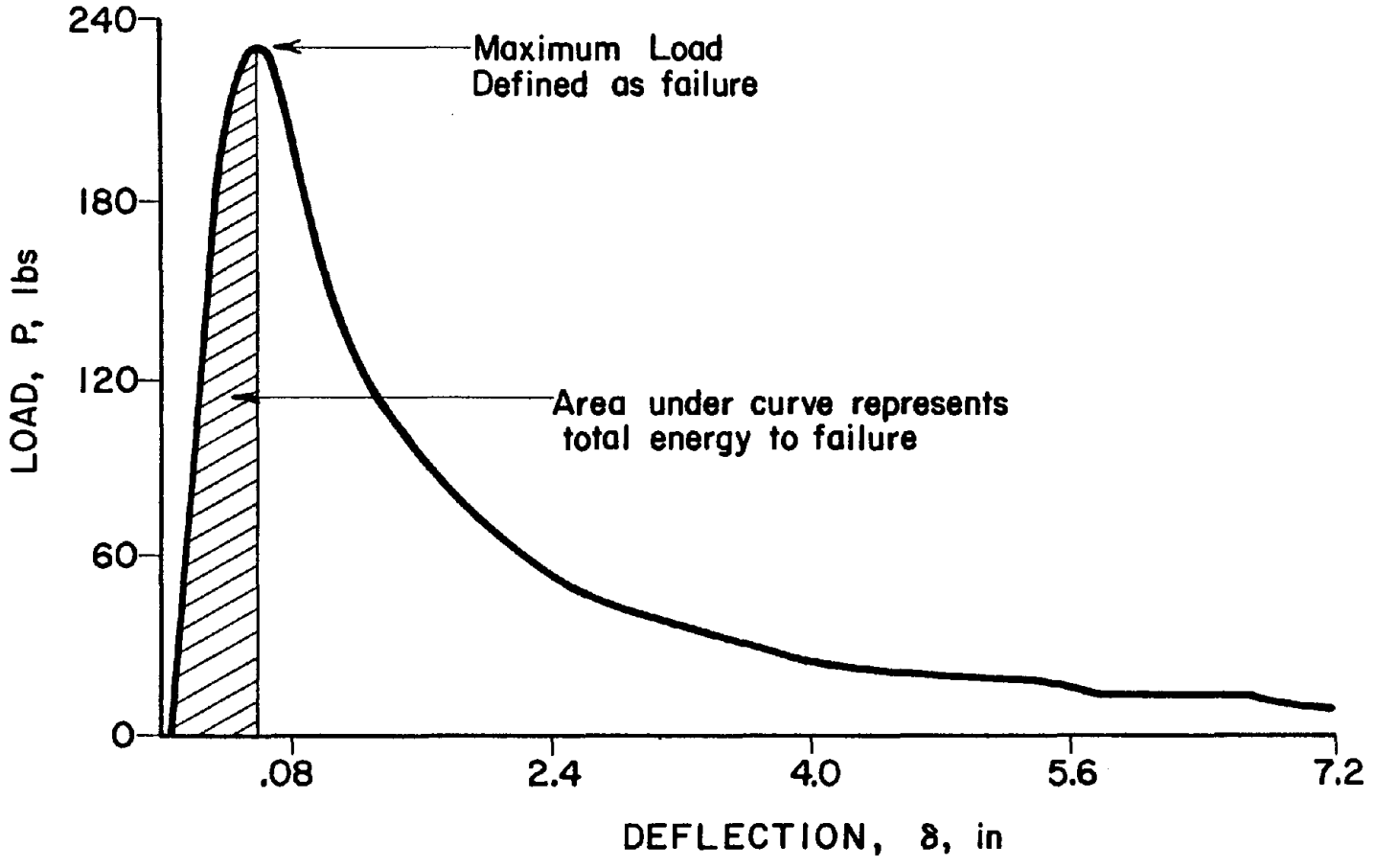

Figure 31. Typical measured load versus deflection curve for notched beam.

Table 18. Compaction sequence for beams.

Lift	Compaction Effort
1st lift	48 blows, 90 lb/in^2 48 blows, 125 lb/in^2 48 blows, 250 lb/in^2
2nd lift	48 blows, 90 lb/in^2 48 blows, 125 lb/in^2 48 blows, 250 lb/in^2 48 blows, 350 lb/in^2
2nd lift	Leveling load, 40 lb/in^2 at 0.25 in/in load rate

Note: Each lift is approximately 1.5 in (38 mm) thick.
1 lb/in^2 = 6.89 MPa.

No standard procedure exists for determining the fracture mechanics properties of notched asphalt concrete beams. The following procedures and recommendations were adopted for the project and are recommended for future work in this area:

- ASTM specification designation C31-69 for flexure tests specifies that the minimum beam dimension should be three times the maximum aggregate size. Maximum aggregate size in the mix used in this study was 3/8 in (9.15 mm), which satisfies the specification requirement.

- According to ASTM E 813, the span of the beam should be chosen such that the span to depth ratio equals 4. An overall length of 16 in (406 mm), a span length of 12 in (305 mm) and a depth of 3 in (76 mm) were used in this study, which meets these requirements.

- It is suggested by the research team that, for low-temperature fracture tests, the notch length to beam depth ratio (a/d) should be greater than or equal to 0.5. This ratio is in accordance with ASTM E 813 specifications for J_{Ic} testing of metals. At least three distinct notch depths, a, should be used.

The loading frame used to conduct the fracture test is shown in figure 32. Loading of the specimens was accomplished with the MTS model 810-14.2 closed-loop electrohydraulic testing machine. The specimens were loaded monotonically to failure using a ramp function. A ramp rate was chosen to give a load of 1.5 lb/s (680 g/s). This loading rate represents an average of loading rates used by others.[57,58] Loads were measured with an electronic load cell mounted between the hydraulic actuator and the specimen.

The deformation-measuring equipment consisted of two LVDTs supported by a rod fastened to the base plate, figure 32. The tests were performed at and below 60 °F (16 °C). Preliminary testing showed that there was no visible or measurable deformation in the beam at the point of contact between the 1/2-round supports and the beam, figure 32. Therefore, it was assumed that, during any given test, the deflection measured with the LVDTs was due solely to the deflection of the beam. Consequently, deflection measurements were made on the underside of the beam by attaching aluminum clips to the beam and referencing the LVDTs to the strips.

The deflection-measurement system is shown in figure 33. Two LVDTs were used, one on each side of the beam, to obtain an accurate measurement of

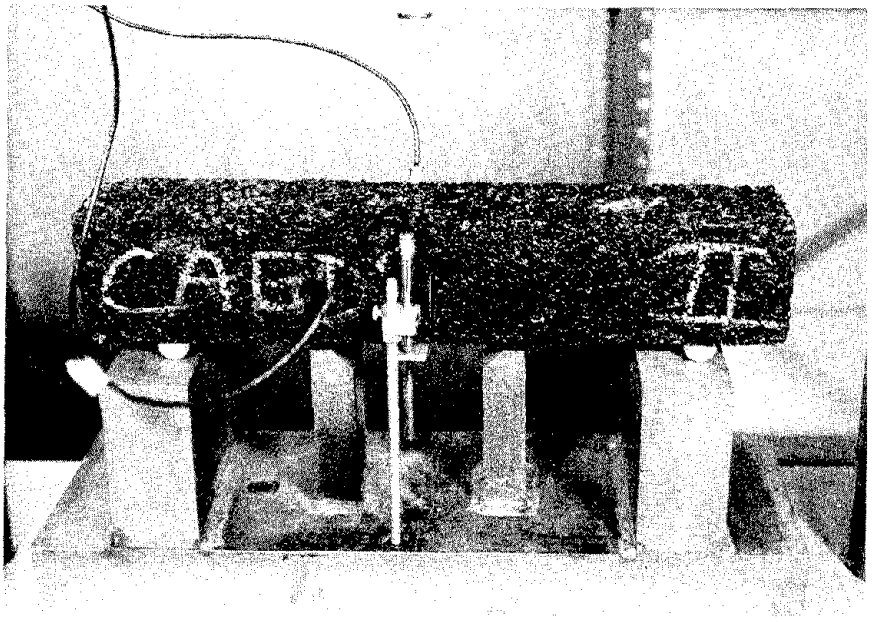

Figure 32. Photograph of fracture mechanics testing fixture.

Figure 33. Photograph illustrating details of fracture beam deflection measuring technique.

deflection. The individual signals were monitored and summed using the data acquisition software. The load and deflection signals were sampled with a Data Translation Model DT-2801A analog to digital I/O board mounted in an IBM PC. ASYST, a scientific programming environment, was used as an interface between the A/D board and the computer.[86]

The fracture testing was conducted at five temperatures: 40 °F (4.4 °C), 25 °F (-3.9 °C), 10 °F (-12.2 °C), and -5 °F (-20.6 °C). Cracks were sawed at the midpoint on the underside of each beam. A small diamond-blade saw was used for this purpose, giving a very smooth surface and a crack width of approximately 1/8 inch (3 mm). The depths of the notches were such that the ratio of the notch depth to the beam depth varied between 0.5 and 0.65. The notch tip was sharpened using a 24 teeth/in (1 tooth/mm) hacksaw blade just before testing.

Values of J_{1c} were determined as follows:

1. The total energy to failure, U_T, was calculated by summing the area under the load-deflection diagram, up to the point of maximum load, as shown in figure 31. Failure was defined by the maximum load. The area was summed using the acquired data and the trapezoidal rule for determining the area under a curve.

2. U_T/b, the energy per unit thickness, was then plotted against notch depth, as shown in figure 34. The slope $(1/b)(dU_T/da)$, was obtained through regression. This procedure was repeated for each test temperature and mixture.

3. The critical strain-energy release values, J_{1c}, were then determined for each test temperature from the slope of the energy versus notch length plots (figure 34) using equation 37.

The results of the fracture testing for each beam are given in table 19 as the energy per unit thickness, U_T/b, that was necessary to fail the beam. The results of the J_{1c} calculations for the individual mixes are summarized in table 20.

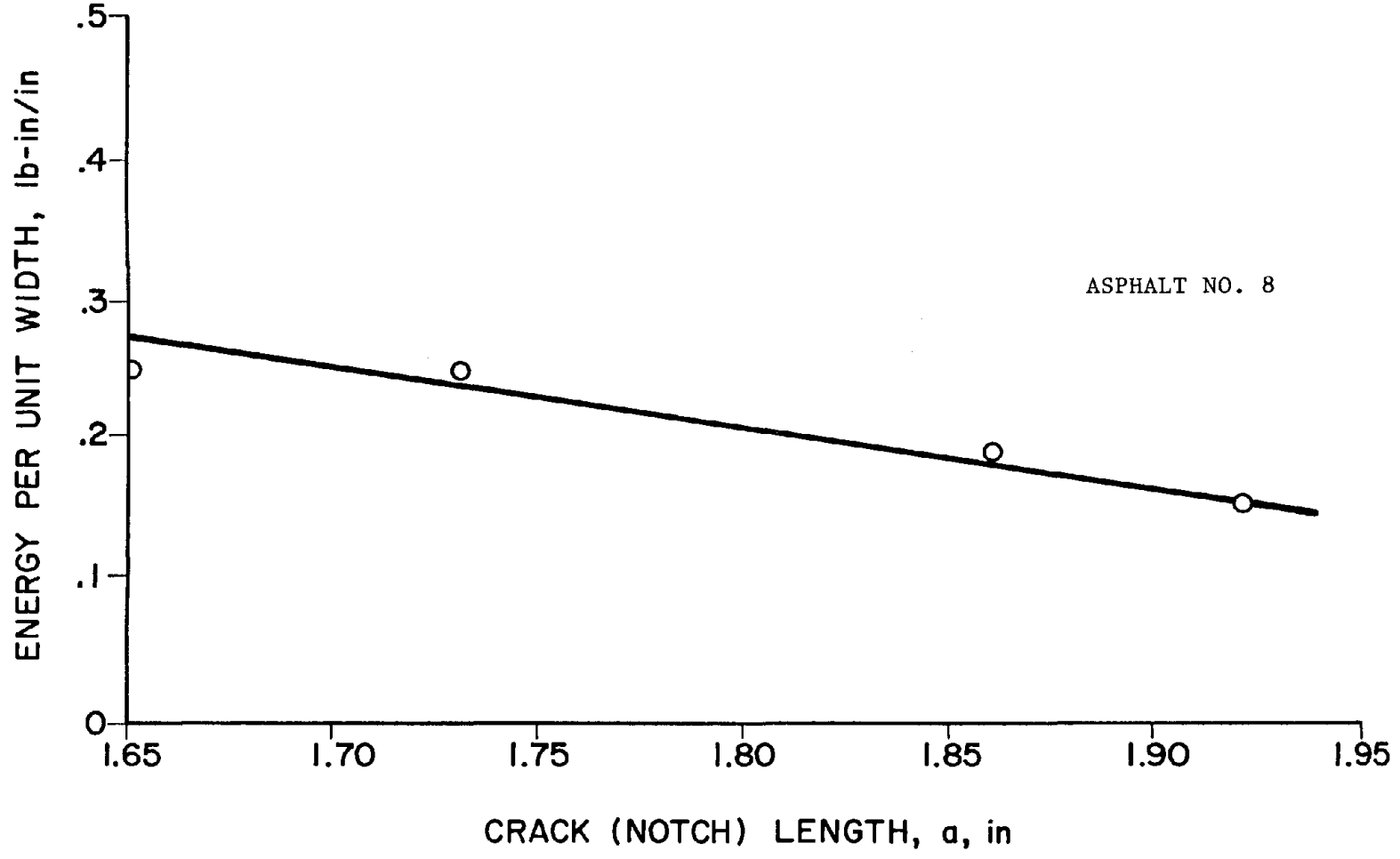

Figure 34. Typical plot of energy versus notch depth, asphalt No. 8.

Table 19. Energy to fracture data for notched beams.

Asphalt Number	-5 °F		8 °F		10 °F		15 °F	
	Crack Length, in	Energy, U_t/width, lb/in	Crack Length, in	Energy, U_t/width, lb/in	Crack Length, in	Energy, U_t/width, lb/in	Crack Length, in	Energy, U_t/width, lb/in
1	1.45	0.42	NT	NT	NT	NT	1.50	0.88
	1.70	0.39	NT	NT	NT	NT	1.71	0.70
	1.85	0.46	NT	NT	NT	NT	1.85	0.33
2	1.55	0.62	NT	NT	1.48	0.86	NT	NT
	1.65	0.47	NT	NT	1.69	0.74	NT	NT
	1.83	0.42	NT	NT	1.85	0.56	NT	NT
4	1.50	0.57	NT	NT	1.50	0.78	NT	NT
	1.75	0.35	NT	NT	1.75	0.46	NT	NT
	1.92	0.21	NT	NT	1.92	0.27	NT	NT
5	1.42	0.53	NT	NT	1.50	0.91	NT	NT
	1.70	0.27	NT	NT	1.75	0.53	NT	NT
	1.95	0.19	NT	NT	2.00	0.34	NT	NT
7	1.50	0.69	NT	NT	NT	NT	1.50	0.52
	1.72	0.22	NT	NT	NT	NT	1.68	0.65
	2.00	0.26	NT	NT	NT	NT	1.91	0.37
8	1.66	0.22	1.65	0.25	NT	NT	NT	NT
	1.75	0.16	1.73	0.25	NT	NT	NT	NT
	1.86	0.12	1.86	0.19	NT	NT	NT	NT
	1.91	0.16	1.92	0.15	NT	NT	NT	NT
11	1.50	0.36	NT	NT	1.50	0.20	NT	NT
	1.73	0.24	NT	NT	1.72	0.20	NT	NT
	1.82	0.37	NT	NT	1.92	0.28	NT	NT
12	1.52	0.60	NT	NT	1.50	0.65	NT	NT
	1.68	0.71	NT	NT	1.70	0.52	NT	NT
	1.85	0.60	NT	NT	1.85	0.59	NT	NT
13	1.63	0.82	1.52	0.91	NT	NT	NT	NT
	1.70	0.42	1.60	0.81	NT	NT	NT	NT
	1.80	0.41	1.72	0.88	NT	NT	NT	NT
			1.80	0.66	NT	NT	NT	NT
14	1.49	0.56	NT	NT	1.40	1.70	NT	NT
	1.68	0.69	NT	NT	1.68	0.61	NT	NT
	1.85	0.48	NT	NT	1.93	0.53	NT	NT
16	1.50	0.33	NT	NT	NT	NT	1.59	0.52
	1.75	0.20	NT	NT	NT	NT	1.66	0.44
	1.85	0.25	NT	NT	NT	NT	1.92	0.21
17	1.55	0.34	NT	NT	1.55	0.98	NT	NT
	1.70	0.32	NT	NT	1.67	0.62	NT	NT
	1.89	0.35	NT	NT	1.90	0.47	NT	NT

Note: NT indicates that no tests were conducted for this asphalt at this temperature. Tests were conducted at four temperatures. The test temperatures were selected according to the stiffness of the asphalt concrete.

Table 19. Energy to fracture data for notched beams (continued).

Asphalt Number	25 °F		40 °F		60 °F	
	Crack Length, in	Energy, U_t/width, lb/in	Crack Length, in	Energy, U_t/width, lb/in	Crack Length, in	Energy, U_t/width, lb/in
1	NT	NT	1.50	1.41	1.47	7.03
	NT	NT	1.64	0.92	1.64	5.05
	NT	NT	1.93	0.64	1.91	3.59
2	1.50	0.84	1.48	9.38	NT	NT
	1.75	0.72	1.69	7.28	NT	NT
	1.88	0.69	1.89	5.84	NT	NT
4	1.45	1.35	1.50	1.27	NT	NT
	1.70	0.67	1.70	1.09	NT	NT
	2.02	0.30	2.00	0.73	NT	NT
5	1.48	1.21	1.50	4.11	NT	NT
	1.65	0.80	1.69	4.18	NT	NT
	2.00	0.37	1.95	1.45	NT	NT
7	NT	NT	1.51	1.07	1.50	6.58
	NT	NT	1.70	0.85	1.75	3.54
	NT	NT	1.98	0.64	1.98	3.82
8	1.65	0.52	1.45	1.07	1.50	3.52
	1.73	0.37	1.69	0.74	1.62	3.77
	1.80	0.40	1.79	0.49	1.82	3.20
	1.90	0.37	1.90	0.46	1.90	1.94
11	1.50	1.00	1.50	0.93	NT	NT
	1.70	0.91	1.69	0.69	NT	NT
	1.82	0.48	1.95	0.55	NT	NT
12	1.42	1.21	1.55	4.91	NT	NT
	1.70	1.26	1.78	4.43	NT	NT
	1.90	0.81	1.90	5.00	NT	NT
13	1.60	4.19	1.60	5.88	NT	NT
	1.70	3.20	1.89	3.63	NT	NT
	1.95	2.09	2.00	2.61	NT	NT
14	1.41	1.45	1.53	9.14	NT	NT
	1.65	0.84	1.70	5.93	NT	NT
	1.95	0.48	1.88	3.86		
16	NT	NT	1.58	1.01	1.50	7.47
	NT	NT	1.71	1.00	1.70	5.22
	NT	NT	1.93	0.65	1.93	3.75
17	1.45	0.86	1.50	4.43	NT	NT
	1.69	0.82	1.68	2.45	NT	NT
	1.90	0.42	1.92	1.67	NT	NT

Note: NT indicates that no tests were conducted for this asphalt at this temperature. Tests were conducted at four temperatures. The test temperatures were selected according to the stiffness of the asphalt concrete.

Table 20. Summary of J-integral data for notched beams.

Asphalt No.	J_{1c}, in-lb/in^2						
	-5 °F	8 °F	10 °F	15 °F	25 °F	40 °	60 °F
1	0.66	NT	NT	1.50	NT	1.67	7.67
2	0.66	NT	0.81	NT	0.49	8.64	NT
4	0.45	NT	1.22	NT	1.80	1.09	NT
5	0.64	NT	1.14	NT	1.56	6.20	NT
7	0.82	NT	NT	0.40	NT	0.90	5.85
8	0.28	0.39	NT	NT	NT	1.45	3.57
11	0.10	NT	NA	NT	1.51	0.81	NT
12	0.20	NT	0.21	NT	0.76	2.09	NT
13	0.13	0.66	NT	NT	5.71	7.74	NT
14	0.20	NT	2.24	NT	1.77	2.58	NT
16	0.28	NT	NT	0.95	NT	1.10	8.58
17	0.15	NT	1.37	NT	1.91	6.39	NT

Note: NT indicates that no tests were conducted at this temperature for this asphalt cement.

NA indicates that the test data were not considered valid at this temperature for this asphalt cement.

4.9 CALCULATED PARAMETERS

A wide variety of temperature-susceptibility and other parameters have been proposed by various researchers. These calculated parameters, etc., were calculated from the laboratory data. Values for each of these parameters, along with the method of calculation, are given in appendix E. These parameters were used in the data analysis, as described in chapter 6.

5. PREDICTION OF THERMAL CRACKING USING SELECTED MODELS AND PROCEDURES

A review of the models that have been developed by others for predicting thermal cracking was presented in chapter 3. Two computer models, programs TC-1 and THERM, and the Hills nomographic procedure, were selected for further study. The rationale for choosing these models and the results of their application to the data obtained from this project are discussed below. In the next chapter the cracking predicted from these models is compared with the cracking and temperature-susceptibility indices that were developed in chapter 4.

The ideal thermal cracking model should possess the following attributes:

- The model must be based on mechanistic analysis so that the model can be reliably extrapolated to new conditions.
- The model must be based on fundamental engineering properties of the asphalt cement and asphalt mixture.
- The model must be capable of predicting thermal fatigue as well as low-temperature shrinkage cracking.
- The model must predict cracking in terms of performance indicators, such as cracking indices, rather than an expected cracking temperature. Predictions of the severity of the cracking with increasing service life are also needed.
- The model must be accurate and not overly sensitive to one or more of the input parameters.

These criteria were used in the selection of the models that were recommended for further consideration as producing reference data for the evaluation of temperature susceptibility parameters and their surrogates, and for inclusion in a field verification study.

5.1 MODELS AND PROCEDURES SELECTED FOR PREDICTING THERMAL CRACKING

Table 3 summarizes the five available computer programs that were investigated. Although not computer based, the Hills procedure, when presented in nomographic form, is very simple to use.[41] Incremental stress/strain calculations form the basis for this method. Hills' method,

which was the basis for the Asphalt Institute design procedure, considers only the asphalt cement, excluding any consideration of mix properties such as air voids and maximum aggregate size. The method gives only the temperature at which cracking is likely to occur and not the time or extent of cracking. The Hills procedure was included in this study primarily because of its simplicity and because it is solely dependent upon asphalt properties. It was felt that comparing the critical temperatures found using Hills' nomograph with the results of the computer models would provide useful information on the effects of the various submodels used in the more complex computer programs.

The Shahin-McCullough program (TC-1) and Lytton's program (THERM) predict the cracking index as a function of time.[38,59] In contrast, the COLD program, the Ruth model, and the Hills procedure predict critical temperatures or stiffnesses at which cracking can be anticipated.[39,40,41] Programs THERM and TC-1 also include provision for asphalt aging effects, which may be very important because aging occurs at varying rates and may dramatically affect asphalt stiffness.

The Hajek-Haas model, although a relatively unsophisticated statistical model, has been effective in predicting low-temperature cracking in northern climates. The Hajek-Haas model was not selected for further study because it is empirical, does not account for thermal fatigue, and does not predict the extent of cracking as a function of time.

As summarized in table 3, and discussed previously, programs TC-1 and THERM are two of the more inclusive programs in that they take into account the specific material properties of the asphalt, aging effects, mixture strength, and both low-temperature cracking and thermal fatigue. However, programs TC-1 and THERM differ in the techniques used to predict cracking as a function of time or temperature. Program COLD is also inclusive and based on many of the same assumptions as program TC-1. Programs TC-1 and COLD use some of the same concepts and both are mechanistic/empirical. Program THERM is also based on a mechanistic/empirical model, but uses a fracture mechanics approach, whereas TC-1 and program COLD are based on purely elastic systems. A serious deficiency of program COLD is that it does not predict the time to cracking, predicting instead a cracking temperature.

Programs TC-1 and THERM were recommended for use with the test data obtained from this project because each uses some of the same variables, but the predictions are based on different techniques (elastic beam versus fracture mechanics). Ruth's model was not selected because it has not been verified in the field, as have programs TC-1 and THERM.

The following asphalt cement or asphalt concrete properties are required for the use of TC-1, THERM, or Hills' procedure:

- Asphalt cement or mixture stiffness versus temperature for a loading time of 7,200 s, static compression modulus, lb/in^2 (Pa).
- Original penetration of the asphalt at 77 °F (25 °C).
- Original ring and ball softening point temperature of the asphalt, °F (°C).
- Thin film oven test, percent weight loss.
- Kinematic viscosity at 275 °F (135 °C), cSt.
- Indirect tensile strength, lb/in^2 (Pa), versus temperature, °F (°C).

5.2 APPLICATION OF THE MODELS TO THE PROJECT DATA

The data obtained in the laboratory were used to predict the cracking potential of each of the asphalt cements. Hills' procedure was applied to the complete set of 17 asphalts because mixture data are not required for this procedure. The results of this procedure are shown in table 21 along with a numerical ranking of the predicted limiting stiffness temperature. In general the results are as expected: for a given source of asphalt, the cracking temperature increased with grade in accordance with increases in the relative stiffness of the asphalt. The waxy asphalt, No. 17, had one of the lowest predicted cracking temperatures, -45 °F (-43 °C), but after being air blown (now called No. 16), this asphalt sample had one of the highest predicted cracking temperatures, -18 °F (-28 °C).

The data obtained from this study were used with TC-1 and THERM to predict the cracking temperatures of mixtures made with each asphalt. Minimum

Table 21. Predicted cracking temperatures for asphalts tested as part of this project; Hills' procedure.

Asphalt Number	Source	Limiting Stiffness Temperature, °F	Susceptibility to Cracking, Rank (best to worst)
1	A	-29	11
2	B	-42	4
3	B	-35	7
4	B	-26	12
5	C	-31	9
6	C	-24	13
7	C	-22	15
8	D	-15	17
9	E	-36	5
10	E	-31	9
11	E	-24	13
12	F	-47	2
13	G	-49	1
14	G	-36	6
15	H	-35	7
16	I	-18	16
17	I	-45	3

pavement temperatures calculated as part of a previous study for six different locations were used in these predictions:[44]

- Albany, New York (ALBY), minimum pavement temperature, 6 °F (-14 °C).
- Dallas-Fort Worth, Texas (DFW), minimum pavement temperature, 30 °F (-1 °C).
- Fargo, North Dakota (FARGO), minimum pavement temperature, -9 °F (-23 °C).
- Phoenix, Arizona (PHX), minimum pavement temperature, 31 °F (-1 °C).
- Spokane, Washington (SPKN), minimum pavement temperature, 10 °F (-12 °C).
- Tallahassee, Florida (TALL), minimum pavement temperature, 39 °F (4 °C).

Cracking indices predicted with TC-1 are given in table 22. These indices were predicted for the six locations listed above. Because mixture data are required for TC-1, predictions were made only for the 12 asphalt cements for which mixture data were obtained. All of the asphalts, even the AC-5 grades, showed some cracking for the Fargo, North Dakota, location although, in some cases, the cracking was minimal. Only the asphalt from source 7 showed significant cracking at the Albany, New York, location; the TC-1 program predicted that no cracking would occur at the other sites. The ranking with regard to the severity of cracking was approximately the same for the Fargo and the Albany locations.

The data given in table 22 are shown graphically in figure 35, where the total predicted cracking after 10 years is plotted versus the minimum pavement temperature for Spokane, Washington; Albany, New York; and Fargo, North Dakota. This plot presents a pictorial ranking of the asphalts with regard to cracking severity. Asphalt No. 7, an AC-20, is known to be a poor performer and exhibits severe cracking in West Texas. The corresponding AC-5 grade, asphalt No. 5, showed little cracking, which is in agreement with the field experience with this asphalt.

Asphalt No. 1, which is used in Montana, also has a poor field performance record with regard to thermal cracking. The poor performance

Table 22. Predicted cracking indices for asphalt concrete tested as part of this project; TC-1 model.

Asphalt Number	Location Code	Cracking Index, ft/1000 ft^2									
		Years after construction									
		1	2	3	4	5	6	7	8	9	10
1	Albany							.02	.08	.26	.73
	Dallas-Ft. Worth										.00
	Fargo	.04	.23	.98	2.37	4.76	8.35	13.10	19.35	28.45	38.97
	Phoenix										.00
	Spokane									.02	.10
	Tallahasee										.00
2	Albany									.03	.10
	Dallas-Ft. Worth										.00
	Fargo	.01	.04	.08	.17	.52	1.27	2.63	4.99	9.09	14.99
	Phoenix										.00
	Spokane										.01
	Tallahasee										.00
4	Albany										.00
	Dallas-Ft. Worth										.00
	Fargo		.00	.01	.02	.01	.03	.10	.24	.47	.82
	Phoenix										.00
	Spokane										.00
	Tallahasee										.00
5	Albany										.00
	Dallas-Ft. Worth										.00
	Fargo		.00	.02	.12	.36	.77	1.42	2.57	4.13	6.42
	Phoenix										.00
	Spokane										.00
	Tallahasee										.00
7	Albany				.00	.01	.08	.30	1.04	3.07	7.50
	Dallas-Ft. Worth										.00
	Fargo	.22	1.13	2.77	5.35	9.68	16.75	26.70	40.08	56.86	74.13
	Phoenix										.00
	Spokane					.00	.00	.04	.19	.75	2.50
	Tallahasee										.00
8	Albany										.00
	Dallas-Ft. Worth										.00
	Fargo	.08	.03	.03	.08	.12	.17	.21	.24	.27	.30
	Phoenix										.00
	Spokane										.00
	Tallahasee										.00

Table 22. Predicted cracking indices for asphalt concrete tested as part of this project; TC-1 model (continued).

Asphalt Number	Location Code	Cracking Index, ft/1000 ft^2 — Years after construction 1	2	3	4	5	6	7	8	9	10
11	Albany										.00
	Dallas-Ft. Worth										.00
	Fargo		.00	.01	.01	.00	.01	.03	.07	.15	.29
	Phoenix										.00
	Spokane										.00
	Tallahasee										.00
12	Albany								.00	.02	.10
	Dallas-Ft. Worth										.00
	Fargo	.00	.16	.39	.57	1.15	3.07	6.00	10.30	16.14	23.39
	Phoenix										.00
	Spokane										.00
	Tallahasee										.00
13	Albany										.00
	Dallas-Ft. Worth										.00
	Fargo	.00	.05	.21	.43	.61	.75	1.27	2.50	4.43	7.50
	Phoenix										.00
	Spokane										.00
	Tallahasee										.00
14	Albany										.00
	Dallas-Ft. Worth										.00
	Fargo	.00	1.07	2.84	1.50	.32	.77	1.23	1.63	2.03	2.03
	Phoenix										.00
	Spokane										.00
	Tallahasee										.00
16	Albany										.00
	Dallas-Ft. Worth										.00
	Fargo	.00	.00	.03	.07	.12	.21	.34	.61	1.10	2.08
	Phoenix										.00
	Spokane										.00
	Tallahasee										.00

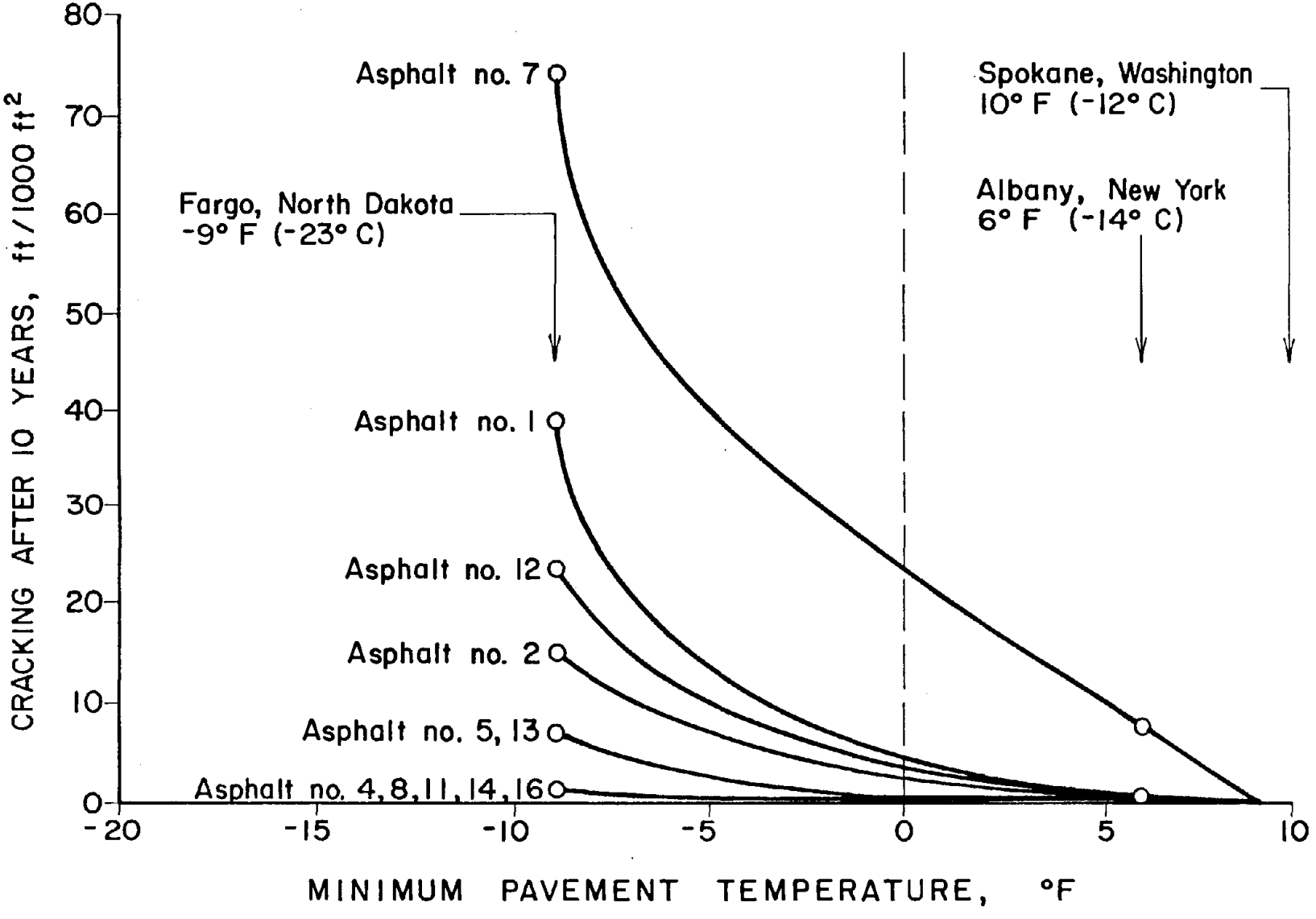

Figure 35. Cracking index after 10 years service predicted from TC-1 versus minimum pavement temperature at test site.

record of asphalt No. 12 in California is verified by its position on the graph. Asphalt No. 4, from a source supplied to Pennsylvania, has shown slight cracking tendencies in the field in Pennsylvania. For this asphalt TC-1 predicts minimal cracking only for Fargo, North Dakota, which is a significantly colder climate than Pennsylvania.

Some anomalies present in the results for the remaining asphalts can be explained by the fact that program TC-1 uses stiffness values estimated from Van der Poel's nomograph, and not measured stiffness values. Furthermore, the TC-1 program uses original asphalt stiffness and an empirical model to predict asphalt stiffness as a function of service life.

The cracking indices predicted by program THERM were unrealistically large. The erroneous results were traced to the unrealistic pavement temperatures predicted by the program's temperature subroutine.[87] The iteration procedure in this subroutine must be modified before the program will qualify for general use. Efforts to correct the program were unsuccessful, and the results from the program were used with reservation in the analyses that follow. Because of its rational basis, this program has the best potential for future development but should be modified extensively to include an energy approach to characterize fracture, direct measurements of fracture parameters and stiffness values, and a revised aging algorithm. Program THERM also uses the same aging model as TC-1, and this contributes to the unrealistic values predicted by both models.

5.3 COMPARISON OF MODELS AND SENSITIVITY ANALYSIS

A comparison of the cracking indices predicted by TC-1 for the various asphalts at Fargo, North Dakota, 10 years after construction, and the cracking temperature from the Hills procedure is shown in figure 36. In this figure, the asphalts that exhibit severe thermal cracking in the field are shown with a filled circle; moderate cracking, with a half-filled circle; and little or no cracking, with an open circle. Two distinct sets of data are shown: those close to the drawn line and those close to the temperature axis. Asphalt No. 7 is known as a poor performer with respect to thermal fatigue cracking; however, Hills' procedure does not account for thermal fatigue. Asphalt No. 1

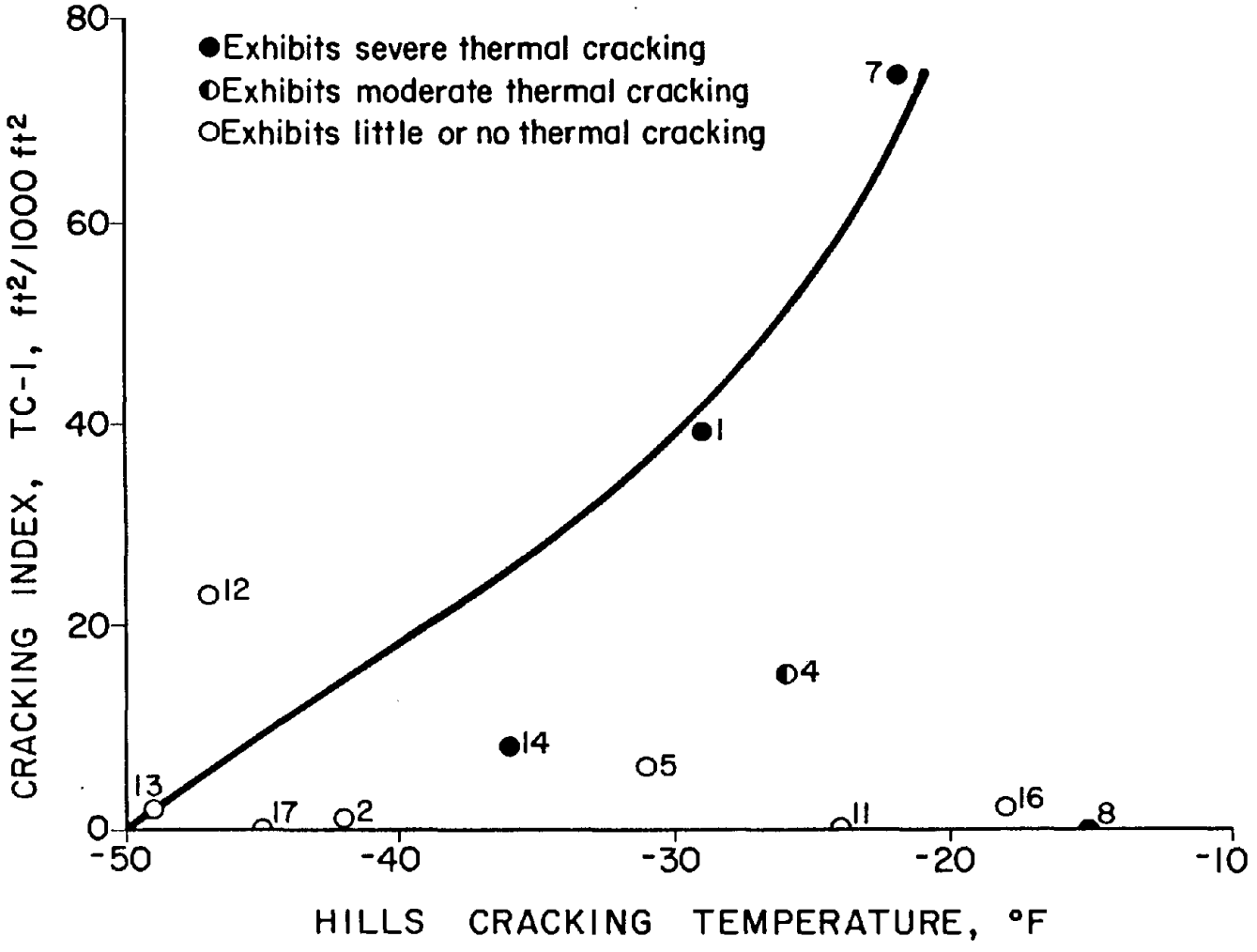

Figure 36. Cracking index predicted by TC-1 versus Hills' cracking temperature.

performs poorly in Montana and is shown as such by both procedures. In general, the ranking offered by TC-1 and Hills' procedure is not in the same order. For example, asphalt No. 12 does not exhibit thermal cracking in the field and asphalt No. 8 exhibits severe cracking in the field. These inconsistencies can be explained by the influence of the aging model in TC-1 and the lack of an aging model and thermal fatigue considerations in the Hills procedure.

A sensitivity analysis was conducted with TC-1 by allowing the original penetration, softening point, and percent retained penetration (appendix E) to assume the measured mean as well as $\pm$ 1 standard deviation from the mean. Standard deviation values were obtained from the respective ASTM specifications, and, in each case, these values were somewhat larger than those measured during the study. The following standard deviation values were obtained from the respective specifications:

- Penetration, ASTM D5: 2.8 percent of the mean for penetration values equal to or greater than 50 penetration units (0.1 mm) and $\pm$ 1.4 penetration units (0.1 mm) for penetrations less than 50 penetration units (0.1 mm)
- Ring and ball softening point temperature, ASTM D36: $\pm$ 2.3 °F ($\pm$ 1.3 °C)

No precision statements are presented by ASTM for the percentage of retained penetration for rolling thin-film oven residue. As a conservative estimate, multilaboratory standard deviations for penetration were applied to the measured penetration for the RTFOT residue for each of the two asphalts. The three resulting values for penetration, corresponding to the mean and $\pm$ 1 standard deviation from the mean, were then divided by the measured penetration of the unaged asphalt, giving three values for retained penetration. To maintain consistency throughout the analysis, these same values for percentage of retained penetration were used for each of the nine combinations of unaged penetration and ring and ball softening point temperature.

Allowing the three variables to assume three values (mean, mean +1 standard deviation, mean -1 standard deviation) gave 27 combinations of

input values, shown in table 23. These combinations were used with TC-1 to predict the 27 cracking indices shown in table 23. Two asphalts, No. 2 and 7, were used in the analysis. No. 7 is highly susceptible to cracking, whereas No. 2, a soft AC-5 grade, is highly resistant to cracking. The results of the sensitivity analysis are shown in table 23. To better illustrate the effects of variation in each of the variables, two-way interaction plots are shown in figures 37 and 38. These were obtained by averaging the cracking indices for one of the variables and plotting the individual values for the remaining two variables. For example, in figure 38, for each percent retained penetration (-1 standard deviation, mean, +1 standard deviation) and each penetration (-1 standard deviation, mean, +1 standard deviation) there are three values of ring and ball softening point temperature. The three predicted cracking index values for the three ring and ball softening point temperatures were averaged, giving the nine data points shown in figure 38.

A $\pm$1 standard deviation error in any of the three variables had little effect on the soft asphalt, No. 2. However, a much different pattern emerges for asphalt No. 7. In this case the percent retained penetration has a very large effect, seen in figures 37 and 38, much greater than would be expected, further evidencing the need to re-evaluate the aging model in TC-1. The decrease in cracking index with increasing softening point temperature seen in figure 37 may at first seem anomalous. However, this is explained by the decrease in temperature susceptibility which occurs with increasing softening point temperature at a given value for penetration. This decrease in temperature susceptibility results in lower estimated stiffnesses at low temperatures, and hence lower cracking indices, even though the asphalt consistency is stiffer at high temperatures, as indicated by the softening point temperature.

In summary, the authors are not satisfied with any of the cracking models:

- The assumptions inherent in the Hills procedure are unrealistic; the procedure ignores mixture variables, cannot be used for thermal fatigue, and does not predict time to cracking.
- The aging model in TC-1 must be updated, and the updated model should be verified in the field with a new data set.

Table 23. Results of sensitivity analysis for TC-1.

Penetration at 77 °F 0.1 mm		Softening Point Temperature, °F		Retained Penetration, percent		Cracking Index ft/1000 ft^2	
No. 2	No. 7	No. 2	No. 7	No. 2	No. 7	No. 2	No. 7
184	58	100	118	49	54	6.7	139
184	58	100	118	51	57	2.5	81
184	58	100	118	52	59	1.1	41
184	58	102	120	49	54	3.7	124
184	58	102	120	51	57	1.2	80
184	58	102	120	52	59	0.4	31
184	58	104	122	49	54	2.3	125
184	58	104	122	51	57	0.6	70
184	58	104	122	52	59	0.2	15
189	60	100	118	49	54	2.8	133
189	60	100	118	51	57	0.9	77
189	60	100	118	52	59	0.4	38
189	60	102	120	49	54	2.6	121
189	60	102	120	51	57	0.8	74
189	60	102	120	52	59	0.3	26
189	60	104	122	49	54	1.2	121
189	60	104	122	51	57	0.3	62
189	60	104	122	52	59	0.1	14
194	62	100	118	49	54	2.1	127
194	62	100	118	51	57	0.6	73
194	62	100	118	52	59	0.2	34
194	62	102	120	49	54	1.6	117
194	62	102	120	51	57	0.5	69
194	62	102	120	52	59	0.2	22
194	62	104	122	49	54	0.5	116
194	62	104	122	51	57	0.1	54
194	62	104	122	52	59	0.0	13

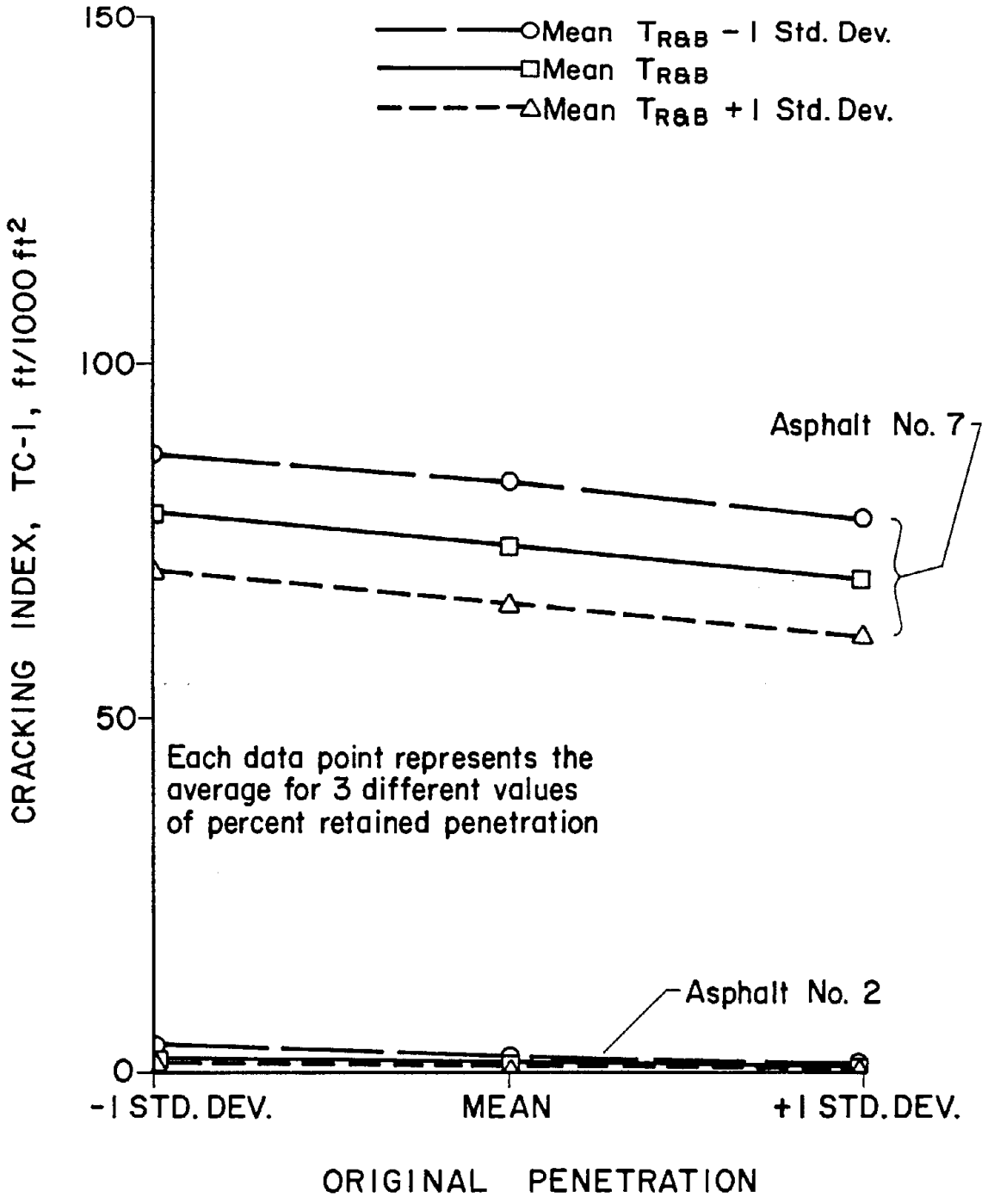

Figure 37. Interaction diagram for TC-1 cracking indices versus penetration averaged over percent retained penetration.

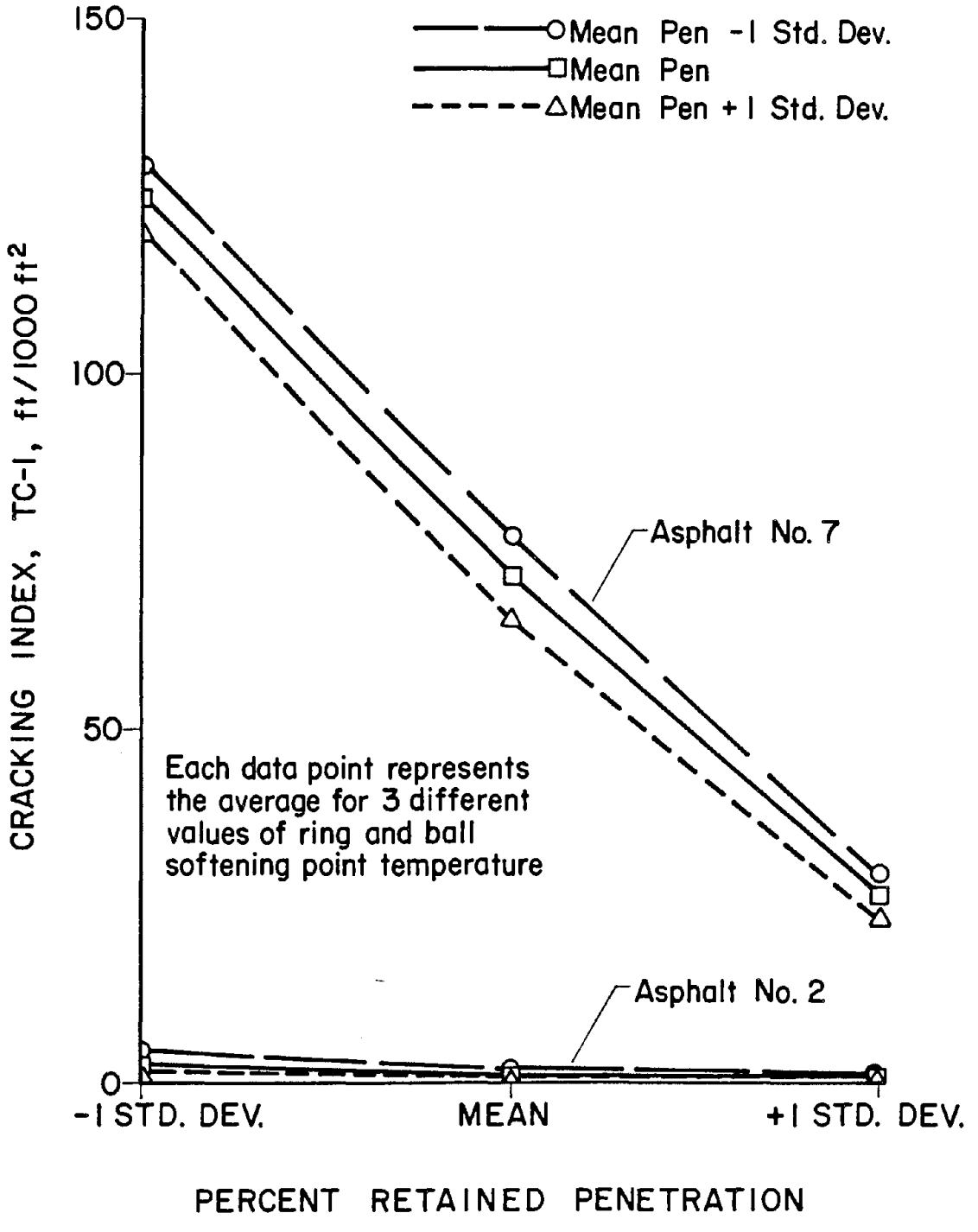

Figure 38. Interaction diagrams for TC-1 cracking indices versus penetration averaged over ring and ball softening point temperature.

- THERM is not workable in the form in which it was supplied to the authors. The aging model suffers the same deficiency as the aging model used in TC-1, and the procedure for calculating pavement temperature is unreliable. THERM has the greatest potential of any of the models, but measured properties should be substituted for the predicted values that are currently used in the program. The revised version of THERM model should be included in the field verification study because of the promise that it offers if future refinements are made.

6. ANALYSIS OF LABORATORY DATA

The laboratory testing program was specifically designed to address a number of questions:

- Are measures such as T_g and HP-GPC acceptable surrogates for asphalt stiffness or mechanical properties in ranking susceptibility to cracking?
- Are indirect estimates of stiffness (nomographic methods) acceptable surrogates for direct measurements?
- Are PVN and PI interchangeable as estimates of temperature susceptibility and thermal cracking?

6.1 STATISTICAL APPROACH

The analysis of the data required to answer the above and other questions was complicated by the number of tests, variables, models, and asphalts and asphalt concrete mixtures that were involved. To provide a meaningful analysis, extensive use was made of correlation matrices and linear regression.

A correlation matrix is a matrix that contains the correlation coefficients for linear regression, R, for all pairs of variables in the matrix. As such, the correlation matrix can be used to identify variables that show a high degree of correlation when paired with any of the other variables in the marix and to select variables that warrant further analysis. Initially, 30 of the variables that were either measured or calculated were identified by the research team as justifiable variables in the statistical analysis. The 30 variables are listed in table 24. To reduce the number of variables to a more manageable number, the variables that did not have at least one correlation coefficient, R, greater than 0.81 were excluded from further analysis and are so indicated in table 24 by an asterisk. Variables with at least one R value greater than 0.81 were retained for further analysis; T_{vis4GP} was retained even though its largest R value was 0.79. This was done so that an equiviscous temperature determined from viscosity measurements alone would be included in the subsequent analysis. It should be pointed out that, except as noted, all of the neat asphalt cement analysis in this chapter was done with RTFOT residue.

Table 24. List of variables used in initial correlation matrix.

1.* Asphalt viscosity grade, or for residual and penetration graded asphalts, nearest viscosity grade as indicated by test data.

2. Fraass brittle point temperature; °F (°C), T_{Fraass}.

3.* Log-penetration temperature susceptibility: slope of best-fit line on a plot of log-penetration versus temperature in °C; A.

4.* Penetration index based on ring and ball softening point temperature and penetration at 77 °F (25 °C); PI.

5.* Penetration index based on log-penetration data; $PI_{log-pen}$.

6.* Penetration index based on Fraass brittle point temperature and penetration at 77 °F (25 °C); PI_{Fraass}.

7.* Penetration-viscosity number based on viscosity at 140 °F (60 °C) and penetration at 77 °F (25 °C); PVN_{140}.

8.* Penetration-viscosity number based on viscosity at 275 °F (135 °C) and penetration at 77 °F (25 °C); PVN_{275}.

9.* Viscosity temperature susceptibility: slope of line through log log-viscosity (cSt) versus log absolute temperature (°R); VTS.

10.* Viscosity ratio: ratio of viscosity at 140 °F (60 °C) to viscosity at 275 °F (135 °C), in consistent units; R_{η}.

11. Temperature, °F, where the penetration is 1.2, as estimated from log-penetration versus temperature data; $T_{pen1.2}$.

12. Temperature, °F, where the viscosity is 4.0 GP, as estimated from log log-viscosity versus log absolute temperature data; T_{vis4GP}.

13. Temperature, °F, at a stiffness of 1.0 GPa at 30 min, as estimated from Van der Poel's nomograph using ring and ball softening point temperature and PI to enter the nomograph; T_{1GPA}.

14. Temperature, °F, at a stiffness of 1.0 GPa at 30 min, as estimated from Van der Poel's nomograph and using T_{Pen800} and $PI_{log-pen}$ to enter the nomograph; T_{1GPa}.

NOTES: Equations and calculated values for derived parameters are listed in appendix E. All variables for neat asphalts are for RTFOT residue. Variables marked with an asterisk did not correlate well with any other variables ($R < 0.80$) and were excluded from further statistical analysis.

Table 24. List of variables used in initial correlation matrix (continued).

15. Temperature, °F, at a stiffness of 1.0 GPa at 30 min, as estimated from Van der Poel's nomograph and using $T_{Pen800F}$ and PI_{Fraass} to enter the nomograph; T_{1GPa}.

16. Temperature, °F, at a stiffness of 200 MPa at 2 h, as estimated from Van der Poel's nomograph using ring and ball softening point and PI to enter the nomograph; T_{200MPa}.

17. Temperature, °F, at a stiffness of 200 MPa at 2 h as estimated from Van der Poel's nomograph using T_{Pen800} and $PI_{log-pen}$ to enter the nomograph; T_{200MPa}.

18. Temperature, °F, at a stiffness of 200 MPa at 2 h as estimated from Van der Poel's nomograph using $T_{Pen800F}$ and PI_{Fraass} to enter the nomograph; T_{200MPa}.

19. Temperature, °F, at a stiffness of 200 MPa at 2 h as estimated from McLeod's modification of Heukelom and Klomp's version of Van der Poel's nomograph, using the base temperature and PVN_{140} to enter the nomograph; T_{200MPa}.

20. Hills cracking temperature: temperature, °F, at which pavement cracking is expected, found using a nomograph produced by the Asphalt Institute[37] based on incremental stress and strain calculations first proposed by Hills and Brien; T_H.

21.* Percent large molecular size, as found in Montana HP-GPC tests; LMS.

22.* Number average molecular weight, as found in Penn State HP-GPC tests; $\bar{M}_n$.

23.* Weight average molecular weight, as found in Penn State HP-GPC tests; $\bar{M}_w$.

24.* Polydispersity index: ratio of weight average to number average relative molecular weight, as found in Penn State HP-GPC testing; PDI.

25.* Glass transition temperature, from differential scanning calorimetry, lowest observed transition temperature, °F; T_g.

26.* Glass transition temperature, from dynamic mechanical analysis, temperature, °F, at observed peak in loss modulus; T_g.

27. Mix tensile strength temperature shift: temperature, °F, at a mixture tensile strength of 300 lb/in^2 (2.1 MPa) and 32 °F (0 °C), measured in indirect tension at a loading rate of 0.10 in/min (2.5 mm/min).

NOTES: Equations and calculated values for derived parameters are listed in appendix E. All variables for neat asphalts are for RTFOT residue. Variables marked with an asterisk did not correlate well with any other variables ($R < 0.80$) and were excluded from further statistical analysis.

Table 24. List of variables used in initial correlation matrix (continued).

28.	Mix modulus temperature shift: temperature, °F, at a mixture static modulus of 730,000 lb/in^2 (5.0 GPa) and 32 °F (0°C), measured in indirect tension at a loading rate of 0.1 in/min (2.5 mm/min).
29.*	Cracking index as predicted by program TC-1, ft/1000 ft^2.
30.*	Cracking index as predicted by program THERM, ft/1000 ft^2.

NOTES: Equations and calculated values for derived parameters are listed in appendix E. All variables for neat asphalts are for RTFOT residue. Variables marked with an asterisk did not correlate well with any other variables ($R < 0.80$) and were excluded from further statistical analysis.

The characteristic temperatures, which include limiting stiffness, equiviscous and cracking temperatures, with correlation coefficients greater than 0.81, were used to construct the correlation matrix shown in table 25. Included in table 25 are T_{vis4GP}, $T_{Penl.2}$, Fraass brittle point temperature, temperature shifts based on mixture tensile strength and static modulus, and seven different limiting stiffness temperatures. These seven temperatures were found by specifying two values of limiting stiffness--145,000 lb/in^2 (1.0 GPa) at 30 min and 29,000 lb/in^2 (200 MPa) at 2 h--and by using either Van der Poel's nomograph or McLeod's modification of Heukelom and Klomp's version of Van der Poel's nomograph as follows:

- Van der Poel's nomograph used with $T_{R\&B}$ and PI as entrance parameters.
- Van der Poel's nomograph used with $T_{Pen800F}$ and $PI_{log-pen}$ as entrance parameters.
- Van der Poel's nomograph used with T_{Pen800} and PI_{Fraass} as the entrance parameters.
- McLeod's modification of Heukelom and Klomp's version of Van der Poel's nomograph used with the base temperature, T_B, and PVN_{140} as entrance parameters. Because this nomograph only extends to temperature 180 °F (100 °C) below the softening point, limiting stiffness temperatures for 145,000 lb/in^2 (1.0 GPa) at 30 min could not be calculated for this method. As a consequence only seven limiting stiffness temperatures are shown in table 25.

The average correlation coefficient for each parameter is shown at the bottom of table 25. Mixture tensile strength temperature shifts showed the largest average correlation coefficient, 0.83. The temperature at a viscosity of 4.0 GP, T_{vis4GP}, showed the smallest average correlation coefficient, 0.51, and none of the correlations containing T_{vis4GP} as one of the variables showed a correlation coefficient greater than 0.79 (R^2 greater than 0.62).

Linear regression techniques were used with pairs of the characteristic temperature variables, table 25, that showed correlation coefficients, R, greater, than 0.90 (R^2 greater than 0.81). Linear regression with pairs of variables was considered appropriate because the objective was to determine if the variables could be used as surrogates or replacements for each other. The results are shown in table 26 where the dependent and independent variables,

Table 25. Correlation matrix for characteristic temperatures with at least one correlation greater than 0.80.

	T_{vis4GP} °F	$T_{Pen1.2}$ °F	Fraass Brittle Point Temp, °F	Hills' Cracking Temp, °F	Temperature, °F, where: S_B = 1.0 GPa at 30 min based on nomograph using			Temperature, °F, where: S_B = 0.2 GPa at 2 h based on nomograph using				Temperature Shift, °F, for Tensile	
					Pen 77-TR&B	log-Pen	Pen 77-Fraass	Pen 77-TR&B	log-Pen	PVN-vis	Pen 77-Fraass	Strength	Modulus
Variable Number	1	2	3	4	5	6	7	8	9	10	11	12	13
1	(1.00)	.31	.72	.31	.55	.10	.62	.68	.24	.53	.70	.79	.60
2	.31	(1.00)	.65	.99	.79	.95	.52	.77	.99	.82	.60	.84	.89
3	.72	.65	(1.00)	.65	.78	.49	.96	.83	.61	.75	.98	.91	.71
4	.31	.99	.65	(1.00)	.79	.94	.51	.77	.98	.82	.58	.82	.88
5	.55	.79	.78	.79	(1.00)	.67	.67	.98	.75	.83	.75	.84	.80
6	.10	.95	.49	.94	.67	(1.00)	.38	.63	.97	.71	.44	.70	.80
7	.62	.52	.96	.51	.67	.38	(1.00)	.71	.48	.58	.97	.79	.51
8	.68	.77	.83	.77	.98	.63	.71	(1.00)	.73	.87	.76	.88	.85
9	.24	.99	.61	.98	.75	.97	.48	.73	(1.00)	.80	.55	.82	.90
10	.53	.82	.75	.82	.83	.71	.58	.87	.80	(1.00)	.69	.82	.91
11	.70	.60	.98	.58	.75	.44	.97	.76	.55	.69	(1.00)	.88	.65
12	.79	.84	.91	.82	.84	.70	.79	.88	.82	.82	.88	(1.00)	.89
13	.60	.89	.71	.88	.80	.80	.51	.85	.90	.91	.65	.89	(1.00)
Average	.51	.76	.75	.75	.77	.65	.64	.79	.74	.76	.71	.83	.78

Note: T_{vis4GP} is included in this table so that a viscosity-based equiviscous temperature will be included in the analysis.

Table 26. Summary of regression models with R^2 greater than 0.81.

Variable A	Variable B	R^2	Variable A versus B: Intercept, °C	Slope	Prediction Interval, °C	Variable B versus A: Intercept, °C	Slope	Prediction Interval, °C
$T_{Pen1.2}$, °C	T_H, °C	0.97	21	0.93	± 1.6	-23	1.1	± 1.7
$T_{Pen1.2}$, °C	T_{1GPa}, °C 30 min, $PI_{log-pen}$	0.90	18	0.71	± 3.0	-27	1.3	± 4.0
$T_{Pen1.2}$, °C	T_{200MPa}, °C 2 h, $PI_{log-pen}$	0.98	18	0.95	± 1.4	-19	1.0	± 1.5
T_{Fraass}, °C	Tensile Strength Temp. Shift, °C	0.83	-16	0.90	± 3.8	15	0.93	± 3.9
T_H, °C	T_{1GPa}, °C 30 min, $PI_{log-pen}$	0.88	-4	0.75	± 3.5	0	1.2	± 4.4
T_H, °C	T_{200MPa}, °C 2 h, $PI_{log-pen}$	0.96	-4	1.0	± 2.1	2	0.96	± 2.1
T_{1GPa}, °C 30 min, PI	T_{200GPa}, °C 2 h, PI	0.96	-4	1.2	± 2.0	2	0.80	± 1.7
T_{1GPa}, °C 30 min, $PI_{log-pen}$	T_{200MPa}, °C 2 h, $PI_{log-pen}$	0.95	-2	1.2	± 3.0	0	0.76	± 2.4
T_{200MPa}, °C 2 h, $PI_{log-pen}$	Tensile Modulus Temp. Shift, °C	0.82	-33	0.74	± 5.3	36	1.1	± 6.5
T_{200MPa}, °C 2 h, PVN	Tensile Modulus Temp. Shift, °C	0.83	-35	0.65	± 4.5	46	1.3	± 6.3
T_{200MPa}, °C 2 h, PI_{Fraass}	T_{1GPA}, °C 30 min, PI_{Fraass}	0.91	2	0.79	± 2.8	-6	1.1	± 3.4

90 percent prediction level, and the slope and intercept of the regression equation are shown. The limiting stiffness temperatures that were calculated using PI_{Fraass} were not regressed against T_{Fraass} since these variables are strongly interdependent. This resulted in a total of 11 regression models, table 26. These results and their significance are discussed in greater detail in sections 6.4 and 6.7.

6.2 COMPARISON OF DIFFERENT PENETRATION INDICES AND PENETRATION-VISCOSITY NUMBERS

One of the objectives of this project was to study the interchangeability of PI and PVN numbers computed from a number of different methods. A correlation matrix containing all of the temperature susceptibility parameters from table 24 is shown in table 27. Generally, a low level of correlation is observed between the pairs of parameters implying that the different temperature susceptibility parameters, PI, PVN, and VTS, cannot be used as replacements for each other. This is in agreement with the findings of previous research studies.[66,88,89] Of the temperature susceptibility parameters, only PVN_{140} and VTS were strongly correlated ($R = 0.90$). This is not totally unexpected given that both parameters are dependent upon the coefficient of viscosity at 140 °F (60 °C) for their determination, and both describe the upper branch of the plot on the BTDC chart. This correlation is not of significance to this study because VTS describes temperature susceptibility within a range of temperatures well above room temperature.

To determine if aging had an effect on temperature susceptibility, an analysis of variance was conducted using the different penetration indices and both penetration-viscosity numbers as class variables; these were the only parameters for which data on both aged and unaged asphalts were available. In the model, asphalt source and grade, calculation method, and aging treatment (aged/unaged) were used as main effects. An interaction term between the calculation method and aging treatment was also included. A total of 203 observations were included in the model; however, many of these observations were pseudo-replicates, calculated from individual penetration, viscosity, and softening point measurements. The results of this model show a significance level of 0.35 for aging treatment, and 0.46 for the interaction of aging

Table 27. Correlation matrix for temperature susceptibility parameters.

	PI	$PI_{log-pen}$	PVN_{140}	PVN_{275}	VTS	PI_{Fraass}
PI	(1.00)	0.53	0.49	0.57	0.30	0.42
$PI_{log-pen}$	0.53	(1.00)	0.16	0.58	-0.15	0.21
PVN_{140}	0.49	0.16	(1.00)	0.69	0.90	0.35
PVN_{265}	0.57	0.58	0.69	(1.00)	0.30	0.20
VTS	0.30	-0.15	0.90	0.30	(1.00)	0.05
PI_{Fraass}	0.42	0.21	0.35	0.20	0.05	(1.00)

treatment and calculation method. This indicates that aging in the rolling thin-film oven, on the average, does not significantly change the values of penetration index or penetration-viscosity number calculated as described above. This is in contrast to the results shown by others where the PI has been shown to change significantly upon aging while the PVN has remained relatively unchanged.[66,89]

6.3 COMPARISON OF EQUIVISCOUS TEMPERATURES

The Fraass brittle point temperature, T_{Fraass}, and the temperature at which the penetration value extrapolates to 1.2, $T_{Pen1.2}$, have been reported by others as equiviscous temperatures at which the coefficient of viscosity is 4.0 GP. As noted above, and in table 25, the correlation coefficients for these variables show poor correlation. The results of linear regression with pairs of these variables gave the following coefficients of determination:

- $T_{Pen1.2}$ versus T_{Fraass}, $R^2 = 0.42$ ($R = 0.65$).
- T_{vis4GP} versus T_{Fraass}, $R^2 = 0.52$ ($R = 0.72$).
- $T_{Pen1.2}$ versus T_{vis4GP}, $R^2 = 0.10$ ($R = 0.31$).

On the basis of these R^2 data, the researchers have concluded that these parameters are not strongly correlated with each other and therefore cannot be used as surrogates for each other.

6.4 COMPARISON OF LIMITING STIFFNESS AND EQUISTIFFNESS TEMPERATURES

One of the objectives of this study was to compare the different limiting stiffness and equistiffness temperatures and determine if they are surrogates for each other. The pairs of limiting stiffness or equistiffness temperatures with correlation coefficients greater than 0.90, table 25, are shown in table 26 along with the 90 percent prediction interval at the mean value of the independent variable, and the slope and intercept of the corresponding regression equations. The regression coefficients are given for variable A versus B and variable B versus A. The researchers arbitrarily assumed that

the variables are acceptable surrogates if the 90 percent prediction levels for variables A versus B and variables B versus A are both less than ± 5.4 °F (± 3.0 °C). In table 26, four pairs of limiting or equistiffness temperatures meet this requirement:

- T_{200MPa}, 2 h, (based on $PI_{log-pen}$), as a surrogate for $T_{Pen1.2}$.
- Hills' cracking temperature, as a surrogate for $T_{Pen1.2}$.
- T_{1GPa}, 30 min (based on PI), as a surrogate for T_{200MPa}, 2 h (based on PI).
- T_{200MPa}, 2 h (based on $PI_{log-pen}$), as a surrogate for Hills' cracking temperature.

Each of the above relationships is shown graphically in figures 39 through 42. As seen from the figures, the correlation between these pairs of variables is highly significant, implying that they can be used as surrogates for each other. In other words, the variables in the pairs can be exchanged for each other but only through the regression equations. For example, the limiting stiffness temperature defined at a stiffness of 145,000 lb/in^2 (1.0 GPa) at 30 min found using $PI_{log-pen}$ can be interchanged with $T_{Pen1.2}$ by the following relationship (table 26):

$$T_{200MPa,\ 2\ h,\ PI_{log-pen},\ °C} = -19 + 1.0\ (T_{Pen1.2,\ °C}) \qquad (38)$$

and

$$T_{Pen1.2,\ °C} = 18 + 0.95\ (T_{200MPa,\ 2\ h,\ PI_{log-pen},\ °C}) \qquad (39)$$

For this relationship, although 90 percent of the new predictions of T_{200MPa} should be within ± 2.7 °F (± 1.5 °C) of the true value of $T_{Pen1.2}$, the magnitudes of the two variables differ by approximately 34 °F (19 °C).

The regression equations in table 26 also show that the different loading time/stiffness level conditions given in the literature may not produce equivalent temperatures. For example, when the limiting stiffness temperature is defined as the temperature where the stiffness is 145,000 lb/in^2 (1.0 GPa) after 30 min loading (PI method) and 29,000 lb/in^2 (200 MPa) after 2 h loading (PI method), the limiting stiffness temperatures for these two sets of

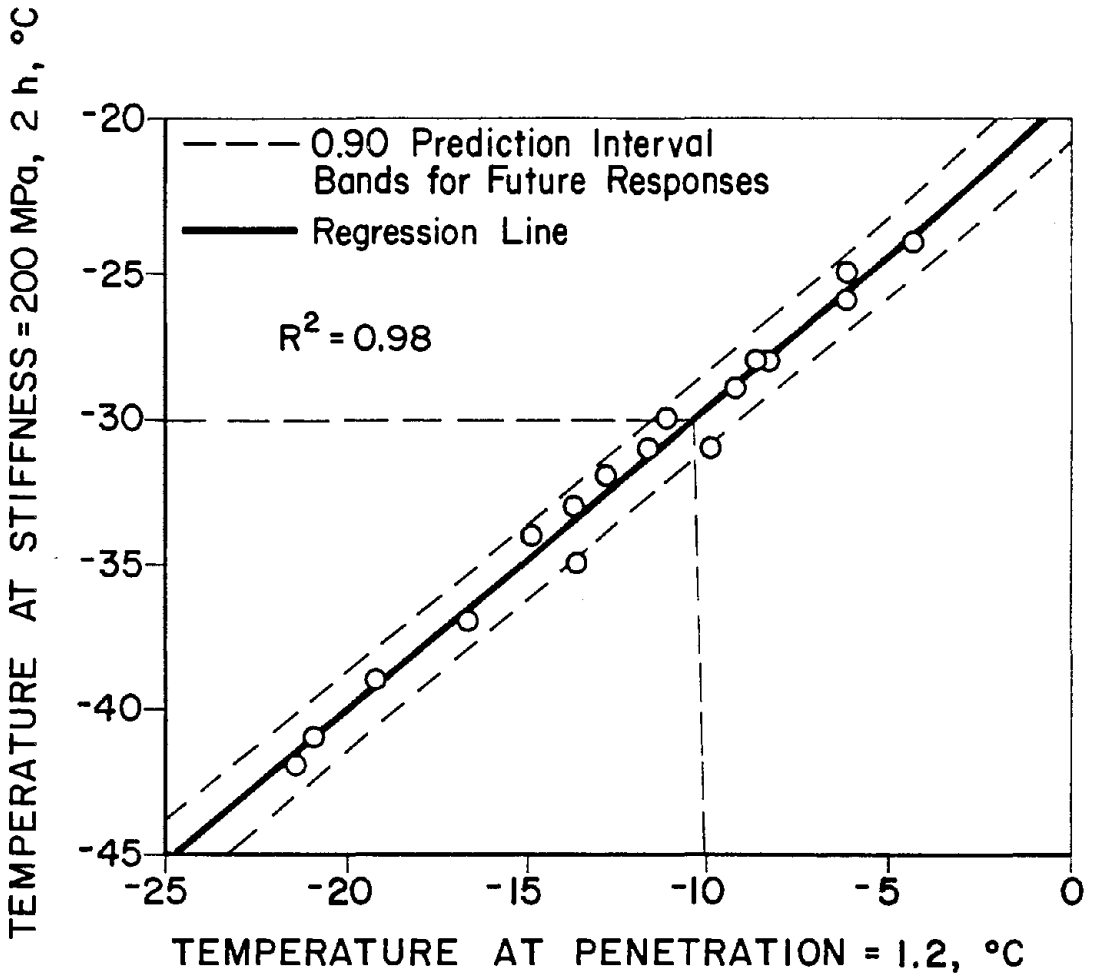

Figure 39. Regression of limiting stiffness temperature, 0.2 GPa, 2 h, °C, ($PI_{log\text{-}pen}$ method) on $T_{Pen1.2}$.

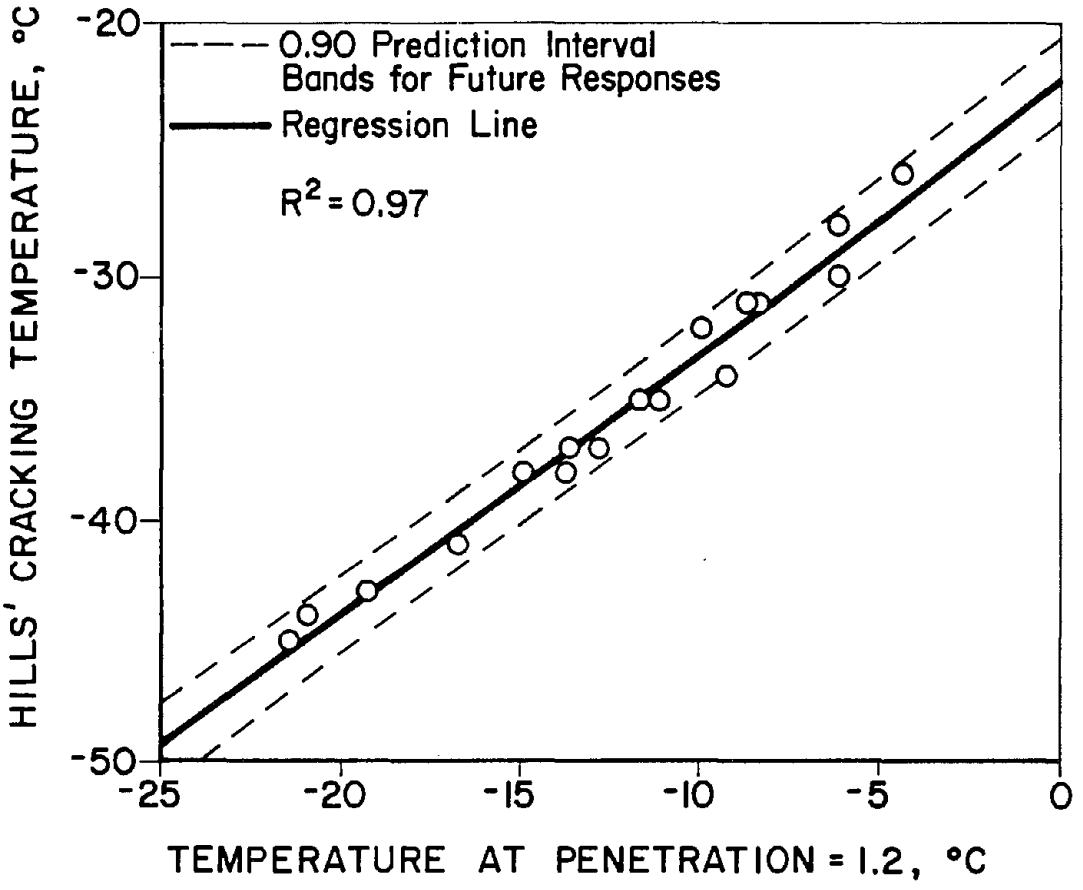

Figure 40. Regression of Hills' cracking temperature versus $T_{Pen1.2}$.

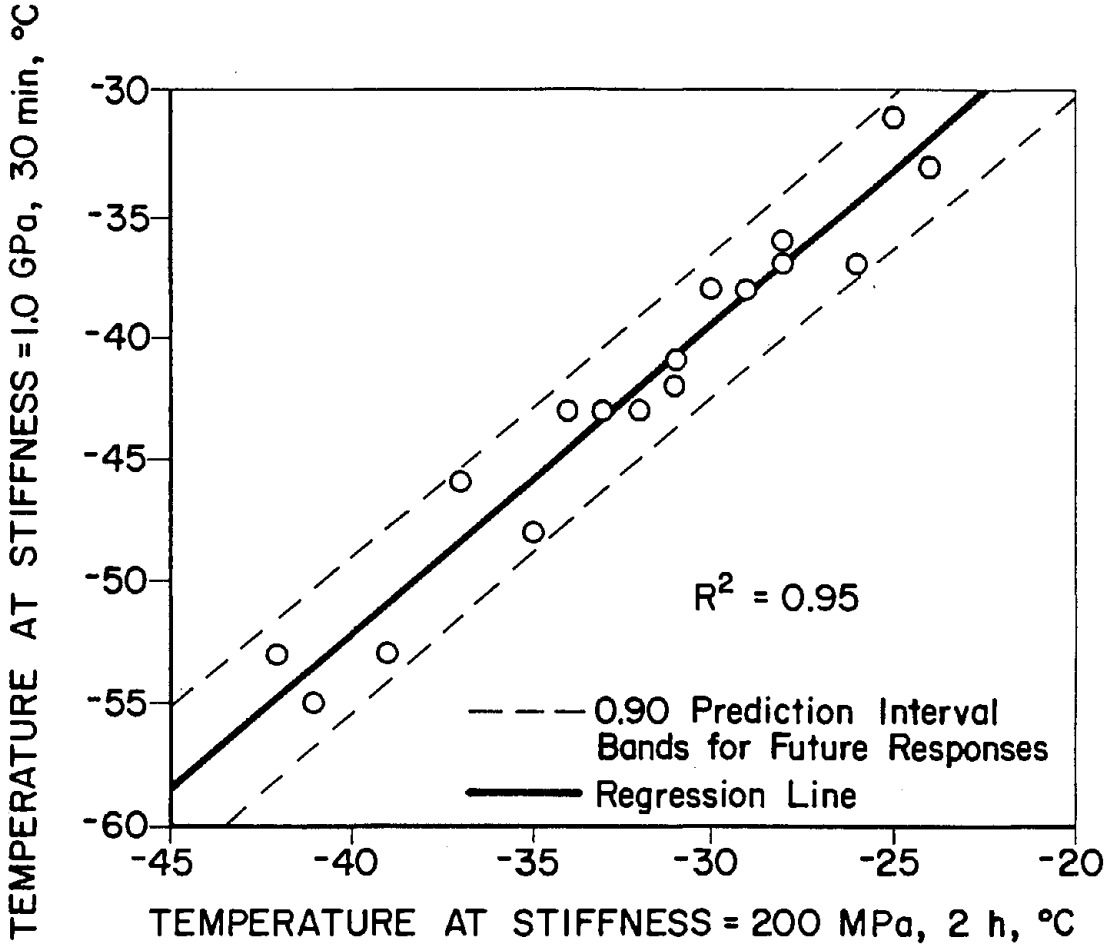

Figure 41. Regression of limiting stiffness temperature for stiffness of 1.0 GPa after 30 min loading time ($PI_{log\text{-}pen}$) versus limiting stiffness temperature for stiffness of 200 MPa after 2 h loading time ($PI_{log\text{-}pen}$).

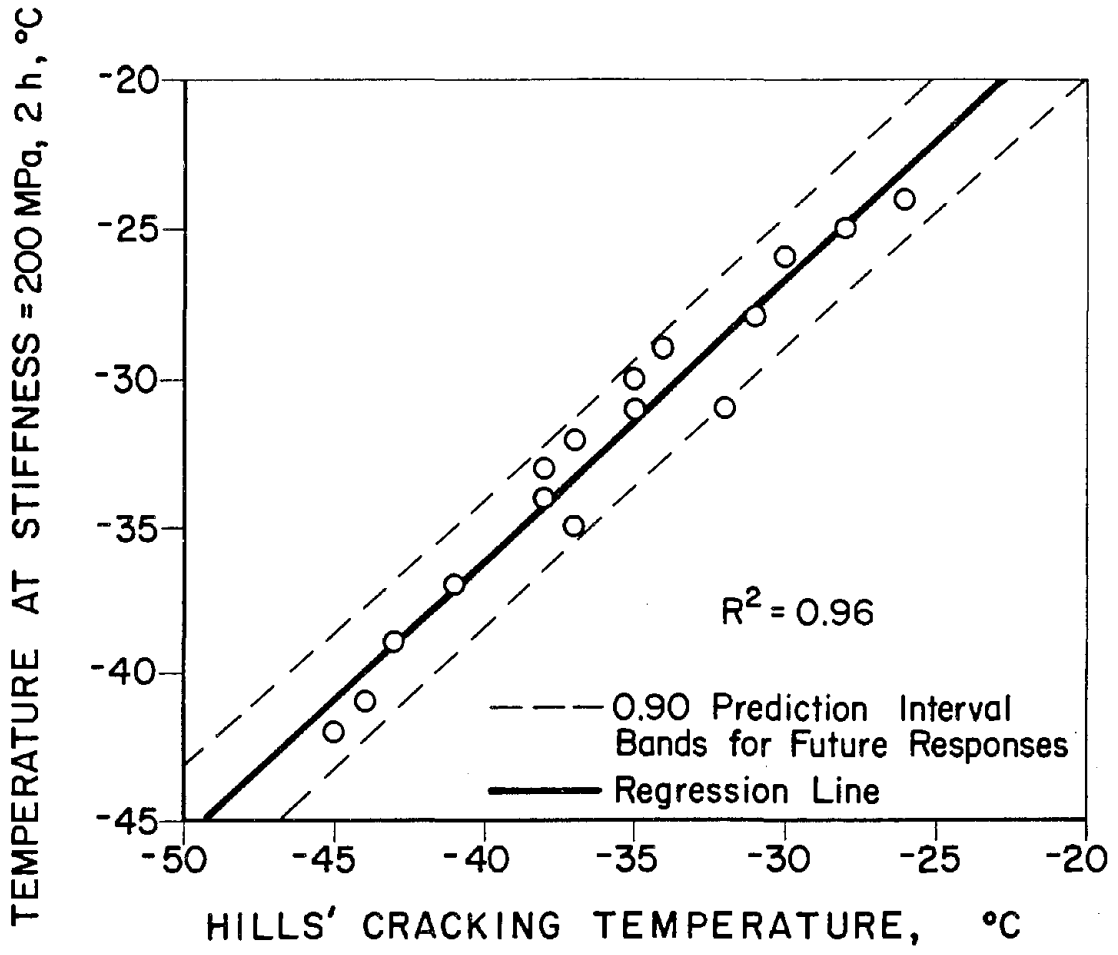

Figure 42. Regression of limiting stiffness temperature for stiffness of 200 MPa after 2 h loading time ($PI_{log-pen}$) versus Hills' cracking temperature.

conditions differ by 13 to 22 °F (7 to 12 °C) in the region of interest (figure 43). When the $PI_{log\text{-}pen}$ is used in the calculations, the difference is similar in magnitude, table 26 and figure 41.

When the average limiting stiffness temperatures for the different methods are calculated, the following comparison can be made (averaged over all asphalts for each method, appendix E):

1 GPa, 30 min, PI method: -48 °F (-44 °C)
1 GPa, 30 min, $PI_{log\text{-}pen}$ method: -44 °F (-42 °C)
1 GPa, 30 min, PI_{Fraass} method: -52 °F (-47 °C)

200 MPa, 2 h, PI method: -29 °F (-34 °C)
200 MPa, 2 h, $PI_{log\text{-}pen}$ method: -26 °F (-32 °C)
200 MPa, 2 h, PI_{Fraass} method: -31 °F (-35 °C)
200 MPa, 2 h, PI_{PVN140} method: -31 °F (-35 °C)

Hills' cracking temperature: -32 °F (-36 °C)

From these data it is clear that the different loading times/stiffnesses are not equivalent. Furthermore, the 145,000 lb/in^2 (1.0 GPa), 30 min condition is not realistic given that asphalt cement approaches a glassy modulus (stiffness) of 380,000 lb/in^2 (2.6 GPa) at very low temperatures.[2]

Figures 42 and 44 are closely related plots, showing the results of regressions of limiting stiffness temperatures based on $PI_{log\text{-}pen}$, but for different loading times and stiffnesses, versus Hills' cracking temperature. The variability seen in figure 44 is fairly large, as reflected in the R^2 which is 0.88 compared with 0.96 for figure 42. Furthermore, the slope is closer to one for the 29,000 lb/in^2 (200 MPa), 2 h loading condition compared with the model using the 145,000 lb/in^2 (1.0 GPa), 30 min loading condition ($PI_{log\text{-}pen}$ method, both cases). Thus Hills' cracking temperature more closely approximates the limiting stiffness temperature for the 200 MPa, 2 h loading condition than for the 145,000 lb/in^2 (1.0 GPa), 30 min loading conditions.

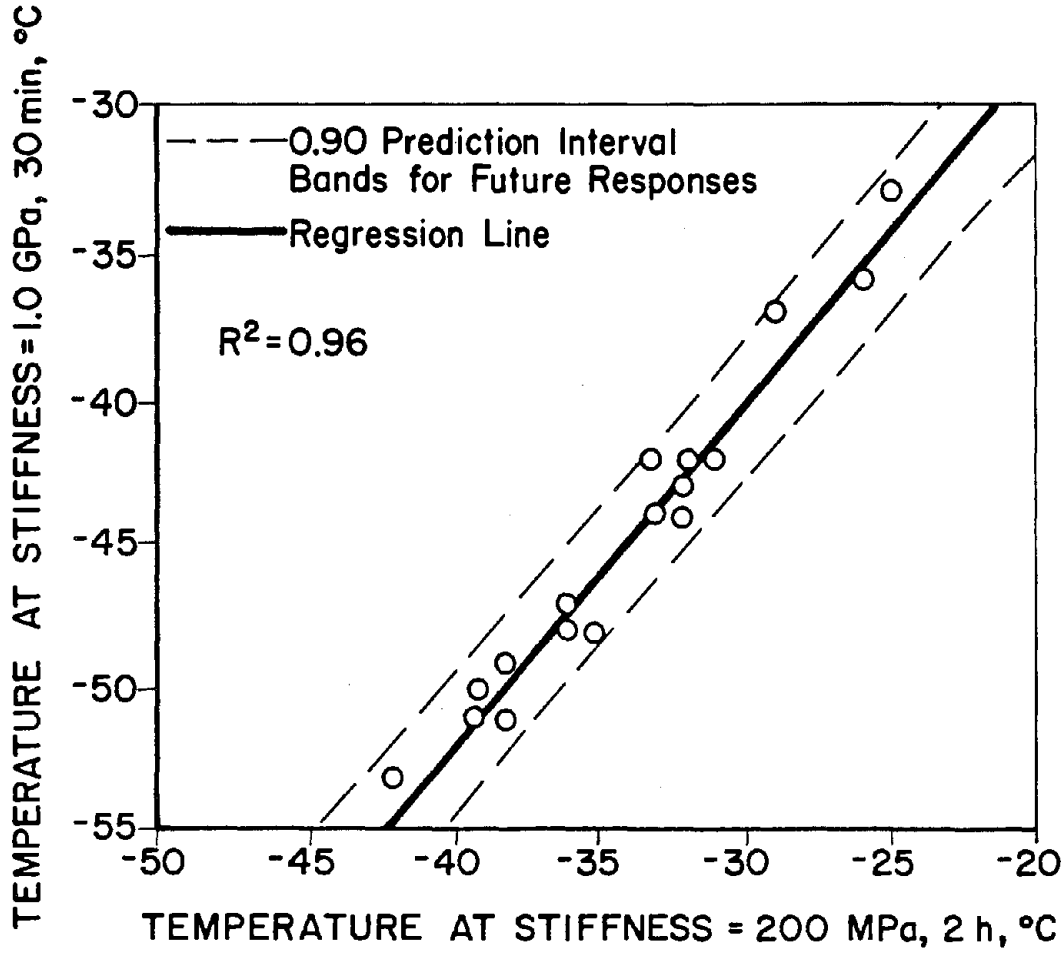

Figure 43. Regression of limiting stiffness temperature for stiffness of 1.0 GPa after 30 min loading time (PI) versus limiting stiffness temperature of 200 GPa after 2 h loading time (PI).

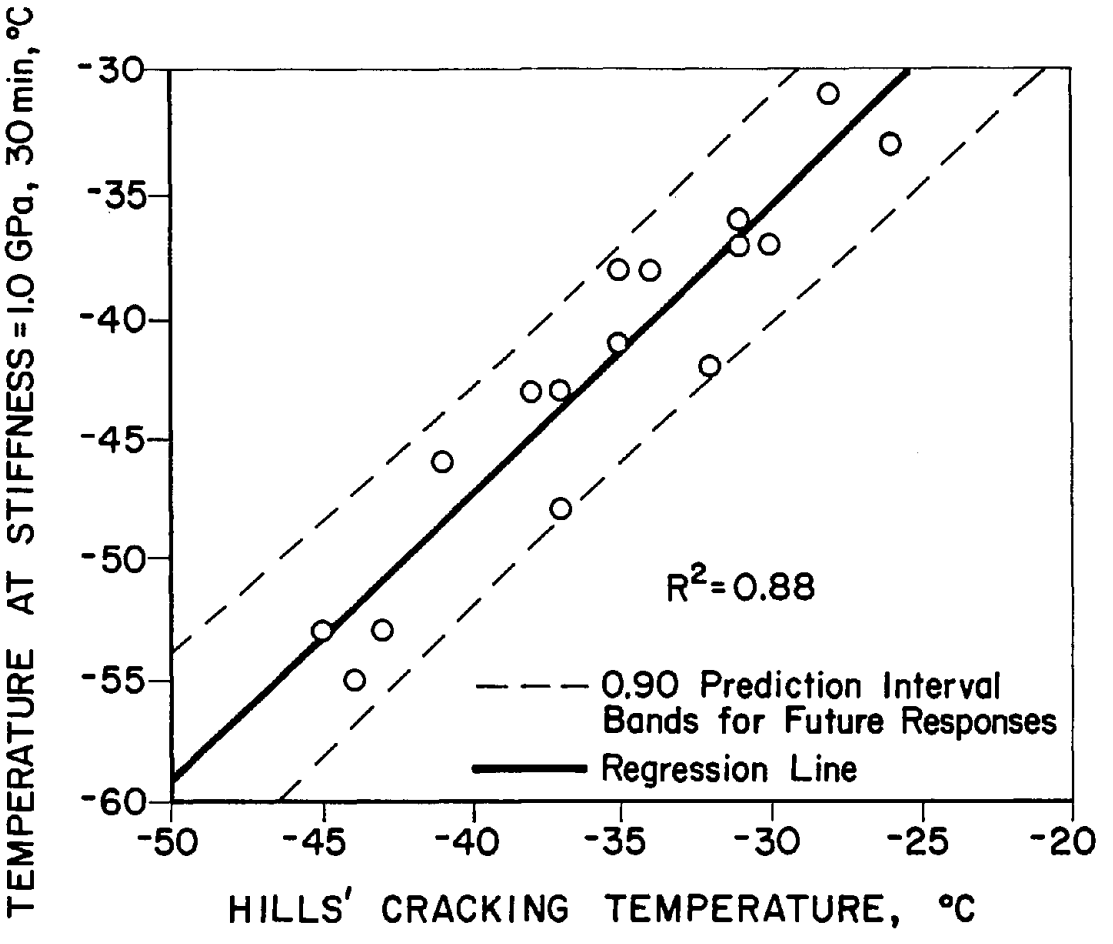

Figure 44. Regression of limiting stiffness temperature for stiffness of 1.0 GPa after 30 min loading time ($PI_{log\text{-}pen}$) versus Hills' cracking temperature.

The Fraass brittle point temperature does not correlate well with any of the limiting stiffness temperatures (see R values, table 25), except those calculated using T_{Fraass}, and therefore is not a surrogate for them. The low R values for T_{Fraass} in table 25 indicate that the prediction intervals will be larger than $\pm$ 5.4 °F ($\pm$ 3 °C), the criterion for interchangeability. $T_{Pen1.2}$ correlates well with the limiting stiffness at 29,000 lb/in^2 (200 MPa), 2 h loading time and with 1 GPa, 30 min only when $PI_{log-pen}$ is used to estimate the stiffness. T_{vis4GP} does not correlate with any of the limiting stiffness temperatures.

To further evaluate the relationships between the three variables--limiting stiffness/loading time, temperature, and method of estimate--an analysis of variance was conducted, table 28. Asphalt, nomographic method, and limiting stiffness/loading time were used as class variables. In addition to the two limiting stiffness/loading time values discussed above, a third limiting stiffness/loading time was added to this phase of the analysis: 20,000 lb/in^2 (140 MPa) at 20,000 s; this value has been suggested by McLeod.[48] A two-factor interaction term for nomographic method and limiting stiffness/loading time was also included in the model. A significant interaction term indicates that the change in the predicted limiting stiffness temperature when different limiting stiffness/loading time values are used (e.g., 145,000 lb/in^2 (1.0 GPa), 30 min versus 29,000 lb/in^2 (200 MPa), 2 h) depends on the nomographic method used. Individual measurements chosen using the D2S values from the appropriate ASTM specifications were randomly assigned in calculating values for entrance into the nomographs so that replicate observations could be generated. A total of 456 observations were made in the analysis. The results of the analysis of variance are summarized in table 28. In examining the results of an analysis of variance, the significance level is usually examined. This level is an indication of the probability of incorrectly concluding that a given parameter is not significant. Therefore, the lower the significance level, the greater the probability that the variable has a significant effect.

As seen from the significance levels listed in table 28, all of the main effects were highly significant, whereas the interaction between the nomographic method and limiting stiffness/loading time was not nearly as

Table 28. Summary of analysis of variance for limiting stiffness temperatures.

Model:

$$Y_{ijk} = \beta_o + \beta_i + \beta_j + \beta_k + \beta_{jk} + \varepsilon_{ijk}$$

where

Y_{ijk} = observed limiting stiffness temperature, °C, for asphalt i using nomograph method j and limiting stiffness/loading time value k

β_o = overall average limiting stiffness temperature, °C

β_i = effect of asphalt i on limiting stiffness temperature, °C

β_j = effect of nomographic method j on limiting stiffness temperature, °C

β_k = effect of limiting stiffness/loading time k on limiting stiffness temperature, °C

β_{jk} = effect of interaction between nomograph method j and limiting stiffness/loading time k

ε_{ijk} = error term

Source of Variation		Degrees of Freedom	F-Ratio	Significance Level
A	Asphalt	16	50.3	0.0000
B	Nomograph Method	3	14.3	0.0000
C	Limiting Stiffness/ Loading Time	2	344.8	0.0000
B*C	Interaction of B and C	6	1.5	0.1752
	Residual	429	----	----
	Total	456	----	----

Limiting stiffness temperature, Means for different methods		Limiting stiffness temperature, Means for different limiting stiffness/loading time values
PI_{Fraass}:	-38 °F (-39 °C)	1 GPa at 30 min: -47 °F (-44 °C)
PVN_{140}:	-37 °F (-38 °C)	200 MPa at 2 h: -30 °F (-34 °C)
PI:	-36 °F (-38 °C)	140 MPa at 20,000 s: -30 °F (-34 °C)
$PI_{log-pen}$	-33 °F (-36 °C)	

significant. A comparison of the mean values for limiting stiffness temperature found by using the various nomographic methods shows only slight differences: the smallest mean was for the PI_{Fraass} method, -38 °F (-39 °C); the largest was for the $PI_{log-pen}$ method, -33 °F (-36 °C). However, a much larger difference was seen in the values of limiting stiffness temperature when different loading conditions were used: 145,000 lb/in^2 (1.0 GPa), 30 min gave an average temperature of -47 °F (-44 °C), whereas 29,000 lb/in^2 (200 MPa), 2 h gave a much higher temperature, -30 °F (-34 °C). Using a limiting stiffness value of 145,000 lb/in^2 (1.0 GPa), 30 min apparently predicts cracking temperatures 17 °F (9 °C) lower, on average, than the temperatures predicted using the other two limiting stiffness/loading time conditions. This discrepancy is significant. Which of these stiffness values is most appropriate can be determined only through field evaluation. The conservative approach would be to use either the 29,000 lb/in^2 (200 MPa) at 2 h value, or McLeod's value of 20,000 lb/in^2 (140 MPa) at 20,000 s, since these give higher values for limiting stiffness temperatures.

6.5 DERIVATION OF CLASS INDEX

After a thorough study of the data, the authors suspected that some of the variation among the limiting stiffness temperatures calculated by the different methods could be explained in terms of bitumen class, as defined by Heukelom.[22] The bitumen class is found by plotting viscosity and penetration data at different temperatures on the Bitumen Test Data Chart (BTDC), figure 45. The BTDC is constructed with temperature as the abscissa and penetration and viscosity as the ordinates. The scales for penetration and viscosity were chosen by Heukelom so that the data for a typical straight-run, or class S, asphalt will plot as a single straight line.[22] Blown, or class B, asphalts show lower temperature susceptibilities as indicated by the slope of the penetration branch of the plotted test data. Waxy, or class W, asphalts show higher temperature susceptibilities at intermediate to high penetration temperatures, since the wax present is melting within this temperature range. The asphalts tested in this study showed a range of behavior from class W to class B as shown in the plots of the data that are given in appendix F.

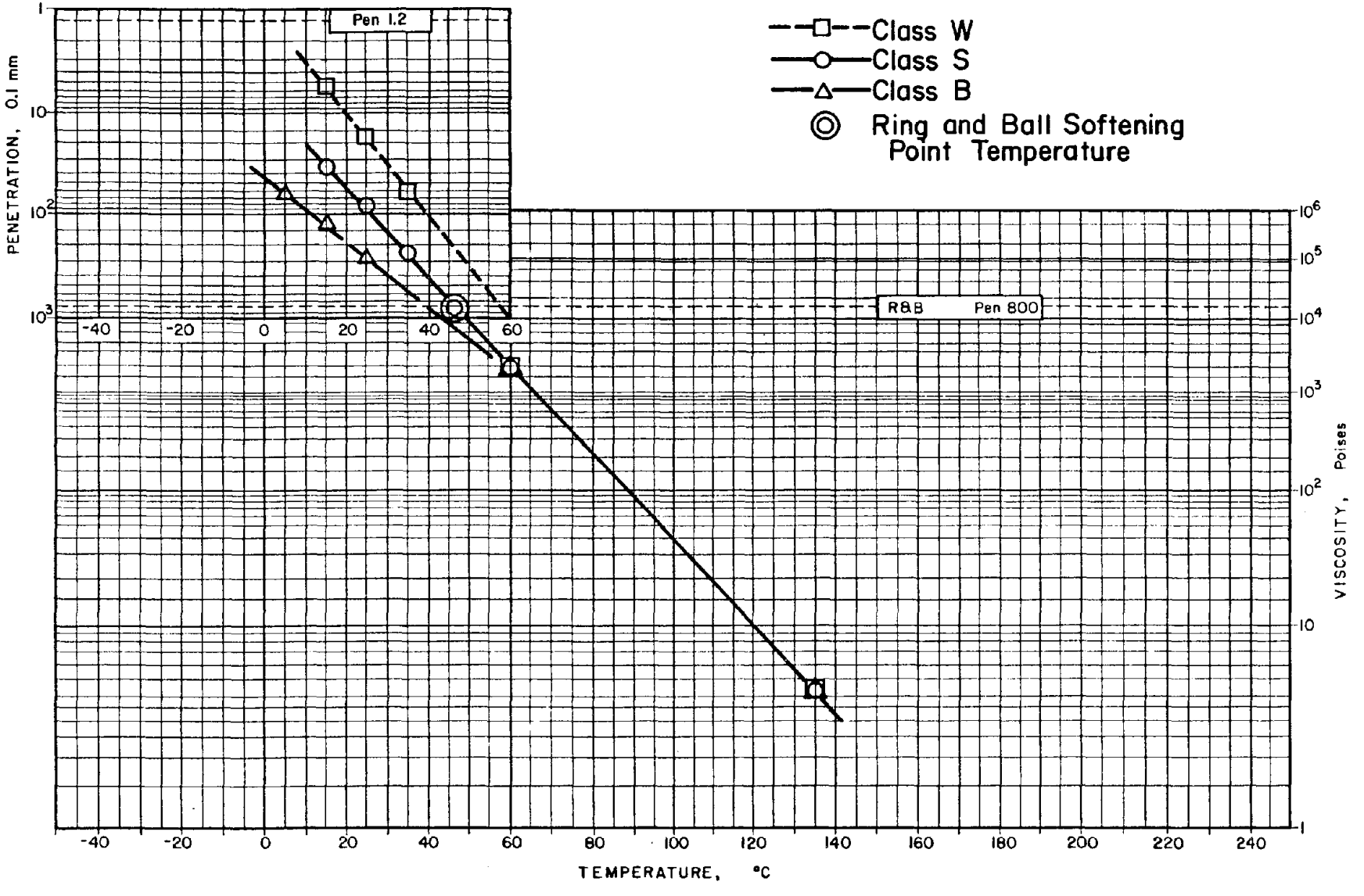

Figure 45. Different classes of asphalt shown on the Bitumin Test Data Chart.

To include the effect of asphalt class in statistical models, the research team developed the following method for quantitatively describing bitumen class. The log-pen temperature susceptibility, A, was calculated as the absolute value of the slope of the penetration branch of the plot on the Shell BTDC chart. From formulas, given by Heukelom, the absolute value of the slope of the viscosity branch of the BTDC chart, A', can be calculated from the following equation:[22]

$$A' = \left| \left[\frac{46.07(\eta''_{275} - \eta''_{140})}{72.25 + 8.5\,(\eta''_{275} + \eta''_{140}) + \eta''_{275}\,\eta''_{140}} \right] [1/75] \right| \quad (40)$$

where

$$\eta''_{275} = \log \left[\frac{\text{viscosity at 275 °F (135 °C), poises}}{13{,}000} \right] \quad (41)$$

$$\eta''_{140} = \log \left[\frac{\text{viscosity at 140 °F (60 °C), poises}}{13{,}000} \right] \quad (42)$$

The ratio of the two temperature susceptibility parameters, A/A' gives an indication of bitumen class as indicated by the BTDC. Class S bitumens will have values of A/A' close to one; class B bitumens will tend to have values significantly less than one; and class W asphalts will have values greater than one. If the difference, ΔT, between the ring and ball softening point temperature, $T_{R\&B}$, and T_{Pen800} is plotted versus the ratio A/A', the asphalts used in this study plot roughly as a straight line, as shown in figure 46. A regression line (solid line in figure 46) through the data points intercepts the y-axis at 9.5 °F (-12.5 °C), with a slope of 22.1 °F (12.3 °C), and the temperature difference is approximately equal to zero when A/A' is equal to 1.0. In this plot, asphalts at the lower left are more like class B asphalts, while those at the upper right tend toward class W characteristics. The class S asphalts, by definition, have an A/A' ratio close to 1.0 and a temperature difference approaching 0 °F (0 °C).

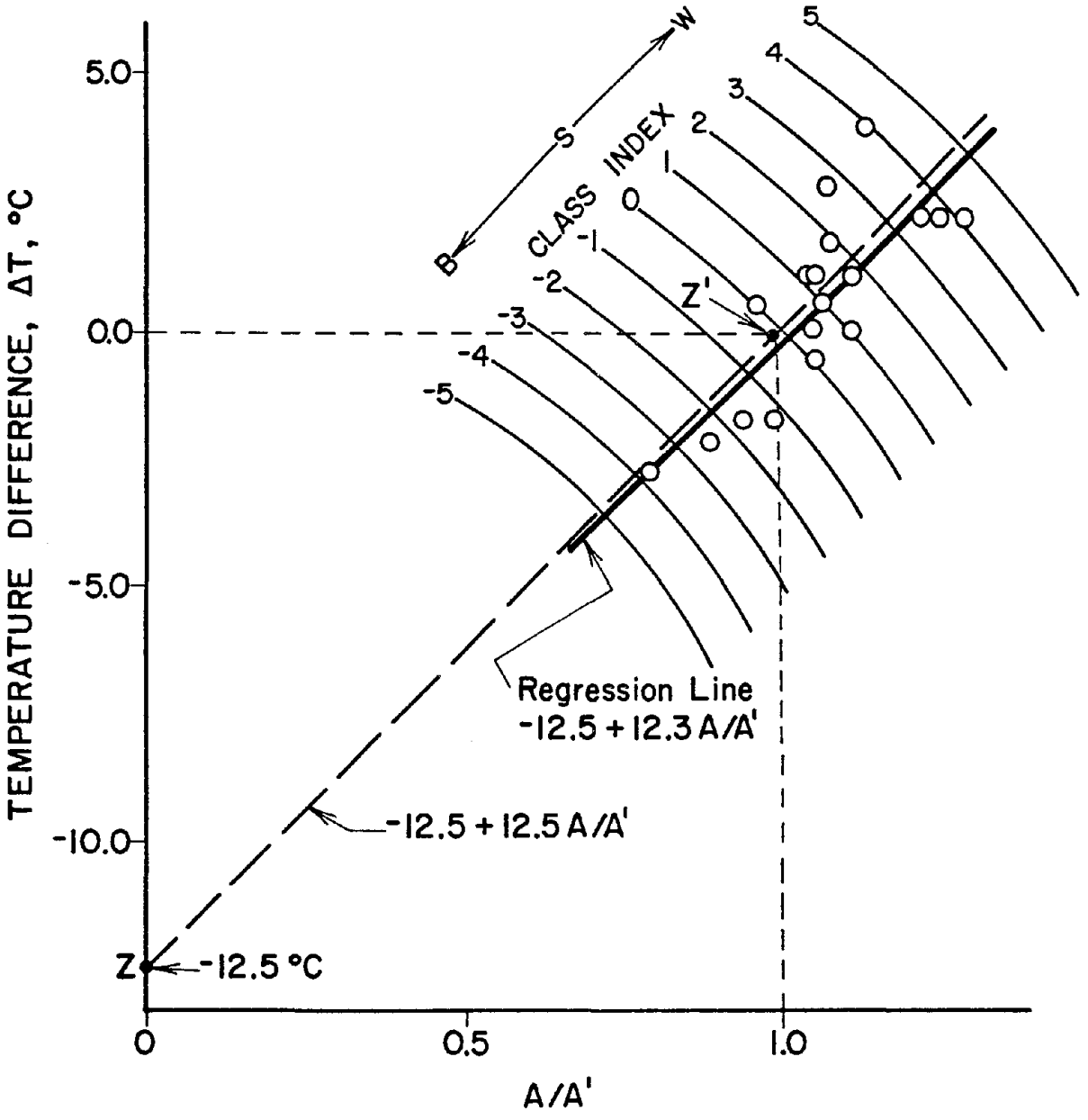

Figure 46. Derivation of class index.

The plot in figure 46 lends itself to the development of a parameter called the Class Index (C.I.), which is an indicator of the relative position of the data points along the regression line, $\Delta T = -12.5 + 12.3\ A/A'$. The regression line (solid line) in figure 46 was divided into different curvilinear zones created by generating circular contours about the point, $\Delta T = -12.5$ °C and $A/A' = 0.0$. The scale in figure 46 has been adjusted so that the physical distance on the graph between $\Delta T = -12.5$ °C and 0 °C and between $A/A' = 0$ and 1.0 are equal. This is equivalent to multiplying the values of the abscissa by 12.5. With this adjustment, the radius of the contour, centered at point Z, -12.5 and passing through point 1.0, 0.0 is given by:

$$\overline{ZZ'} = [(12.5\ (A/A'))^2 + (12.5)^2]^{1/2} \qquad (43)$$
$$= 17.68$$

where

$\overline{ZZ'}$ = distance between points Z and Z'
A = log-penetration temperature susceptibility
A' = slope of plot of viscosity branch of BTDC plot, as defined above

Distances along the radii $\overline{ZZ'}$ measured with respect to point Z' are defined as class index values where negative values are by definition measured from point Z' toward point Z. The distances are given by:

$$C.I. = [(-12.5 - \Delta T)^2 + (12.5\ A/A')^2]^{1/2} - 17.68 \qquad (44)$$

where

$\Delta T = T_{R\&B} - T_{Pen800}$, °C
A = log-penetration temperature susceptibility
A' = slope of plot of viscosity branch of BTDC plot, as defined above

Values for the A, A/A', ΔT, and the calculated class index (C.I.) are shown in table 29. Larger (more positive) values for C.I. indicate class W behavior while smaller (more negative) values indicate class B behavior. The

Table 29. Asphalt class index (RTFOT residue).

Asphalt Number	Asphalt Source	A	A'	A/A'	$T_{R\&B} - T_{Pen800}$ °C	Class Index
1	A	.0476	.0455	1.047	1.1	1.2
2	B	.0452	.0430	1.051	0.0	0.4
3	B	.0456	.0429	1.065	2.8	2.6
4	B	.0440	.0421	1.045	1.1	1.1
5	C	.0497	.0448	1.110	1.1	1.7
6	C	.0491	.0449	1.105	0.0	0.9
7	C	.0461	.0441	1.046	-0.6	0.0
8	D	.0500	.0471	1.061	0.6	0.9
9	E	.0494	.0383	1.292	2.2	4.1
10	E	.0483	.0385	1.255	2.2	3.8
11	E	.0474	.0386	1.229	2.2	3.5
12	F	.0381	.0426	.895	-2.2	-2.5
13	G	.0433	.0437	.993	-1.7	-1.3
14	G	.0466	.0435	1.071	1.7	1.8
15	H	.0414	.0441	.938	-1.7	-1.8
16	I	.0528	.0468	1.129	3.9	3.9
17	I	.0378	.0474	.799	-2.8	-3.8

class index values for asphalts 9 through 11 are relatively large, indicating a waxy behavior. These asphalts, all from the same source, contain very few asphaltenes and are, therefore, somewhat anomalous. Asphalt 16 is a waxy asphalt, in agreement with its large class index, 3.9. Asphalt 17 was processed from the same crude as asphalt 16 except that air blowing was used during its manufacture. As expected, the class index changed, from 3.9 to -3.8, the latter value indicative of a class B or blown asphalt.

In figure 47, the temperature difference between the limiting stiffness (1 GPa at 30 min) temperatures found using the PI method and the $PI_{log\text{-}pen}$ method are plotted versus class index. The 90 percent prediction interval for new observations is also shown on the plot. A fairly strong relationship is seen: as class index increases (the asphalt becomes more waxy), the PI method produces lower limiting stiffness temperatures relative to the $PI_{log\text{-}pen}$ method. This can be explained physically by the anomalously high softening points seen in waxy paving grade asphalts, which result in higher values of calculated penetration index (PI), and hence, lower predicted limiting stiffness temperatures. It can be concluded that bitumen class is an important parameter in explaining the lack of agreement between the PI and $PI_{log\text{-}pen}$ methods for estimating stiffness and limiting stiffness temperatures. For many asphalts, the penetration-viscosity versus temperature curve departs from ideal (linear) behavior, and the class index is a measure of this deviation. Therefore, the class index is a convenient method of quantifying the shape of the plot on the BTDC.

6.6 DSC AND HP-GPC PARAMETERS

As is evident from the variables eliminated from the correlation matrix, table 25, none of the HP-GPC parameters investigated correlated well with any of the other paameters. This does not necessarily mean that asphalt chemistry as reflected in HP-GPC analysis does not affect cracking, only that it is not a strong primary factor or that it acts in concert with other factors. Glass transition temperatures found by differential scanning calorimetry also did not correlate well with any of the other parameters. The DSC thermogram generally showed multiple, diffuse peaks and were difficult to interpret. In

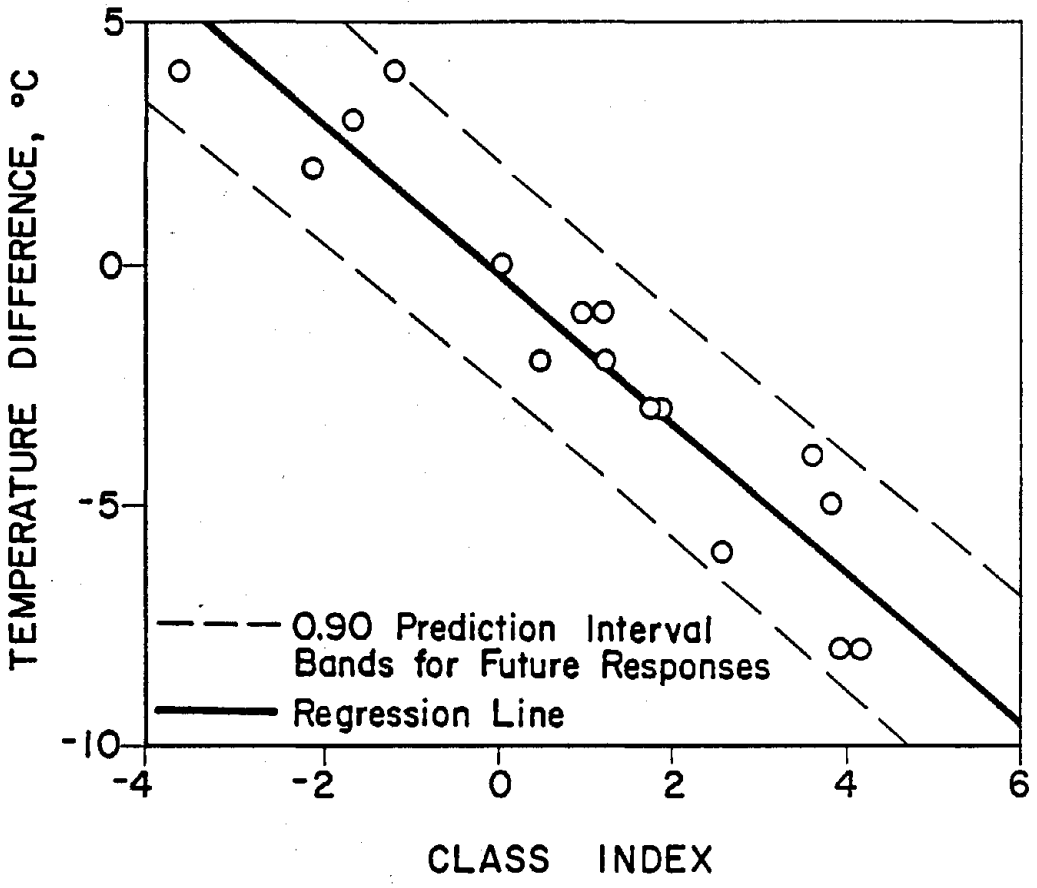

Figure 47. Plot of difference in predicted temperature at a stiffness of 145,000 lb/in^2 (1 GPa) at 30 min (PI - $PI_{log\text{-}pen}$ method) versus class index.

the opinion of the authors, the use of DSC data to characterize asphalt properties and internal structure merits additional study; however, further study was beyond the scope of this project.

6.7 DIAMETRAL TENSION TESTING OF MIXES

Marshall sized specimens, 2.5 in by 4.0 in (64 mm by 102 mm), were loaded diametrally at four temperatures, and the indirect tangent modulus and tensile strength were calculated for each specimen. A comparison of these test results is shown in figure 48, where tensile strength is plotted versus the logarithm of the static modulus. As has been shown by other researchers, the data show a general relationship between diametral tensile strength and the logarithm of static modulus, figure 48. It should be emphasized that the data in figure 48, although they represent a range of temperatures, are for a single mixture (aggregate size, gradation, and source), and the relationship illustrated in this figure should not be extended to mixes in general. However, from the data presented in figure 48, it can be concluded that, for a given mix, the values for static diametral tensile modulus and strength are ranked in the same order as they are affected by asphalt properties. In other words, the effect of asphalt properties on the diametral static modulus is in the same order of effectiveness as for the diametral tensile modulus. Therefore, the same general ranking would be obtained according to stiffness or tensile strength.

Figure 49 is a plot of mixture indirect tensile strength temperature shift versus Fraass brittle point temperature. There is a moderately strong relationship, $R^2 = 0.83$, showing that the Fraass brittle point temperature is reflected in the mixture properties; higher Fraass brittle point temperatures correlate with larger tensile strength shift temperatures. The indirect tensile modulus temprature shift is plotted versus limiting stiffness temperature at 29,000 lb/in^2 (200 MPa) at 2 h, $PI_{log\text{-}pen}$ method, in figure 50. Here again, although a fairly strong correlation is seen, these measurements cannot be considered interchangeable according to the previously established criterion that the prediction interval be less than $\pm$ 5.4 °F ($\pm$3.0°C). Whereas the asphalt cement properties (stiffness, T_{Fraass}) do correlate with the mixture properties, the correlations are not as strong as when simlar correlations are made for the neat asphalt.

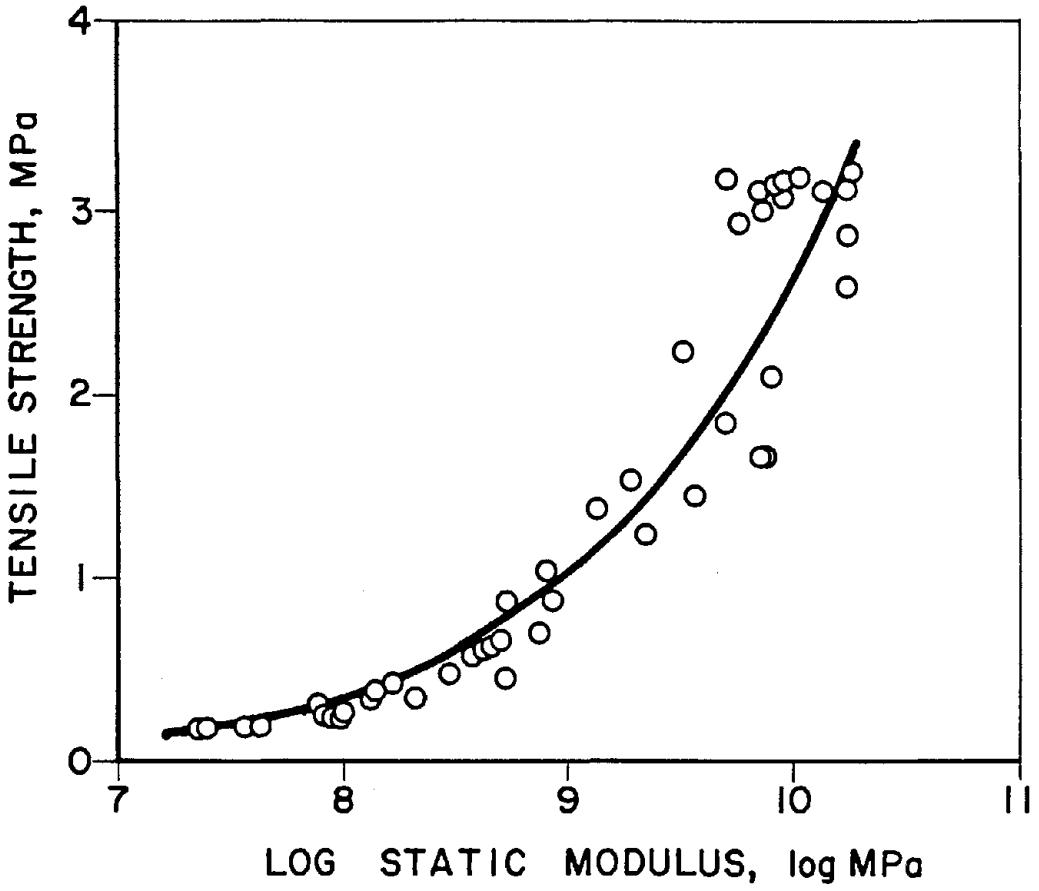

Figure 48. Plot of mixture tensile strength versus log mixture tensile modulus.

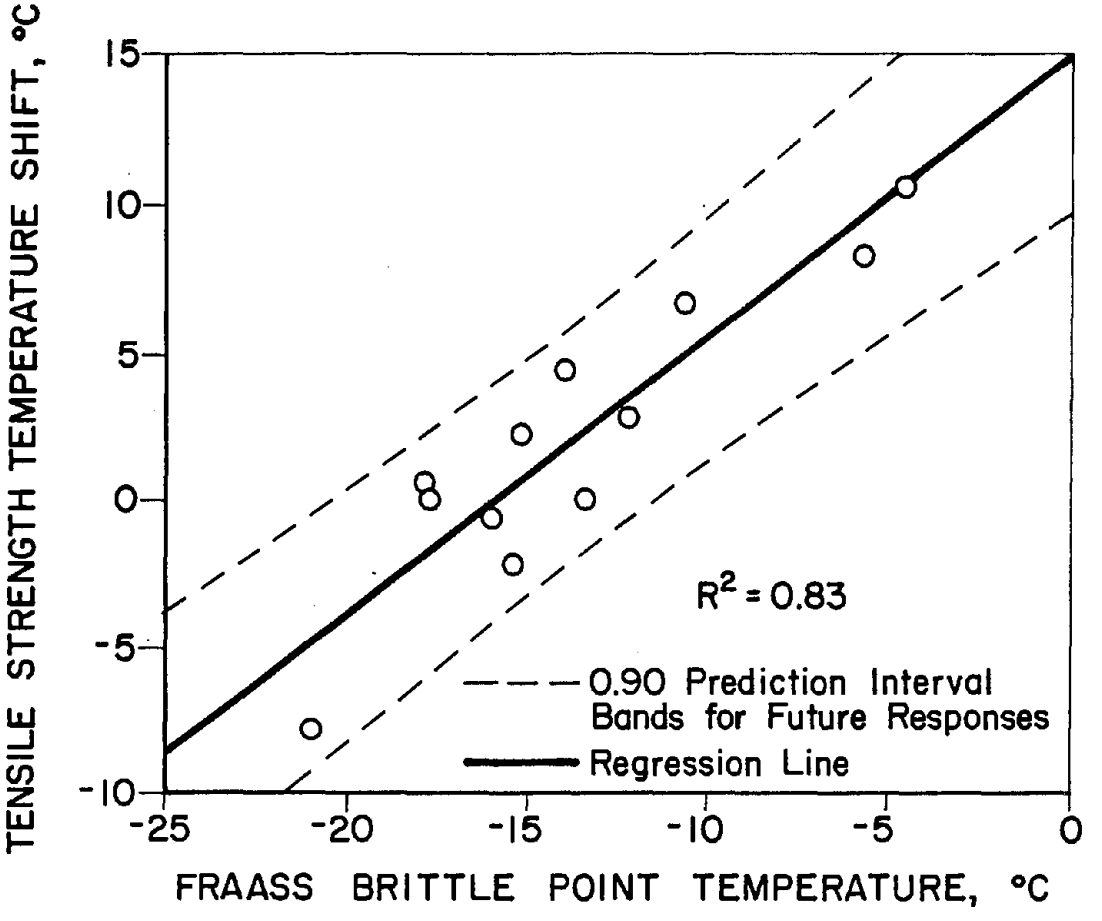

Figure 49. Plot of tensile strength temperature shift versus Fraass brittle point temperature.

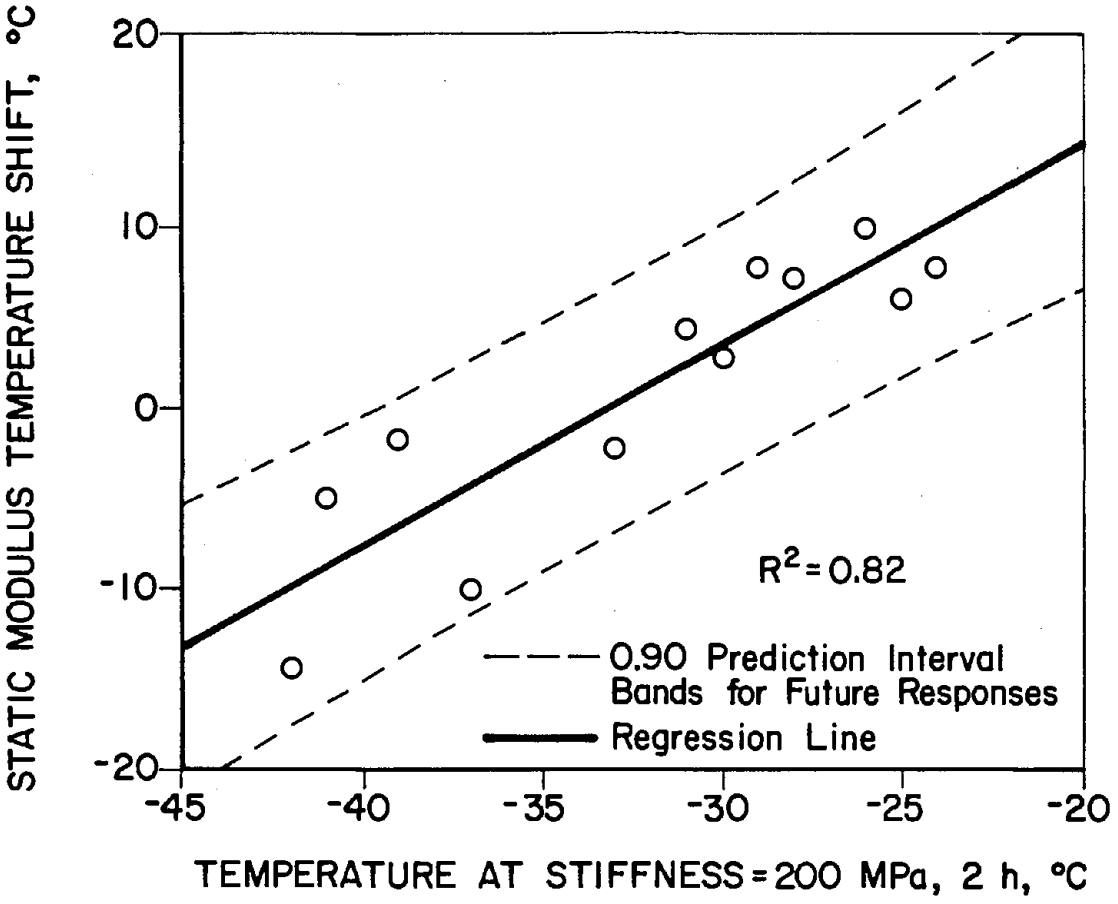

Figure 50. Plot of static modulus temperature shift versus temperature where stiffness equals 200 MPa after 2 h loading time ($PI_{log-pen}$).

6.8 COMPARISONS WITH PREDICTED CRACKING INDICES

The equistiffness temperatures were also compared graphically with the cracking indices predicted by the TC-1 and THERM programs for the Fargo, North Dakota, location. Examples of these plots are shown in figures 51 through 53, where the cracking predicted by TC-1 is plotted versus T_{Fraass}, $T_{Pen1.2}$, and the limiting stiffness temperature for 29,000 lb/in^2 (200 MPa) at 2 h loading time, based upon T_{Pen800} and $PI_{log\text{-}pen}$. The plots containing the TC-1 cracking indices, figures 51 through 53, reflect not a linear relationship between the variables but two separate relationships: the one described by the solid line and the other by the points that plot on or near the abscissa.

The solid line, which has been sketched in figure 51, appears to approximately represent the expected trend in the data: cracking showed an increase with increasing Fraass brittle point temperature. Asphalt number 8, with the highest Fraass brittle point temperature, should be associated with considerable cracking, whereas TC-1 predicts little or no cracking. If a valid relationship does exist between the cracking index and the Fraass brittle point temperature, then asphalt number 16 should also be considered to show anomalous behavior, with TC-1 underpredicting the cracking that would be expected given its Fraass brittle point temperature.

Figures 52 and 53 were prepared with $T_{Pen1.2}$ and an equistiffness temperature as the respective abscissa. The two figures show nearly identical trends, which might be expected given the excellent correlation, figure 39, that was shown previously between $T_{Pen1.2}$ and the equistiffness temperature based on $PI_{log\text{-}pen}$ and T_{Pen800}. Asphalt numbers 8, 11, 12, and 16 evidence anomalous behavior in figures 52 and 53. Relative to the $T_{Pen1.2}$ and equiviscous temperatures, TC-1 overpredicts the cracking for asphalt number 12 and underpredicts the cracking for asphalt number 8. Based on field experience, asphalt number 12 would not be expected to show significant cracking, whereas asphalt number 8 would be expected to crack significantly. On the basis of their grade and field record, asphalt numbers 11 and 16 would be expected to be resistant to thermal cracking. TC-1 predicts minimal thermal cracking for these asphalts, but they have the second and fourth highest Fraass brittle point temperatures of all the asphalts.

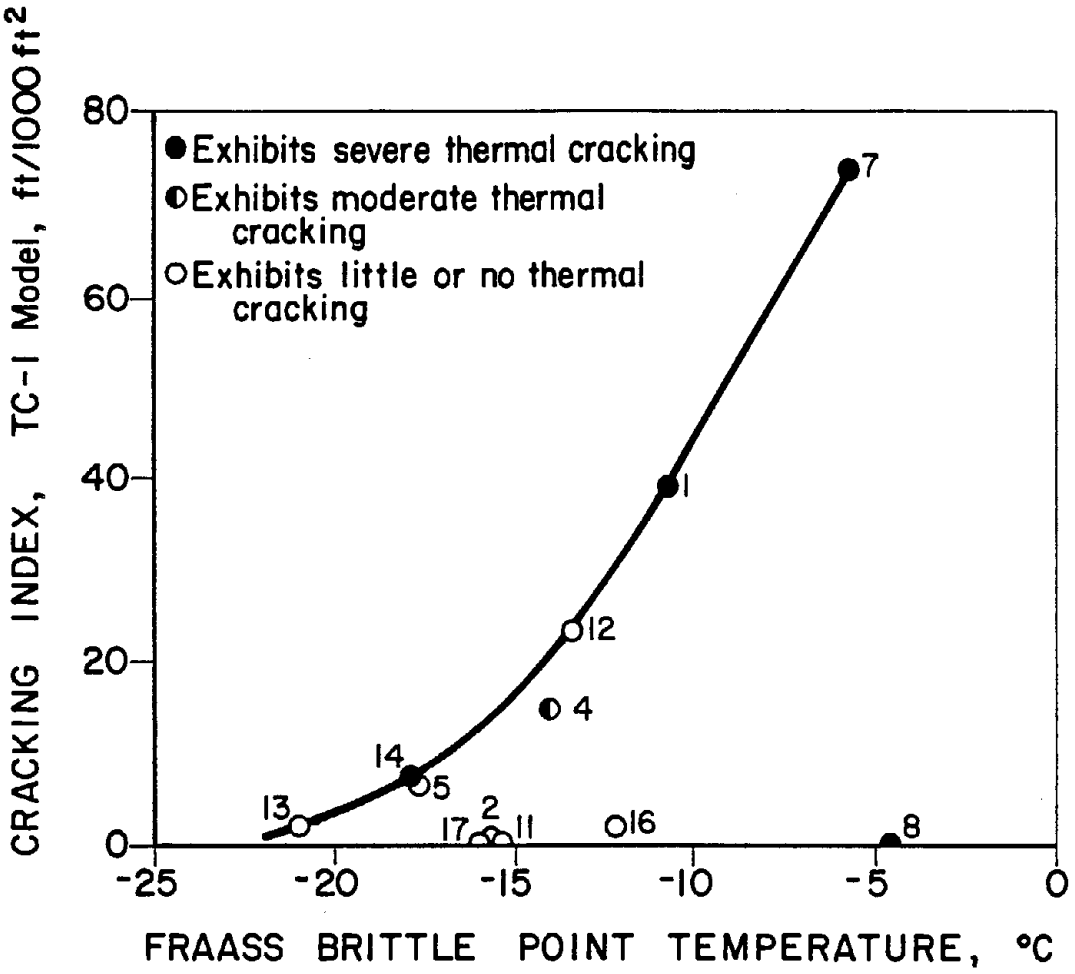

Figure 51. Cracking index as predicted by TC-1 versus Fraass brittle point temperature, Fargo, ND.

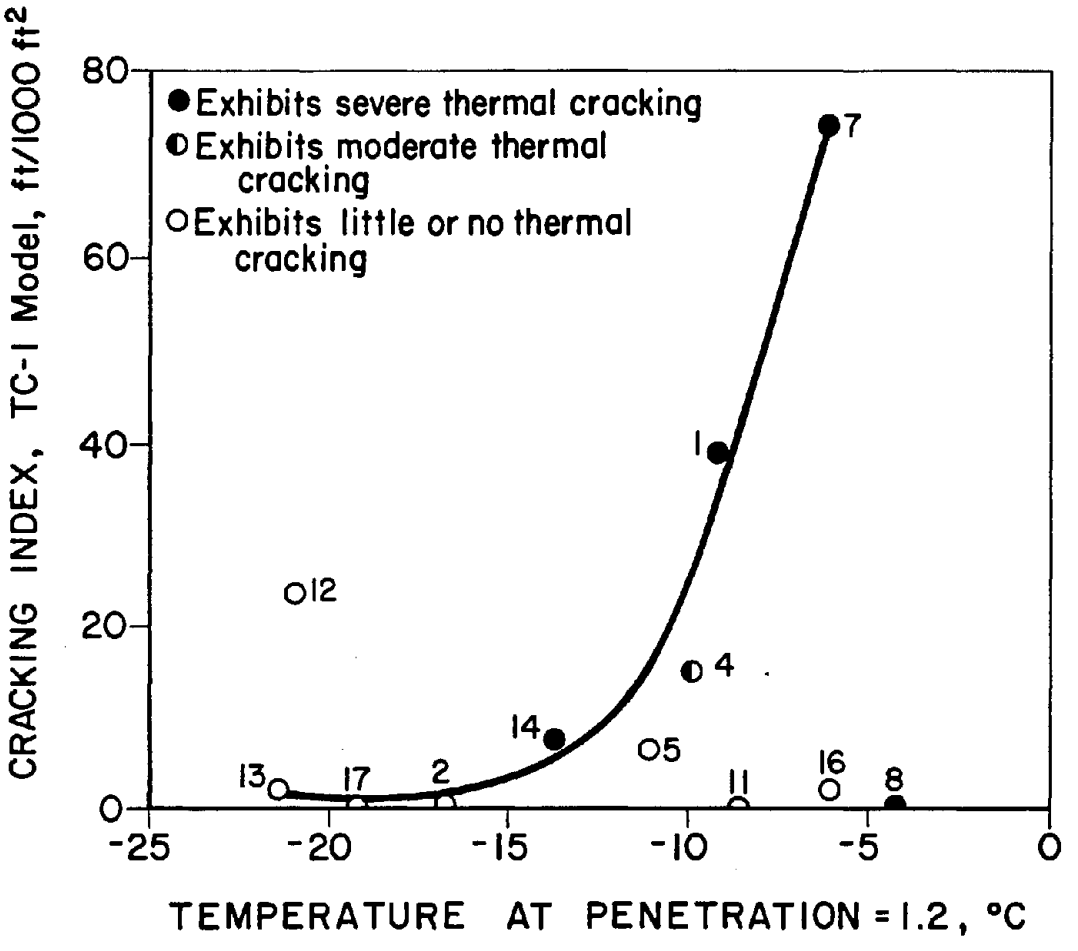

Figure 52. Cracking index as predicted by TC-1 versus temperature where penetration is equal to 1.2, Fargo, ND.

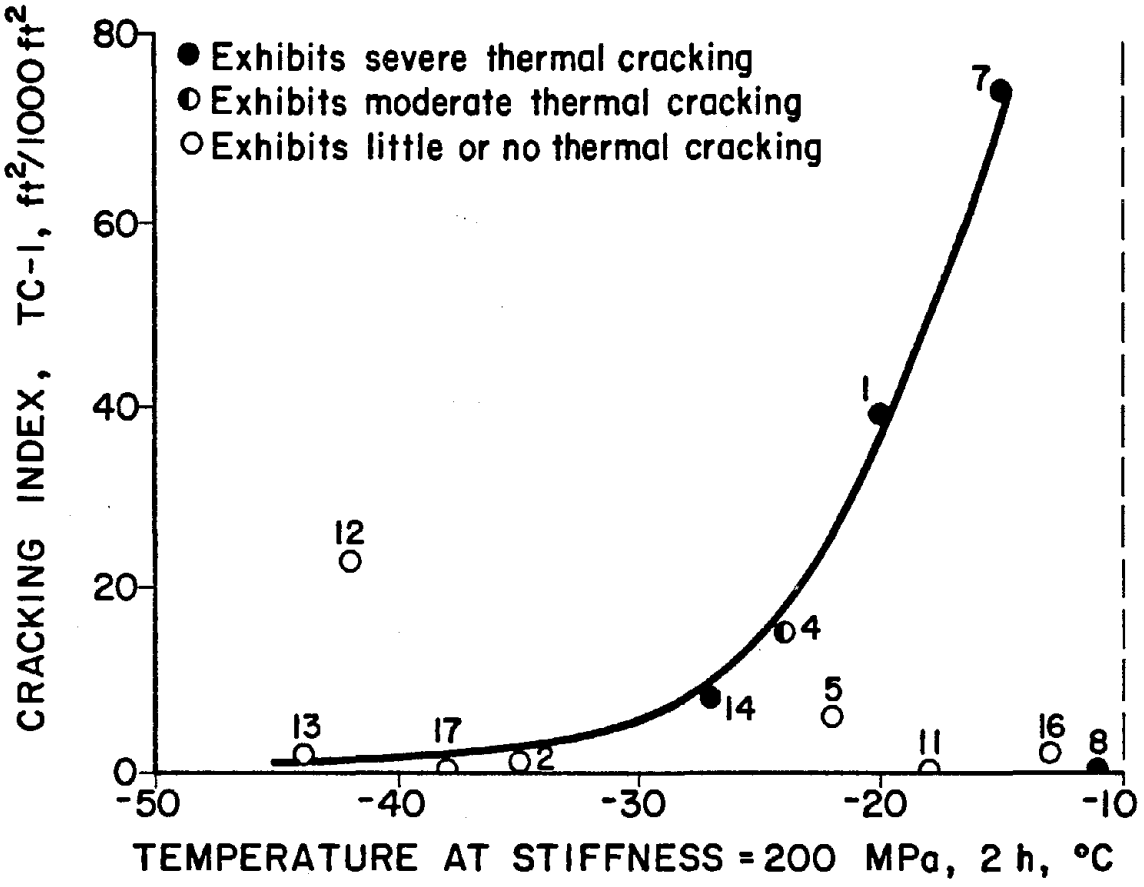

Figure 53. Cracking index as predicted by TC-1 versus temperature where stiffness is equal to 200 MPa at 2 h, °C, using T_{Pen800} and $PI_{log-pen}$, Fargo, ND.

Asphalt numbers 7 and 5 (Texas) and 14 and 13 (Canada) offer a comparison of materials differing in grade but from the same source. In both cases the softer grade (numbers 5 and 13) have a lower equistiffness temperature and a smaller predicted cracking index than their stiffer counterpoints (numbers 7 and 14). Asphalt 16 is a waxy asphalt and shows a high Fraass brittle point temperature, figure 5) and a high equistiffness temperature (figures 52 and 53). When processed with air blowing (asphalt number 17), the asphalt from this crack shows a reduced Fraass brittle point temperature, figure 51, and equistiffness temperature, figures 52 and 53; this TC-1 cracking index is insensitive to the blowing.

The cracking indices predicted by program THERM are plotted versus the Fraass brittle point temperature in figure 54. No discernible relationship is shown, verifying the authors' previous comments regarding needed improvements to the program, chapter 5.

6.9 PRECISION ESTIMATES

Estimates of precision were calculated for the consistency measurements, temperature susceptibility parameters, and limiting stiffness temperatures. The precision estimates are given as values of D2S, which is the difference between two repeated measurements which will be exceeded only 1 time in 20. The D2S precision is calculated simply by multiplying the standard deviation by two times the square root of two. Table 30 lists estimated precisions for the routine test data. These precision values were found using simple analysis of variance techniques where the individual determinations were treated as replicates and then pooled for the 17 asphalts. Where available, ASTM precision statements are also listed in this table for comparison.

Of particular interest in table 30 are the relatively large D2S values for DMA loss peak temperature, indicating that improvements in the test procedure or the use of different sample geometry (e.g., cone and plate or parallel sliding plate) is needed. Replicate measurements were not obtained for the HP-GPC and DSC tests, and, therefore, no precision estimates were made for them.

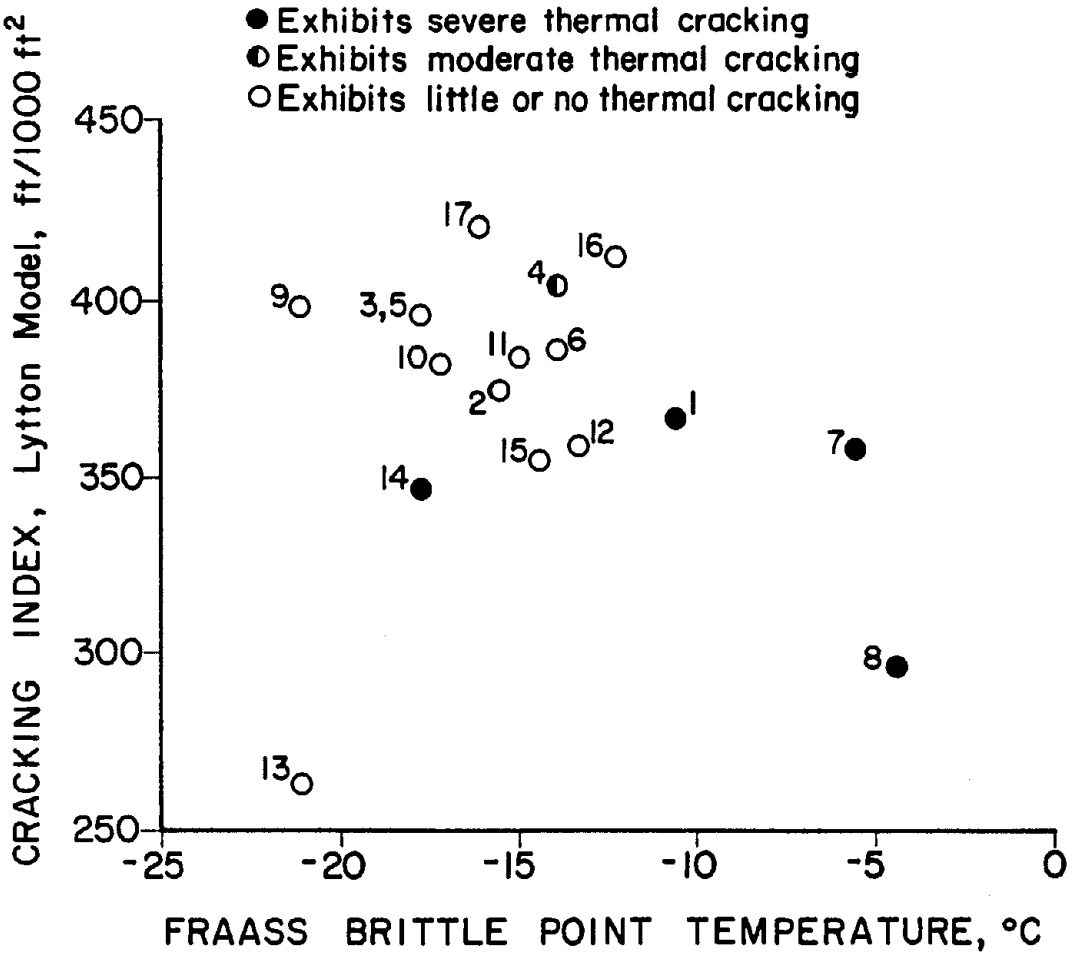

Figure 54. Cracking index as predicted by Lytton (THERM) model versus Fraass brittle point temperature.

Table 30. Precision summary for laboratory tests, D2S precision, single operator[1].

Procedure	ASTM	Unaged	RTFOT Residue	Observed Range, RTFOT
Viscosity at 140 °F	7.0%	3.7%	2.3%	917 to 8150 P
Viscosity at 275 °F	1.8%	1.5%	2.8%	274 to 894 cSt
Penetration:				
At 42 °F	1.0 1/10 mm	--	1.0 1/10 mm	8 to 17 1/10 mm
At 59 °F	1.0 1/10 mm	--	1.4 1/10 mm	11 to 44 1/10 mm
At 77 °F	3.0%	2.9%	3.5%	36 to 125 1/10 mm
At 95 °F	3.0%	--	2.0%	92 to 213 1/10 mm
Softening Point	1.8 °F	1.1 °F	1.2 °F	108 to 132 °F
RTFOT Loss	14%	14%	--	-0.328 to 1.502
Fraass Temperature	--	--	2.9 °F	-6 to 24 °F
DMA Loss Peak Temperature:				
1 replicate	--	--	5.8 °F	38 to 68 °F
2 replicates	--	--	3.2 °F	

[1] Maximum expected difference between two determinations.

The temperature susceptibility parameters and limiting stiffness temperatures are estimated from nomographs that require a pair of variables, such as penetration and ring and ball softening point temperature. Triplicate measurements were made for penetration and duplicate measurements were made for ring and ball softening point temperature. To obtain random pairs of measurement values that could be used with the nomographs, one of the softening point temperatures was randomly chosen and then randomly assigned to one of the penetration values. The remaining softening point temperature was then randomly assigned to one of the two remaining penetration values end the third penetration value was ignored. This was repeated for all 17 asphalts, producing 34 pairs of values for estimating the penetration index. The same technique was used for the other calculated temperature susceptibility and limiting stiffness parameters.

Precision estimates for the various temperature susceptibility parameters are given in table 31. The D2S values for the penetration-viscosity numbers, and viscosity temperature susceptibility (VTS), are significantly smaller than for the other parameters, probably because the viscosity measurements are more repeatable compared with softening point and penetration measurements. The precision for $PI_{log\text{-}pen}$, when penetration is determined at only two temperatures, is 0.86, which is unacceptably large. When using this procedure for calculating penetration index, measurements at three temperatures should be used to improve the precision.

Estimated precision values for stiffness values predicted from der Poel's nomograph, and McLeod's modification of Heukelom and Klomp's version of Van der Poel's nomograph, are given in table 32. The estimated precision for Van der Poel's nomograph (all methods) is 31 percent and for McCleod's version of the nomograph, 25 percent. For all practical purposes, the precision of these nomographs should be considered equal and generally acceptable. The estimated precision for limiting stiffness temperatures using all techniques is 7.2 °F (4.0 °C). All nomographs used in this project were enlarged to approximately 24 by 30 in (60 by 75 cm). Using a smaller scaled version of the nomographs, as generally published in the literature, will probably increase the magnitude

Table 31. Precision summary for temperature susceptibility parameters, D2S precision, single operator[1].

Parameter	Unaged	RTFOT Residue	Observed Range, RTFOT
Penetration Index, 77 Pen/$T_{R\&B}$	0.34	0.34	-1.29 to -0.10
Penetration Index, Log-Pen Data:			
2 Temperatures	--	0.86	-1.76 to 0.38
3 Temperatures	--	0.44	
Penetration Index, 77 Pen/Fraass Temperature	--	0.45	-1.44 to 0.15
Penetration Viscosity Number:			
77 Pen/140 vis	0.11	0.11	-1.07 to 0.12
77 Pen/275 vis	0.07	0.08	-1.36 to 0.16
Viscosity Temperature Susceptibility	0.033	0.065	-3.89 to -3.08

[1] Maximum expected difference between two determinations.

Table 32. Precision summary for Van der Poel's and McLeod's nomograph.

Procedure	D2S Precision, Single Operator	Observed Range, RTFOT
Stiffness Estimate; Original Van der Poel Nomograph	31%	130 to 3,000 lb/in^2
McLeod's version of Van der Poel's Nomograph	25%	130 to 3900 lb/in^2
Limiting stiffness temperature, All methods	7.2 °F (4.0 °C)	-67 to -11 °F

of reading errors, thereby decreasing the repeatability of stiffness values read from the nomograph.

6.10 ANALYSIS OF FRACTURE MECHANICS DATA FOR ASPHALT CONCRETE MIXES

The critical value of J-integral, J_{1c}, is a measure of the rate of the strain-energy released during fracture. Thus, increasing values of J_{1c} reflect increasing resistance to cracking. Values of J_{1c}, were calculated from the experimental data using two methods. The first method, called method 1 hereafter, was explained in chapter 4. In this method, J_{1c} is calculated from the following equation:

$$J_{1c} = [-1/b][dU_T/da] \tag{45}$$

where

b = width of beam, in (mm)
U_T = total strain energy to failure, lb-in (J)
a = crack (notch) length, in (mm)

Rice showed that J-integral is a path-independent contour integral which is a mathematically valid formulation for evaluating energy to failure in the presence of limited plasticity at the crack tip.[85] Values of J_{1c} calculated from plots, figure 34, of total energy per unit width versus initial crack (notch) length, method 1, were given in table 20.

Method 1 was proposed as part of the initial work plan; however, a second method, method 2, is also commonly used to calculate J_{1c}. An advantage of this method is that only a single specimen is needed to define J_{1c}. This method, for three-point bending, was suggested by Merkle et al. (figure 30):[90]

$$J_{1c} = \eta(U_T - U_e^{nc})/b(d-a) \tag{46}$$

where

η = constant dependent on crack geometry
U_T = total strain energy to failure, lb-in (J)

U_e^{nc} = stored elastic energy in a beam with no crack, lb-in (J)

b = width of beam, in (mm)

d = depth of beam, in (mm)

It should be noted that failure is obtained when a maximum load is reached on the load-deflection diagram. In this study the beams that were tested measured 3 in (76 mm) by 3 in (76 mm) by 16 in (406 mm). Sumpter and Turner have discussed equation 46 in more detail.[91] They found from experiments, done for metals and polymers, that for beam length to beam depth ratios (L/d) equal to 4, the contribution of U_e^{nc} in equation 46 is negligible, in which case that equation becomes:[90]

$$J_{1c} = \eta U_T/b(d-a) \tag{47}$$

Sumpter and Turner also observed that for beam length to depth ratios (L/d) equal to 4 and crack (notch) length to beam depth ratios (a/d) between 0.5 and 0.7, the constant, η, in equation 47 is equal to 2.[91] Therefore, equation 47 can be stated as:

$$J_{1c} = 2\ U_T/b(d-a) \tag{48}$$

This relationship is valid only for the beam length to depth and crack (notch) length to beam depth ratios given above. The specimens used in this study satisfied these requirements. Values of J_{1c} calculated using method 1 (equation 37) and method 2 (equation 48) are given in table 33.

When J_{1c} values calculated from the two methods were compared they were found to be in reasonably good agreement for most of the asphalts. Linear regression was used to compare the J_{1c} values obtained from the two methods. A coefficient of determination, R^2, was obtained for each asphalt by regressing the J_{1c} value obtained from method 2 against the J_{1c} value obtained from method 1. In general the coefficients of determination showed good to excellent correlation between the J_{1c} values obtained from the two methods. For two of the asphalts, numbers 12 and 14, there was no correlation between the two methods; the coefficient of determination was 0.09 and 0.06, respectively. Examination of the data for these two asphalts shows a

Table 33. Summary of fracture mechanics characterization.

Asphalt Number	Method	J1c, lb-in/in^2 -5 °F	8 °F	10 °F	15 °F	25 °F	40 °F	60 °F	Coefficient of Determination R^2, Method 1 vs. Method 2
1	Method 1	.66	NT	NT	1.50	NT	1.67	7.7	
	Method 2	.67	NT	NT	1.11	NT	1.47	8.3	.98
	G_{1c}	.41	NT	NT	.97	NT	10.9	35.	
2	Method 1	.66	NT	.81	NT	.49	8.6	NT	
	Method 2	.76	NT	1.08	NT	1.11	11.2	NT	.85
	G_{1c}	.48	NT	2.0	NT	7.8	27.	NT	
4	Method 1	.45	NT	1.22	NT	1.80	1.09	NT	
	Method 2	.54	NT	.62	NT	1.10	1.54	NT	.75
	G_{1c}	.39	NT	.49	NT	1.87	7.5	NT	
5	Method 1	.64	NT	1.14	NT	1.56	6.2	NT	
	Method 2	.55	NT	.84	NT	1.16	4.9	NT	.90
	G_{1c}	.31	NT	.86	NT	3.9	23.	NT	
7	Method 1	.82	NT	NT	.40	NT	.90	5.9	
	Method 2	.58	NT	NT	.65	NT	1.30	7.2	.89
	G_{1c}	.33	NT	NT	.56	NT	1.44	5.0	
8	Method 1	.28	.39	NT	NT	NT	1.45	3.6	
	Method 2	.29	.38	NT	NT	NT	1.10	4.6	.84
	G_{1c}	.25	.47	NT	NT	NT	6.4	91.	
11	Method 1	.10	NT	NA	NT	1.51	.81	NT	
	Method 2	.49	NT	.36	NT	1.15	.99	NT	NA
	G_{1c}	.26	NT	.50	NT	1.10	1.54	NT	
12	Method 1	.20	NT	.21	NT	.76	2.1	NT	
	Method 2	.93	NT	.90	NT	1.68	7.5	NT	.09
	G_{1c}	1.00	NT	2.5	NT	19.2	49.	NT	
13	Method 1	.13	.66	NT	NT	5.7	7.7	NT	
	Method 2	.85	1.26	NT	NT	5.1	5.8	NT	.88
	G_{1c}	.95	4.5	NT	NT	16.8	24.	NT	
14	Method 1	.20	NT	2.24	NT	1.77	2.6	NT	
	Method 2	.90	NT	1.00	NT	1.34	9.4	NT	.06
	G_{1c}	.45	NT	.52	NT	2.40	10.8	NT	
16	Method 1	.28	NT	NT	.95	NT	1.10	8.6	
	Method 2	.39	NT	NT	.69	NT	1.36	8.1	.99
	G_{1c}	.20	NT	NT	.40	NT	7.0	32.	
17	Method 1	.15	NT	1.37	NT	1.91	6.4	NT	
	Method 2	.55	NT	1.05	NT	1.22	4.1	NT	.73
	G_{1c}	.39	NT	1.18	NT	3.6	13.6	NT	

Note: NT indicates that no test was conducted at this temperature.
NA indicates that the data were not available from this test.

consistent relationship with temperature for the method 2 data and a somewhat erratic relationship for the method 1 data. As a consequence of these results, and because method 2 requires fewer specimens and is less tedious and time consuming to conduct, the authors choose method 2 as the preferred method. The method 2 data are used in the analyses that follow.

According to fracture mechanics theory, the elastoplastic strain energy release rate, J_{1c}, should equal the linear elastic strain energy release rate, G_{1c}, at low temperatures where the behavior of the asphalt concrete is linear elastic and when the crack tip plasticity is small. G_{1c} can be described as the amount of energy per unit area available to propagate the crack a distance of one unit length. G_{1c} values were calculated using the relationship:[50]

$$G_{1c} = 0.521\ (1 - \nu^2)\sigma_c^2\ B/S_m(T,t) \qquad (49)$$

where

G_{1c} = linear elastic strain energy release rate for plane strain, lb-in/in^2 (Pa-m)
ν = Poisson's ratio
σ_c = remote critical stress, lb/in^2 (Pa)
B = uncracked ligament length, d-a, in (mm) (see figure 30)
d = depth of beam, in (mm)
a = crack (notch) length, in (mm)
$S_m(T,t)$ = stiffness of asphalt concrete mix, lb/in^2 (Pa)

A value of 0.35 was assumed for Poisson's ratio. The remote critical stress, σ_c, is the stress in the beam at some distance from the crack, where the stresses are not affected by the presence of the crack. The stiffness of the mix, S_m (T,t), was taken from plots of the static diametral tensile modulus versus temperature.

Values of G_{1c} for the mixes prepared with each asphalt are presented in table 33. A cursory examination indicates that the values of J_{1c} and G_{1c}

merge at low temperatures. This was verified by plotting J_{1c} (method 2) versus G_{1c} on a log-log plot, figures 55 through 57. The asphalts were plotted in four groups for convenience in plotting and to reduce the number of plots. At the lower temperatures (where the log of J_{1c} and G_{1c} are negative), J_{1c} and G_{1c} are approximately equal, grouping close to the line of equality. At the higher temperatures, where crack tip plasticity becomes more dominant, the two methods diverge and G_{1c} is larger than J_{1c}. In this region the use of G_{1c} is inappropriate because the plastic strain energy cannot be separated from the calculation of G_{1c}. Although G_{1c} can be used at low temperatures where the asphalt concrete is linear elastic, it is inappropriate for much of the temperature regime of interest.

The J_{1c} values, calculated from method 2, table 33, were plotted versus temperature, as shown in figures 58 through 60, to examine their variation with temperature. From the plotted data it is quite obvious that J_{1c} is dependent upon both crude source and grade. Figure 59 contains asphalts in two grades from two different sources. Examining the temperature dependency of J_{1c} for the four asphalts, the two harder asphalts, numbers 4 and 7, reach an asymptotic value of J_{1c} at a much higher temperature than the two softer asphalts, numbers 2 and 5. Similar differences are also shown between the two sources, number 5 versus 2 and number 7 versus 4. In figure 58 asphalts from four different sources are plotted together and show considerable difference. In figure 60, asphalts 13 and 14 are from the same source but of different grade: the effect of grade is clearly shown. In figure 60 a distinct difference is shown between the vacuum distilled (asphalt 16) and blown waxy (asphalt 17) asphalts. Clearly J_{1c} is asphalt specific, varying with both crude source and grade.

6.11 COMPARISON OF J_{1c} TRANSITION TEMPERATURE TO OTHER VARIABLES

J_{1c} distinguished between the different grades and sources, figures 58, 59, and 60, and the curves for the mixes appeared to have an exponential shape. A quantitative method for determining their relative position on the temperature axis was developed. This position was characterized by a transition temperature or the temperature at which the plotted data become asymptotic with respect to the abscissa as shown in figure 61. The following

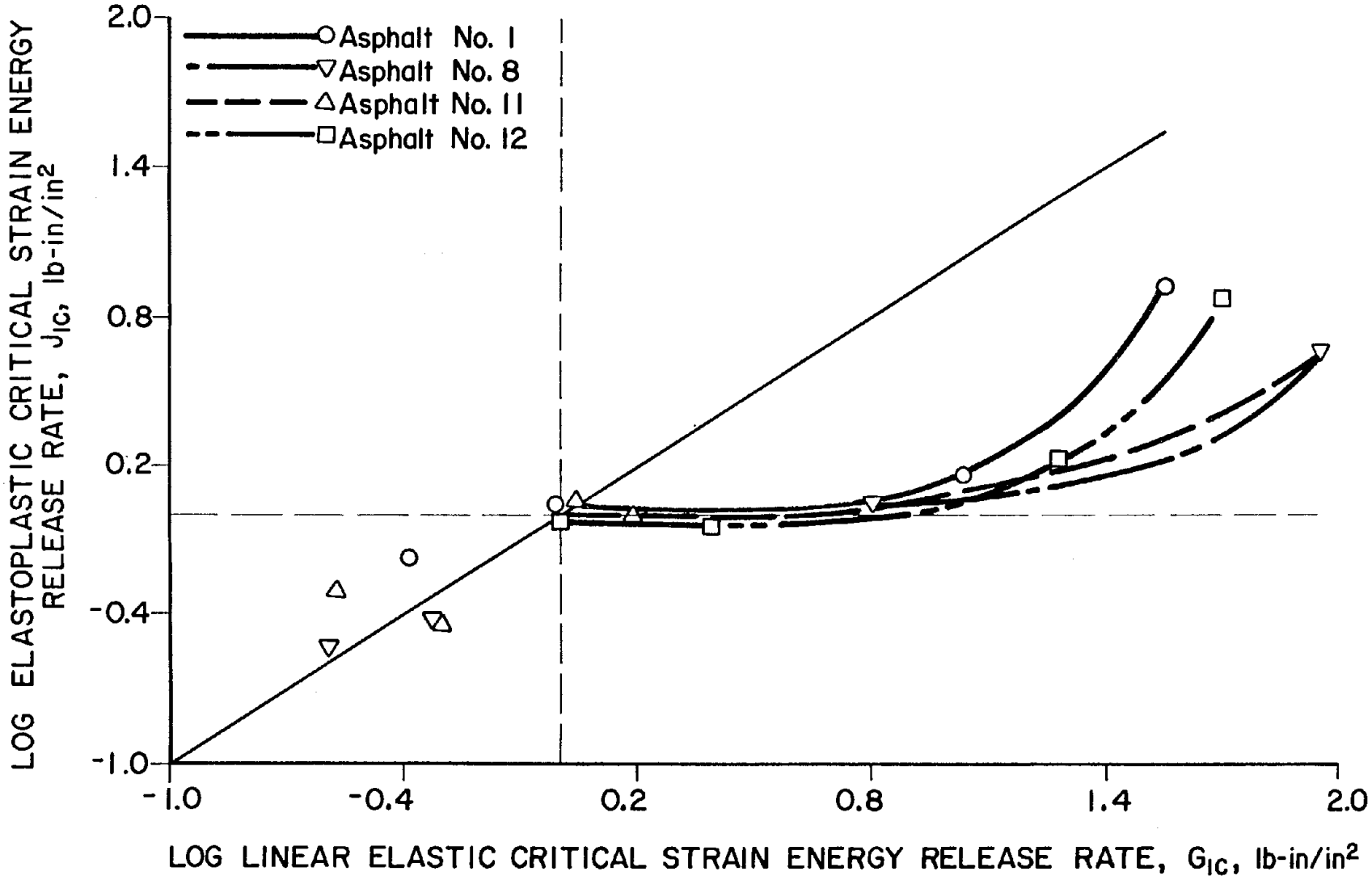

Figure 55. J_{1c} versus G_{1c} for asphalts 1, 8, 11, and 12.

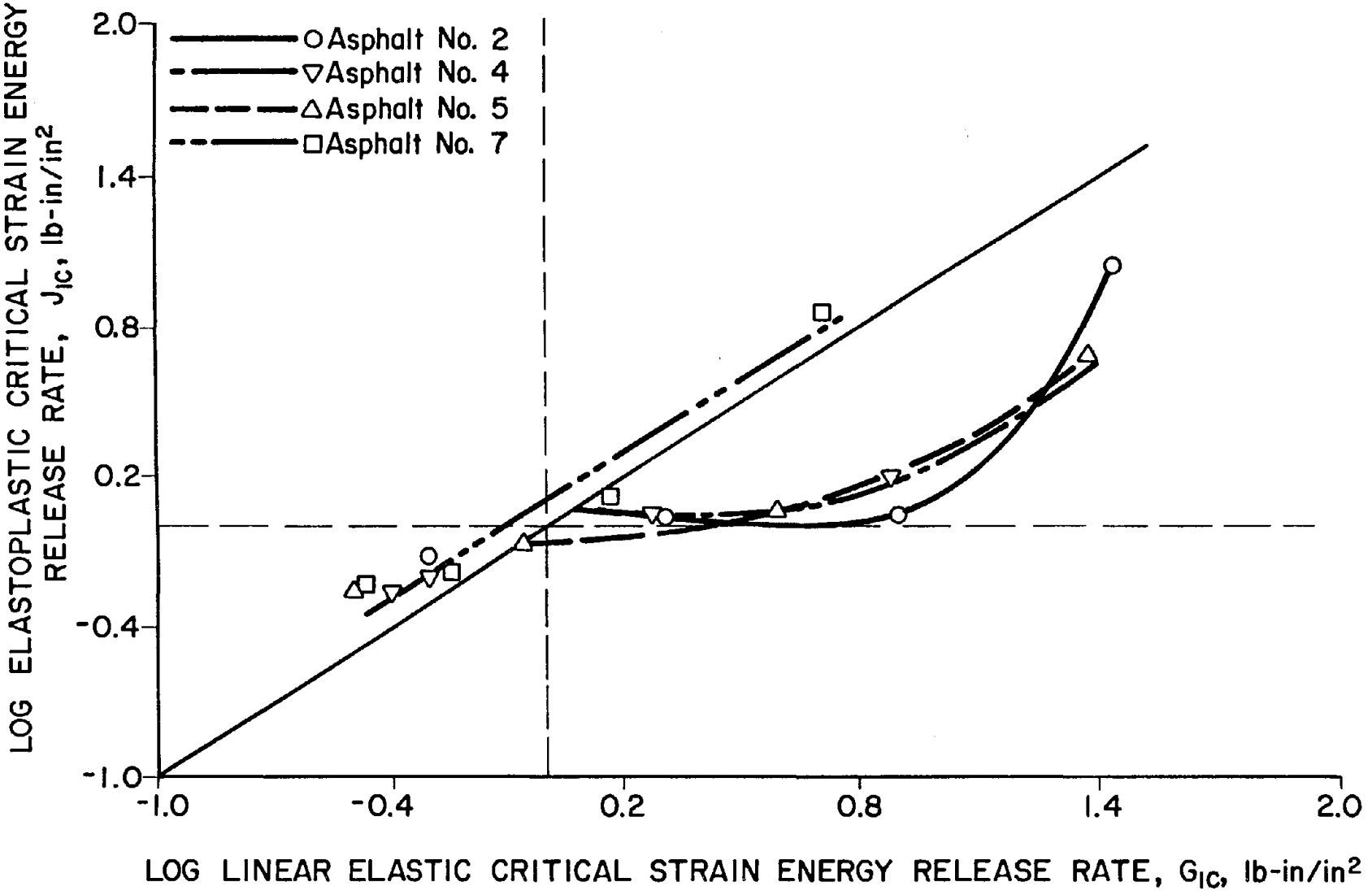

Figure 56. J_{1c} versus G_{1c} for asphalts 2, 4, 5, and 7.

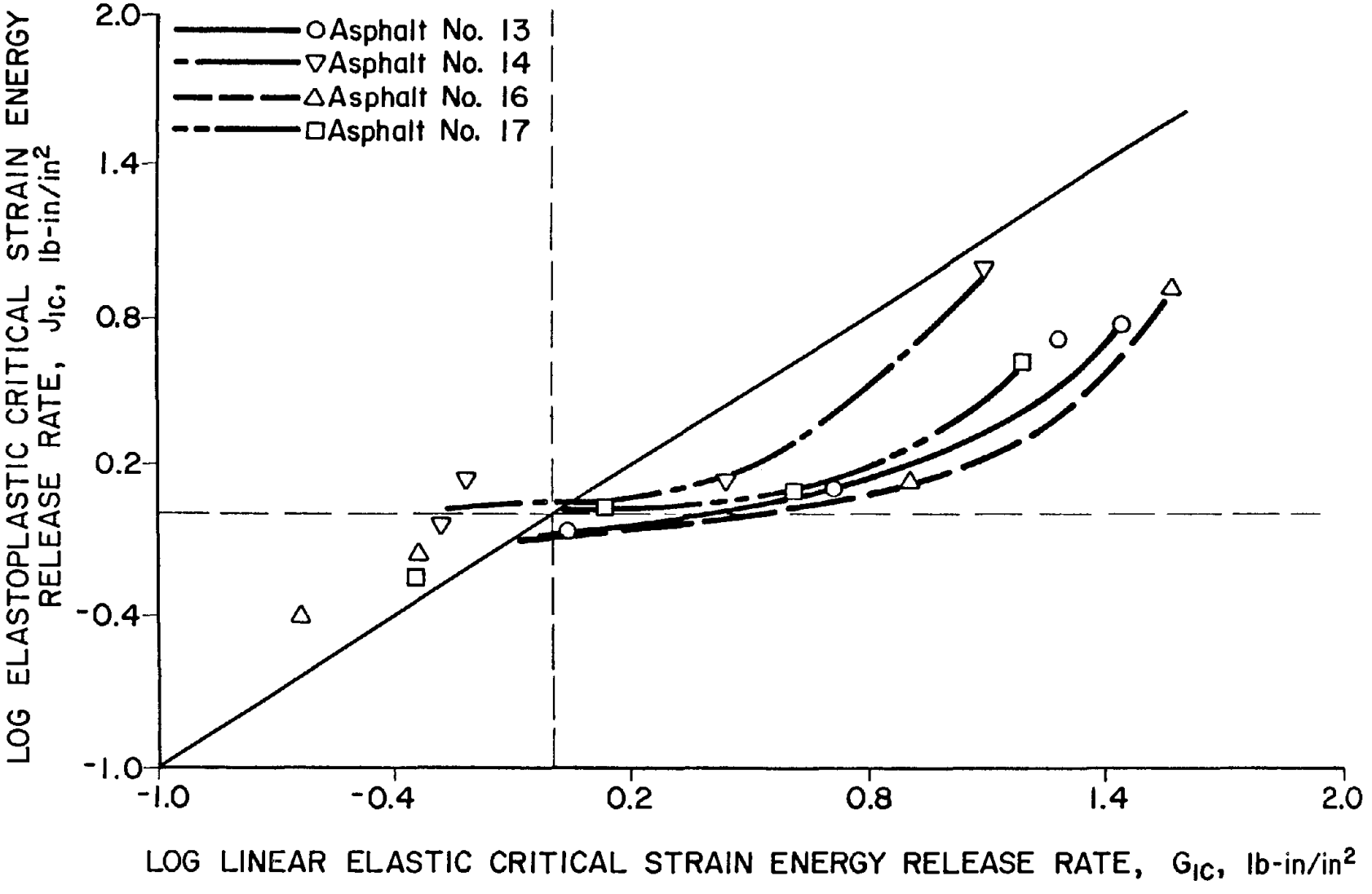

Figure 57. J_{1c} versus G_{1c} for asphalts 13, 14, 16, and 17.

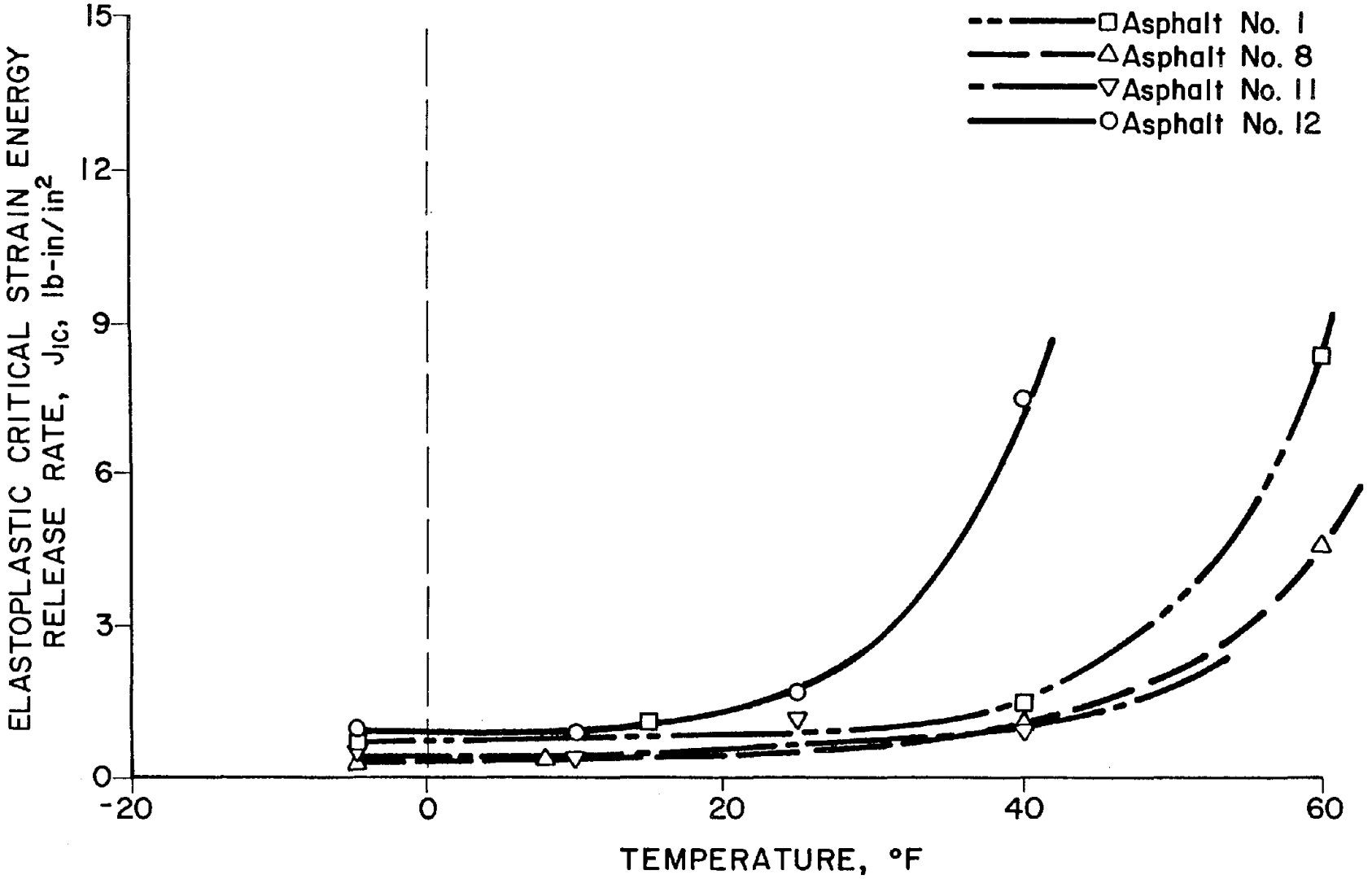

Figure 58. J_{1c} versus temperature for asphalts 1, 8, 11, and 12.

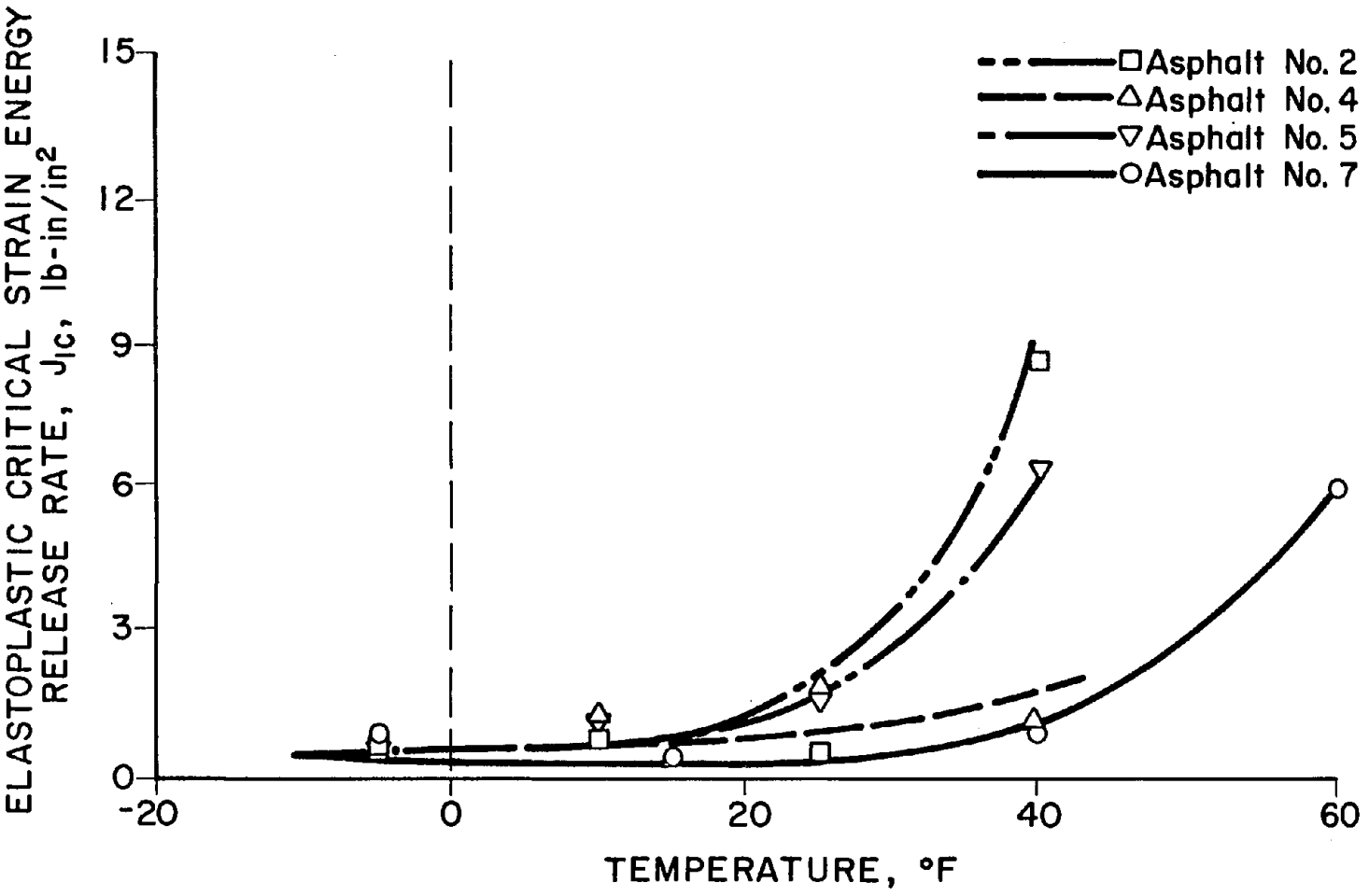

Figure 59. J_{1c} versus temperature for asphalts 2, 4, 5, and 7.

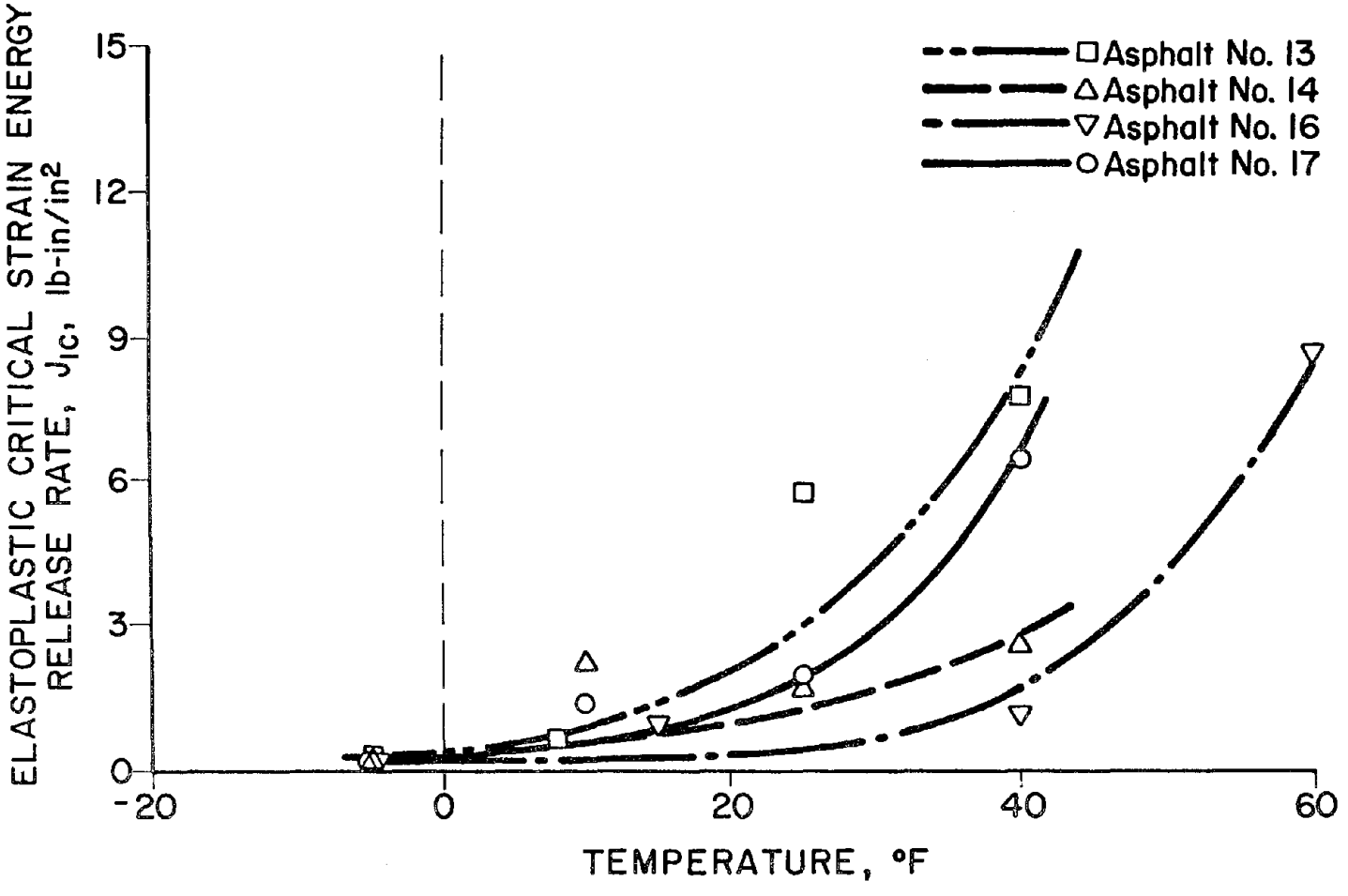

Figure 60. J_{1c} versus temperature for asphalts 13, 14, 16, and 17.

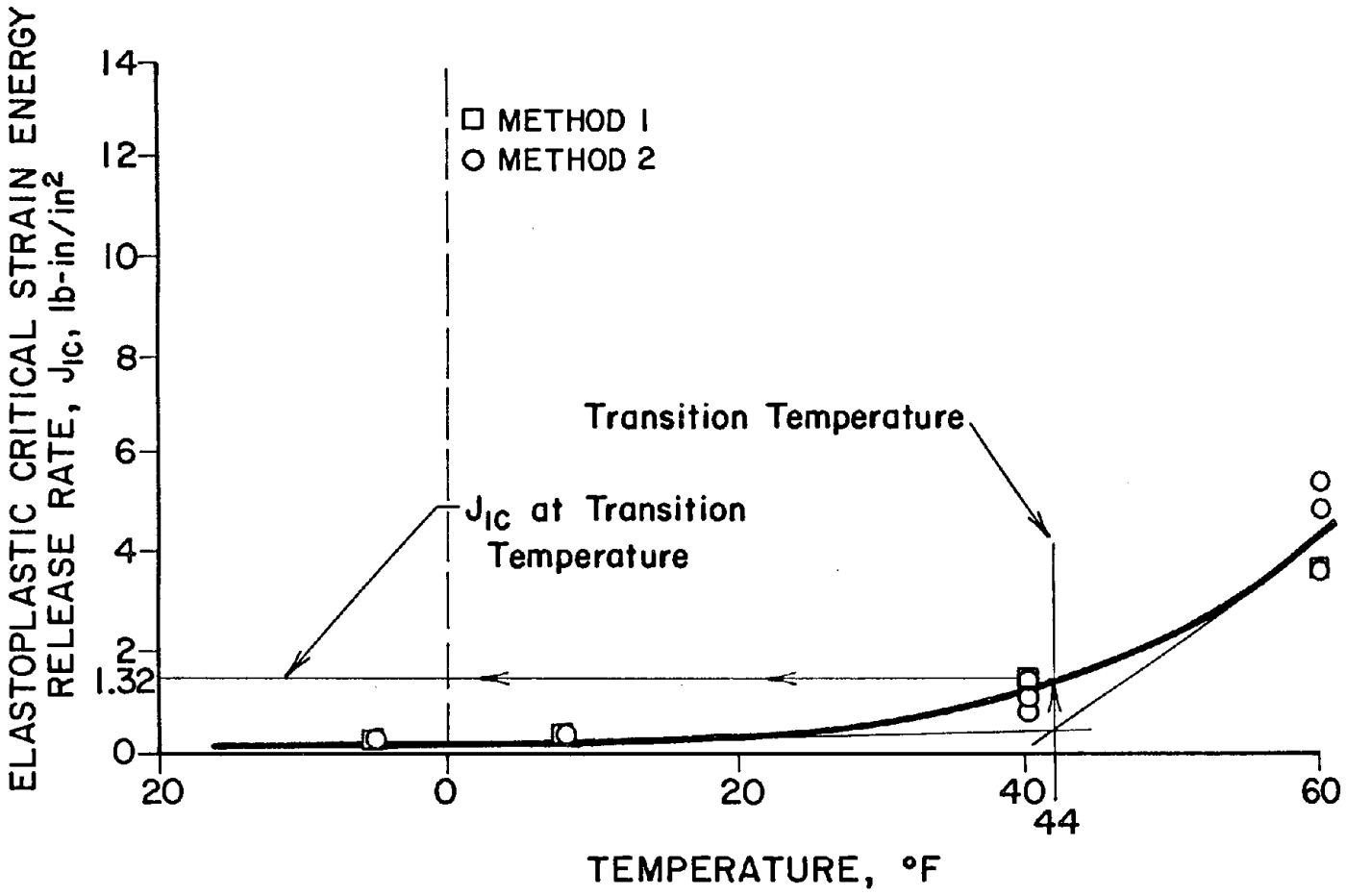

Figure 61. Schematic showing graphic determination of J_{1c} transition temperature.

procedure, as illustrated in figure 61, was used to determine the J_{1c} transition temperature. A line was first drawn parallel to the abscissa and asymptotic to the plotted data. A tangent to the plotted data was drawn to intersect with the asymptotic line as shown in figure 61. The intersection of the asymptotic line and the tangent thus defined the J_{1c} transition temperature. The location of the tangent was selected somewhat arbitrarily but, in general, it was drawn through the data point at the highest test temperature.

The J_{1c} transition temperatures for the asphalt mixtures are given in table 34 along with the temperature shifts (method 2) for the mixes, the Fraass brittle point temperature, and the temperature where the asphalt penetration is 1.2. Because each of these temperatures were obtained under very different test conditions (rates of loading), it is not surprising that they are not equal for a given asphalt. However, they should correlate with each other if they are measures of the same property, in this case, sensitivity to cracking.

To verify the levels of correlation between the J_{1c} transition temperatures and the other variables, the temperature shifts for tensile strength and modulus are plotted versus the J_{1c} transition temperatures in figure 62 where the R^2 values are 0.76 and 0.82, respectively. In figure 63 the Fraass brittle point temperature and $T_{Pen1.2}$ are plotted versus the J_{1c} transition temperatures, yielding R^2 values of 0.60 and 0.75, respectively. These R^2 values indicate that the J_{1c} transition temperature is moderately correlated with the other variables although the correlation is not sufficiently strong to warrant the use of the transition temperature as a surrogate for the other variables. The J_{1c} transition temperature was also compared with the DSC and DMA glass transition temperatures, figure 64, and the resulting correlations were very poor, giving R^2 values of 0.01 and 0.36, respectively. Because of the poor correlation, regression lines are not shown in figure 64.

Another comparison between the J_{1c} transition temperatures and other temperature variables potentially related to the susceptibility to thermal cracking is shown in table 35. In addition to the J_{1c} transition

Table 34. Results of linear regression of J_{1c} transition temperature versus other characteristic temperatures.

Asphalt No.	Source	J_{1c} Transition Temperature °F, method 2	Temperature Shift, °F: Static Tensile Strength	Temperature Shift, °F: Static Tensile Modulus	Fraass Brittle Point Temperature, °F	Temperature at Penetration, 1.2, °F	Temperature, T_g: From DSC, °F	Temperature, T_g: From DMA, °F
1	A	43	12	14	12.8	15.5	-27	55.4
2	B	29	-4	-18	4.3	2.0	-18	42.4
4	B	40	8	8	6.8	14.2	-27	46.0
5	C	29	0	5	0.1	12.0	-34	50.6
7	C	45	15	18	21.7	21.1	-25	48.3
8	D	43	19	14	23.9	24.2	18	68.3
11	E	>40	4	13	4.6	16.6	-28	44.7
12	F	26	0	-9	7.9	-5.6	-27	42.3
13	G	9	-14	-26	-5.8	-6.6	-17	42.0
14	G	31	1	-4	-0.2	7.3	-25	42.3
16	I	49	5	11	10.0	21.1	-26	55.0
17	I	32	-1	-3	3.2	-2.6	-40	37.9
intercept, b_o			-21	-38	-13	-20	-28	33
slope, b_1			0.72	1.13	0.62	0.85	0.15	0.46
coefficient of determination, R^2			0.76	0.82	0.60	0.75	0.01	0.36

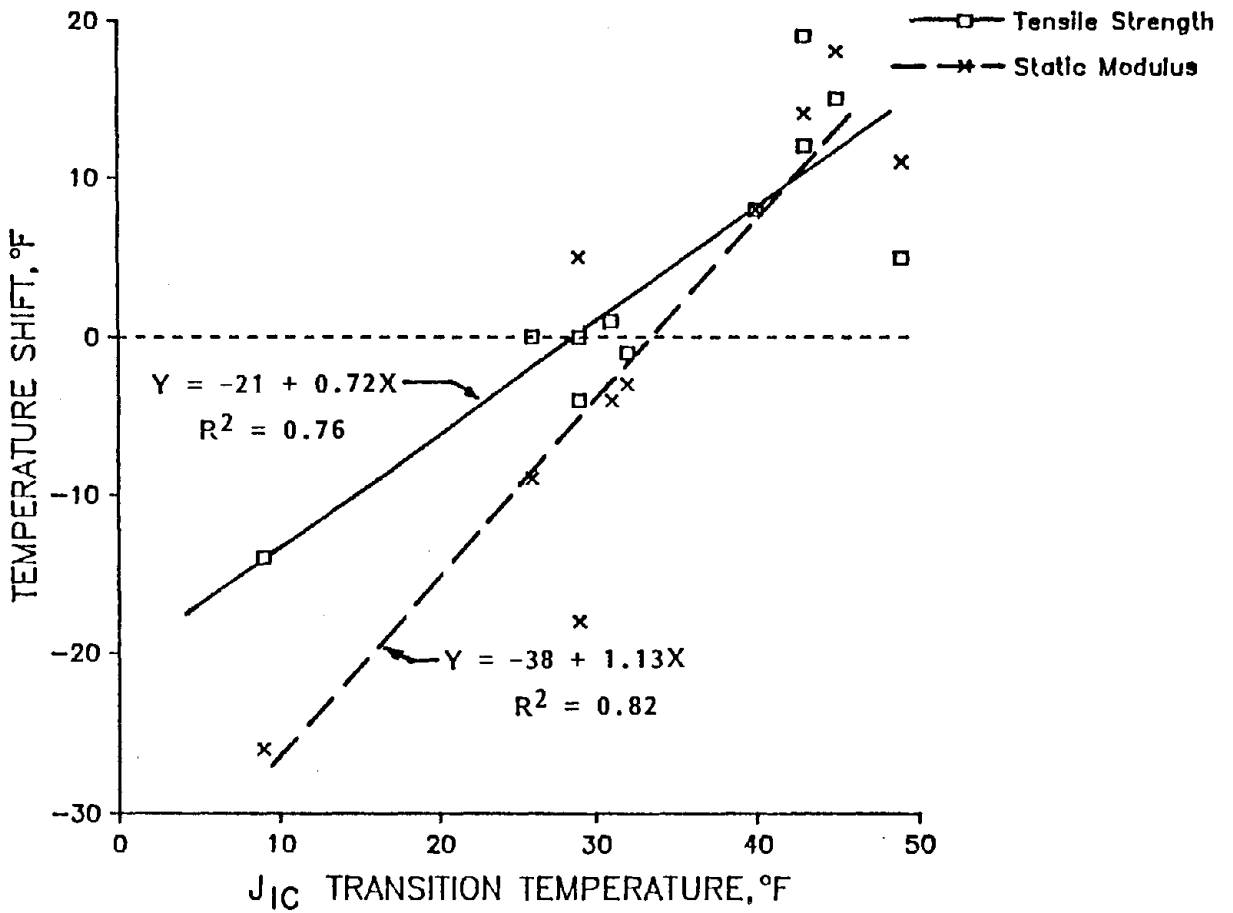

Figure 62. Mixture temperature shift versus J_{1c} transition temperature.

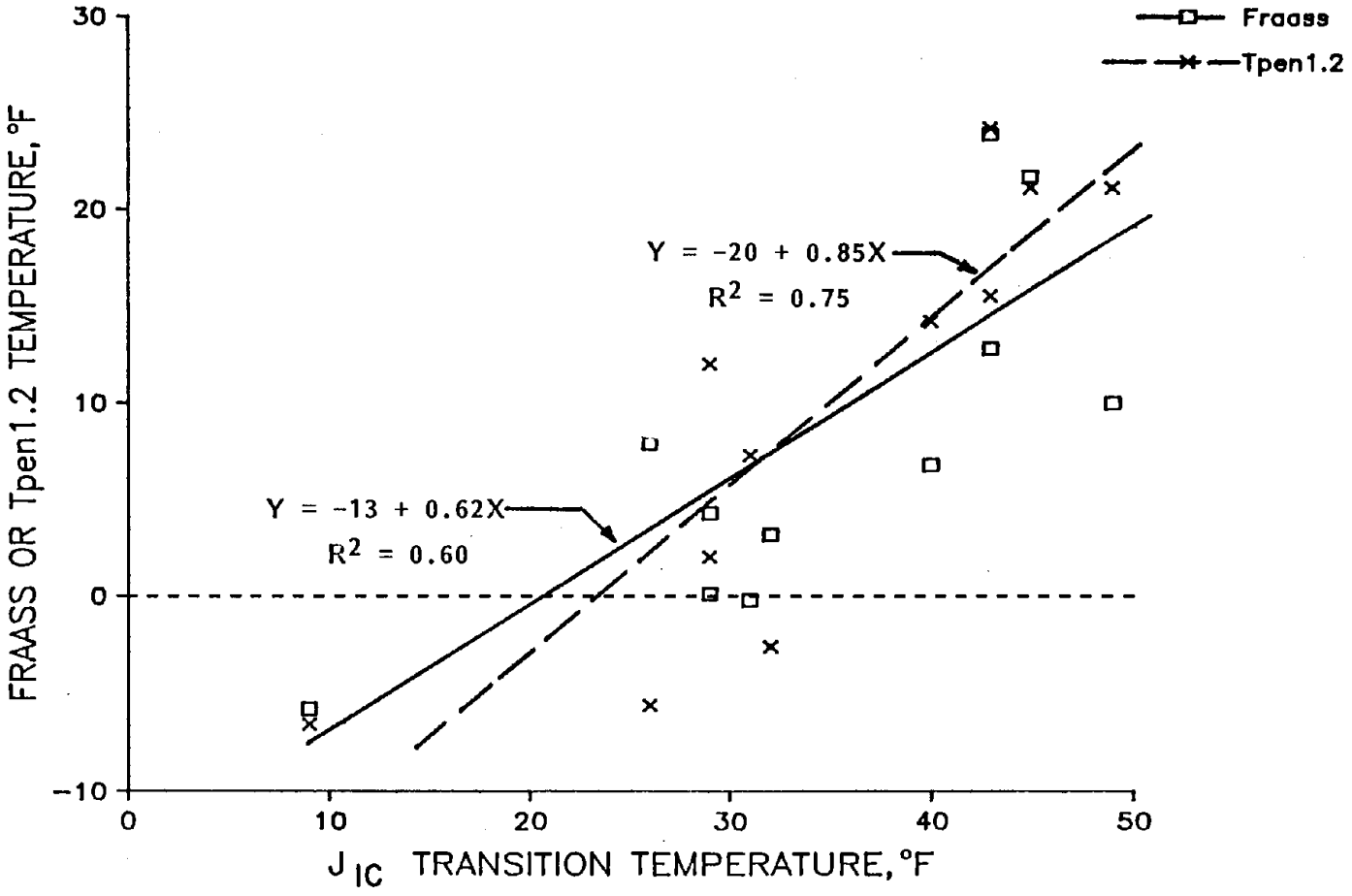

Figure 63. Fraass and $T_{Pen1.2}$ temperatures versus J_{1c} transition temperatures.

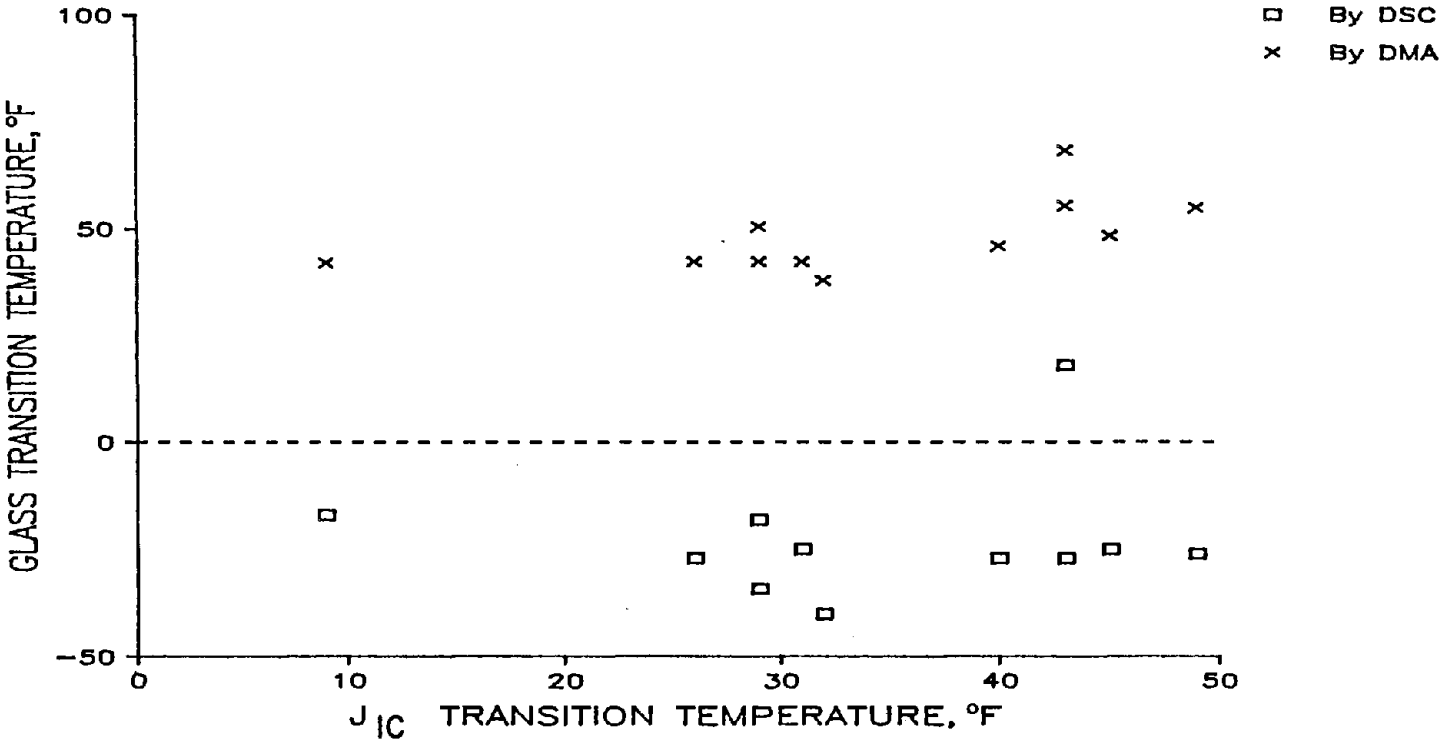

Figure 64. Glass transition temperature versus J_{1c} transition temperature.

Table 35. Ranking of variables that relate to susceptibility to thermal cracking.

Asphalt No.	Source	Grade	Rank and Value of Characteristic Temperature, °F													
			J_{1c} Transition		Tensile Strength Shift		Tensile Modulus Shift		Fraass Brittle Point		$T_{Pen1.2}$		T_g from DSC		T_g from DMA	
			Rank	°F	Rank	°F	Rank	°F	Rank	°F	Rank	°F	Rank	°F	Rank	°F
1	A	85/100	8	43	9	12	9	14	9	13	8	16	3	-27	9	55
2	B	AC-5	3	29	2	-4	2	-18	5	4	4	2	9	-18	2	42
4	B	AC-20	7	40	8	8	7	8	6	7	7	14	4	-27	6	46
5	C	AC-5	4	29	4	0	6	5	2	0	6	12	2	-34	8	51
7	C	AC-20	10	45	10	15	11	18	10	22	9	21	7	-25	7	48
8	D	AR-4000	9	43	11	19	10	14	11	24	11	24	11	18	11	68
12	F	AR-4000	2	26	5	0	3	-9	7	8	2	-6	5	-27	3	42
13	G	200/300	1	9	1	-14	1	-26	1	-6	1	-7	10	-17	4	42
14	G	150/200	5	31	6	1	4	-4	3	0	5	7	8	-25	5	41
16	I	85/100	11	49	7	5	8	11	8	10	10	21	6	-26	10	55
17	I	85/100	6	32	3	-1	5	-3	4	3	3	-3	1	-40	1	38
Sum of absolute value of difference in ranking of J_{1c} transition temperature and ranking for the other characteristic temperatures.					16		12		20		10		46		22	
R^2, J_{1c} versus other characteristic temperatures.					0.76		0.82		0.60		0.75		0.01		0.36	

Note: Asphalt No. 11 could not be ranked because the data were insufficient.

temperatures, other characterizing temperatures listed in table 35 are the mixture shift temperature for tensile strength and modulus, the Fraass brittle point temperature, the temperature at which the penetration of the asphalt cement is 1.2, and the T_g temperatures from DMA and DSC measurements. A comparison of the rankings of the other characteristic temperatures versus the J_{1c} transition temperature was made by summing the absolute values of the differences between the individual rankings for the J_{1c} transition temperatures and the respective ranking for each of the other temperatures. The result, shown at the bottom of table 35, shows the same general trends evidenced in figures 62 through 64.

The J_{1c} transition temperature is a measure of the maximum temperature at which the asphalt concrete departs from linear elastic fracture behavior. The temperature does appear to provide a meaningful ranking of the asphalts. To further characterize each asphalt cement, the magnitude of J_{1c} at the transition temperature, appendix E, was obtained graphically (see figure 61, where J_{1c} at the transition temperature is 1.32 lb-in/in^2). No meaningful correlation with the other variables could be associated with these values of J_{1c}.

The correlations between the J_{1c} transition temperatures and the mixture temperature shifts, $T_{Pen1.2}$, and the Fraass brittle point temperature do verify the dependency of J-integral on asphalt source and grade and warrant the further development of the J-integral approach for hot-mix asphalt and its development as a tool in fracture analyses. Successful use of J-integral has also been reported by Little with sulfur modified asphalt concrete mixes.[92] Further study is needed to refine the measurement of J_{1c} and to integrate J_{1c} into a computer model. The use of J_{1c} and any associated computer model must be verified with a full-scale research study in the field.

7. DEVELOPMENT AND EVALUATION OF THE BENDING BEAM TEST FOR ASPHALT CEMENT

Based upon the review of the literature and of test methods available for measuring asphalt stiffness at low temperature, section 2.11, it was decided to choose the bending beam test for further development and evaluation. This choice, described in sections 2.10 and 2.11, offered direct low-temperature measurements in a low-cost, unsophisticated device. The test can be used in either a three-point or a four-point configuration. After careful consideration, it was decided to use the three-point configuration because of its simplicity and because it results in somewhat larger deflections for a given level of stress. A photograph of the device is shown in figure 65, and a schematic, in figure 66. A complete description of the test apparatus and the associated test procedure is given in appendix G. This test was performed at various temperatures using five of the test asphalts: numbers 4, 6, 13, 16, and 17. These asphalts were chosen because they represent a wide range of rheological behavior.

7.1 CONDUCTING TESTS WITH BENDING BEAM

The bending beam test was conducted using the creep mode with a constant stress. The deflection of the beam was measured using a linear variable differential transformer (LVDT). The electronic signal from the LVDT conditioner was directed to an analog/digital converter board in an IBM PC compatible microcomputer, and the digitized signal was then used to calculate creep stiffness as a function of time.

To ensure that the samples behaved linearly during testing, the maximum tensile bending stress in the specimens was limited to less than 14 lb/in^2 (97 kPa) at low stiffness levels. This limit is based on the shear stress limit of 4.8 lb/in^2 (33 kPa) discussed in chapter 2. The limit given in chapter 2 has been multiplied by a factor of three to account for the three-fold difference in shear and tensile moduli. At larger stiffness levels, the load was limited such that final bending strains were less than 0.1 percent. Temperature control was achieved by placing the apparatus in a

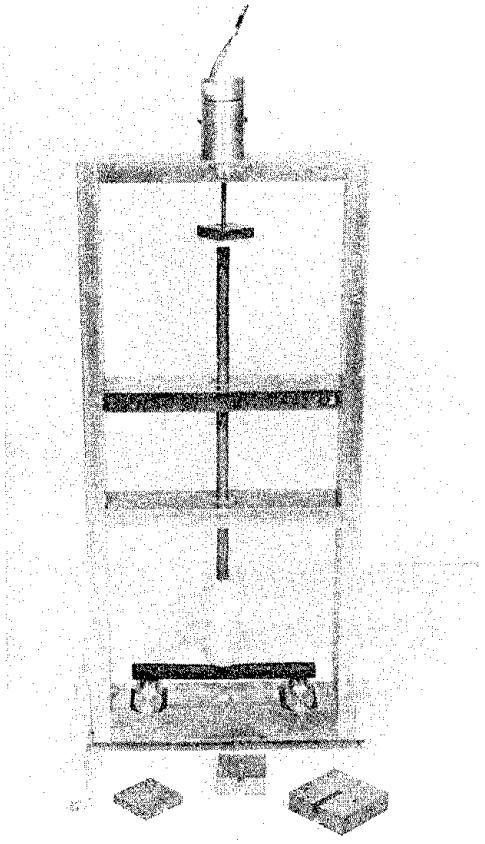

Figure 65. Photograph of bending beam apparatus.

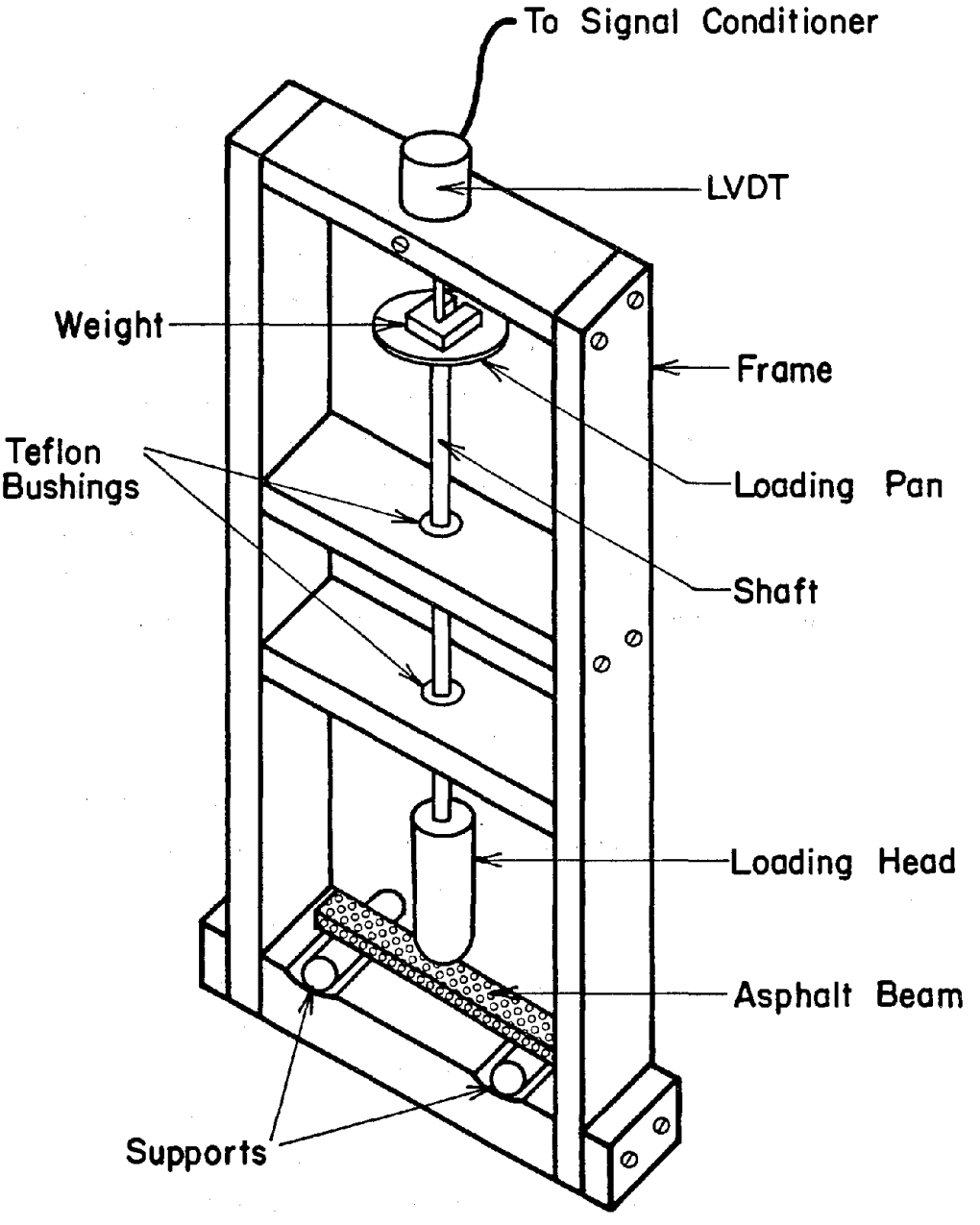

Figure 66. Schematic of bending beam creep test apparatus.

constant temperature bath filled with a mixture of ethylene glycol and water (1:1 mixture, volume base).

To conduct a creep test, the apparatus was placed in the controlled temperature bath, the test specimen was placed on the supports, the LVDT was zeroed, a weight was added to the loading pan, and the deflection of the beam was recorded for 16 min. Creep stiffness was calculated at times of 1, 2, 4, 8, 16, and 30 s, and at 1, 2, 4, 8, and 16 min. The testing temperature varied from 23 °F (-5 °C) to -13 °F (-25 °C). No problems were encountered during the testing except that asphalt No. 13 was too soft to test at the two highest temperatures. Duplicate tests were conducted, and the results were averaged to produce the creep stiffness curves. These curves were shifted by applying the time/temperature superposition principle to form master creep stiffness curves, as explained below in section 7.1. This technique is commonly used for polymeric materials and is a convenient means of extrapolating the range of creep data to longer loading times.[93]

7.2 DEVELOPMENT OF MASTER CURVES

In analyzing creep data for polymers and other linear viscoelastic materials, time/temperature superposition or the method of reduced variables is often applied to produce master stiffness curves. This technique allows creep or stiffness data determined as a function of loading time at various temperatures to be shifted with regard to time, until the stiffness curves obtained at the different temperatures overlap to form a single master curve. This procedure is illustrated in figure 67 where the logarithm of the measured stiffness is plotted as a function of the logarithm of reduced time for three temperatures: T_0, T_1, and T_2. In this example, T_0 is selected as the reference temperature. The stiffness curves at temperatures T_1 and T_2 are then shifted horizontally along the time axis until they overlap with the curve for temperature T_0, forming a single master curve. The distance that each curve is shifted along the time axis is called the shift factor, a(T). The reference temperature in this example was T_0, since data at this temperature were not shifted. Note that the horizontal axis for the master curve is labeled "log reduced time." To completely characterize a viscoelastic material, the shift factor should also be given as a function of temperature, as shown in figure 68, which is a plot of log shift factor versus

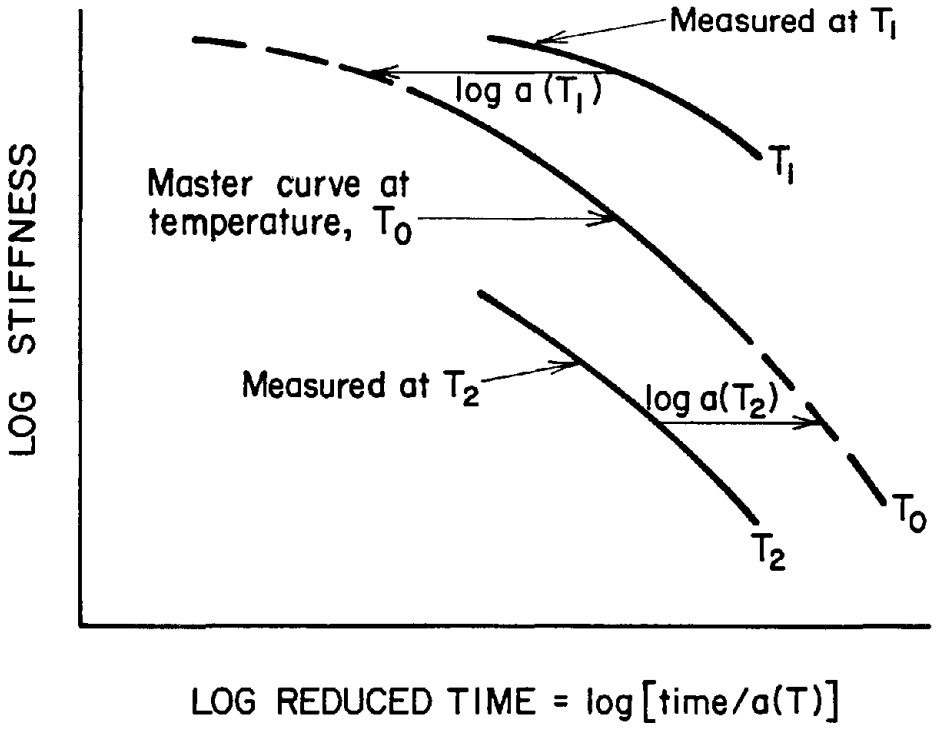

Figure 67. Schematic of time/temperature superposition.

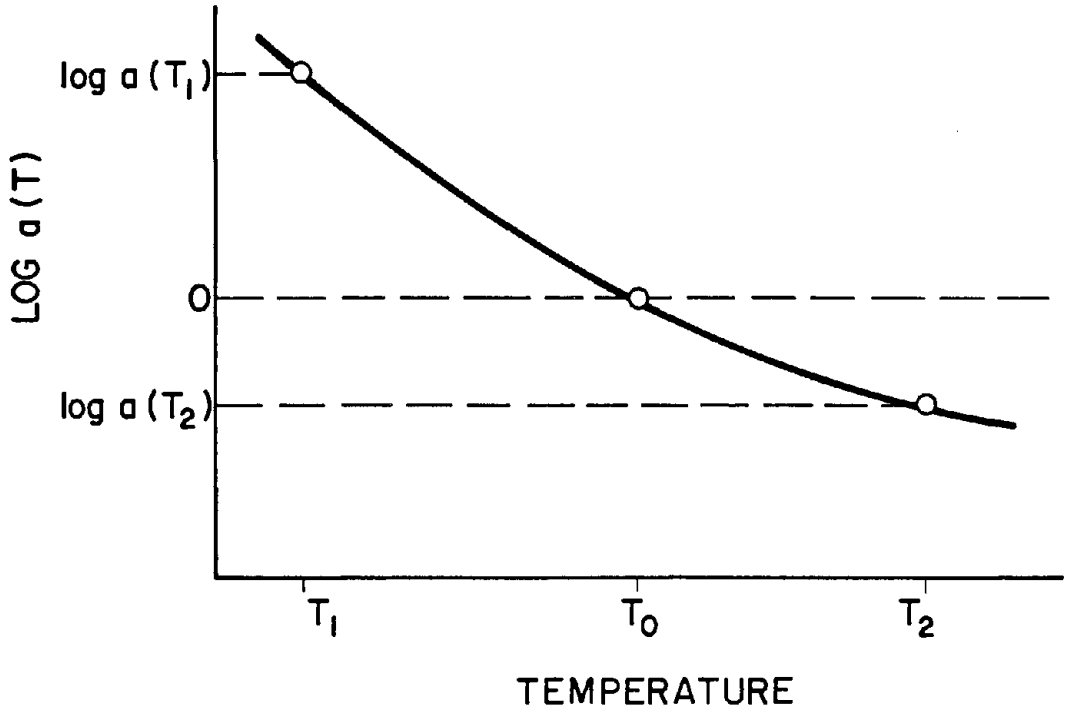

Figure 68. Log shift factor plotted as a function of temperature.

temperature for the example shown in figure 67. Note that the log of the shift factor is zero at the reference temperature, T_0.

The shift factor and the master curve can be used to predict stiffness at other temperatures and times. For example, to use the master curve and shift factor from figures 67 and 68 to predict the stiffness at time t_3 and temperature T_3, first, the log shift factor for temperature T_3, log $a(T_3)$, is found from figure 68. Then t_3 is located on the reduced time axis of the master curve, which has been reproduced in figure 69. The log $a(T_3)$ is graphically subtracted from t_3. Projecting upward to the master curve gives the asphalt stiffness, $S_B(T_3,t_3)$, at the new temperature, T_3, and time, t_3.

In theory, time/temperature superposition should also include a vertical shift that accounts for changes in density, ρ, with temperature.[93] However, this correction can be neglected for the temperature range used to characterize asphalt cement. Ferry gives a more detailed description regarding the reduction of viscoelastic data to form master curves.[93]

As a check on the validity of the bending beam stiffness data, stiffnesses were calculated from the 140 °F (60 °C) and 275 °F (135 °C) viscosity data and the following equation:[21]

$$S_B(T,t) = \frac{3\eta(T)}{t} \qquad (50)$$

where

$S_B(T,t)$ = asphalt stiffness, lb/in^2 (Pa), at temperature T and time t

$\eta(T)$ = coefficient of viscosity, function of temperature, lb-s/in^2 (Pa-s)

t = time, s

Equation 50 is applicable to the straight-line portion of the stiffness curves, at long loading times, where the stiffness is inversely proportional to the loading time and the coefficient of viscosity is constant for any given temperature, T.

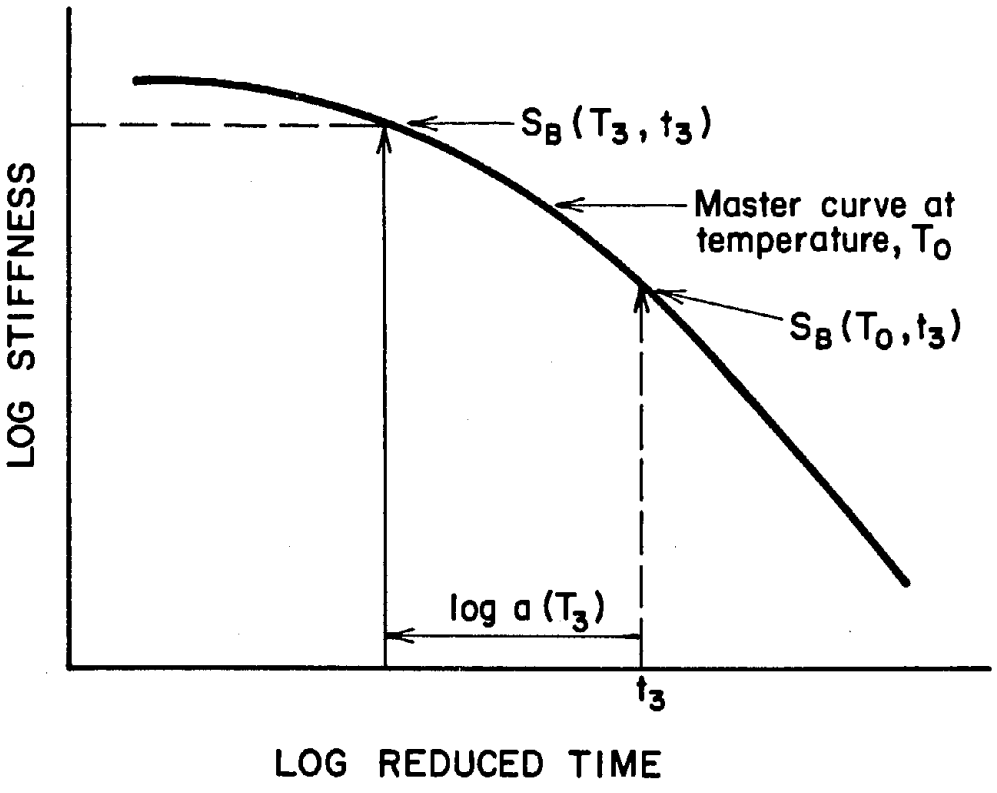

Figure 69. Use of time/temperature superposition to obtain stiffness at specified time/temperature.

When shifted according to the above procedure and plotted on a master curve showing log stiffness versus log reduced time, stiffnesses calculated from 140 °F (60 °C) and 275 °F (135 °C) viscosity data should lie on a line having a 1:1 slope.[93] Additionally, stiffnesses measured by the bending beam should be coincident with the line defined by the points determined from viscosity data. However, to plot stiffnesses calculated from viscosity data on master curves, the data must first be shifted to the reference temperature at some unknown reduced time. In this case, shift factors for calculating the appropriate reduced time were calculated using a method proposed by Dobson as being applicable to most paving-grade asphalt cements.[94] In this technique, two equations are used for predicting the shift factor:

$$\log a(T) = \frac{-8.86\ (T-T_S)}{182.9 + T-T_S} \quad \text{for } T > T_S \tag{51}$$

$$\log a(T) = \frac{-12.5\ (T-T_S)}{256.5 + T-T_S} \quad \text{for } T < T_S \tag{52}$$

where

$\log a(T)$ = log shift factor

T = temperature, °F

T_S = an asphalt specific characteristic reference temperature, °F

Equation 51 is referred to as the WLF equation and has been found to be applicable to a wide range of polymers. Dobson found equation 51 and its coefficients to be applicable to asphalt cements in the Newtonian flow region, generally >140 °F (60 °C), and he suggested that T_S could be accurately estimated for most asphalts from coefficients of viscosity measured at two temperatures in the region of Newtonian flow.[94] T_S is an arbitrary parameter that was selected by Williams et al. to characterize the time/temperature superposition of polymers.[93] T_S is asphalt specific and must be determined experimentally. Equation 52 was proposed by Dobson for calculating the shift factor, a(T), in a viscoelastic region below the reference temperature, T_S. This equation is in the same form as the WLF equation, equation 51, but with differing coefficients. The coefficients in

equation 52 were established experimentally by Dobson and are only applicable for temperatures less than the reference temperature, T_s.[94]

In the region of Newtonian flow, the shift factor is equal to the ratio of the coefficients of viscosity at two different temperatures:

$$a(T) = \frac{\eta_T}{\eta_{T_o}}$$

or

$$\log a(T) = \log (\eta_T) - \log (\eta_{T_o}) \tag{53}$$

where

$a(T)$ = shift factor

η_T = coefficient of viscosity at temperature T

η_{T_o} = coefficient of viscosity at reference temperature T_o (viscosities must be in consistent units)

T_o = any arbitrarily selected reference temperature, °F (°C)

The value of the shift factor between these two temperatures can then be related to T_s by using viscosity data at 140 °F (60 °C) and 275 °F (135 °C) and combining equations 51 and 53, since T_s will normally be less than 140 °F (60 °C):

$$\log a(140) - \log a(275) = \log \left(\frac{\eta_{140}}{\eta_{275}}\right)$$

$$= \frac{-8.86\ (140 - T_s)}{(182.9 + 140 - T_s)} + \frac{8.86\ (275 - T_s)}{(182.9 + 275 - T_s)} \tag{54}$$

where

$\log a(140)$ = log shift factor at 140 °F (60 °C)

$\log a(275)$ = log shift factor at 275 °F (135 °C)

η_{140} = coefficient of viscosity at 140 °F (60 °C)

η_{275} = coefficient of viscosity at 275 °F (135 °C)

T_s = asphalt specific characteristic reference temperature, °F

Equation 54 can be rearranged and solved for T_S, which is asphalt specific, by using the quadratic equation:

$$T_S = 390 \pm [4260 - 218700/\log (\frac{\eta_{140}}{\eta_{275}})]^{1/2} \quad (55)$$

where

T_S = asphalt-specific characteristic reference temperature, °F

η_{140} = viscosity at 140 °F (60 °C)

η_{275} = viscosity at 275 °F (135 °C), consistent units

Observation reveals that the sign for the second term in equation 55 will be negative, since values for T_S would otherwise be much too high. This equation was used to calculate T_S for the five asphalts. Stiffnesses were calculated from capillary viscosity data using equation 50 and the total time of each viscosity test. Using the value of T_S calculated from equation 55, values of log (shift factor) for the viscosity test temperature relative to T_S were found using equation 51. Since the reference temperature for the master curves was arbitrarily selected as 5 °F (-15 °C), the value of log (shift factor) for 5 °F (-15 °C) relative to T_S was calculated using equation 52 and subtracted from the values found using equation 51 to give the total values of log (shift factor) for each viscosity test temperature relative to the reference temperature of 5 °F (-15 °C). The appropriate value of log (reduced time) for plotting the stiffnesses estimated from viscosity data was calculated by subtracting the total log (shift factor) from the logarithm of the total time of each viscosity test. Values of T_S for the asphalt numbers 4, 6, 13, 16, and 17 were 113, 102, 93, 103, and 108 °F (45, 39, 34, 39, and 42 °C), respectively.

7.3 ANALYSIS OF DATA

As an additional check on the accuracy of the bending beam test data, stiffnesses calculated from the DMA were added to the plots of the master curves. DMA stiffnesses, measured at temperatures corresponding to the bending beam test temperatures, were shifted by an amount equal to the shift

factor found for the bending beam data collected at the same temperature. To include the dynamic data in the master stiffness curves, the dynamic frequency must be converted to an equivalent creep loading time. Christensen gives the following approximate relationship for performing this conversion:[95]

$$t \cong 2/\pi\omega \tag{56}$$

where

t = equivalent creep loading time, s

ω = angular frequency, rad/s

Equation 56 was used to convert dynamic frequencies to creep loading times.

Master stiffness curves plotted versus the logarithm of reduced time and plots of log-shift factor versus temperature for asphalts 4, 6, 13, 16, and 17 are shown in figures 70 through 79. Included on the plots of the logarithm of shift factor versus temperature are lines repesenting values of a(T) calculated using Dobson's method. In general, shifting of the data resulted in smooth overlapping and well defined curves for both stiffness and the shift factor. The upper limit for stiffness has been well defined by the dynamic data; the plotted data becomes asymptotic to the generally accepted glassy modulus value of 380,000 lb/in^2 (2.6 GPa) which is common to most asphalts.[2] The dynamic data also overlap smoothly with data from the bending beam test. Stiffnesses calculated from coefficient of viscosity data plotted close to the 1:1 asymptote on the master curves, except for asphalt No. 16, which is a waxy asphalt. Additionally, observed shift factors were reasonably close to those predicted using Dobson's method. The master curves produced using these methods indicate that the bending beam test is a viable method for the measurement of asphalt stiffness at low temperatures.

In figures 80 through 84, asphalt stiffnesses, found using the four nomographic techniques described in chapter 6, are plotted against log time. The experimentally determined stiffness master curve has been included in each plot for comparison with predicted values. These curves show that the various nomographic techniques are in agreement with stiffness values measured at short loading times. Generally, in this region, the observed differences

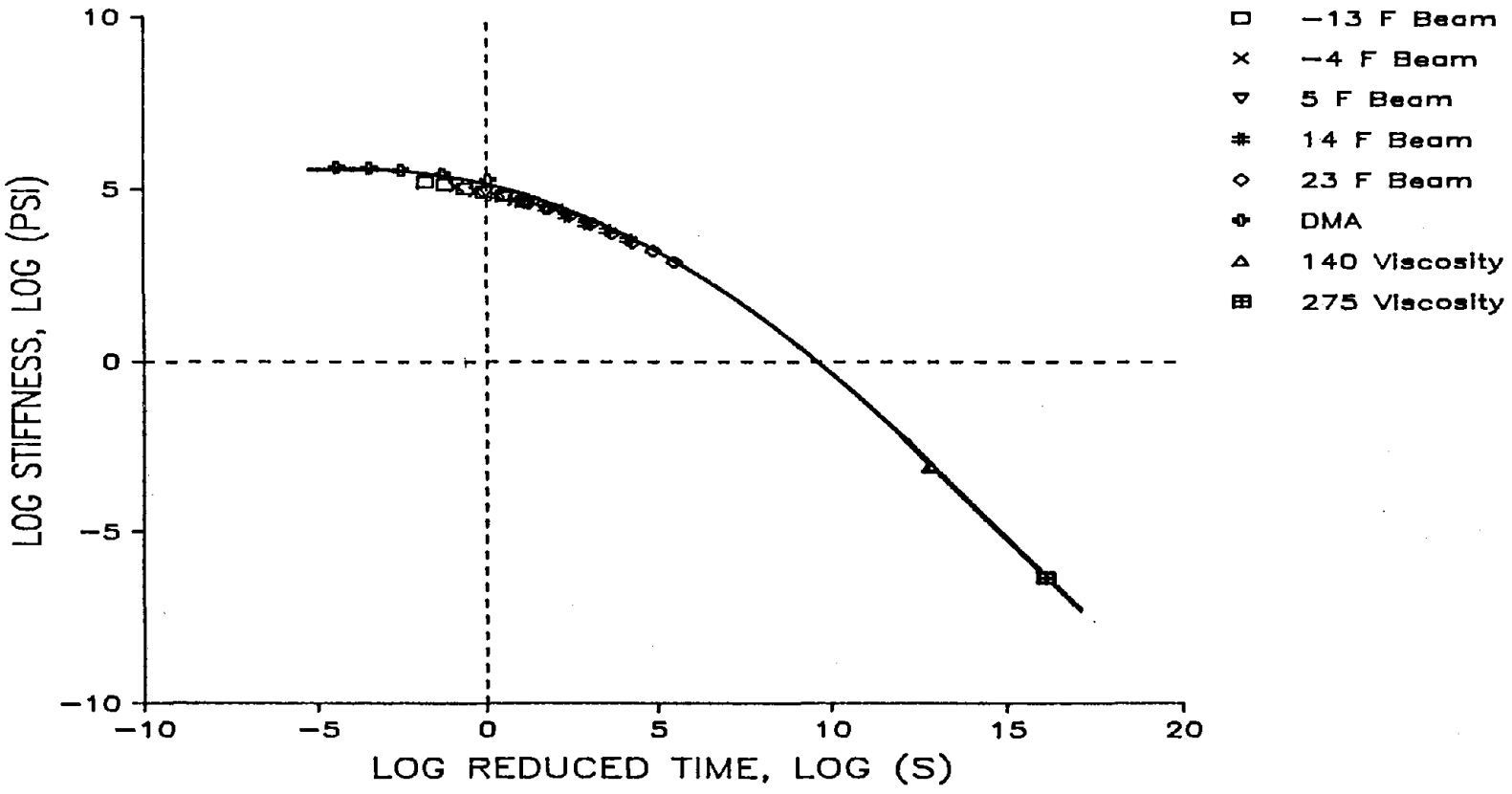

Figure 70. Master creep modulus curve for asphalt No. 4, reference temperature 5 °F (-15 °C).

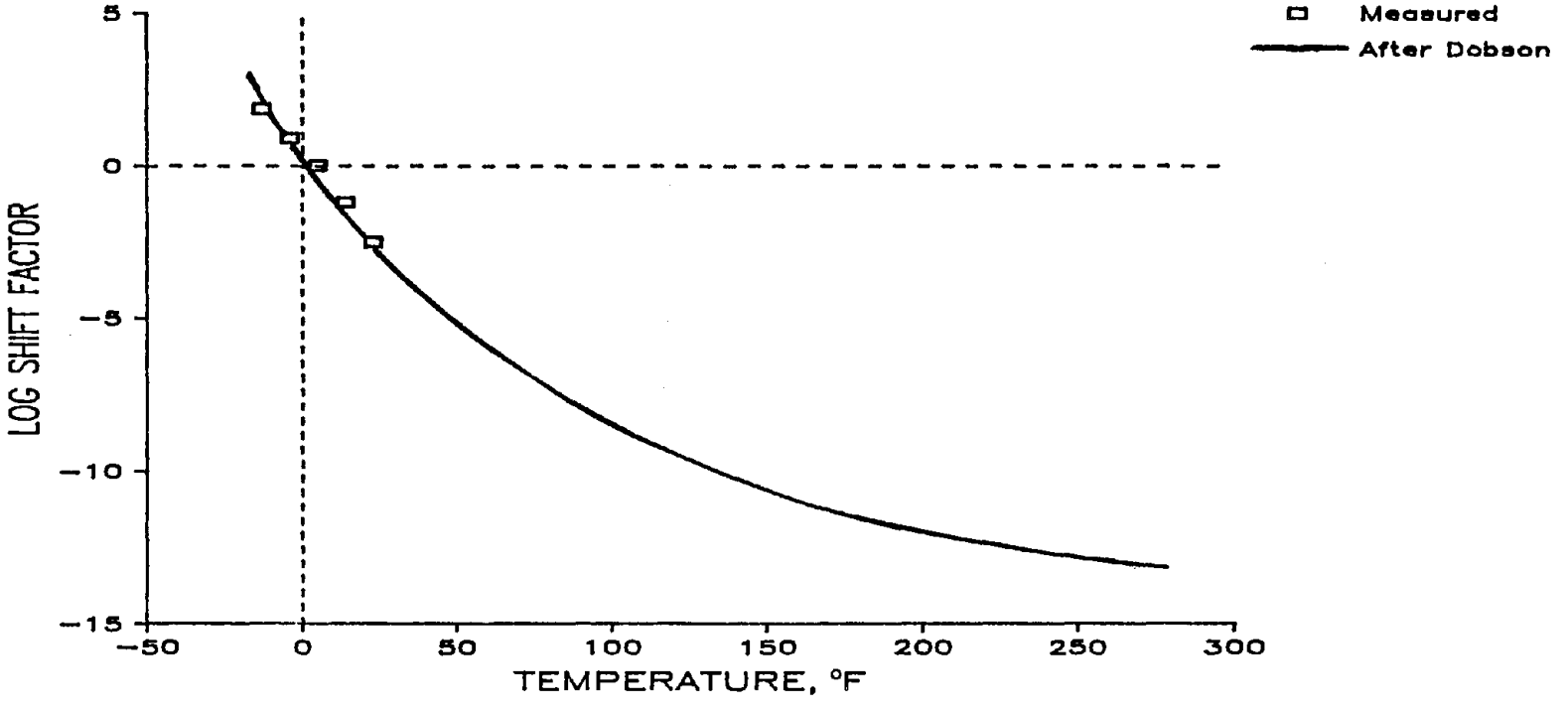

Figure 71. Log shift factor as a function of temperature for asphalt No. 4, reference temperature 5 ^{o}F (-15 ^{o}C).

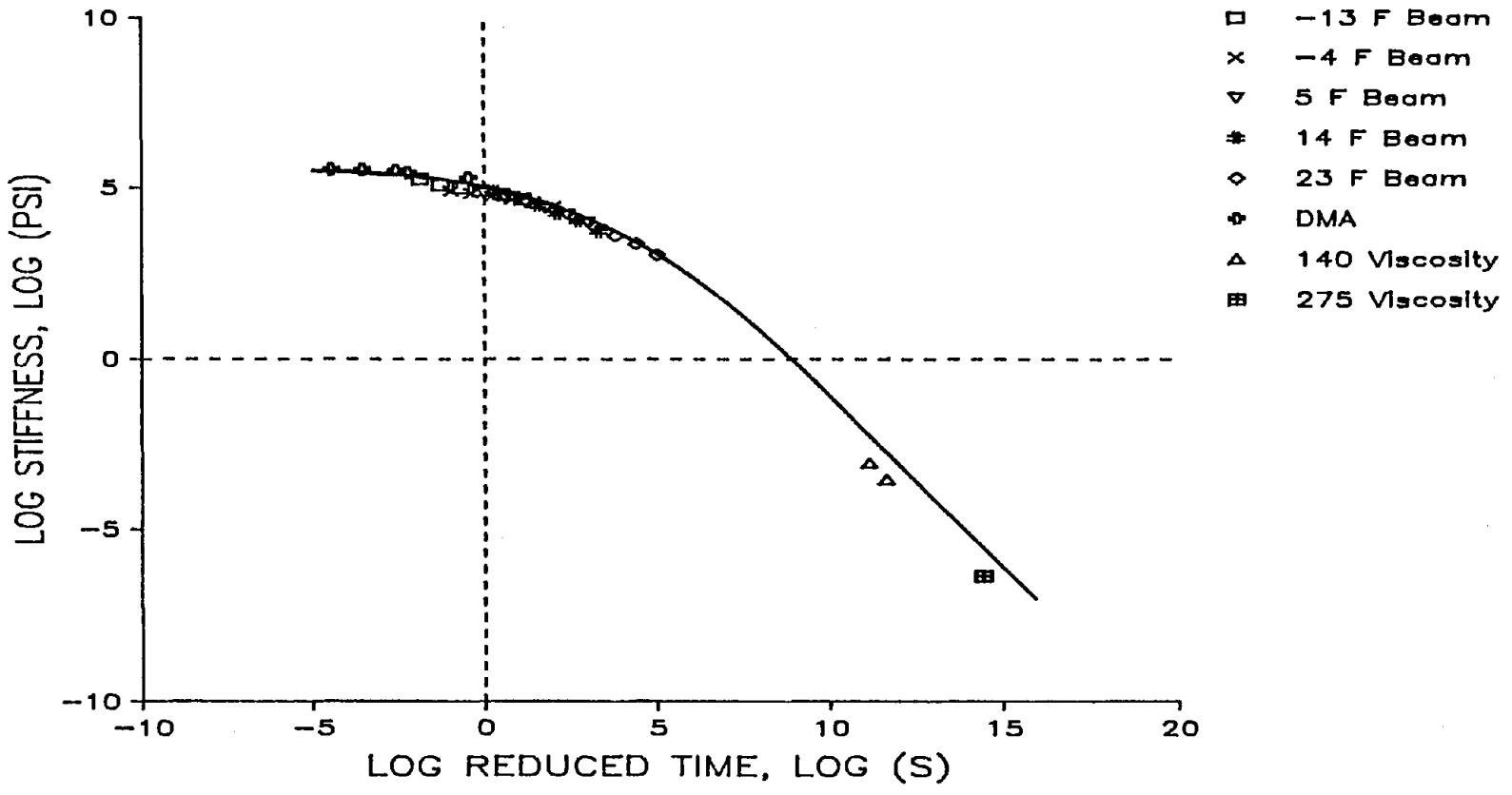

Figure 72. Master creep modulus curve for asphalt No. 6, reference temperature 5 °F (−15 °C).

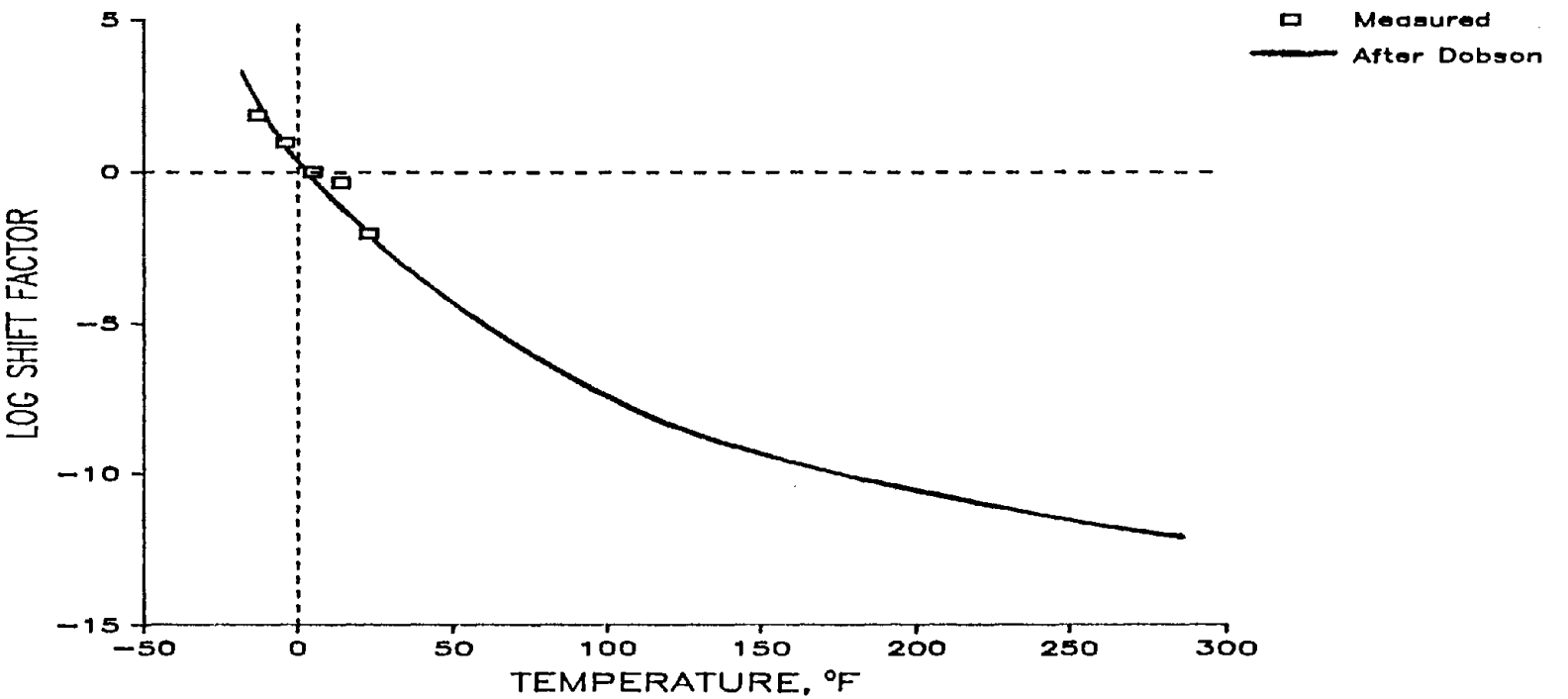

Figure 73. Log shift factor as a function of temperature for asphalt No. 6, reference temperature 5 ^{o}F (-15 ^{o}C).

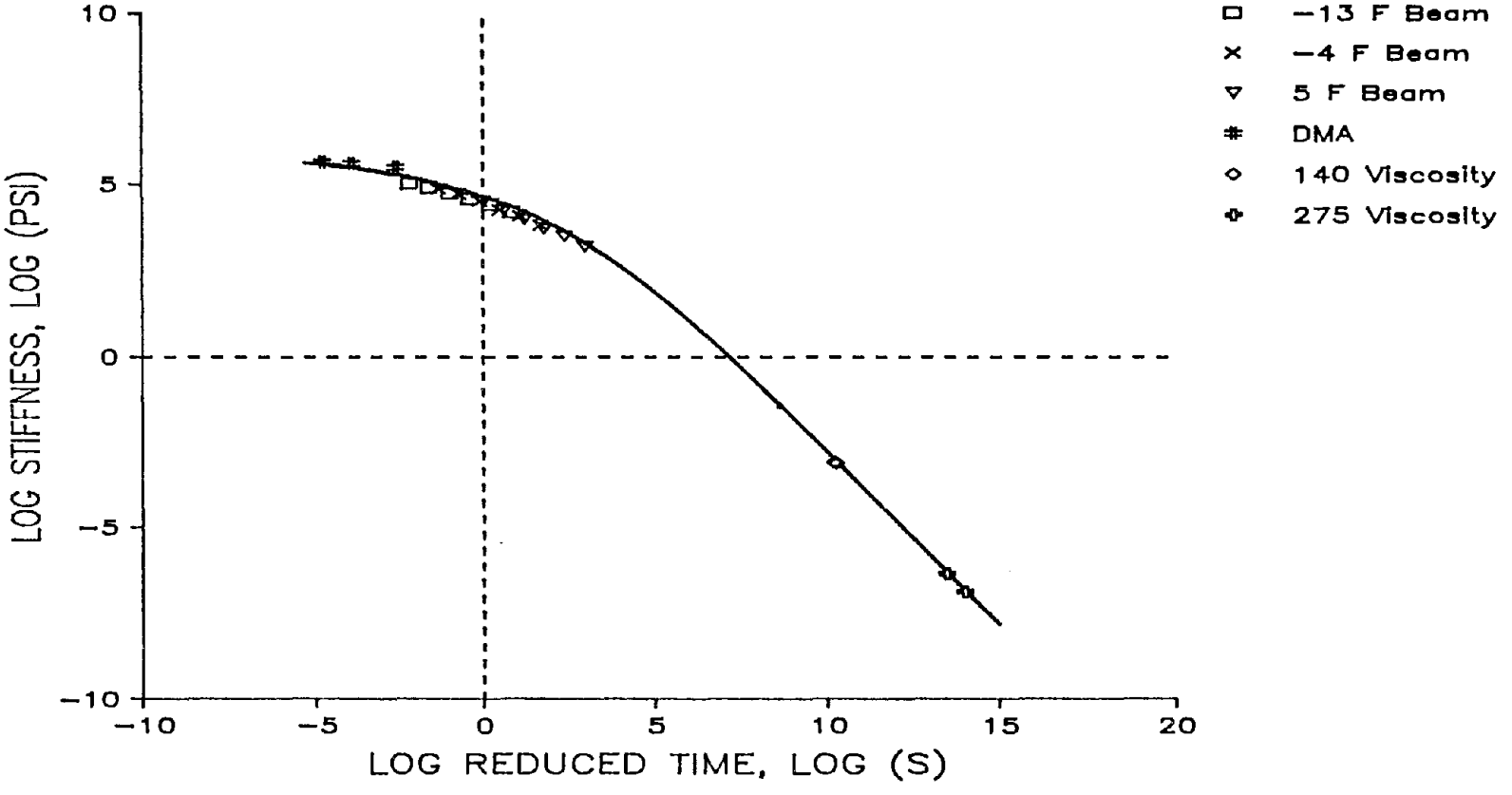

Figure 74. Master creep modulus curve for asphalt No. 13, reference temperature 5 ^{o}F (-15 ^{o}C).

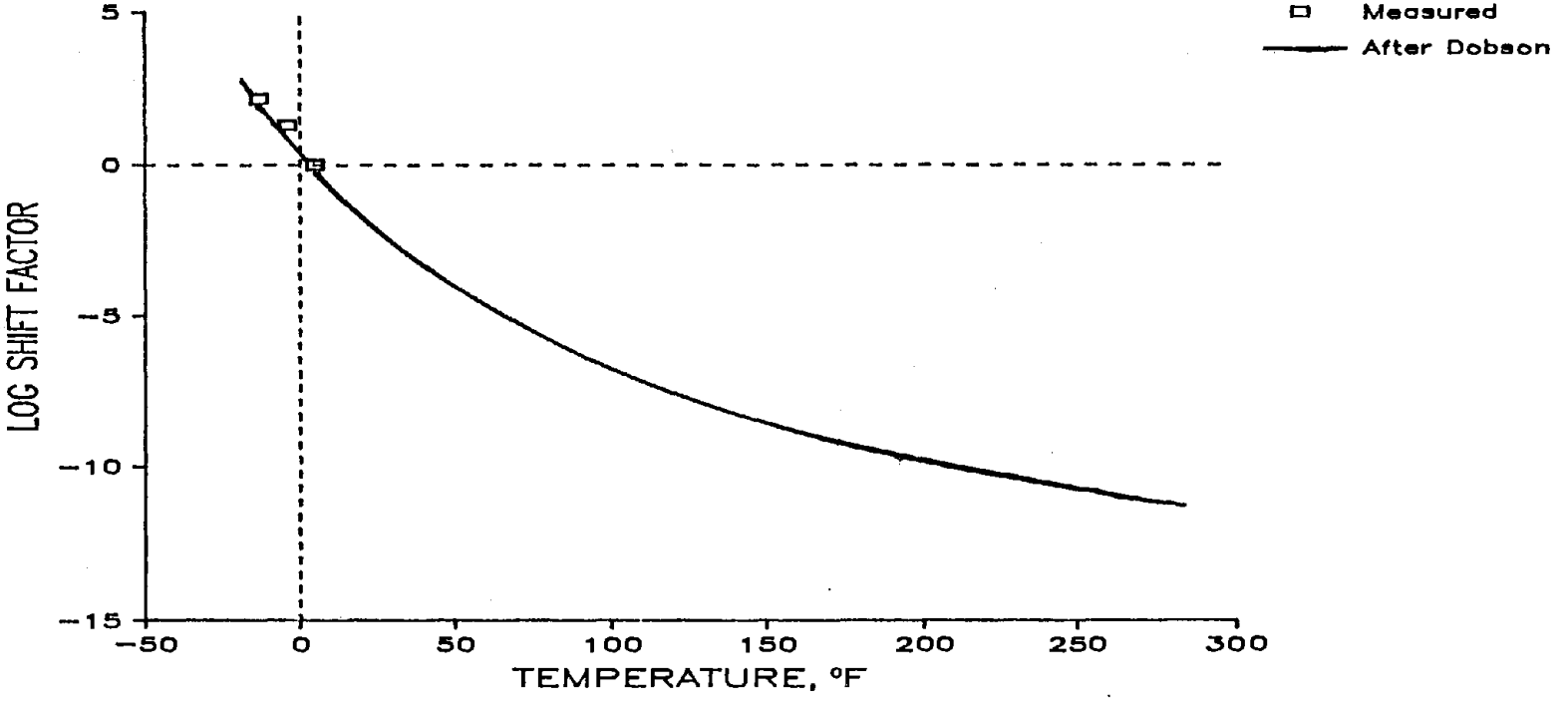

Figure 75. Log shift factor as a function of temperature for asphalt No. 13, reference temperature 5 ^{o}F (−15 ^{o}C).

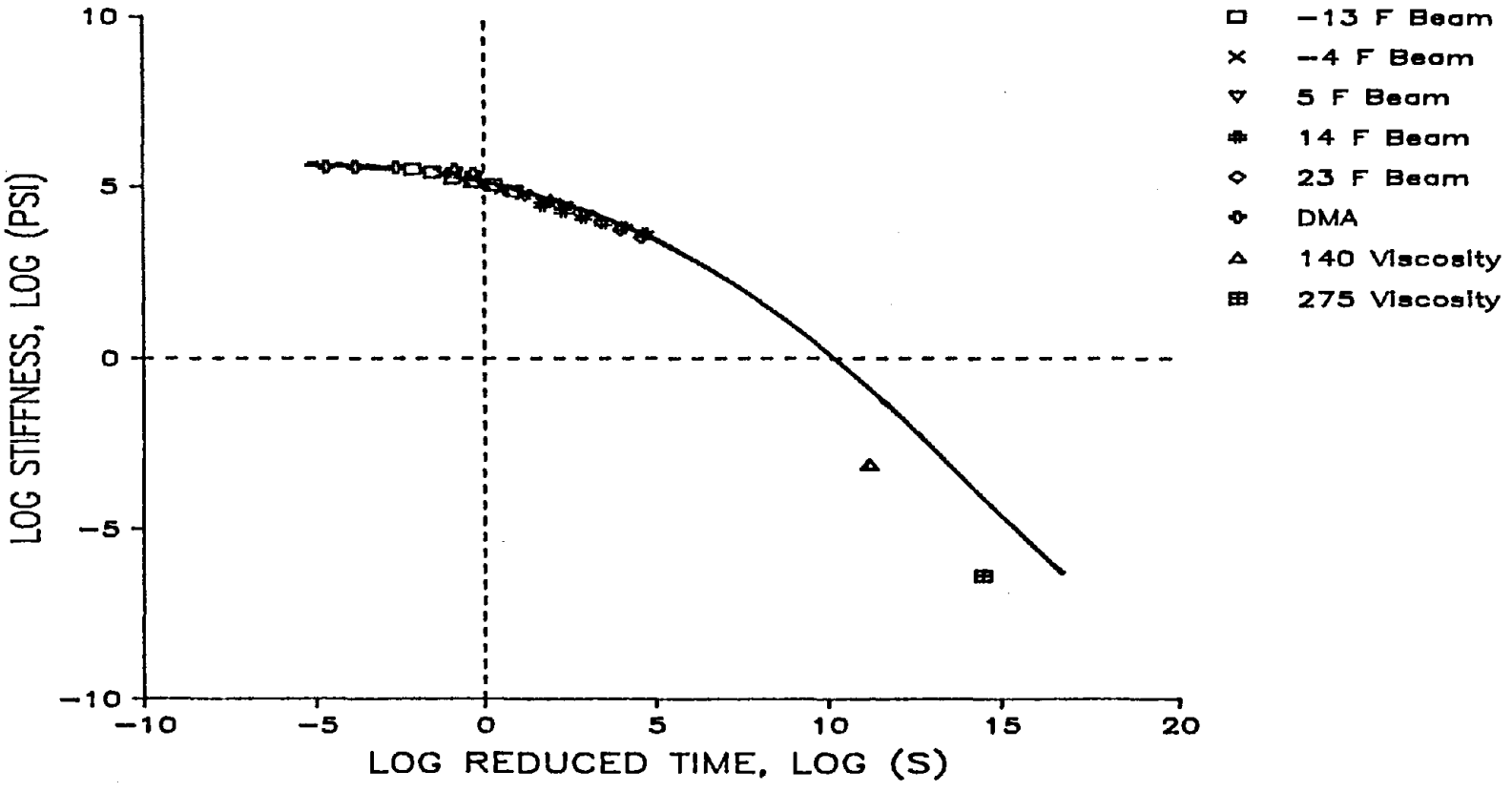

Figure 76. Master creep modulus curve for asphalt No. 16, reference temperature 5 ^{o}F (-15 ^{o}C).

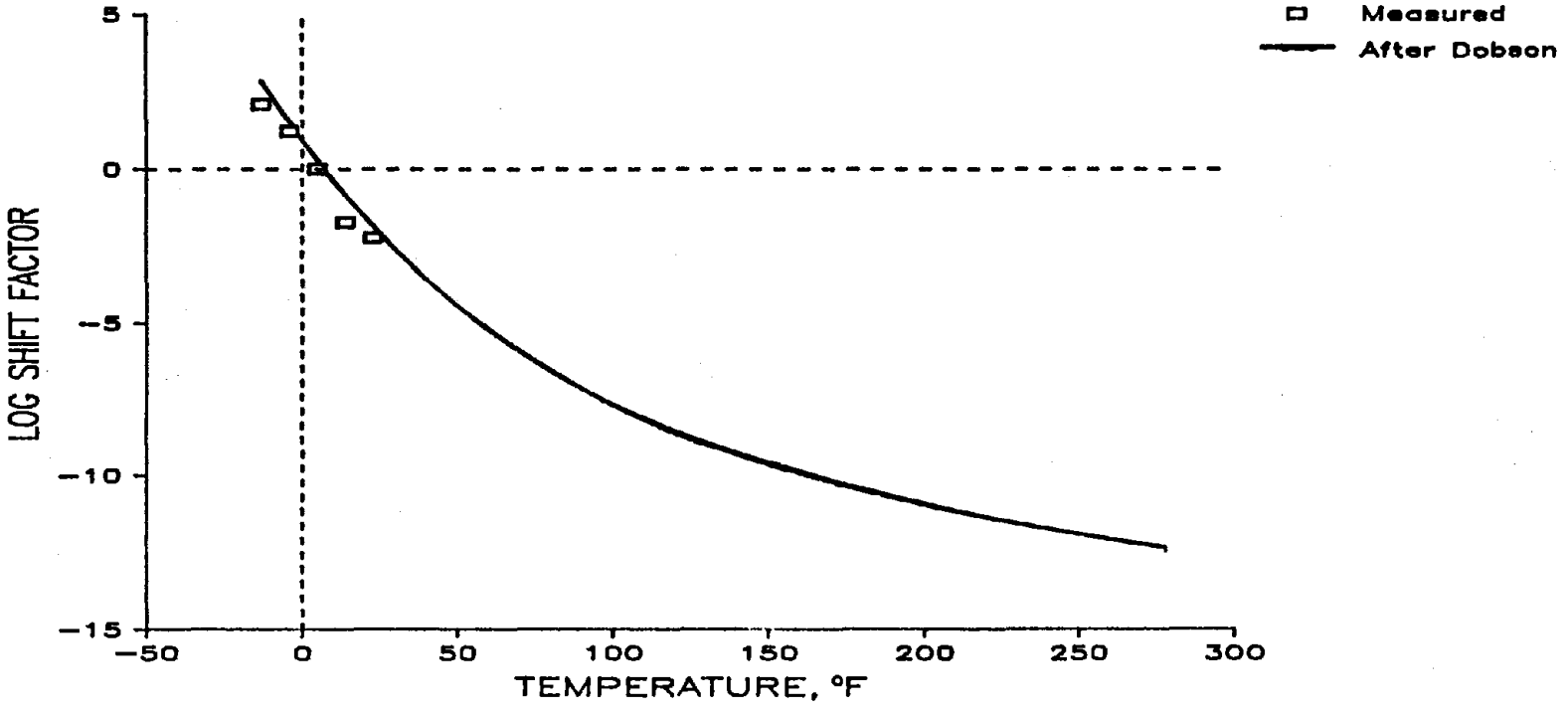

Figure 77. Log shift factor as a function of temperature for asphalt No. 16, reference temperature 5 °F (−15 °C).

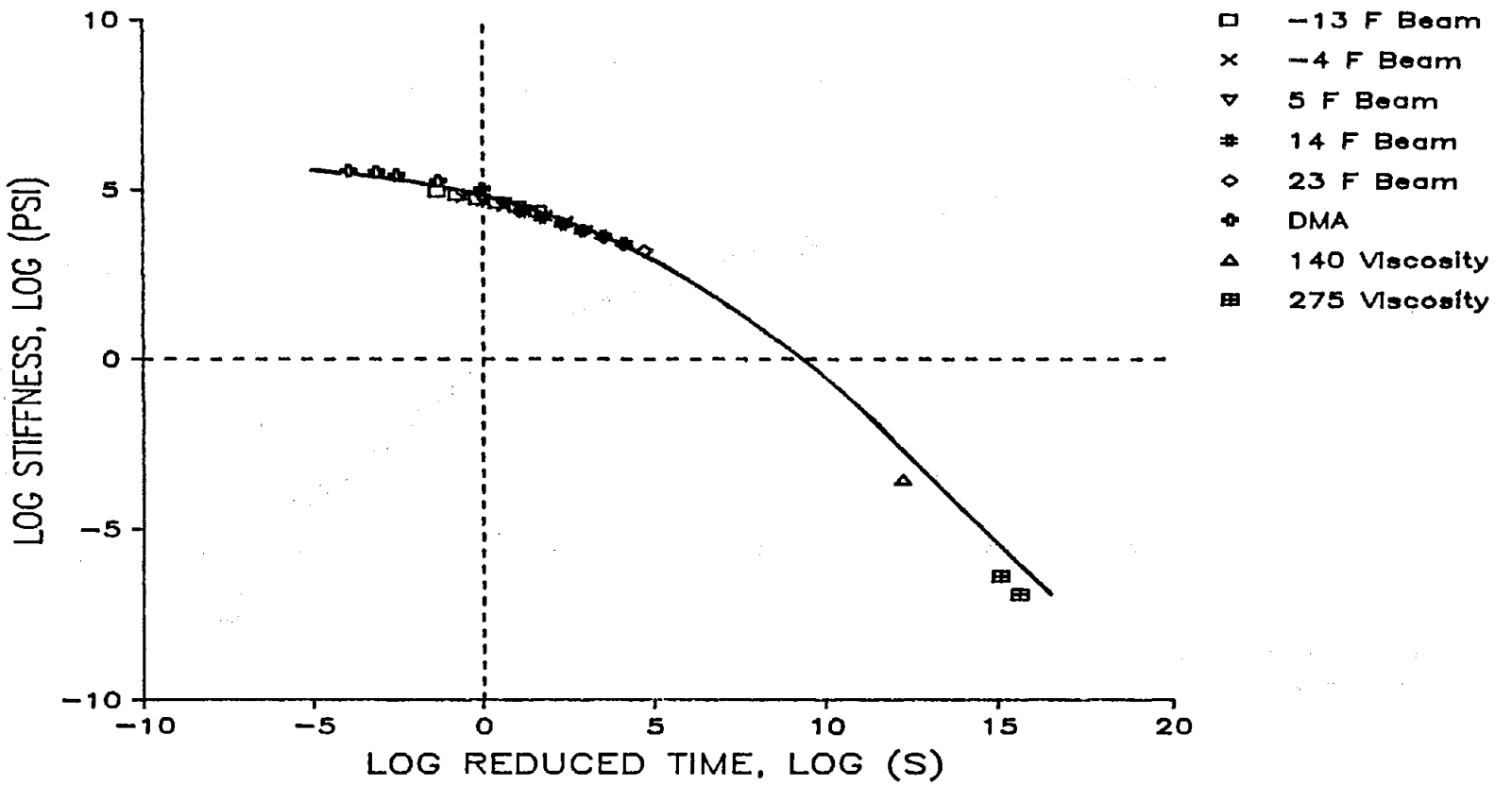

Figure 78. Master creep modulus curve for asphalt No. 17, reference temperature 5 ^{o}F (-15 ^{o}C).

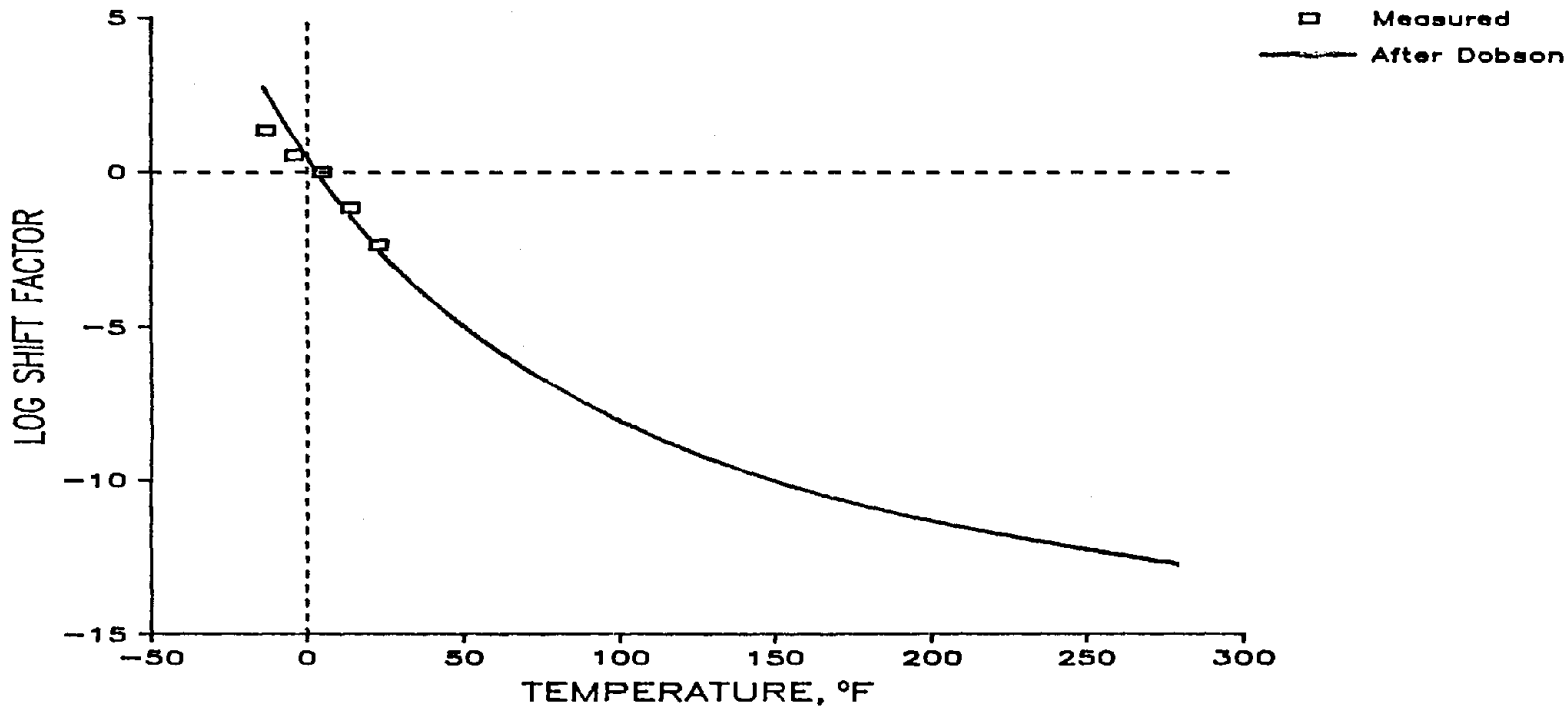

Figure 79. Log shift factor as a function of temperature for asphalt No. 17, reference temperature 5 ^{o}F (−15 ^{o}C).

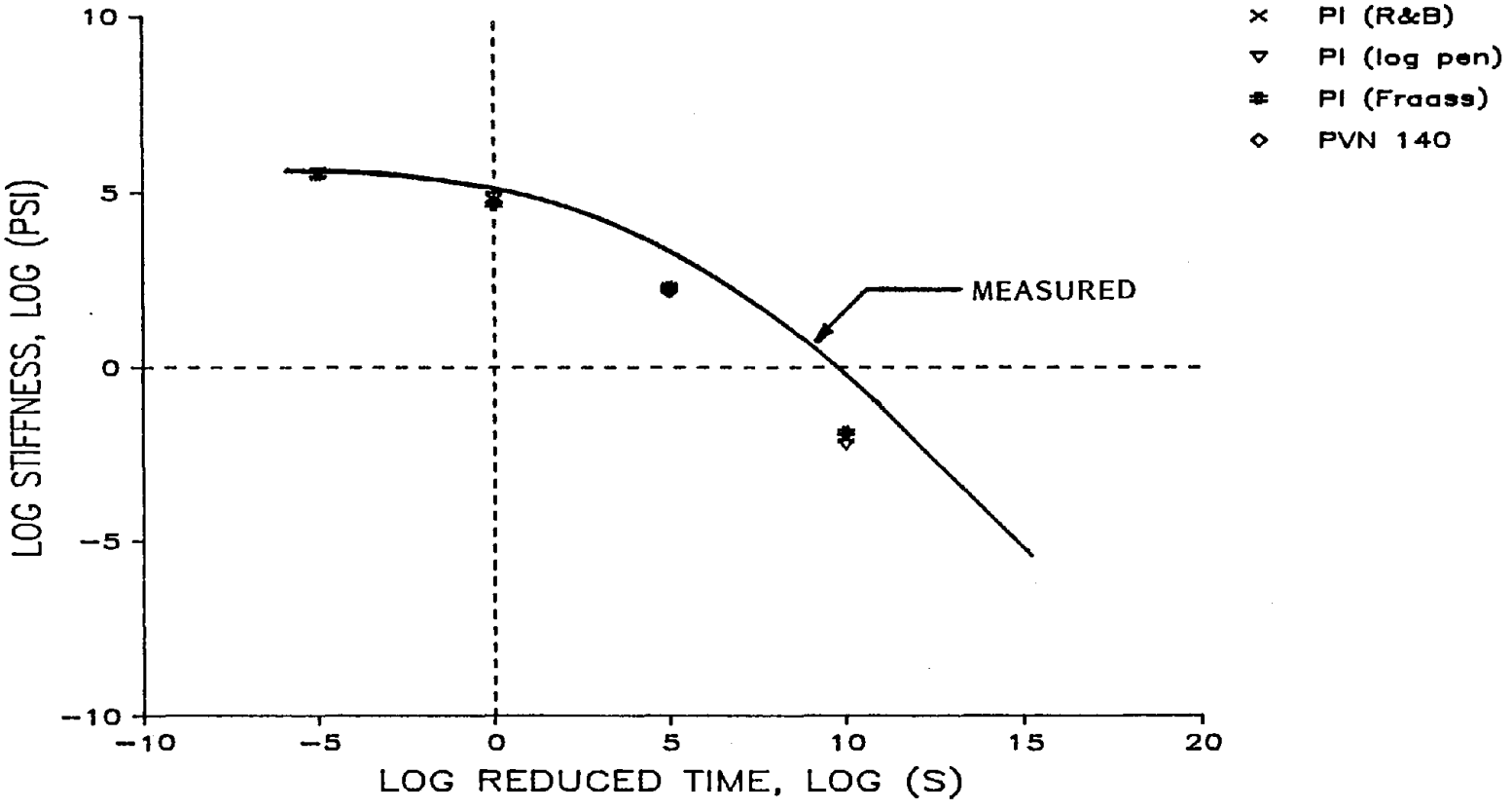

Figure 80. Predicted and measured creep moduli at 5 ^{o}F (-15 ^{o}C) for asphalt No. 4.

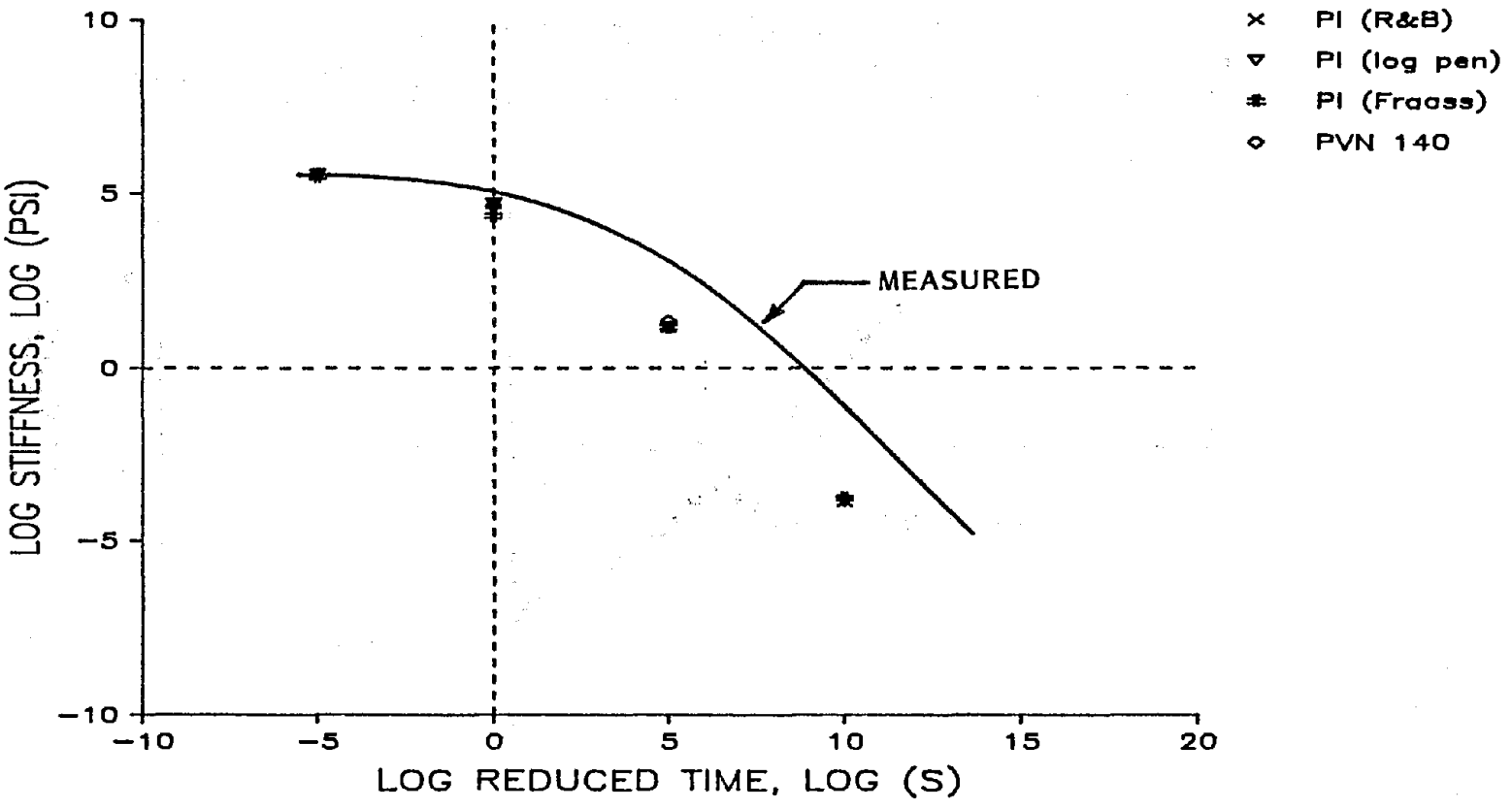

Figure 81. Predicted and measured creep moduli at 5 ^{o}F (-15 ^{o}C) for asphalt No. 6.

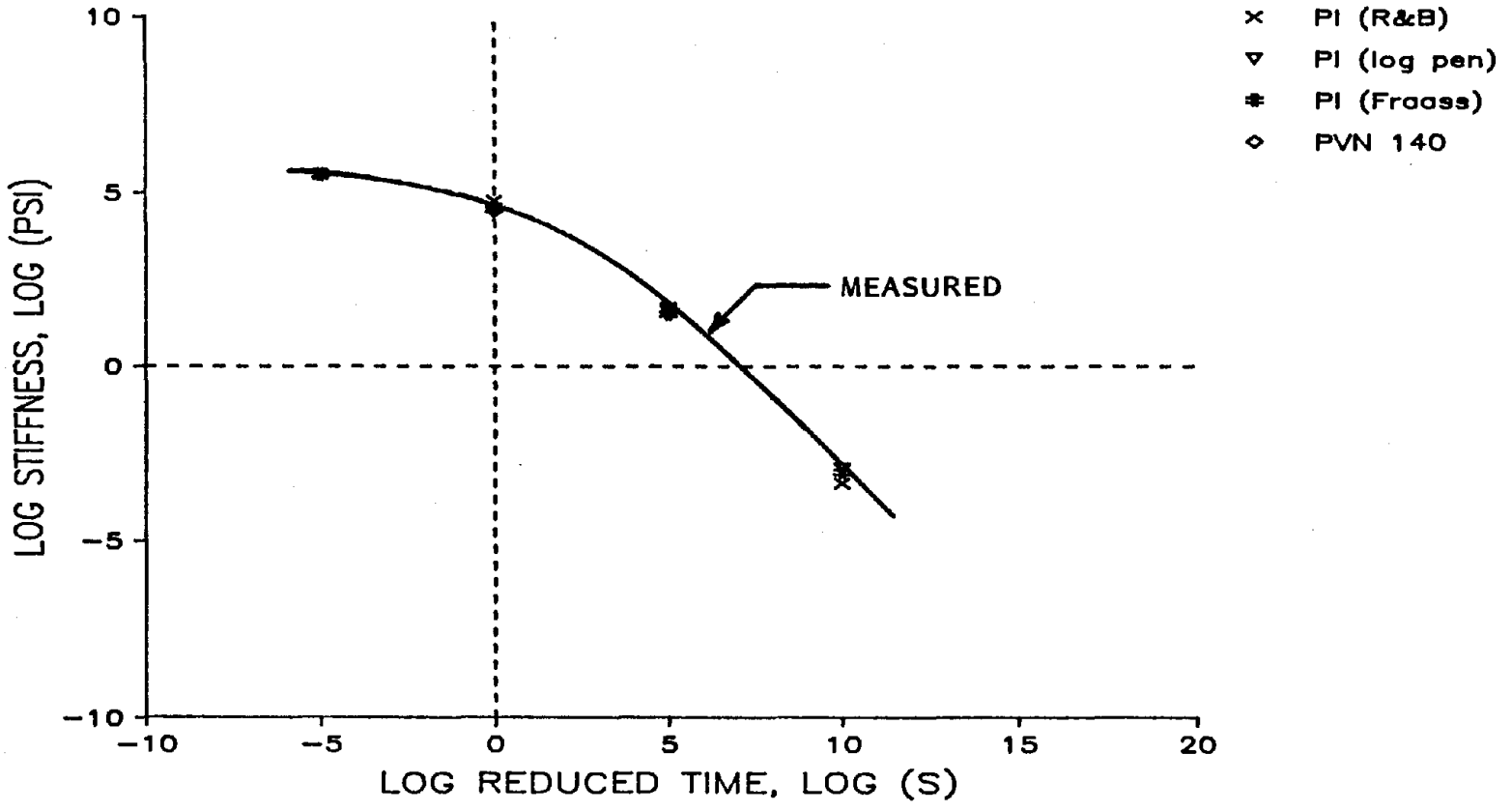

Figure 82. Predicted and measured creep moduli at 5 ^{o}F (-15 ^{o}C) for asphalt No. 13.

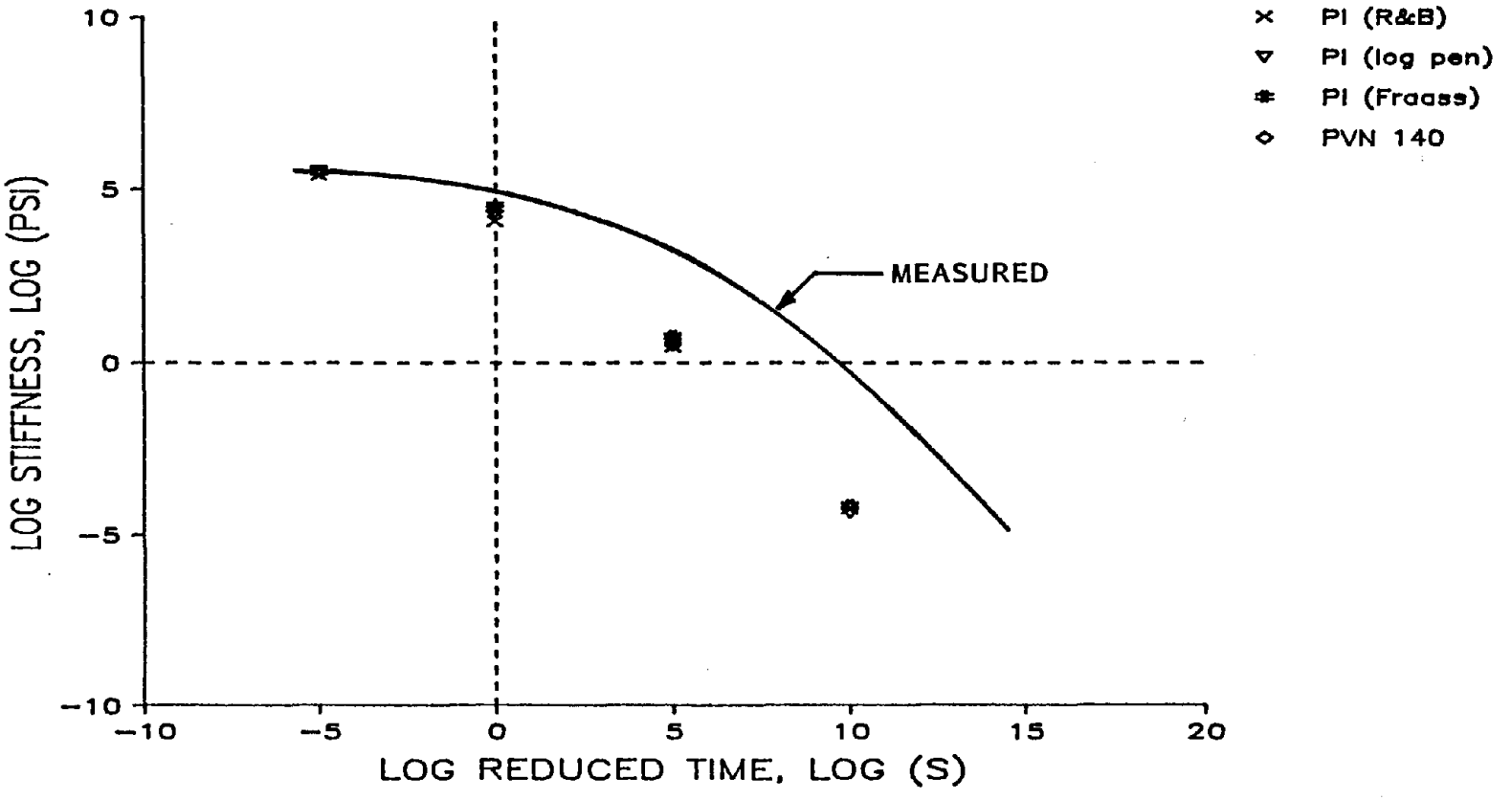

Figure 83. Predicted and measured creep moduli at 5 ^{o}F (-15 ^{o}C) for asphalt No. 16.

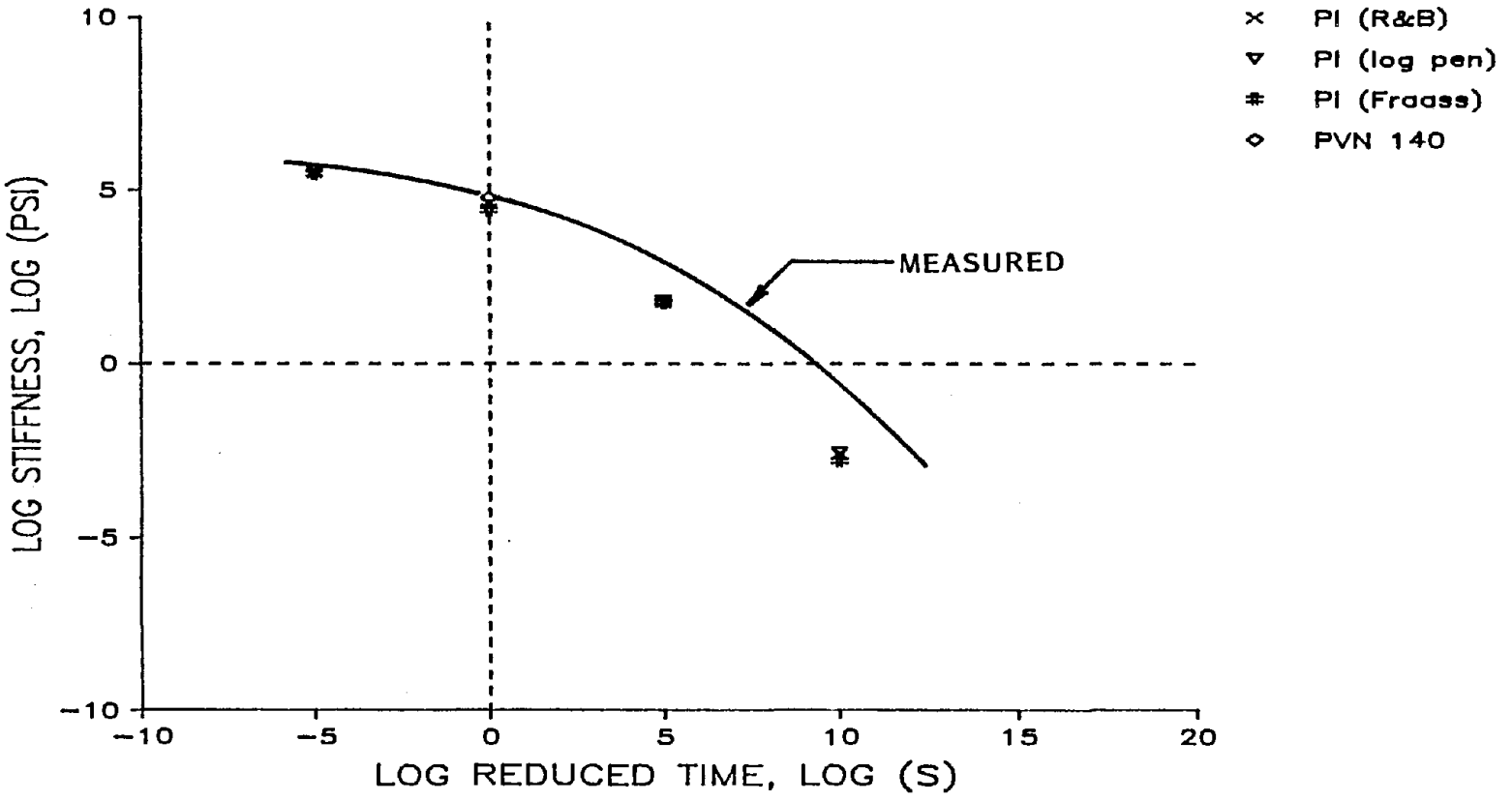

Figure 84. Predicted and measured creep moduli at 5 ^{o}F (-15 ^{o}C) for asphalt No. 17.

between measured and predicted stiffnesses are no more than a factor of about two. However, at long loading times, all of the various nomograph methods significantly underestimate asphalt stiffness. In the first three plots, asphalts 4, 6, and 13, no particular method for predicting asphalt stiffness stands out as being more or less accurate than the others. However, the plots for asphalt 16, which is a waxy asphalt, show differing predictions according to the method used. These differences, which were in the order of 300 to 400 percent, are not readily apparent in the figure because of the scale used in plotting the logarithm of stiffness. This indicates that, for waxy asphalts, the relationships between routine test data and stiffness may be considerably different from those observed for standard asphalts.

As a further comparison of predicted and measured asphalt stiffnesses, the temperature at a stiffness of 29,000 lb/in^2 (200 MPa) at 2 h was calculated using the experimentally determined stiffness master curves and by the four nomographic techniques. These stiffness and time values correspond to a limiting stiffness temperature sometimes used in designing pavements to resist low-temperature cracking.[37] The measured and predicted temperatures are shown in table 36. In almost all cases, the limiting stiffness temperatures of the asphalts are grossly underestimated by nomographic methods. The predicted temperature is an average of 9 °F (5 °C) lower than the experimentally determined value. Nomographic methods for predicting asphalt stiffness, in these instances, significantly underestimated stiffness at long loading times and low temperatures.

The precision of the bending beam test was estimated at a loading time of 30 s. The coefficient of variation of the measured stiffnesses at this loading time was calculated by normalizing and pooling the measured stiffness values for all tests. Fifty-two observations were used in the calculation. The resulting coefficient of variation, for an average of two tests, was 12 percent. This corresponds to a D2S precision of 35 percent--that is, the average of two test results will differ from the average of two other test results by more than 35 percent only 1 time in 20. Although the indicated precision of the bending beam test may appear not to be very good, the device was only a prototype, and modifications to the device or procedure will

Table 36. Limiting stiffness temperatures for 200 MPa, 2 h.

Asphalt Source Number	From Master Creep Curve °F	Predicted from Nomograph			
		PI °F	$PI_{log\text{-}pen}$ °F	PI_{Fraass} °F	PVN_{140} °F
4	-18	-26	-24	-33	-29
6	-18	-20	-18	-29	-22
13	-26	-36	-44	-44	-49
16	-11	-27	-13	-27	-22
17	-31	-31	-38	-33	-26

probably improve the repeatability of the results. The following are likely sources of variability:

- Restraint of longitudinal dimension changes in the beam offered by resistance in the beam supports.
- Eccentric loading of the beam.
- Lateral movement of the beam during loading, either front-to-back, side-to-side, or twisting.
- Friction between the shaft and the bearings during loading of the test specimen.
- Differences in steric hardening of the samples due to differences in elapsed time from sample preparation.

Of these possible sources of variation, it is believed that the most significant cause of error is the binding of the shaft during loading. These problems can be minimized by a more sophisticated design of the loading system.

8. SUMMARY

Thermal cracking of hot-mix asphalt pavements continues to be a problem in both the United States and Canada. Two thermally induced failure mechanisms have been identified: low temperature shrinkage cracking and cracking associated with thermal fatigue. The former mechanism is predominant in the more northerly areas of the United States, and the latter mechanism is associated with more temperate climates that experience rapid temperature excursions.

Current asphalt cement and hot-mix asphalt concrete specifications do not provide sufficient assurance against the occurrence of thermal cracking. Although viscosity graded specifications (ASTM D 3381) do allow some protection against thermal cracking to the extent that they incorporate a penetration-viscosity window, they do not specify the properties of asphalt cement at temperatures less than 77 °F (25 °C). The importance of temperature susceptibility is recognized in ASTM D 3381 with the table I and table II requirements. Table II material is more restrictive with respect to temperature susceptibility and is often specified for colder climates. The inadequacy of the current specifications is mirrored by the multitude of specification variations that have been propagated by State and local agencies. Often ductility or penetration testing at temperatures lower than the customary 77 °F (25 °C) are incorporated, reflecting the need for measurements in the range of the actual service temperatures.

The objectives of this study, listed below, reflect the concern for thermal cracking:

- Investigate the feasibility of developing an uncomplicated test procedure for direct measurement of asphalt stiffness at low temperatures.
- Develop quantitative correlations between the various physicochemical and engineering test procedures used to assess the thermal cracking potential of asphalts.
- Develop a simple, low-cost apparatus that can be used to measure the low-temperature stiffness of asphalt cement and that is suitable for specification use.

- Investigate the applicability of a fracture mechanics approach to the problem of thermal cracking.
- Review the available models that have been developed for predicting thermal cracking.

A comprehensive search of the literature was conducted to identify the various methods available for characterizing the rheological or flow properties of asphalt cements at temperatures lower than room temperature. Mechanical characterization was confined to the relatively simple concept of stiffness where stiffness is defined as a time/temperature-dependent ratio formed by dividing stress by strain. Typical stiffness values for asphalt cement range from 1,000 lb/in^2 (7 MPa) at room temperature to a limiting value of 380,000 lb/in^2 (2.6 GPa) at low temperatures, where it behaves as a glassy solid. This large range in stiffness makes it difficult to design a single, low-cost rheometer that will be reliable over the entire temperature range.

A wide range of testing devices was reviewed, including those traditionally used for testing asphalt cement. Testing geometries such as forced capillary flow, shearing plates, and falling coaxial cylinders are suitable over a limited stiffness range. Whereas bending beams are suitable for very stiff materials, for asphalt cement they are unmanageable at room temperature. The research team was forced to adopt the position that no simple, low-cost device suitable for specification purposes is likely to cover the entire stiffness range. Therefore, attention was given to test configurations that can be used in the stiffness range where asphalt cement behavior transforms from leathery to brittle. In this context, a test that can be used in a go or no-go scenario appeared most attractive. In other words, a test that simply eliminates, at the given design temperature, materials that are too stiff to resist thermal cracking should be appropriate for specification purposes. A simple bending beam appeared to offer the optimal testing configuration that warranted further study.

In contrast to the simple bending beam test is the very sophisticated Rheometrics dynamic mechanical analyzer (DMA), a costly (more than $300,000) device that requires an expert operator. Alternatives to the Rheometrics DMA have become available in recent years and their cost (less than $100,000)

makes them potentially cost effective, even for specification purposes. However, an expert operator is still required for these devices, and the data they yield must be interpreted by someone with at least a rudimentary understanding of the science of rheology. Therefore, such devices are currently unacceptable for specification testing.

Assuming that a rational test method is available for measuring the stiffness of asphalt at low service temperatures, a performance model that allows the stiffness to be related to thermal cracking must be available if rational specification criteria are to be established. Therefore, five of the currently available computer models and a nomographic procedure that have been developed to predict thermal cracking were reviewed. These performance prediction models are categorized as one of three types: statistical, empirical/mechanistic, or fracture mechanics based. Performance prediction models, especially those that accommodate fundamental material properties, such as fracture and stiffness, are essential if these material properties are to be related to performance. The program input requirements, computation methodology, accommodation for and treatment of material properties, and available output were reviewed. Two programs were recommended for further study, the empirical/mechanistic program TC-1 and the relatively untested fracture mechanics model, THERM. While the former has been determined to be the most reliable through field testing, the fracture mechanics model is more fundamental and has the greatest potential for further development. However, neither program proved reliable when it was extrapolated to pavements other than those used in developing the original model. Both models require further development and verification before they can be used routinely.

Program COLD and TC-1 contain submodels for calculating mixture properties, pavement stresses, temperature, and long-term aging effects. The reliability of these submodels for a wide range of conditions is suspect. Direct measurements of mechanical properties are preferred to those estimated from nomographs, especially for waxy or modified asphalts. The applicability of the aging models to a wide range of asphalt cements is also questioned by the research team. In most cases, program TC-1 appeared to predict reasonable cracking indices; however, for several asphalts that were either waxy or exhibited anomalous aging properties, the predicted cracking indices were

unrealistic. Waxy asphalts are a problem because some nomographs may yield inaccurate predictions of stiffness for them, particularly at low temperatures and long loading times.

A laboratory study was conducted with 17 asphalts selected to provide a robust database with a wide range of physical or physicochemical properties. One of the primary objectives of this study was to compare various cracking-related characteristic temperatures and indices measured or calculated as part of the laboratory study and to:

- Examine them for statistically valid relationships.
- Identify temperatures and indices that can be used as surrogates for each other.

As anticipated from the literature search, the various measures of temperature susceptibility (PVN and PI numbers) were poorly correlated, cannot be used as surrogates for each other, and failed to rank the different asphalts equally with regard to thermal cracking.

The temperature at which the penetration extrapolates to 1.2 penetration units, $T_{Pen1.2}$, the temperature at which the viscosity is 4.0 GPa, T_{4GP}, and the Fraass brittle point temperature, T_{Fraass}, have been cited by various researchers as equi-viscous temperatures. Based upon the laboratory data, these three temperatures are not equivalent and the corollary, that these are equi-viscous temperatures, is also not true.

Equi-stiffness temperatures were estimated from Van der Poel's nomograph and McLeod's nomograph. Different limiting stiffness/loading time conditions and different entrance parameters were used to generate a number of equi-stiffness temperatures. In general these temperatures were correlated but not sufficiently to warrant their general use as surrogates for each other. The two loading conditions, 145,000 lb/in^2 (1.0 GPa) at 30 min and 29,000 lb/in^2 (200 MPa) at 2 h are not equivalent:

$$T_{1GPa,\ 30\ min} << T_{200MPa,\ 2\ h}$$

These temperatures differ by approximately 19 °F (11 °C). Specifying 140,000 lb/in^2 (1.0 GPa) as a limiting stiffness is unrealistic because this condition approaches the low-temperature glassy (elastic) modulus for asphalt cement. Applying the 140,000 lb/in^2 (1.0 GPa), 30 min criterion to the study of asphalts would lead to the conclusion that none of them is susceptible to thermal cracking, which is not correct.

In the future, the use of empirical indices and estimated stiffnesses should be discouraged, and, instead, the use of direct measurements of low-temperature stiffness should be encouraged. The bending beam test offers a method for the direct measurement of low-temperature stiffness.

The physicochemical parameters derived from the HP-GPC and the DSC testing did not correlate well with measures of temperature susceptibility, Fraass brittle point temperature, or cracking severity as computed by the models. Compositional parameters alone, such as those from HP-GPC, cannot be expected to correlate with cracking potential. Research has established that compositional parameters must be supplemented with measurements of component compatibility to achieve reasonable correlation with physical properties.[88,89]

The penetration-viscosity number is particularly insensitive to variations in behavior at temperatures below room temperature, and, for low temperature characterizations, the penetration index is preferred over the penetration-viscosity number, especially for waxy asphalts. A quantitative method of characterizing the departure from linearity on the Bitumen Test Data Chart (BTDC) was presented.

Characteristic or transition temperatures were determined in several ways:

- From the temperature corresponding to the peak in the loss modulus (neat asphalt) measured with the DuPont DMA. The temperature at which this peak occurs has been related to the glass transition temperature.
- From plots of the tensile strength and tensile modulus versus temperature which resulted in temperature shifts that are asphalt specific.

- From the fracture mechanics properties plotted versus temperature which resulted in a transition temperature representing the transition from elastoplastic to elastic fracture.
- From the Fraass brittle point temperature.
- From DSC thermograms which can be interpreted to give an apparent glass transition temperature.

In general, these characteristic temperatures exhibited a moderate degree of correlation with each other although there often was considerable offset between the data. Generally, this offset resulted from the use of varying testing rates: in many cases the offset simply represents time/temperature superposition.

It was possible to shift the tensile strength and modulus plots to create a master curve unique to the mix tested. In performing this type of data analysis with mixes, it is important that tests at different temperatures be conducted at the same loading rate. If not, as is practiced by some researchers, then it will be difficult to shift the data and, as a consequence, correlations with the neat asphalt in the mix may also be lost.

The application of fracture mechanics to notched beams of hot-mix asphalt was successful and represents a meaningful method for characterizing fatigue and fracture properties. The incorporation of elastoplastic fracture mechanics and a modification of the THERM program are necessary before the J-integral approach can be added to the program. Short-cut methods, such as correlation of J-integral with creep or relaxation data, for obtaining the fracture parameters, will be necessary if the fracture mechanics approach is to be implemented for routine design or specification purposes.

A simple test procedure for measuring the stiffness of asphalt cement at temperatures less than 77 °F (25 °C) was demonstrated. The test was conducted in the creep mode with a constant applied load. Although the test can be used to generate a master curve, for specification purposes it is best used as a go/no-go test in conjunction with specification criteria including a maximum stiffness at a specified temperature and loading time. Data generated with the beam test overlapped or matched the data obtained with the DMA and

extrapolated reliably to the Newtonian viscosity measured at 140 °F (35 °C). At longer loading times, the beam data showed that the nomographs grossly underestimate stiffness.

Data obtained with the simple bending beam test in the constant strain rate mode were unreliable because of the small loads that were required. Further development of the bending beam test in the constant strain rate mode is probably warranted, but only as a research test. With proper development, the test could be used in this mode to obtain relaxation data or creep data for neat asphalt cement that can be related theoretically to the fracture parameters.

9. CONCLUSIONS

A number of conclusions are valid for the limited range of materials--one aggregate-mix design combination and 17 asphalts--studied in the project. The conclusions are stated as follows:

- The results from the bending beam test, the selection of which was based upon an extensive literature review, support the conclusion that a simple bending beam test is an appropriate test configuration for specifying the low-temperature properties of asphalt cement. The utility of the test was demonstrated using five of the asphalt cements and a prototype testing fixture. The use of this promising test warrants further verification in field trials.

- In comparison with the bending beam test results, the nomographs underestimate stiffness at long loading times. Consequently, when nomographic values of stiffness are used to predict cracking, the stiffness values may be in error by as much as an order of magnitude. The result will be an actual cracking temperature that is higher than predicted. Measured stiffness values are preferred over nomographic predictions of stiffness.

- All of the test data from the bending beam test, the DuPont DMA, and capillary viscometry fall on a single master curve, lending credibility to the reliability of each of the testing systems.

- The accuracy of the thermal cracking models must be improved, and direct measurement of physical properties should be included in the models. The aging submodel in the empirical/mechanistic program, TC-1, and in the fracture-mechanics-based THERM program may be grossly in error for some asphalts. THERM should be modified to permit the direct use of crack growth parameters (J-integral).

- The various temperature-susceptibility parameters do not correlate well with each other, and the penetration-viscosity number, when applied to low-temperature behavior, is questionable for waxy asphalts. Direct measurements of stiffness should be used in the prediction models for thermal cracking rather than nomographic estimates.

- The J-integral approach to fracture behavior is viable for hot-mix asphalt and should be studied further, especially in terms of correlating J-integral with other, more easily measured procedures such as creep behavior.

- The various temperature susceptibility parameters, limiting stiffness temperatures, equiviscous temperatures, and other characteristic temperatures are not, in general, good surrogates of or predictors for each other. The criterion 145,000 lb/in^2 (1.0 GPa) at 30 min is not acceptable as a limiting stiffness for the control of thermal

cracking because it does not discriminate between different asphalts and it approaches the low-temperature glassy modulus. Of the characteristic temperatures, $T_{Pen1.2}$, T_{Fraass}, and the temperature at 29,000 lb/in^2 (200 MPa) at 200 min, $PI_{log-pen}$ basis appear to be more representative of cracking potential than the other parameters. This conclusion is, however, primarily subjective.

- A quantitative method for describing class index was developed. This method accounts for differences between the slope of the two branches of the BTDC chart, as well as the differences between $T_{R\&B}$ and T_{Pen800}.

10. RECOMMENDATIONS

One of the primary objectives of this study was to establish the feasibility of developing a test for measuring the low-temperature stiffness of asphalt cement. Criteria for choosing a test procedure included low cost, ease of performance, suitability for use as a specification test, and reduction to engineering units.

Another objective of the project was to establish a protocol for verifying the validity of the test procedure. A complete protocol must include a predictive model that relates the test results to a cracking mechanism. Ideally the model should account for mix design variations, accommodate both low-temperature shrinkage and thermal fatigue cracking, and predict, as a stochastic variable, the estimated time to cracking as well as the amount of cracking at any time, t.

The above criteria eliminate procedures that simply calculate a limiting stiffness temperature or a temperature at which cracking will occur. Such procedures are severely limited not only because they cannot account for thermal fatigue, but, in addition, they cannot predict the time of cracking or the extent of cracking. Therefore, it is mandatory that the recommended method include an algorithm for predicting time to cracking and the extent of the cracking, as well as accounting for both thermal cracking mechanisms, thermal fatigue and low-temperature thermal shrinkage.

Two models were selected for evaluation, the THERM fracture mechanics model and the empirical/mechanistic TC-1 program. The THERM program was selected for field verification because it is the only model that is based on fracture mechanics and fundamental material properties. However, further development of the model is needed before it can be verified in the field. On this basis, and on the basis of the correlations obtained with project data, the TC-1 program is recommended as the predictive model of choice. However, THERM should not be discounted if the required resources can be acquired to modify the program to accept a fracture mechanics approach and measured

material properties. The accuracy of the aging models in TC-1 and THERM must be improved.

The TC-1 model requires specific input variables. These were summarized in table 3. Many of the data required as input to the program are either environmentally related or can be readily assumed from handbook values. Examples of the latter are mix conductivity, specific heat, and surface absorptivity. The model does require tensile strength as a function of temperature, but the stiffness as a function of temperature is calculated using the Van der Poel nomograph. The model should be calibrated with measured stiffness values. To account for field aging, an empirical aging model is used to predict long-term, inservice aging. This model is suspect with regard to the softer asphalts and the asphalts with unusual properties. Further work needs to be done to update the program if and when improved aging models become available.

TC-1 should also benefit in terms of predictive accuracy if actual stiffness rather than predicted stiffness is used in the model. The nomograph generally underpredicted the stiffness of the mixes. Adoption of actual stiffness as a program input can be done readily and should be done in future applications of the program.

As a consequence of the literature review, the data analyses in chapter 5, and the above discussions, the research team recommends program TC-1, along with measured stiffness as a program input, as an alternative procedure for predicting thermal cracking. Although this program has been developed from field data, the data sets are limited with regard to asphalt properties and mix variables.

With regard to experiment design for a field study on thermal cracking, the first consideration is the number of study variables. The properties of asphalt cement are obviously primary variables. To assess the effect of stiffness, each source should be considered in at least two grades. A wide variety of mixture variables have been purported to affect thermal cracking, but the primary variable appears to be mixture voids or level of compaction.[96]

An important consideration in the design of any experimental study is the number of test sections that can be afforded. The number must be realistic given time and money constraints but must also be reasonable with regard to the ability to fit the sections within a homogeneous environment, namely, one construction job. For this consideration, 16 appears to be a reasonable number of sections. The test sections should preferably be on an interstate or other four-lane road so that loaded and unloaded sections (or at least a lightly traveled passing lane) can be compared. This design gives a total of 32 study sections. The following scheme is compatible with the number of sections:

Source	4
Grade	2
Air Voids	2
Traffic	2
Total = 4 x 2 x 2 x 2 = 32 test sections	

In the proposed study, a full factorial design would be used. The 32 study cells give adequate degrees of freedom for making reliable inferences with regard to the effects of the study variables. The study should be replicated in a least two environmental zones: the northern United States with minimum temperatures of -20 °F (-29 °C) to -40 °F (-40 °C) and a more southerly location where thermal fatigue is encountered.

The algorithms for estimating the components of variance and drawing statistical inferences are well documented for the proposed experimental design. Only two-way interactions would be considered in the analysis of the data; other, higher order interactions would be assigned to the error term. Consequently, any statistical analyses of the data would follow routine statistical procedures.

Ordinary construction practice should be followed except that, to provide two levels of air voids, reduced levels of compaction should be used for one half of the sections. Test sections, each 1,000 ft in length, should be assigned on a random basis to any given combination of the test variables.

The usual construction acceptance would be followed, but in addition, the full schedule of tests conducted for this project should be conducted on the materials.

The proposed experiment will provide a validation of the TC-1 model and, more importantly, will provide a database for the validation or development of newer, more sophisticated models, such as THERM. In fact, with the suggested data measurements, Lytton's THERM model could be field tested. The fracture mechanics program is a mechanistically based model and should provide more reliable predictions than the TC-1 model when it is properly calibrated.

APPENDIX A
DYNAMIC MECHANICAL ANALYSIS TEST DATA

A DuPont Series 9000 DMA testing machine was used to obtain DMA spectra for each of the asphalt cements. Only the RTFOT residue was tested because the authors wanted to test neat asphalt that as nearly as possible duplicates the asphalt cement in the field after construction and laydown. The test specimens were beams, 0.25 in (6.4 mm) by 0.25 in (6.4 mm) by 4 in (101.6 mm) long. The beams were prepared by pouring the hot RTFOT residue into silicone molds at approximately 300 °F (149 °C). After cooling in air at room temperature, the molds were chilled in ice water whereupon the beams were released readily from the molds.

The 9000 DMA operates at the resonant frequency of the test beam, which changes with the stiffness of the beam. Test specimens were pre-cooled in the test apparatus and the stress/strain response was recorded as the beam was heated to room temperature. The test frequency ranged from approximately 40 Hz at -40 °F (-40 °C) to approximately 10 Hz at 77 °F (25 °C). The presence of viscoelastic behavior at the upper end of this temperature regime dampens the beam and reduces its resonant frequency.

The asphalt source is identified by the specimen number in the upper left-hand corner of each plot. Replicate specimens are denoted by an "a" and a "b" following the number. The magnitude of the loss peak and the temperature, T_g, at which it was observed are marked on each plot. The test device was programmed to increase temperature at a rate of 7 °F/min (3 °C/min). However, because of thermal lag between the device and the specimen, the actual temperature increased at an approximate rate of 4 °F/min (2 °C/min). The temperatures given on the horizontal axis of each plot are therefore somewhat higher than the actual asphalt test temperature. No correction was made for the thermal lag because the effect is relatively constant for all of the test specimens.

Replicate specimens were formed from RTFOT residue that was, in general, a mixture of the residue from eight bottles, all from a single RTFOT run. On occasion a second run was performed and the material from the first set of bottles was mixed with the material from the second set of bottles to form a second sample. Test specimens were discarded after they were tested; material was not reused to make replicate specimens.

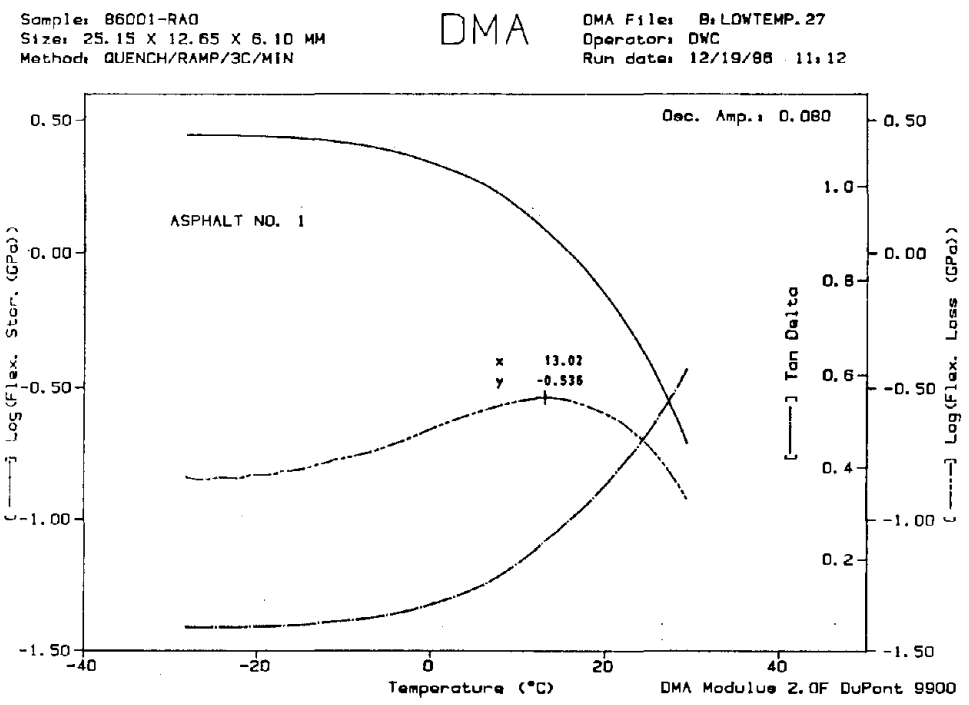

Figure 85. DMA test results for asphalt sample 1.

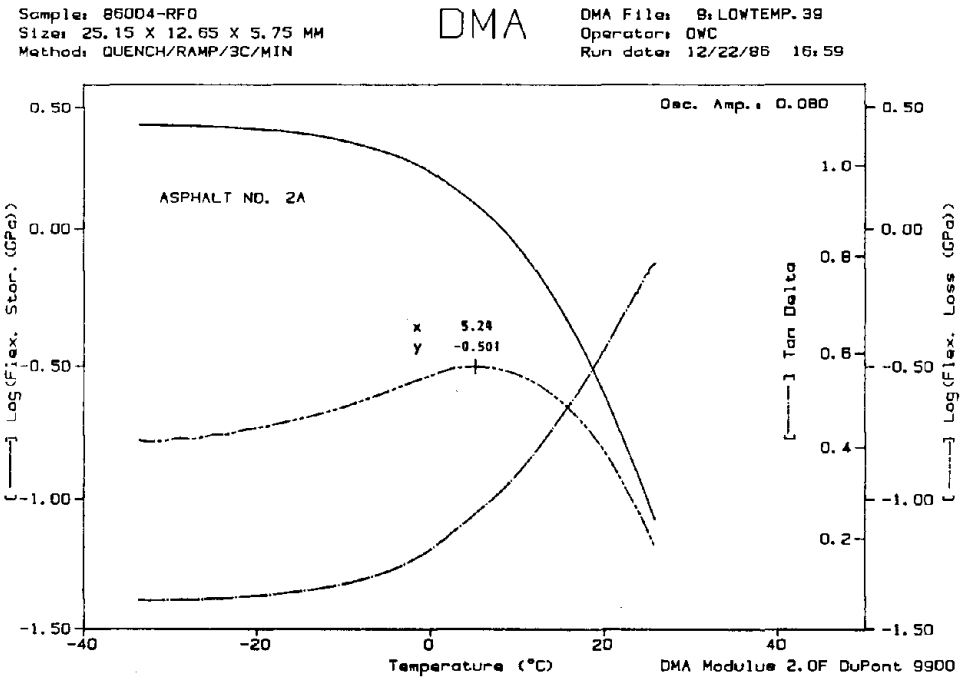

Figure 86. DMA test results for asphalt sample 2a.

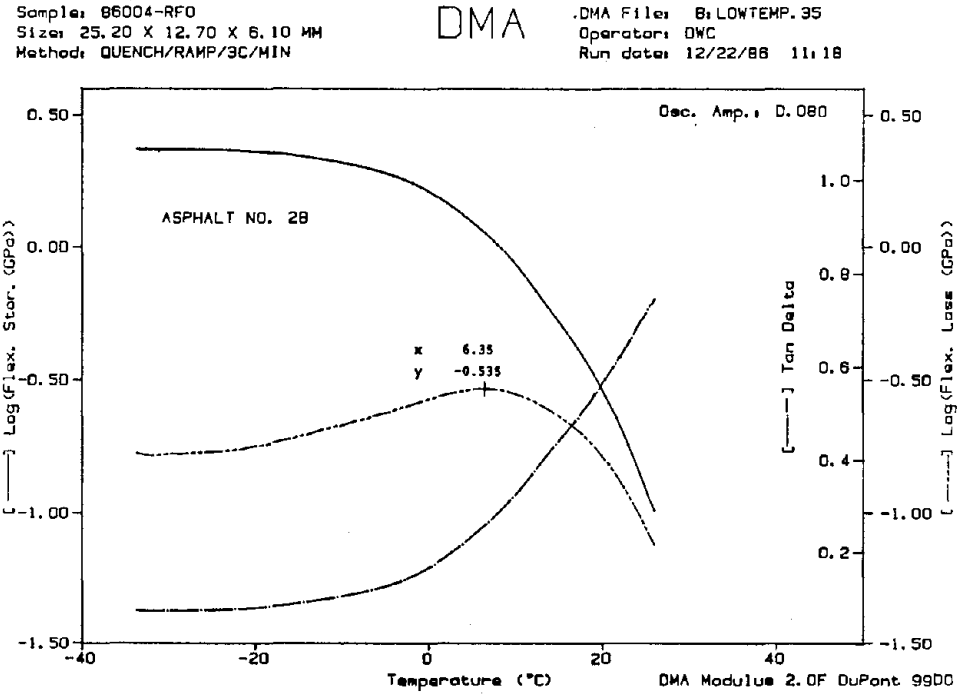

Figure 87. DMA test results for asphalt sample 2b.

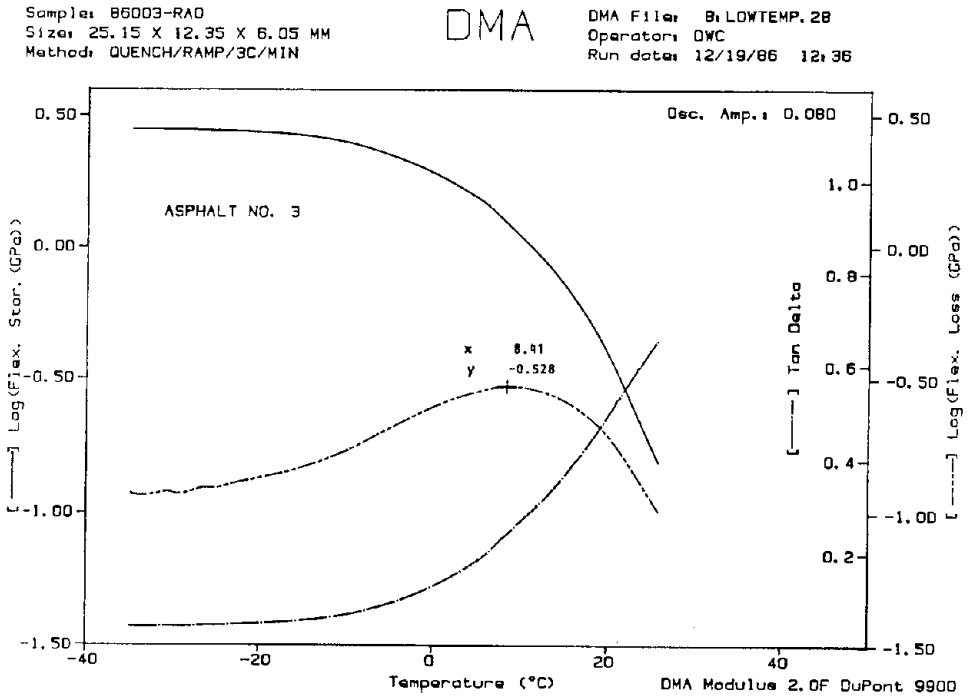

Figure 88. DMA test results for asphalt sample 3.

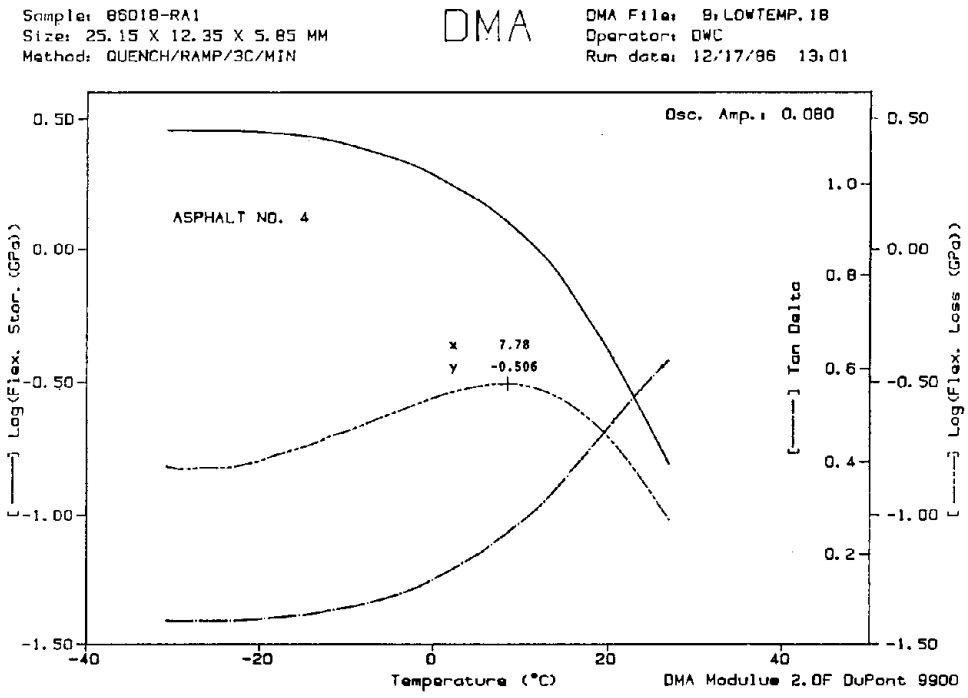

Figure 89. DMA test results for asphalt sample 4.

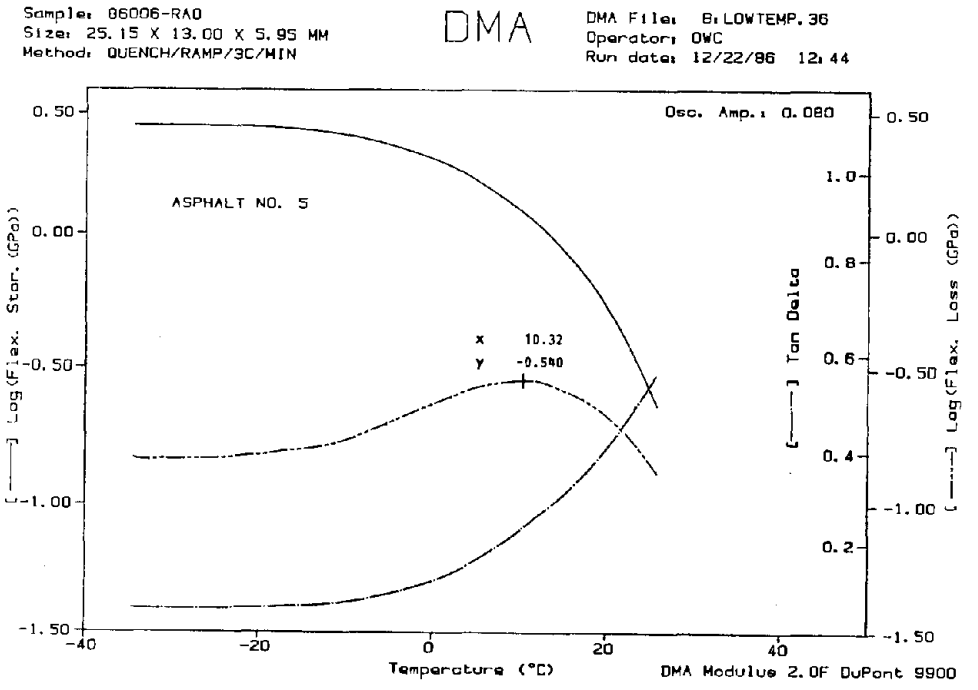

Figure 90. DMA test results for asphalt sample 5.

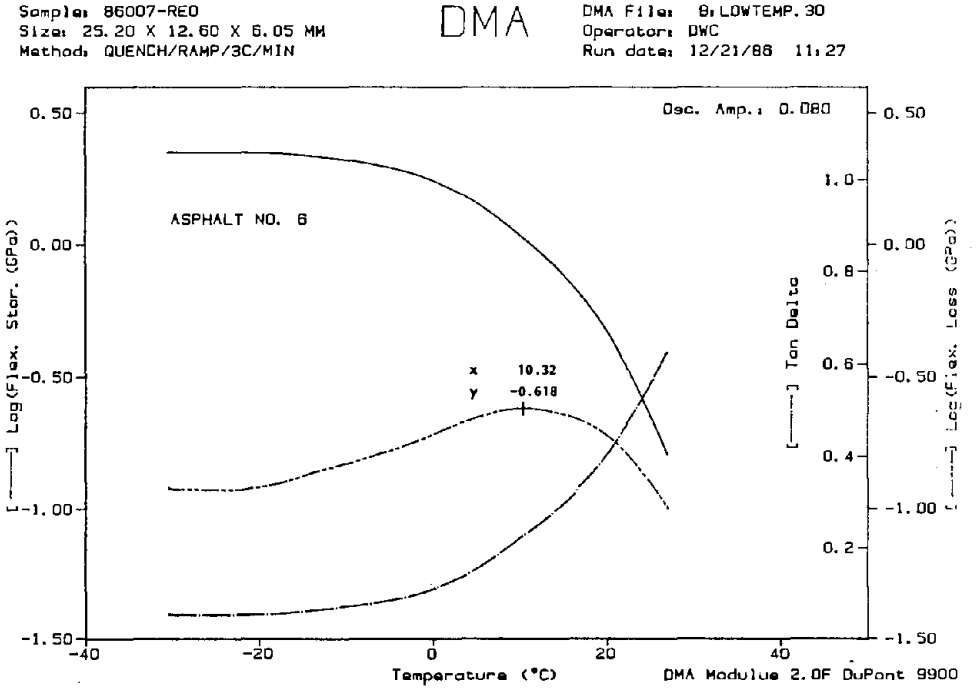

Figure 91. DMA test results for asphalt sample 6.

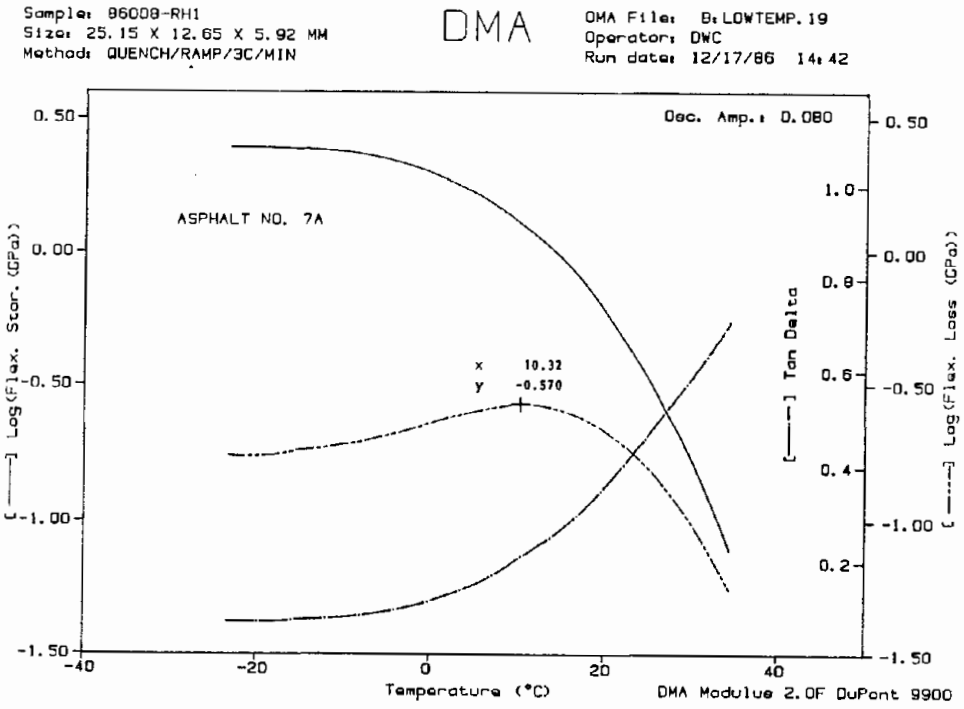

Figure 92. DMA test results for asphalt sample 7a.

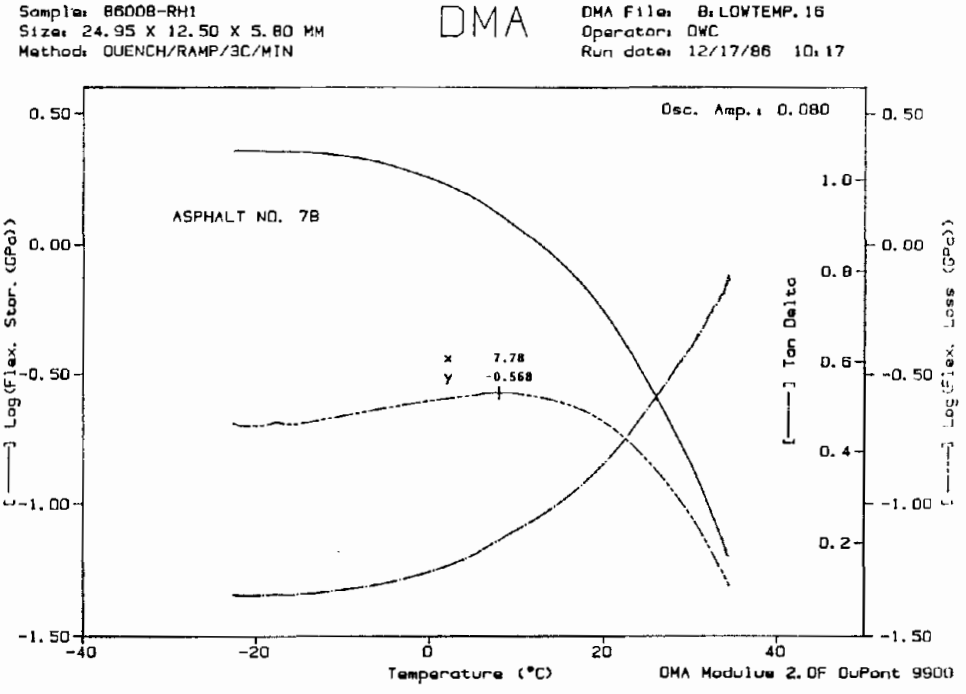

Figure 93. DMA test results for asphalt sample 7b.

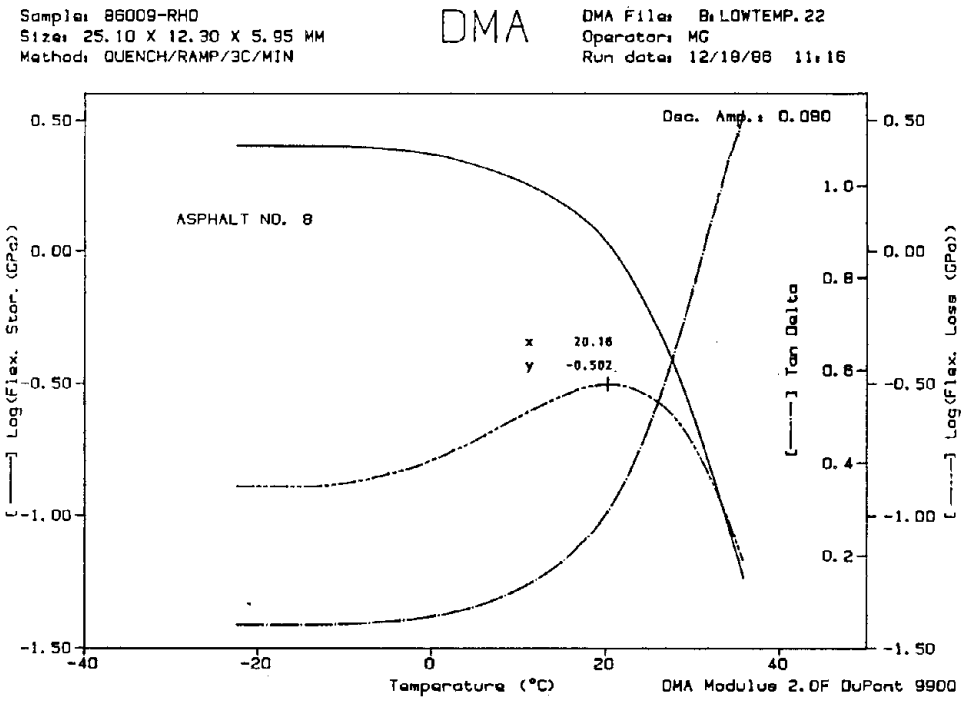

Figure 94. DMA test results for asphalt sample 8.

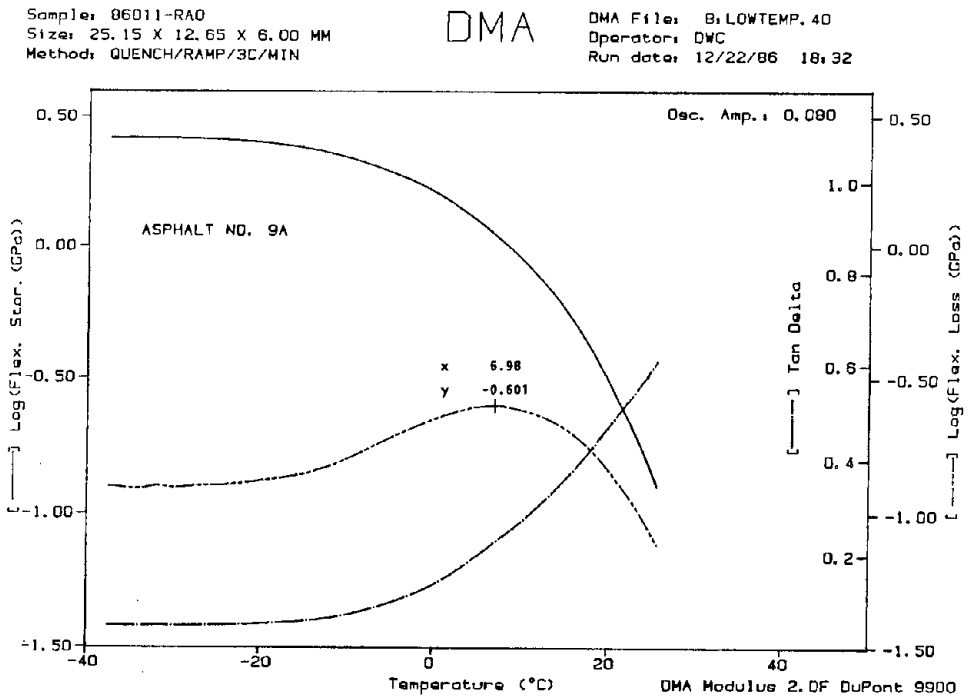

Figure 95. DMA test results for asphalt sample 9a.

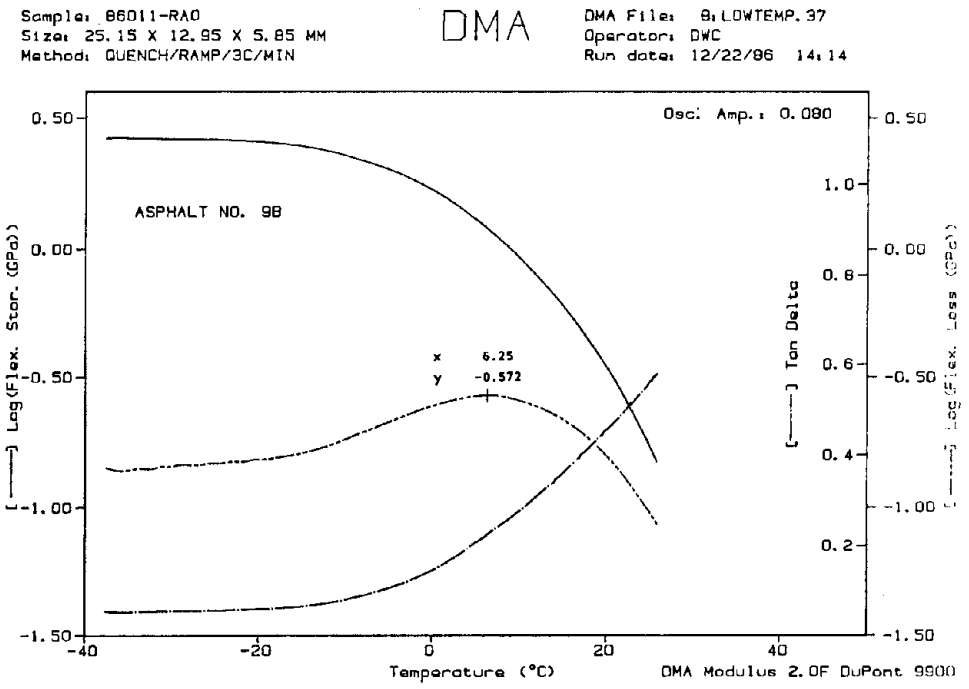

Figure 96. DMA test results for asphalt sample 9b.

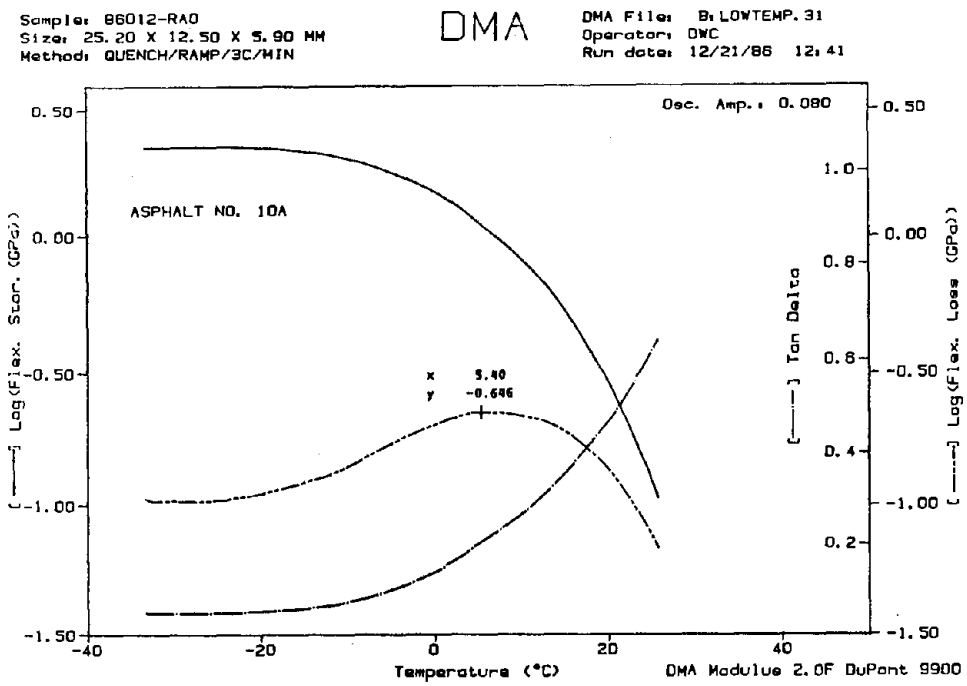

Figure 97. DMA test results for asphalt sample 10a.

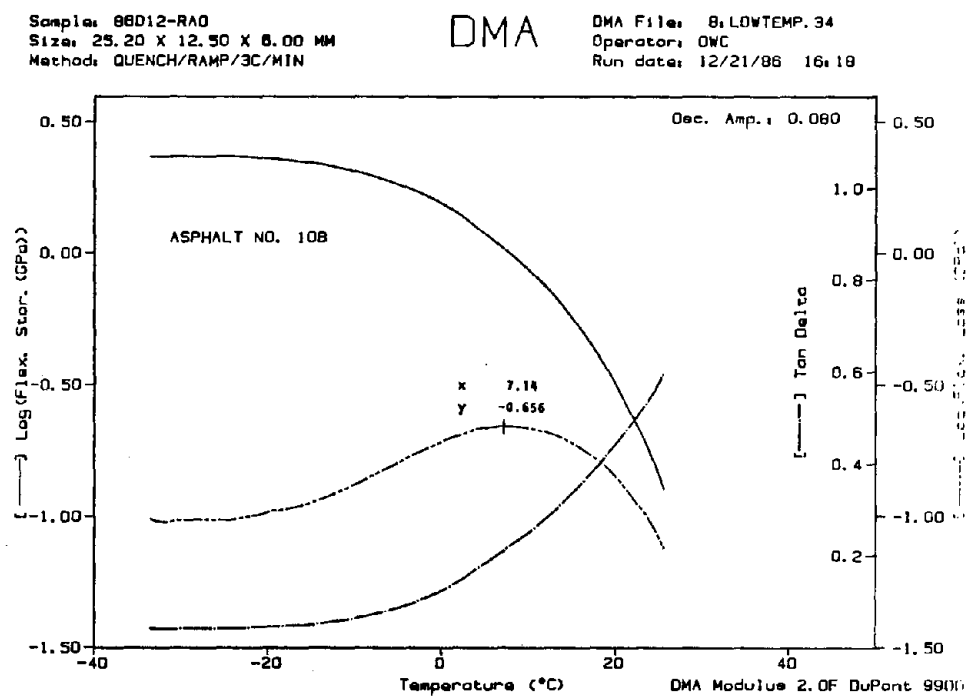

Figure 98. DMA test results for asphalt sample 10b.

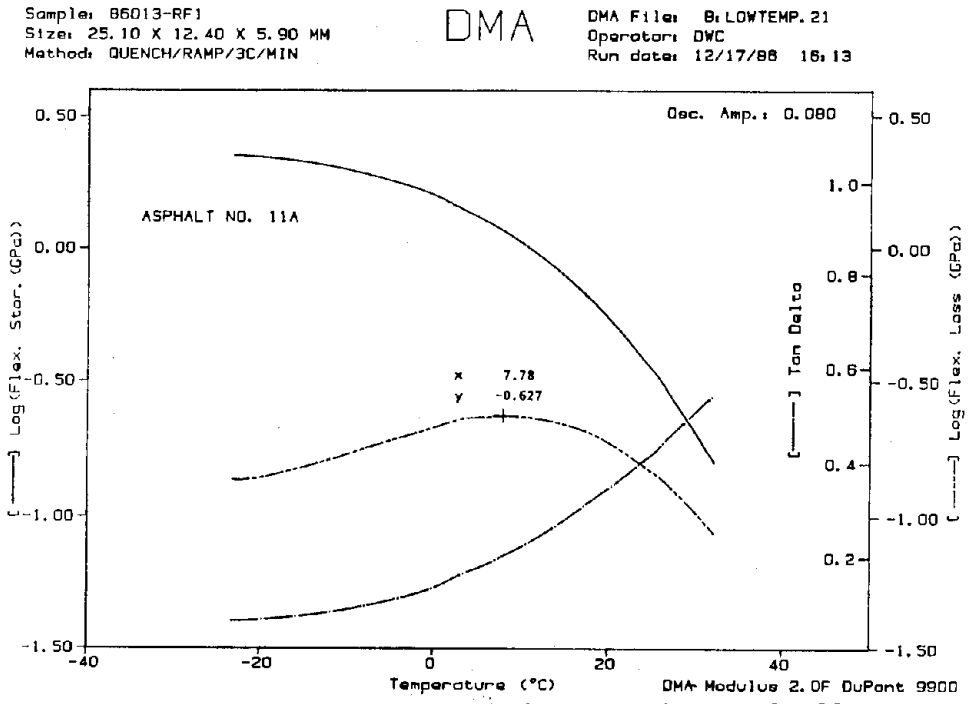

Figure 99. DMA test results for asphalt sample 11a.

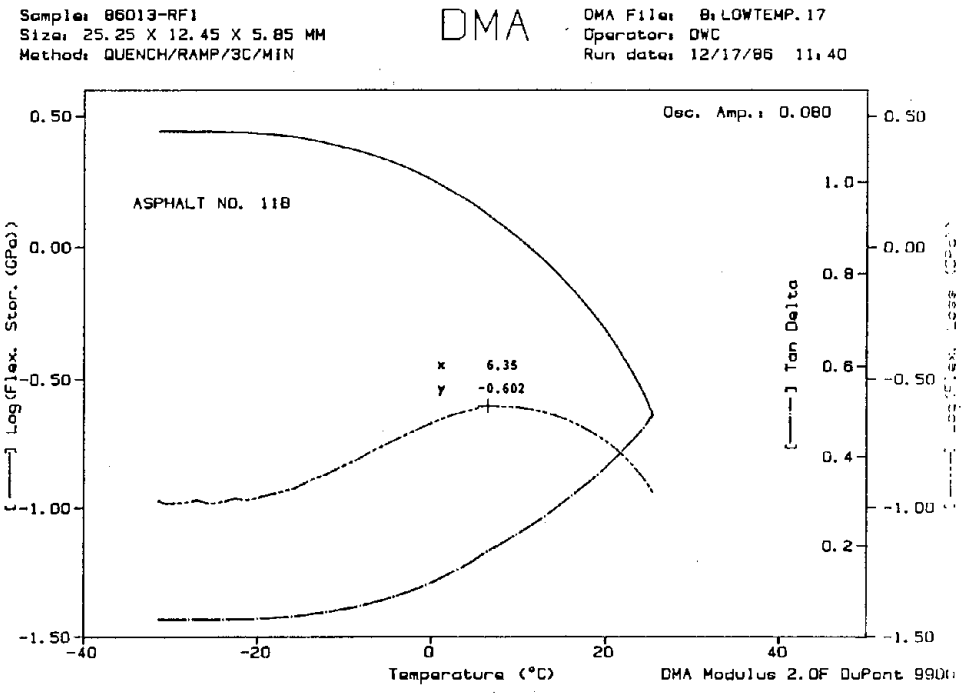

Figure 100. DMA test results for asphalt sample 11b.

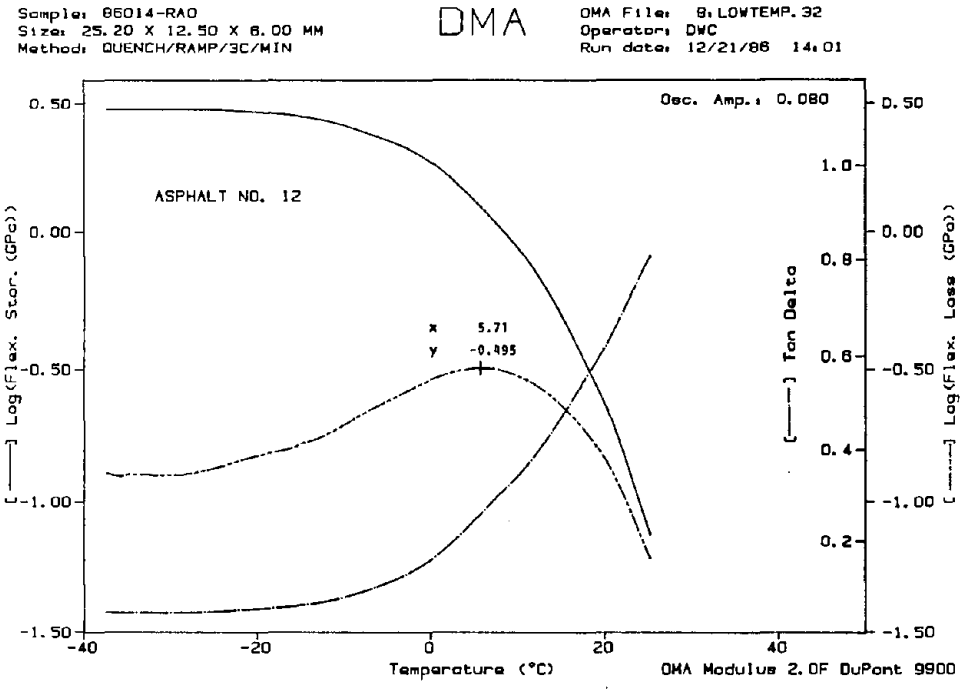

Figure 101. DMA test results for asphalt sample 12.

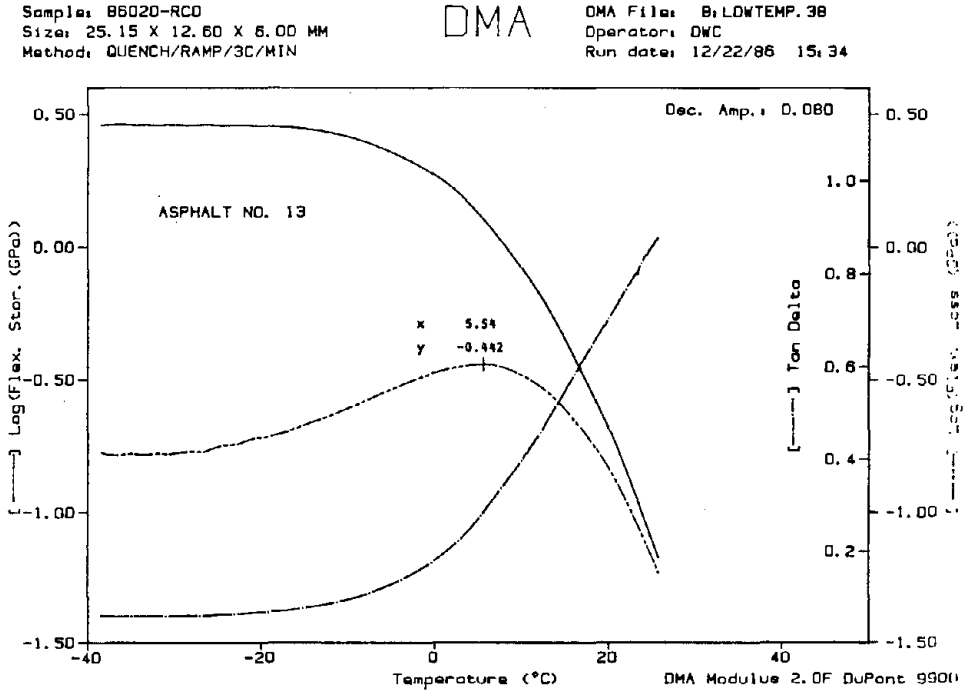

Figure 102. DMA test results for asphalt sample 13.

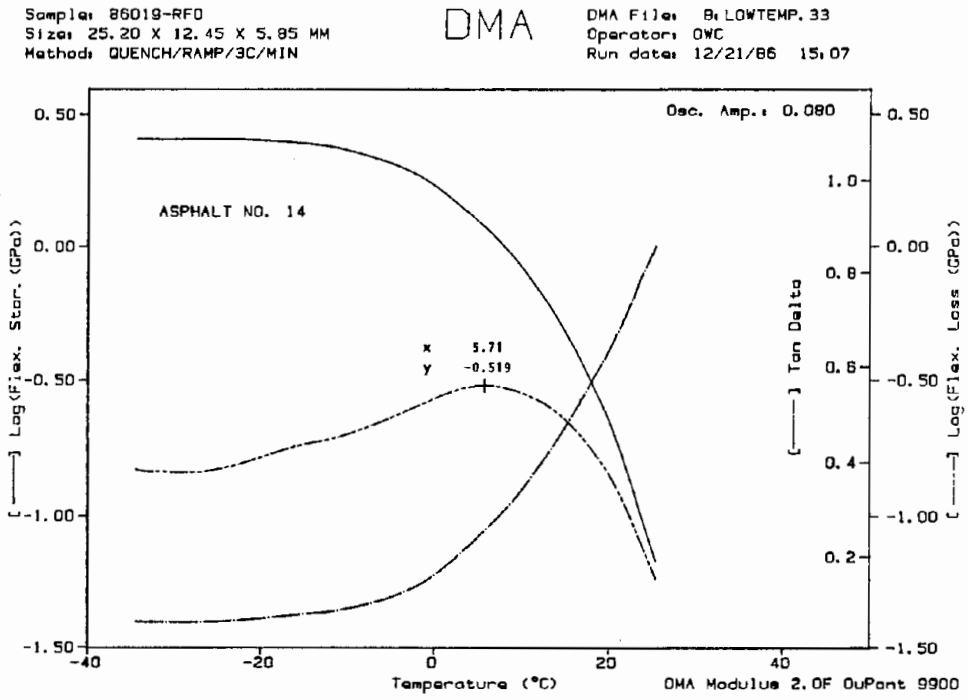

Figure 103. DMA test results for asphalt sample 14.

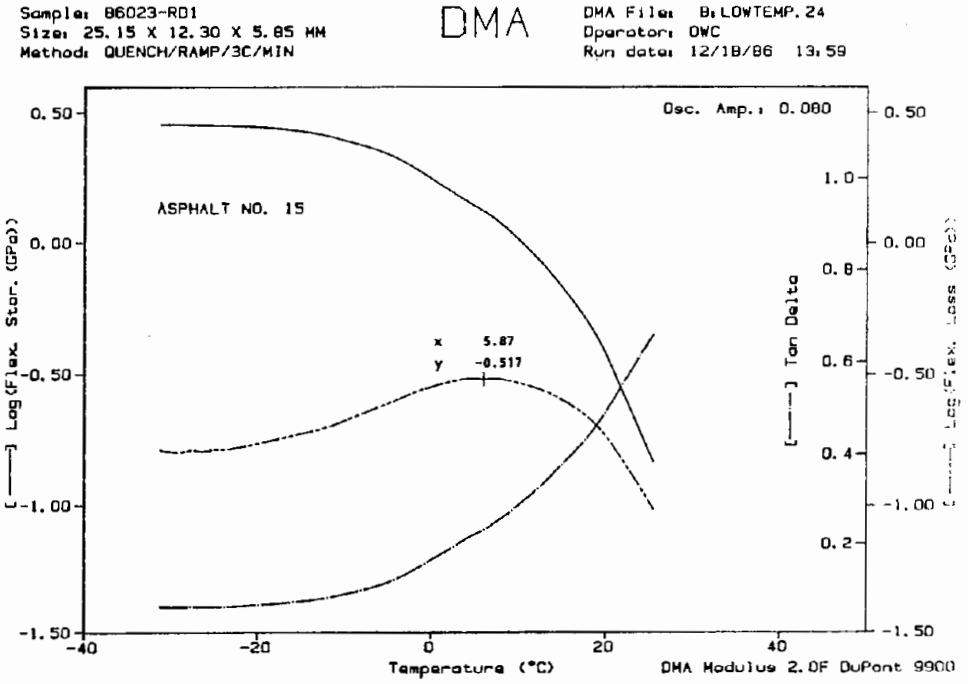

Figure 104. DMA test results for asphalt sample 15.

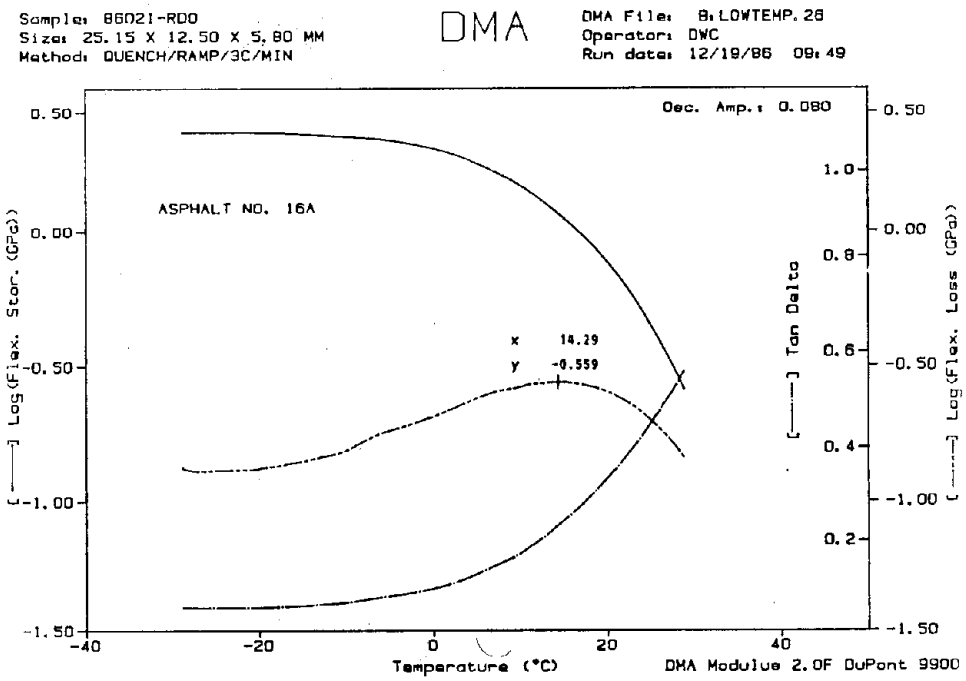

Figure 105. DMA test results for asphalt sample 16a.

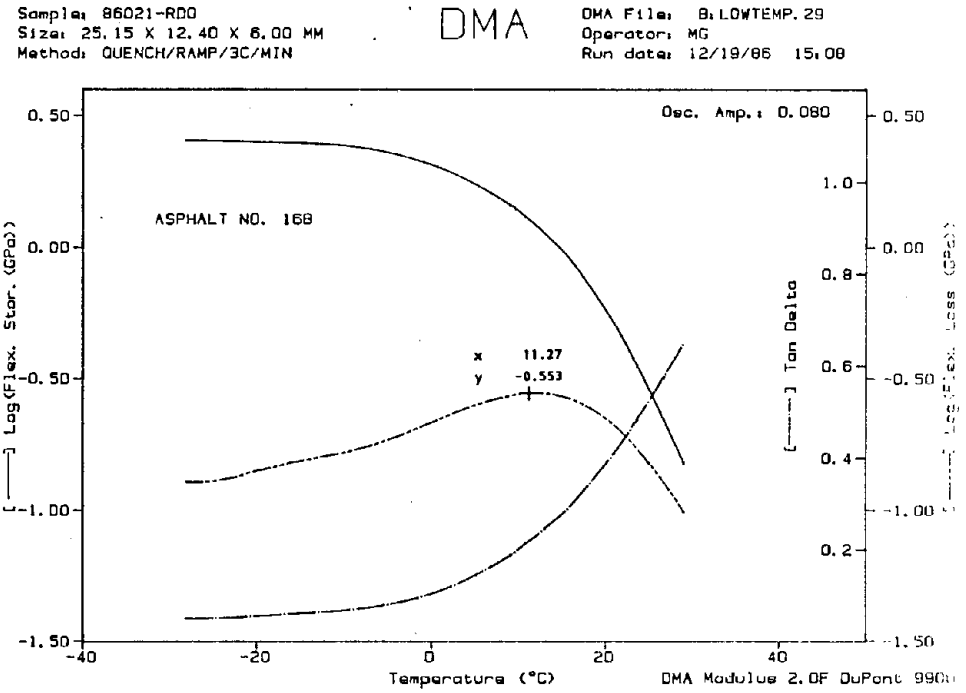

Figure 106. DMA test results for asphalt sample 16b.

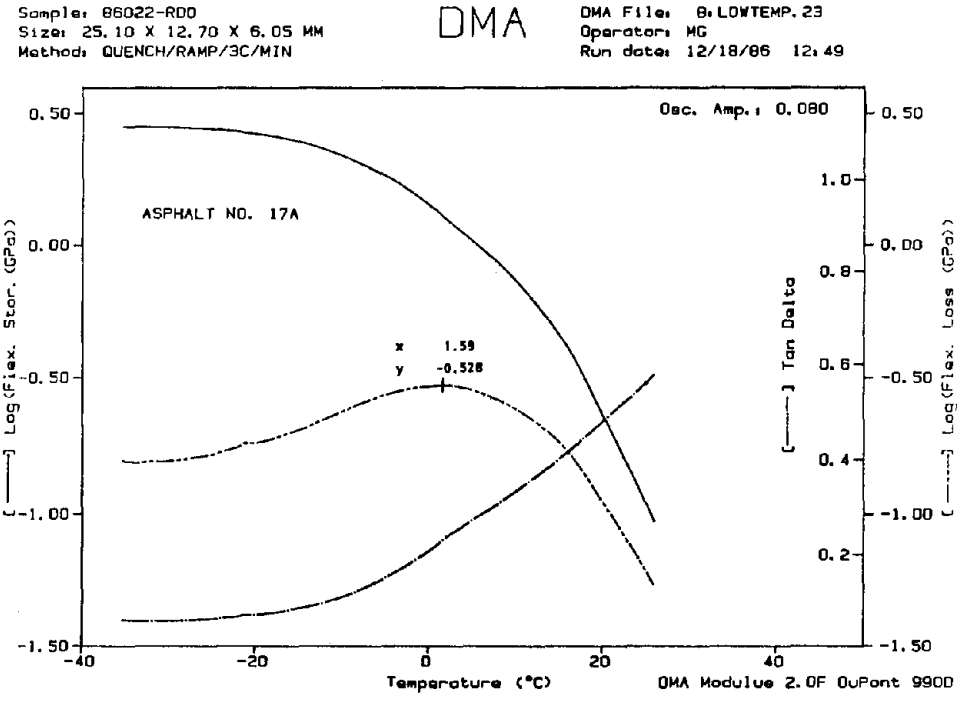

Figure 107. DMA test results for asphalt sample 17a.

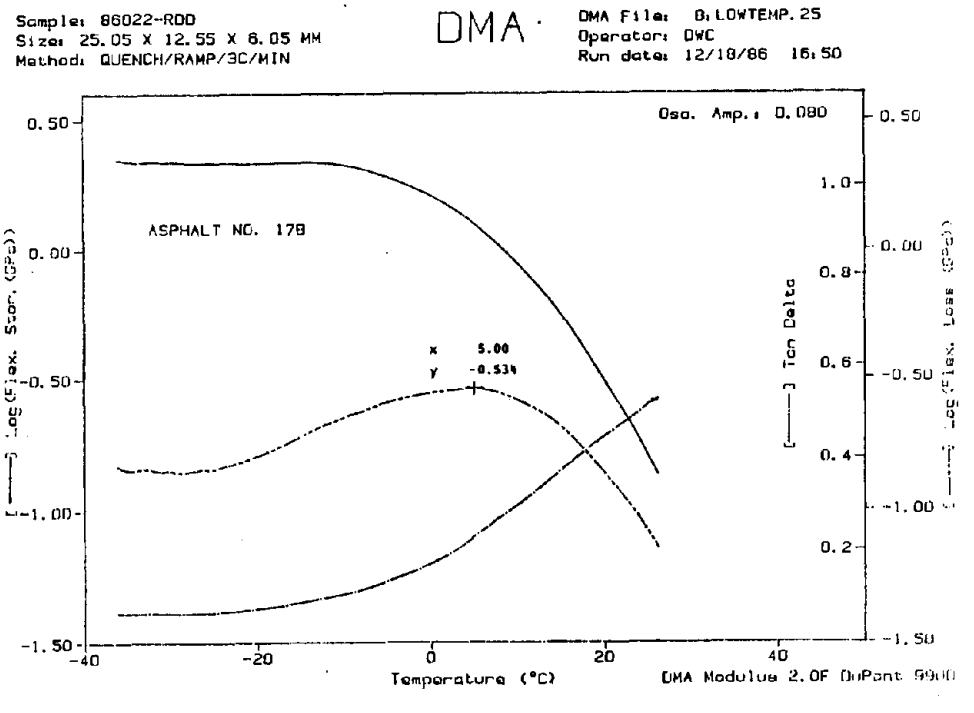

Figure 108. DMA test results for asphalt sample 17b.

APPENDIX B
DIFFERENTIAL SCANNING CALORIMETER THERMOGRAMS

A Perkin-Elmer series 7 differential scanning calorimeter (DSC) was used to obtain a thermogram for the RTFOT residue for each asphalt cement. The sample weights for each DSC run ranged from 10 to 20 mg. The prepared samples were first cooled to -58 °F (-50 °C), and thermograms were recorded as the asphalt cement was heated from -58 °F (-50 °C) to a final temperature of 266 °F (130 °C). The heating rate was 18 °F/min (10 °C/min) for all of the runs.

The individual thermograms were very complicated; the transitions were often very diffuse and difficult to determine. A small-scale study with different heating rates was done to optimize the heating rate, and the 18 °F/min (10 °C/min) rate was selected as the best compromise between the definition of the transitions in the thermogram and the total time required to obtain the thermogram (laboratory productivity).

For simple systems that exhibit well defined transitions, the usual technique for determining a transition temperature is to draw two lines, each parallel to the linear portion of the thermogram on either side of the transition, as shown in figure 23. The point where the midpoint between the two drawn lines and the curve intersects is then recorded as the transition temperature. This simple construction could not be used with most of the thermograms for the asphalt cements. Therefore, for most of the asphalts, the transition points were selected subjectively by examining the shape of the thermograms. Where multiple transitions were observed, the lowest transition temperature was reported. Clearly the interpretation of the thermograms is beyond the capabilities of the average asphalt technician, and, in its current form, DSC testing is not appropriate for routine specification testing.

As an exploratory experiment, several of the samples were quenched immediately after they were heated to 266 °F (130 °C). After quenching, a second thermogram was obtained and, in a number of cases, there were significant differences between the shape of the initial and second thermogram (i.e., the thermogram heated after quenching). Project resources were such that a detailed study of the thermograms obtained after quenching could not be pursued. In the authors' opinion, differential scanning calorimetry warrants further study and may be valuable in studies of asphalt structure, especially in studies of steric hardening.

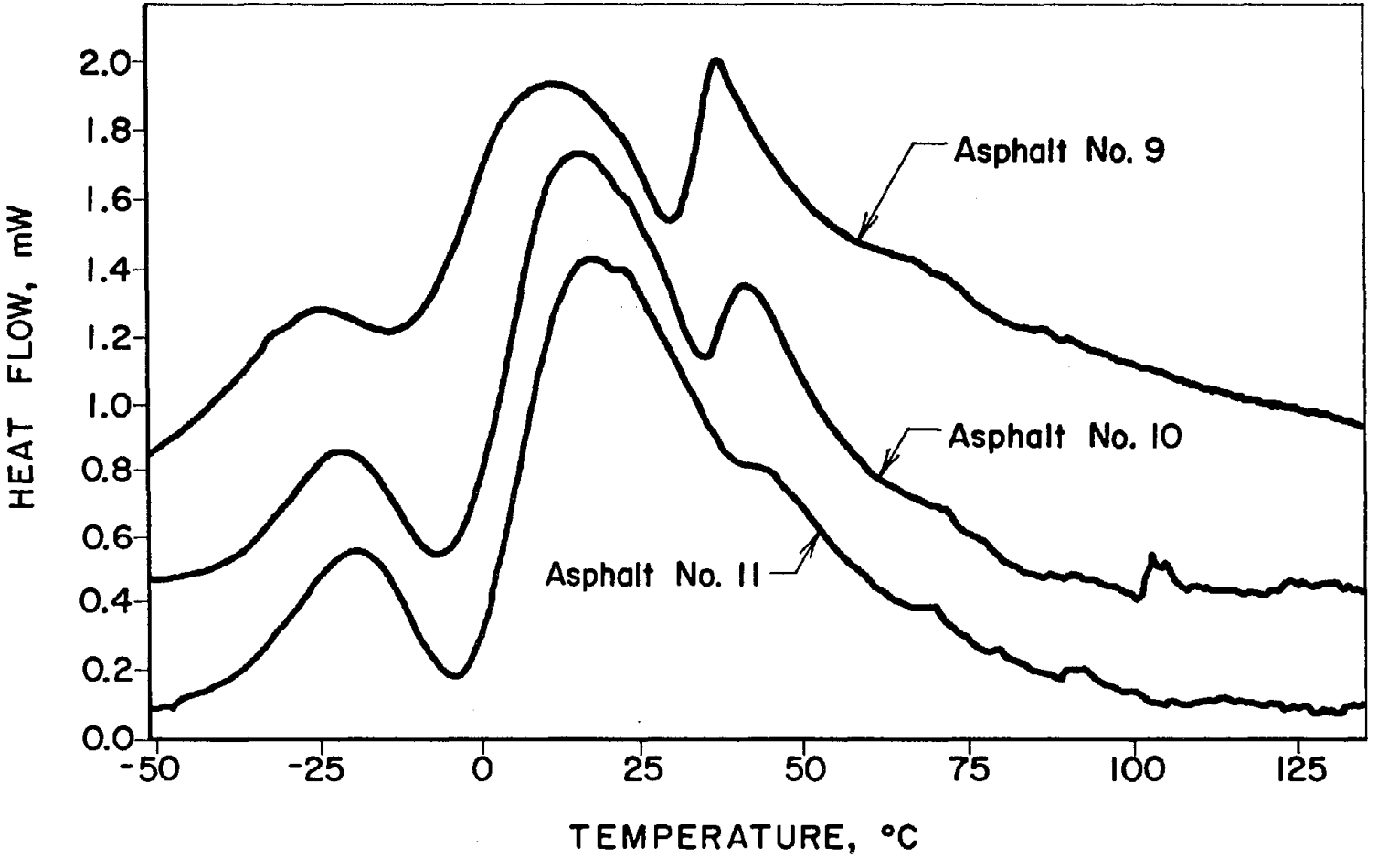

Figure 109. Thermogram for asphalt numbers 9, 10, and 11.

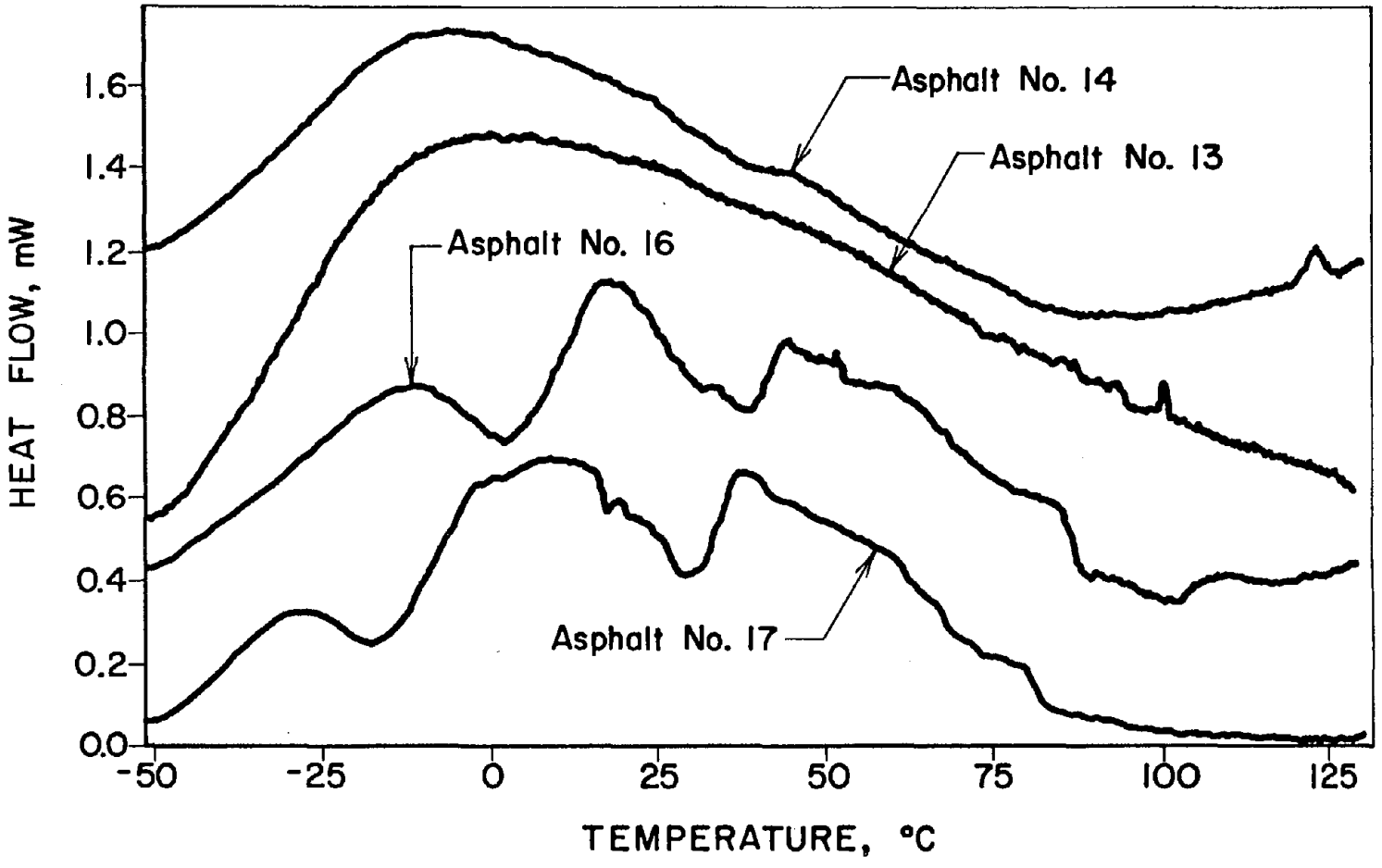

Figure 110. Thermogram for asphalt numbers 13, 14, 16, and 17.

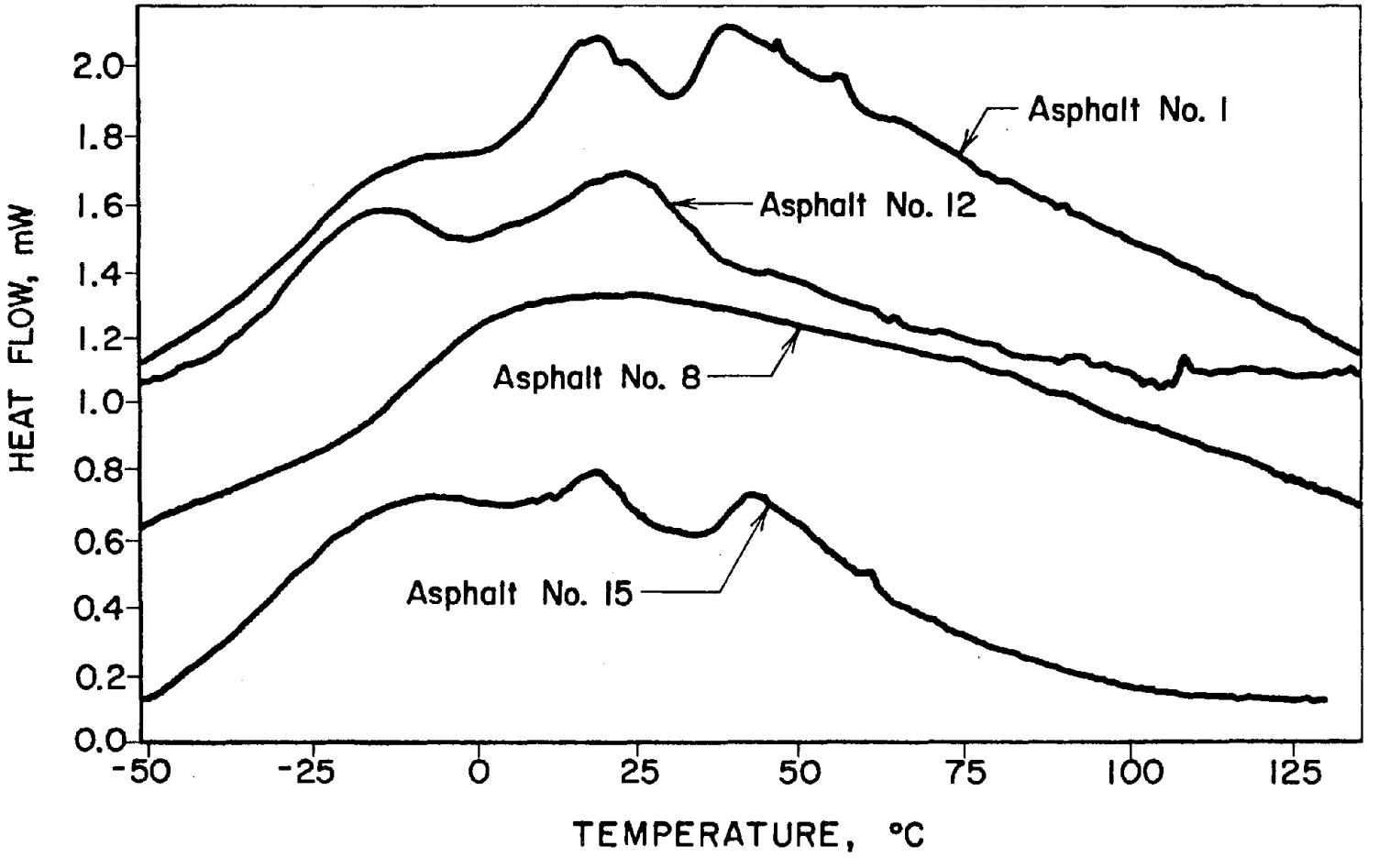

Figure 111. Thermogram for asphalt numbers 1, 8, 12, and 15.

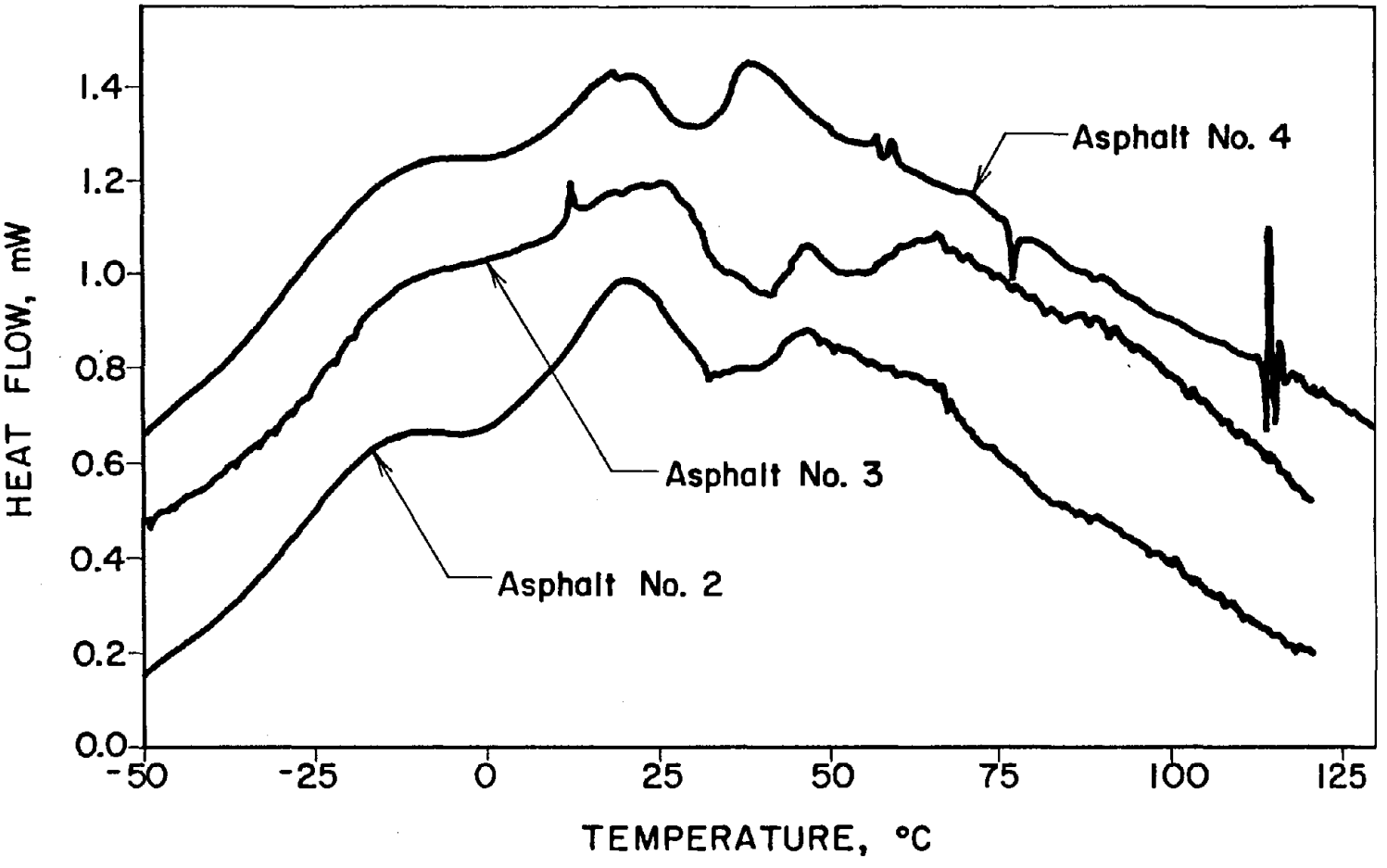

Figure 112. Thermogram for asphalt numbers 2, 3, and 4.

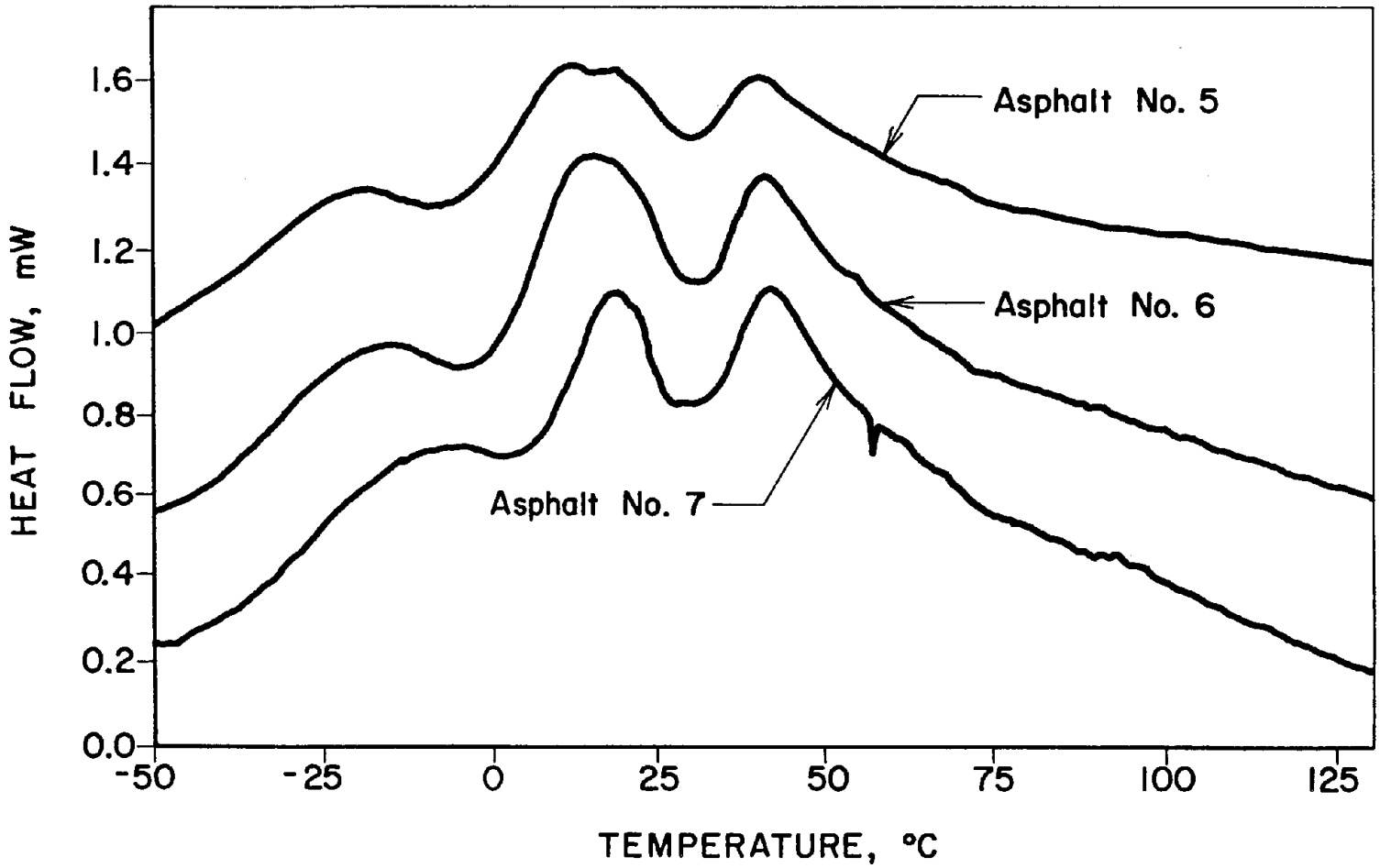

Figure 113. Thermogram for asphalt numbers 5, 6, and 7.

APPENDIX C
HIGH-PRESSURE GEL PERMEATION CHROMATOGRAPHY LABORATORY PROCEDURE

The following procedure is reproduced from a report by Jennings and was followed in the HP-GPC work that was done in the authors' laboratory as well as that done by Pribanic.[83]

ANALYTICAL METHOD

Two high-performance (or pressure) gel permeation chromatography instruments (Waters Associates) were used during this study. Except for minor differences (injectors) that do not affect performance, the instruments were identical. They consisted of a solvent reservoir; a high-pressure pump (Waters model M6000); three Ultrastyragel™ columns (Waters), one 10^3-Å unit followed by two 500-Å units; a refractometer (Waters model R401); and a two-channel absorbance detector at 340 nm (Waters model 440), which was shared, with one channel for each instrument. The solvent reservoir was isolated from the atmosphere by a drying tube and fitted with a tube through which helium was slowly bubbled into the solvent to remove dissolved gases.

A flow meter (Phase Separations, Inc., FLOCOB1) with an analog output was used to monitor and record the actual flow through the instruments. The temperature of the mobile phase, columns, and detectors was controlled at 79 °F (26 °C) by means of a system of tubing and a constant temperature bath. Tetrahydrofuran (THF, Fisher) was checked for water content and was filtered through a 0.45-µm silver membrane filter (Selas) before use.

Using residue from the rolling thin-film oven test, samples were prepared for injection as follows. A small amount of asphalt (0.02 to 0.05 g) was accurately weighed into a 5-dram glass vial. THF (drawn from the solvent reservoir) was added by means of a buret to prepare a 0.5-percent (weight/volume) solution. The solution was transferred to a 5-mℓ bench-top centrifuge tube and was centrifuged for 10 min. These steps were completed just before the sample was to be injected.

The instrument was operated in accordance with the manufacturer's instructions. The sample injection size was 100 µℓ. Flow rate was set at 900 µℓ/min. The data were collected, stored, and manipulated via a Perkin-Elmer data acquisition system.

TECHNICAL NOTES

Ultrastyragel™ columns are delicate; the manufacturer's instructions with regard to instrument startup, flow rates, etc., were assiduously followed to avoid damage. The columns were cleaned weekly (after processing 30 to 40 samples) by injecting 2 to 3 mℓ of pyridine into the system, followed by continued flushing with THF.

After the weekly cleaning, when the equipment was shut down, the restart problems were minimized by maintaining a slow flow of solvent through the system. When all asphalt or pyridine had cleared the system, a closed loop was established by returning the effluent to the solvent reservoir, and a flow rate of 100 µℓ/min was maintained.

Solvents must be "degassed" to avoid troublesome bubbles in the system. This was easily accomplished with a helium purge.

Performance of the system was monitored in several ways. In addition to observing the actual flow rate and pressure, the condition of the columns was checked by periodically running a series of monodisperse polystyrene standards using the ultraviolet detector at 254 nm. In the system configured here, these standards had the following retention times:

Normal	Molecular Weight	Retention Time, min
polystyrene	2.4×10^5	16.45
polystyrene	5.0×10^4	17.38
polystyrene	9.0×10^3	20.38
polystyrene	4.0×10^3	22.85
polystyrene	2.9×10^3	23.77
toluene	92	34.68

These retention times will vary somewhat depending on the individual columns, the precise flow rate, the amount of dead volume in the system, and possibly other factors. Nevertheless, the condition of the system can be monitored by running the polystyrene standard periodically, in addition to each time the machine is started up. For the purposes of the testing done by Pribanic, daily analysis of a standard asphalt was the key means of monitoring the system.[84] The chromatograms of this asphalt were expected to correspond very closely from day to day, and the percentage of large molecular size (LMS) was expected to vary no more than $\pm$ 0.5 percent.

CONTROL OF WATER

All THF used in the HP-GPC system was monitored for water content. Solvent containing less than 0.05 percent water was considered acceptable. An infrared detector (Wilkes-Miran 1A-CUF) set at a transmittance of 2.95 to 2.96 μm was used for this determination; a transmittance of 0.5 or more indicated an acceptable water content. (Each detector must be individually calibrated; therefore, these limits cannot be used universally.)

THF which contained excessive amounts of water was dried by refluxing 4ℓ of THF with sodium (10 g) and benzophenone (30 g) until the solution became deep blue in color. The THF was then distilled through a spinning band unit (B/R Instrument Corp).

Computer System

A Perkin-Elmer 3600 data station consisting of a computer, two interface modules, two disk drives (5 1/4 in, double sided, double density), and a printer-plotter (Model 660) were used for the collection, storage, and manipulation of the HP-GPC data. Analog data from the ultraviolet and refractive index detectors were fed into a chromatography interface module for temporary storage (one analysis capacity), then transferred to the 3600 computer for storage on disk.

The software used in the collection and storage of data was Perkin-Elmer "Chromatographics 2 Software," 0330-0859 Revision C 5/5/83, 1982. Further manipulation (plotting, integration, etc.) was done with Perkin-Elmer "Gel Permeation Chromatography Data Processing," (GPC-5), 0254-0389, Revision B, 1983, software.

APPENDIX D
HPC-GPC CHROMATOGRAMS

Two sets of chromatograms are presented in the appendix: those generated in the authors' laboratory, presented first, and those generated by the subcontractor, which follow.

Two curves are shown in the output from the authors' laboratory: one represents relative intensity; the other represents cumulative intensity. The cumulative intensity curve is the one which approaches 100 percent on the right-hand scale. Both curves were obtained with a refractive index (RI) detector. The abscissa is scaled to show the logarithm of molecular weight, increasing in value from left to right (figure 114), and the ordinate is scaled to show normalized or cumulative area under the intensity curves. It should be noted that, because of detector sensitivity, the relative intensity could not be measured below a molecular weight of about 65, and therefore, the chromatogram is not shown below this value.

The maximum molecular weight shown on the curve is about 25×10^6. The cumulative curve was integrated only over the portion of the relative intensity shown in the graphs, and it was adjusted by the proprietary software such that the cumulative area is zero at the minimum molecular weight, approximately 65.

From the relative intensity data, the software used calculates three parameters. The number average molecular weight is the first moment of the mer units about the mean, while the weight average molecular weight corresponds to the second moment of inertia about the mean. The polydispersity index represents the weight average molecular weight divided by the number average molecular weight.

The chromatograms from the subcontractor include two curves, starting with figure 130. The ordinate for these curves is in millivolts, representing detector intensity. The upper curve was obtained with a uv detector, and the lower curve, with an RI detector. The curves obtained with the RI detector were not used by the subcontractor in the analysis. The abscissa represents elution time in minutes, and the ordinate represents the output from the respective transducer in millivolts. No calibration factor is offered for either axis and one is not needed in the subcontractor's analysis. Longer times, on the abscissa, represent smaller molecular weights.

The percentage of large, medium, and small molecular sizes (LMS, MMS, and SMS) were obtained subjectively by the subcontractor by comparing the shape of the subject asphalt chromatogram to that of a standard laboratory asphalt for which LMS, MMS, and SMS have been arbitrarily assigned. The LMS, MMS, and SMS were obtained subjectively by the subcontractor from this comparison.

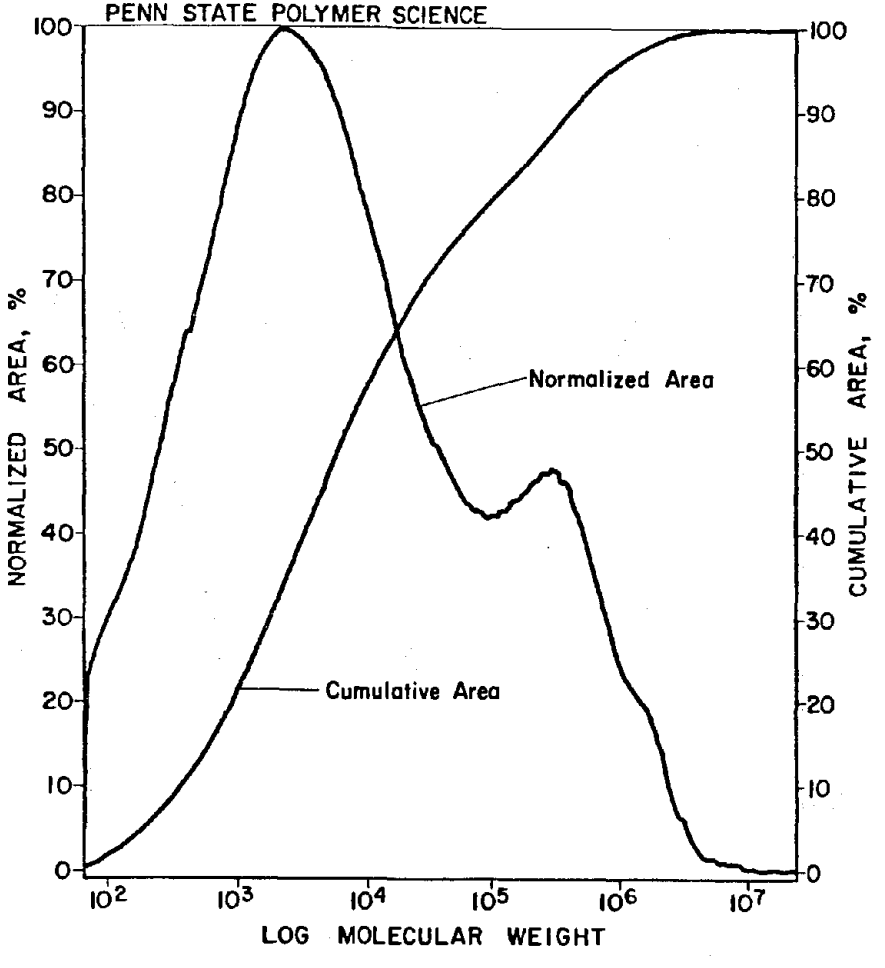

Figure 114. GPC distribution curves for asphalt number 2.

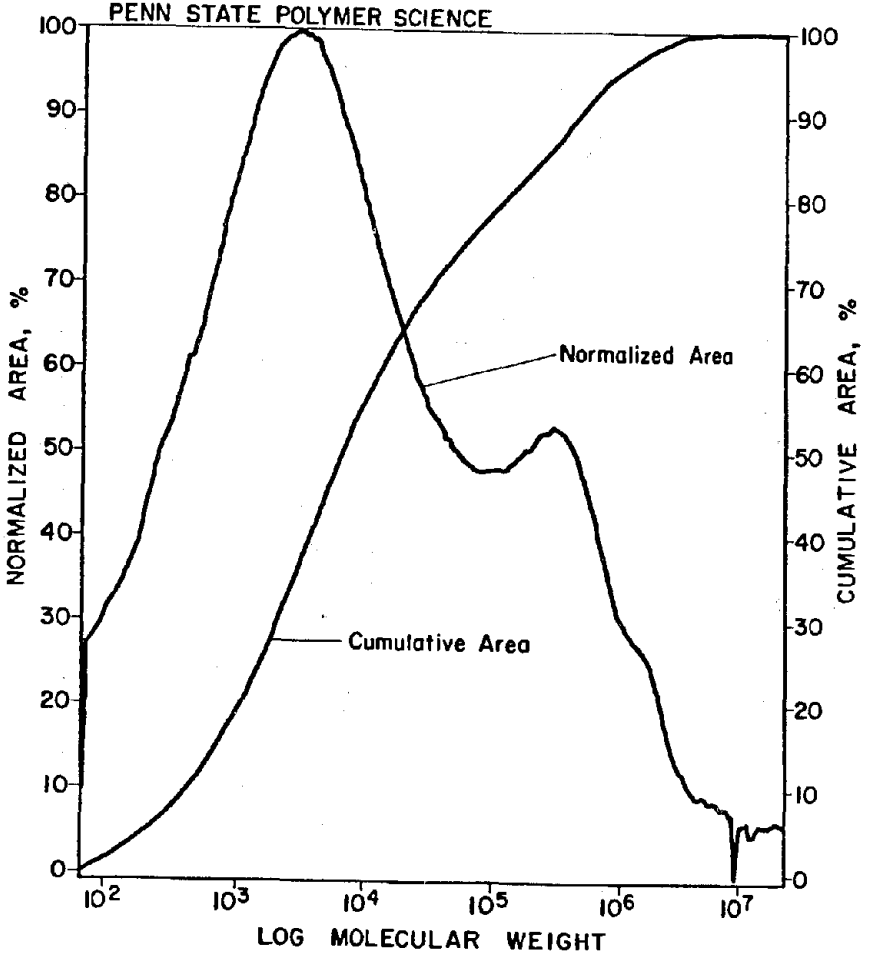

Figure 115. GPC distribution curves for asphalt number 3.

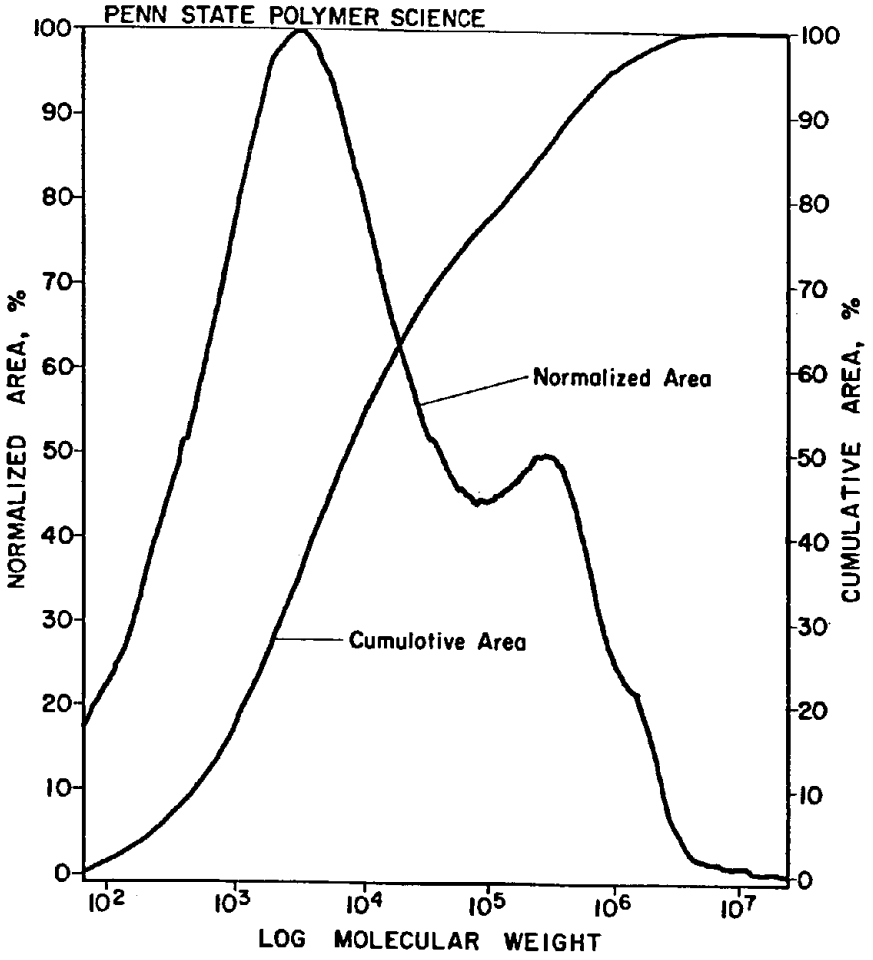

Figure 116. GPC distribution curves for asphalt number 4.

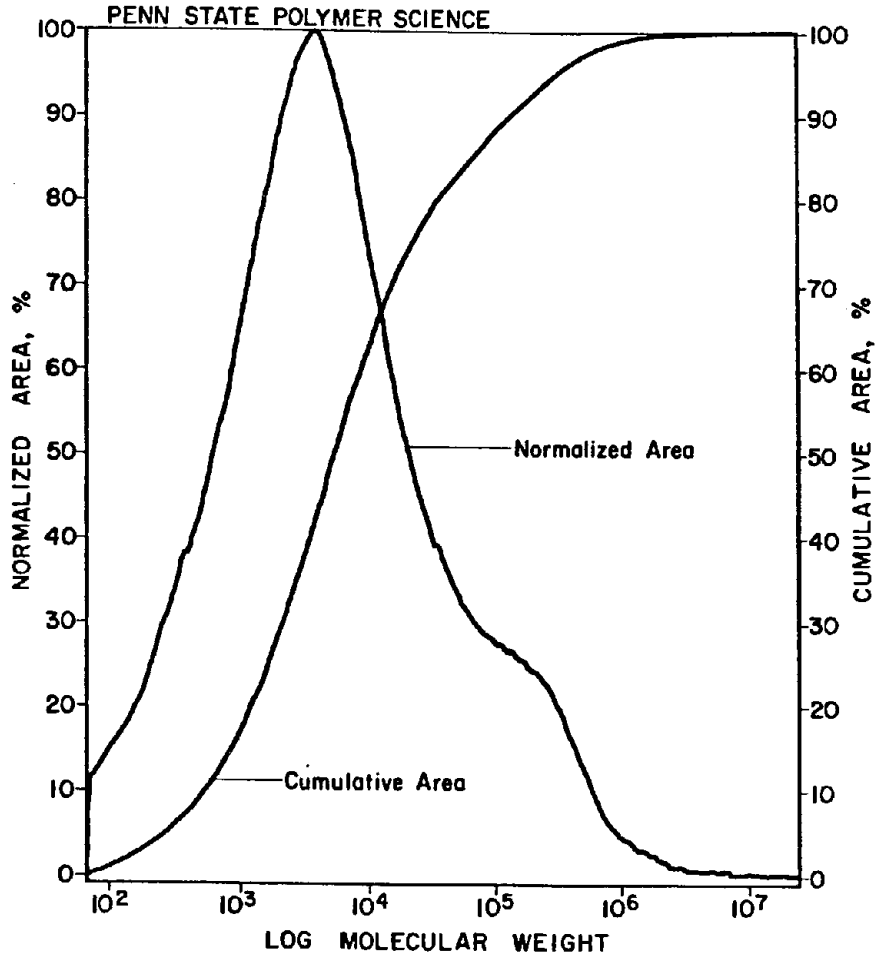

Figure 117. GPC distribution curves for asphalt number 5.

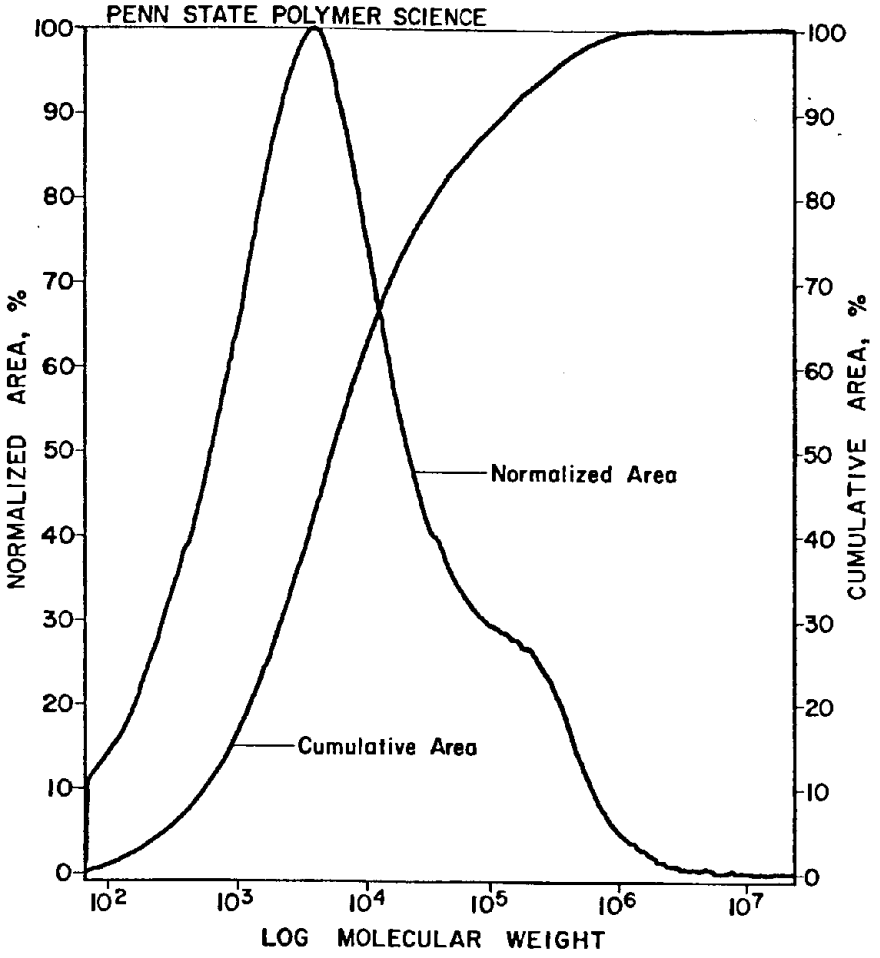

Figure 118. GPC distribution curves for asphalt number 6.

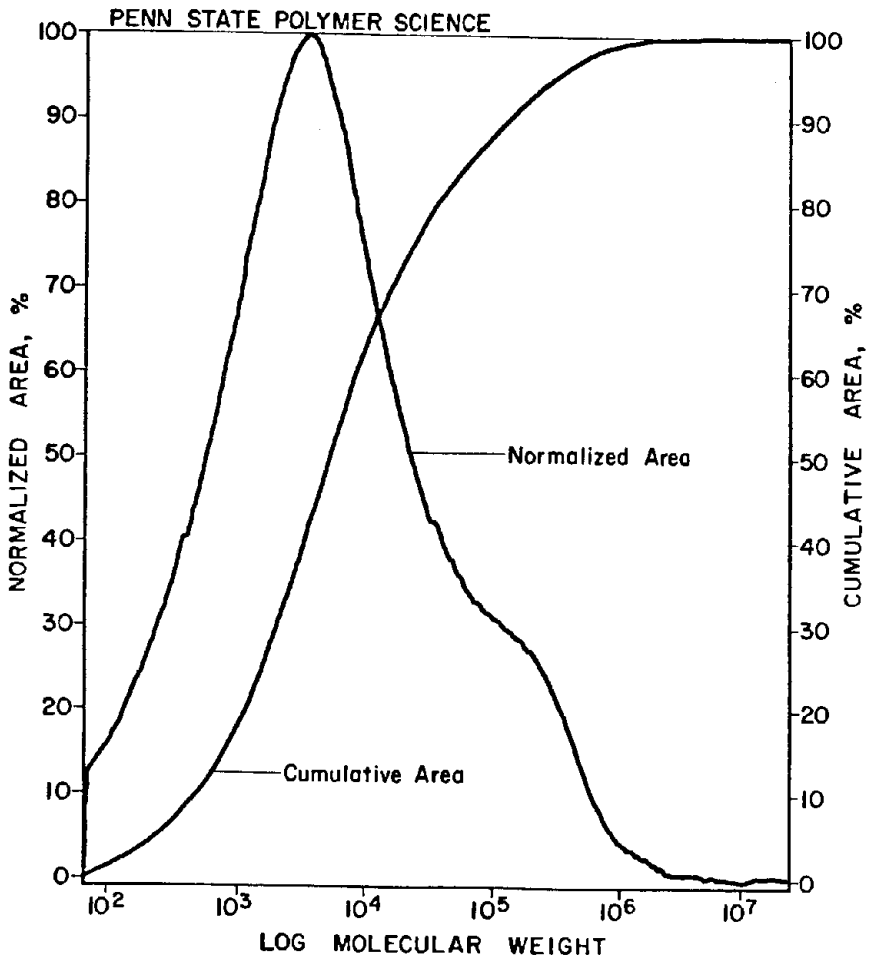

Figure 119. GPC distribution curves for asphalt number 7.

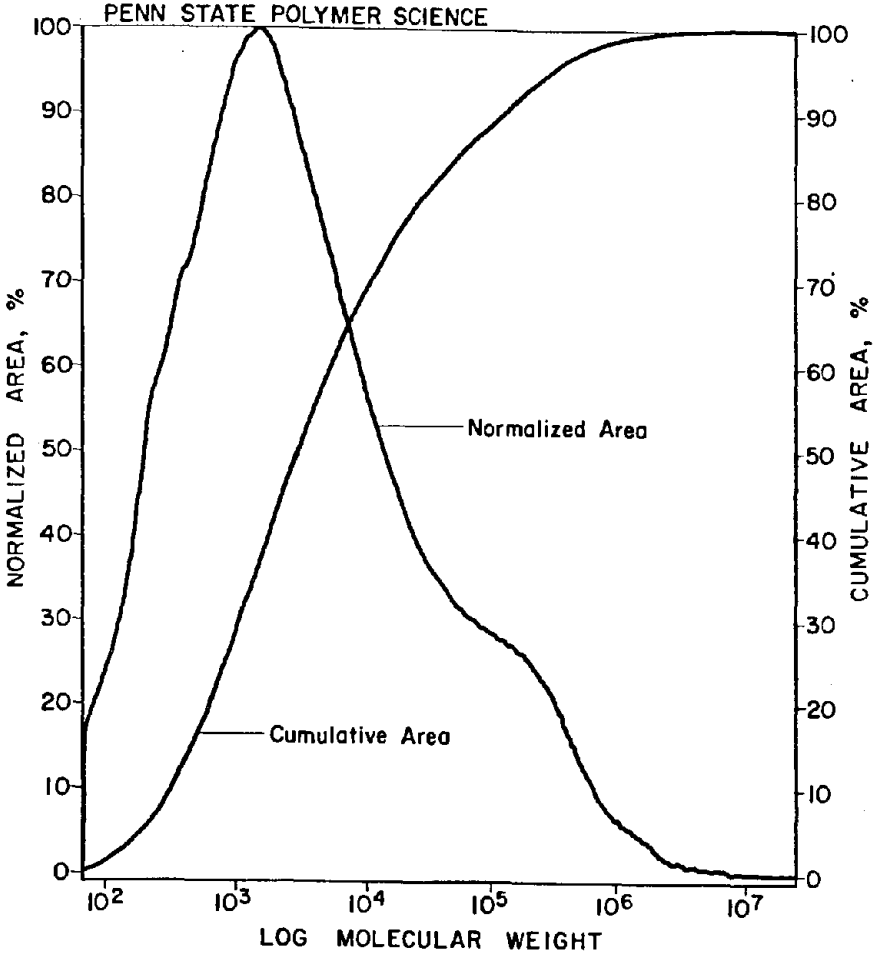

Figure 120. GPC distribution curves for asphalt number 8.

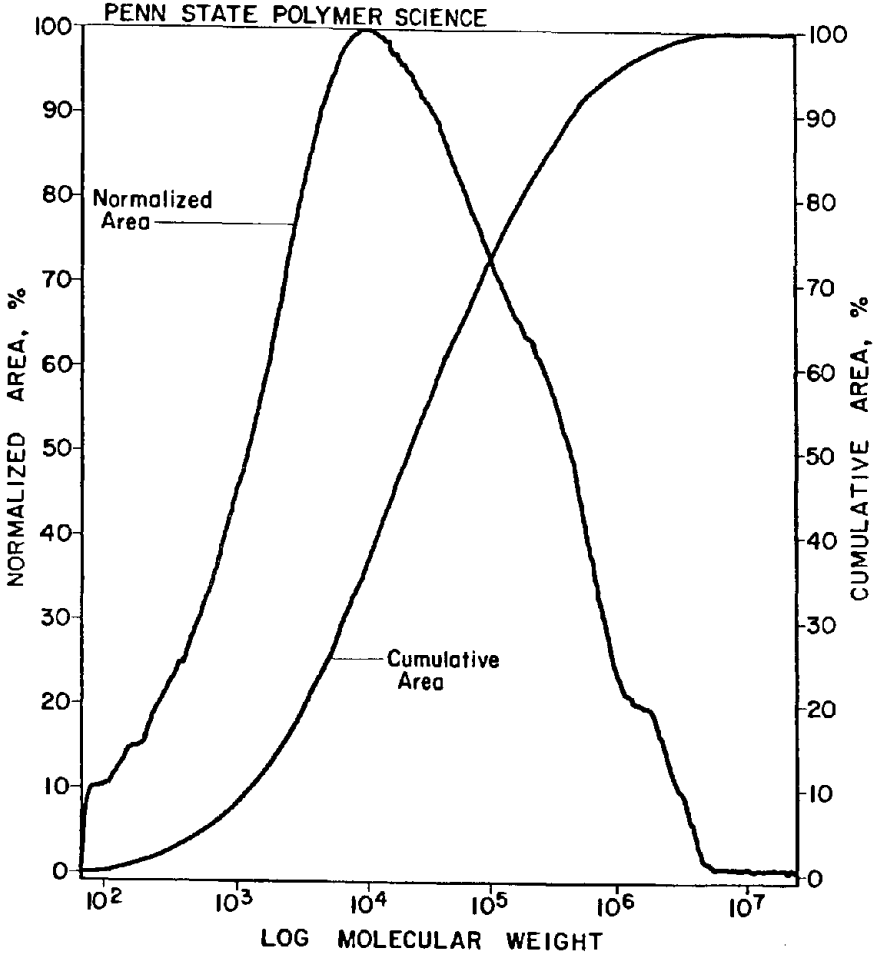

Figure 121. GPC distribution curves for asphalt number 9.

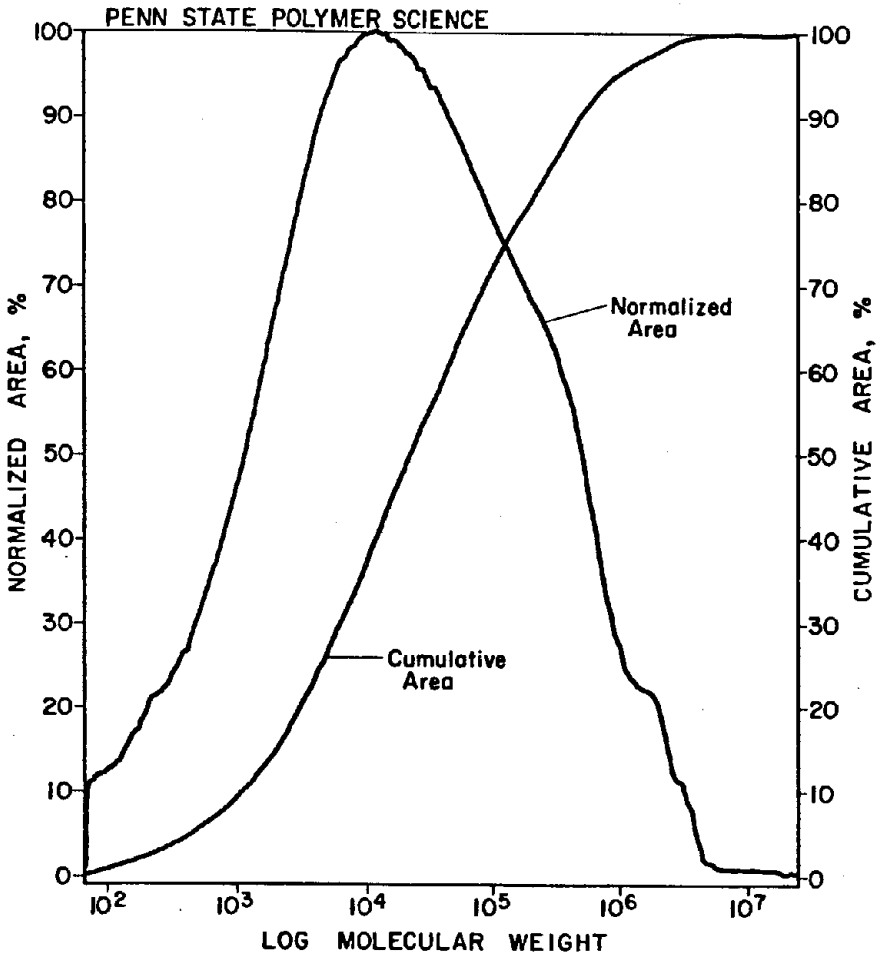

Figure 122. GPC distribution curves for asphalt number 10.

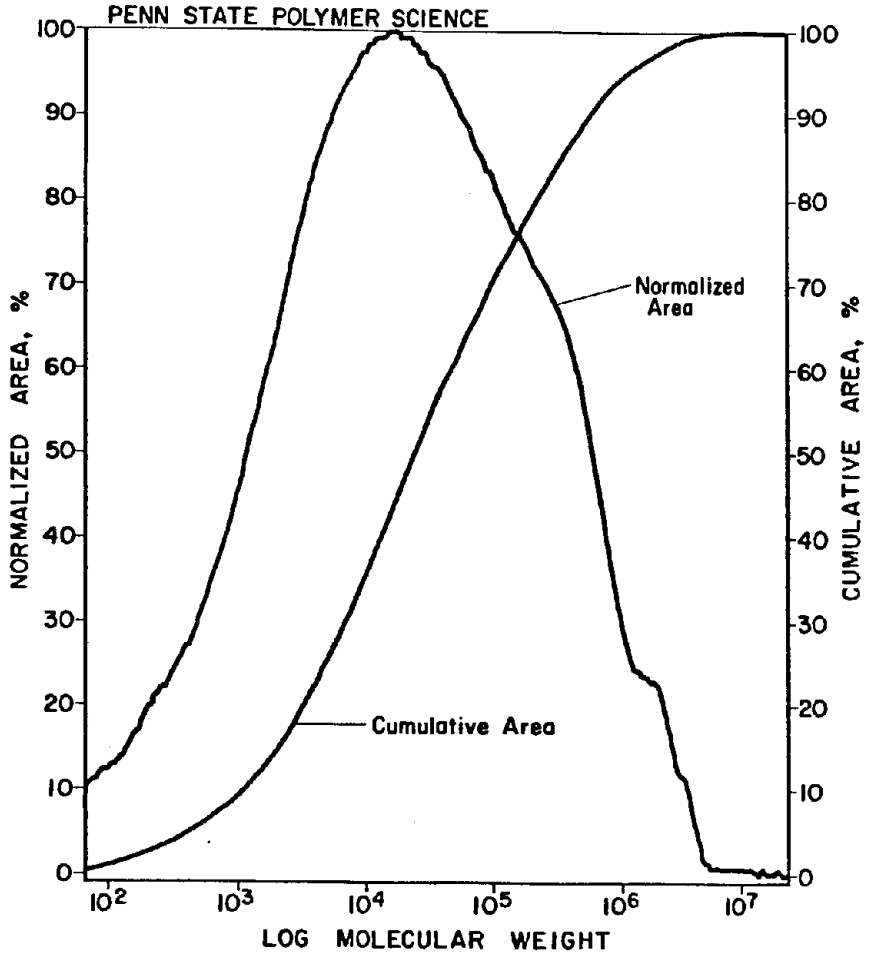

Figure 123. GPC distribution curves for asphalt number 11.

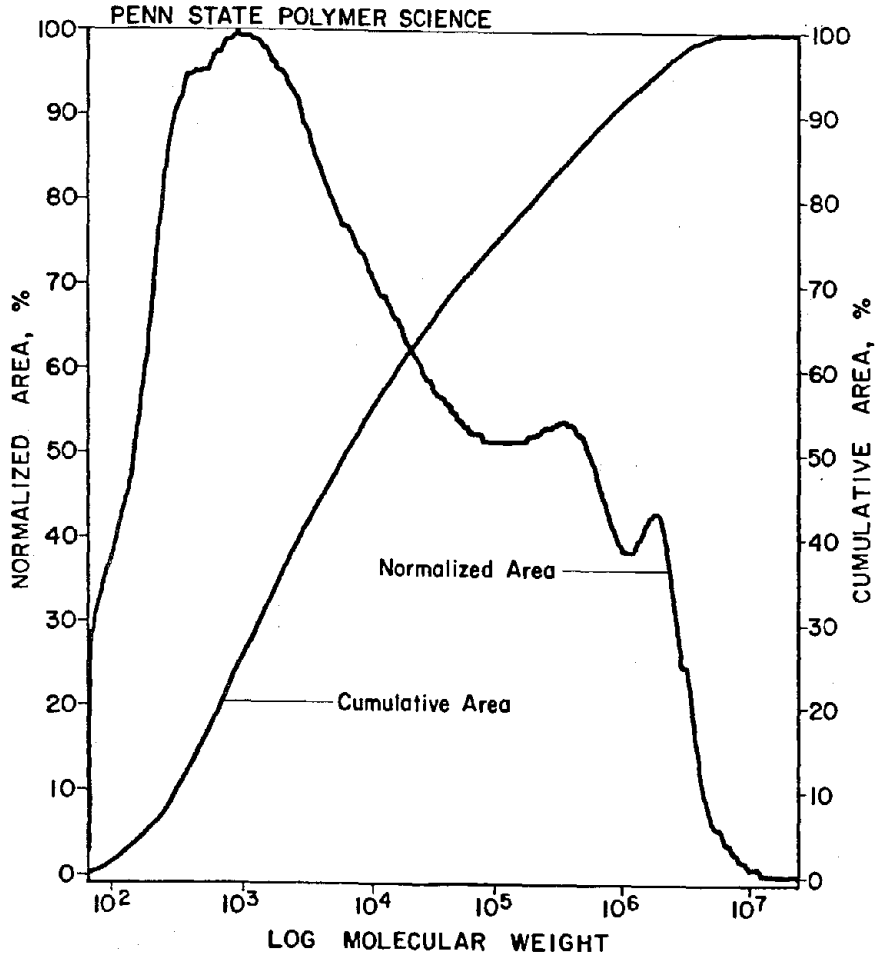

Figure 124. GPC distribution curves for asphalt number 12.

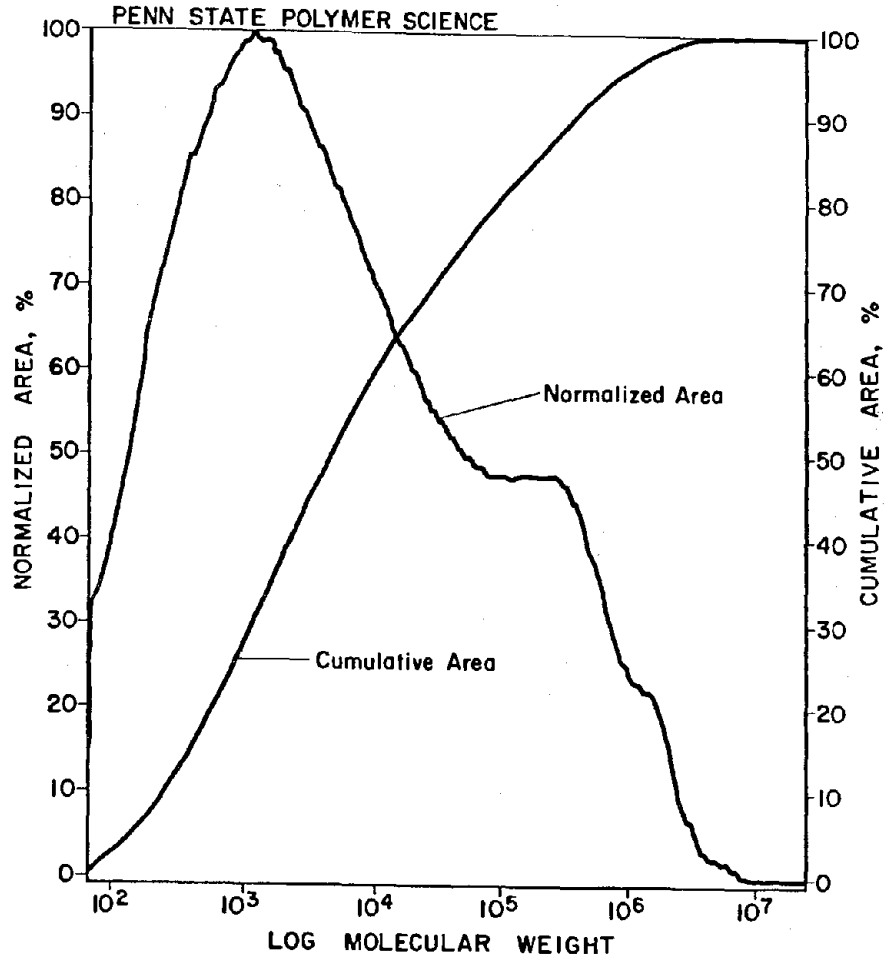

Figure 125. GPC distribution curves for asphalt number 13.

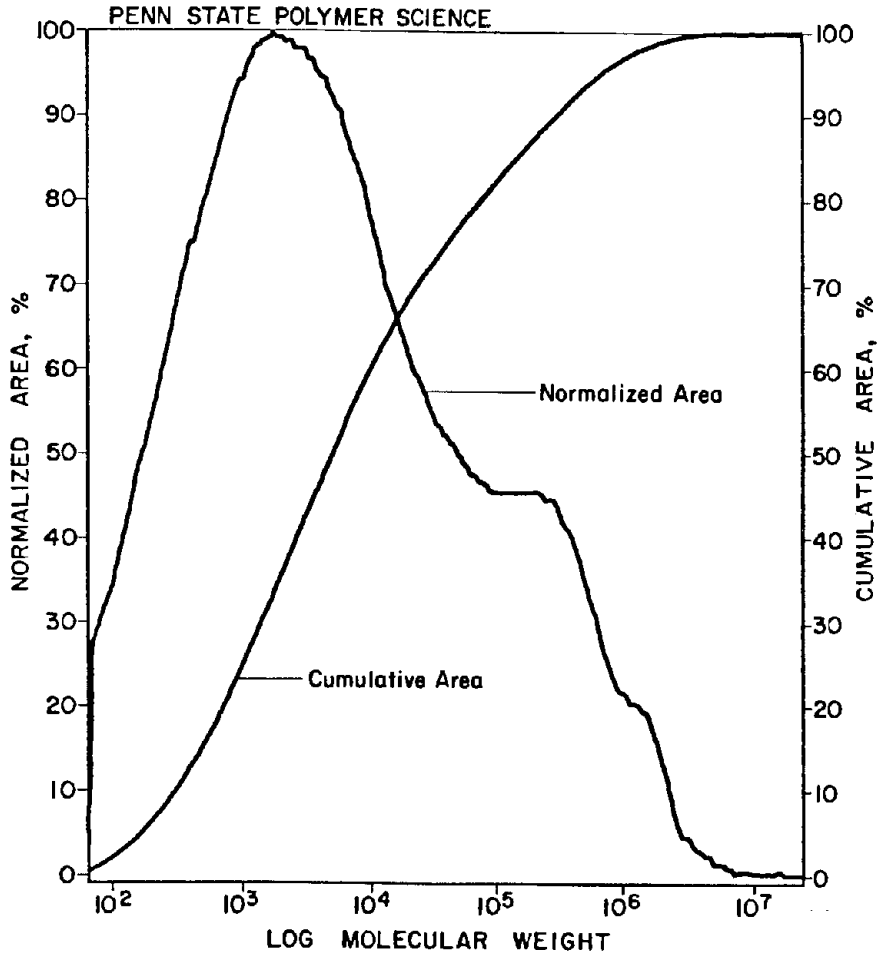

Figure 126. GPC distribution curves for asphalt number 14.

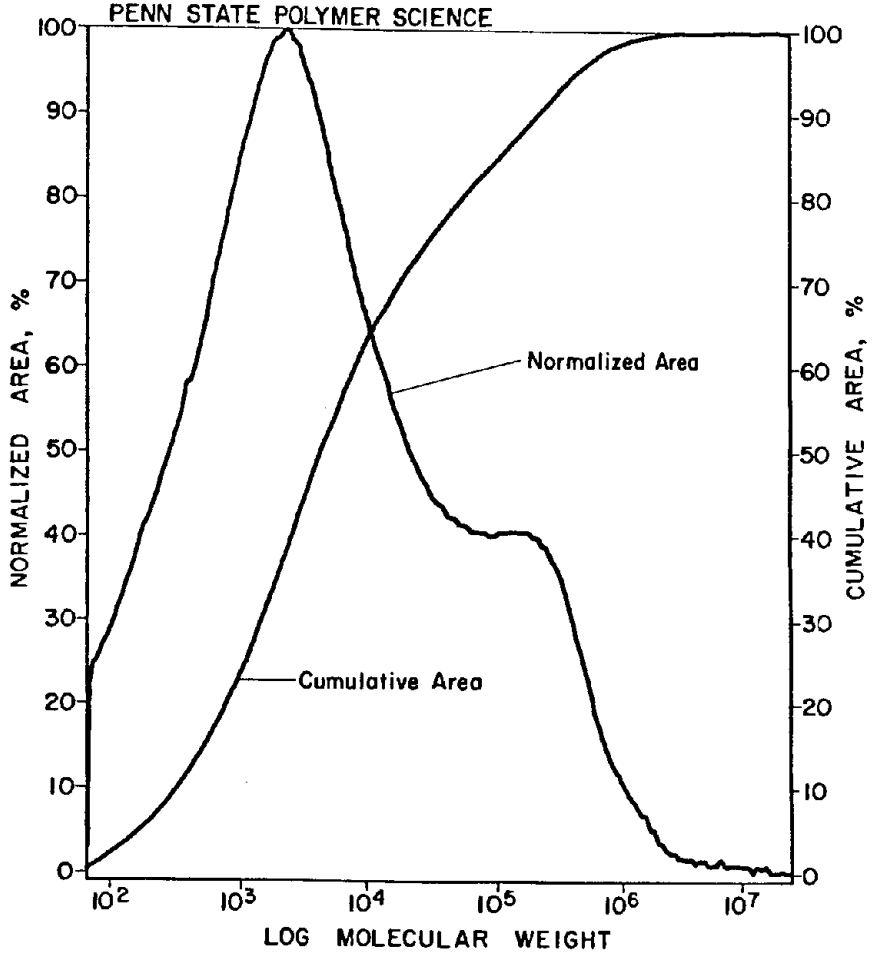

Figure 127. GPC distribution curves for asphalt number 15.

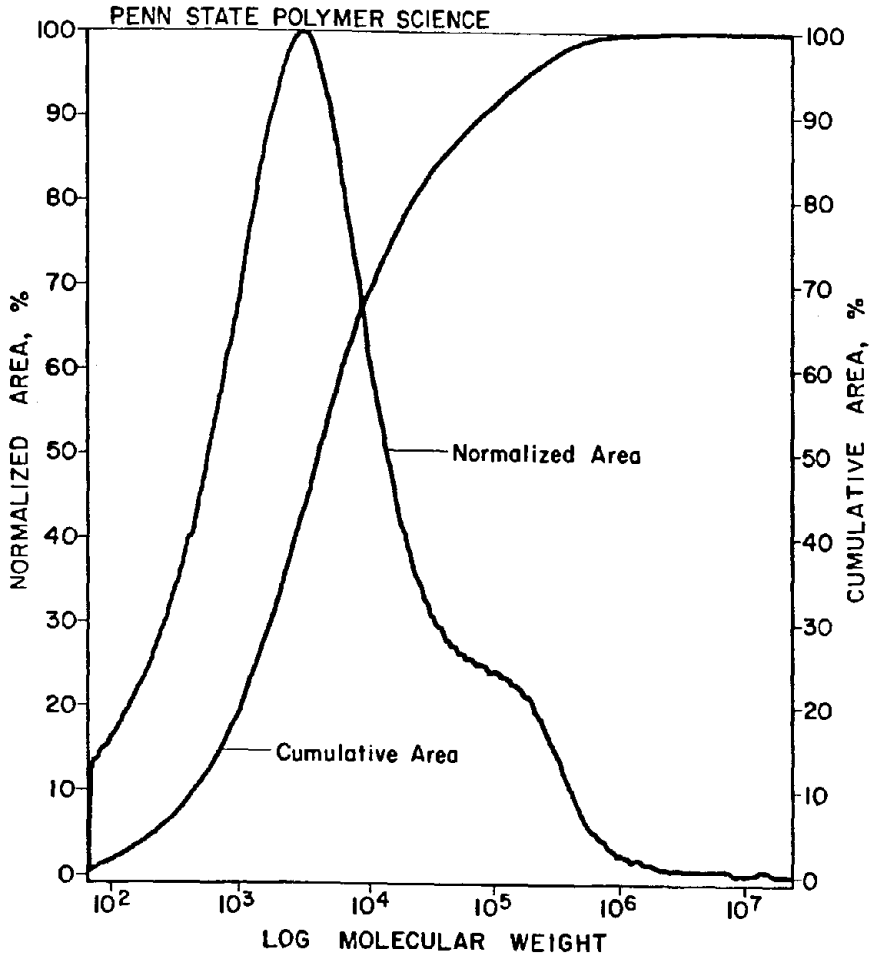

Figure 128. GPC distribution curves for asphalt number 16.

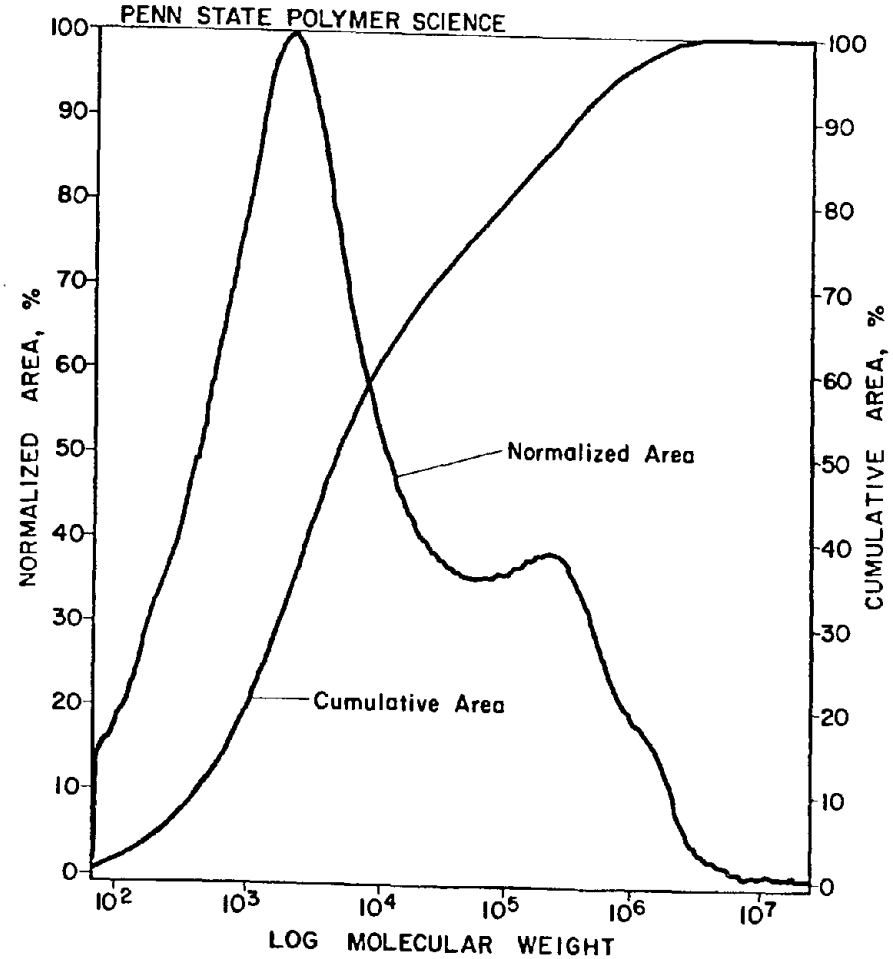

Figure 129. GPC distribution curves for asphalt number 17.

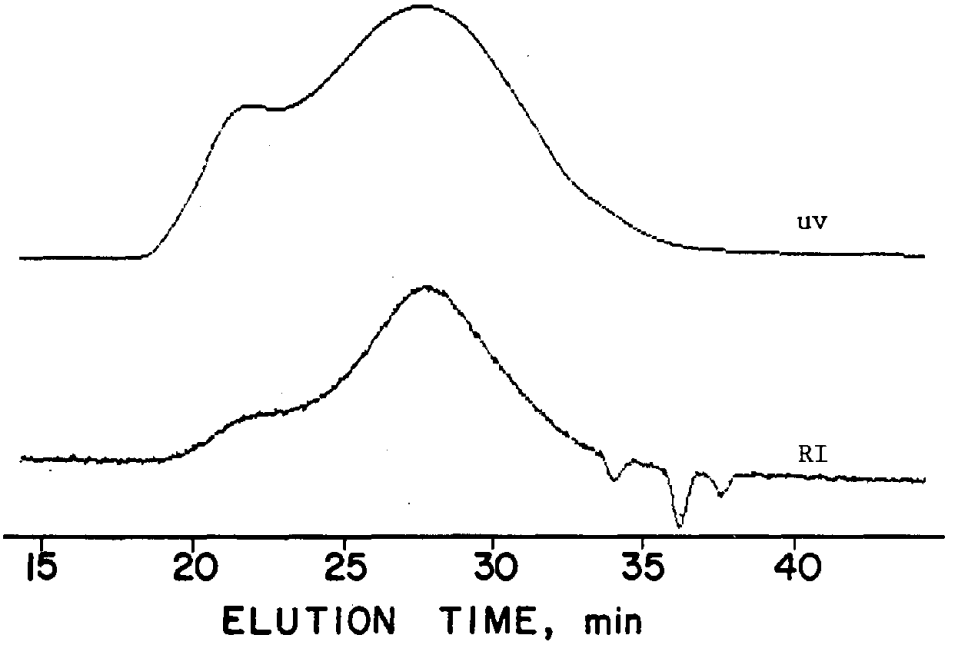

Figure 130. GPC chromatograms for asphalt No. 1m.

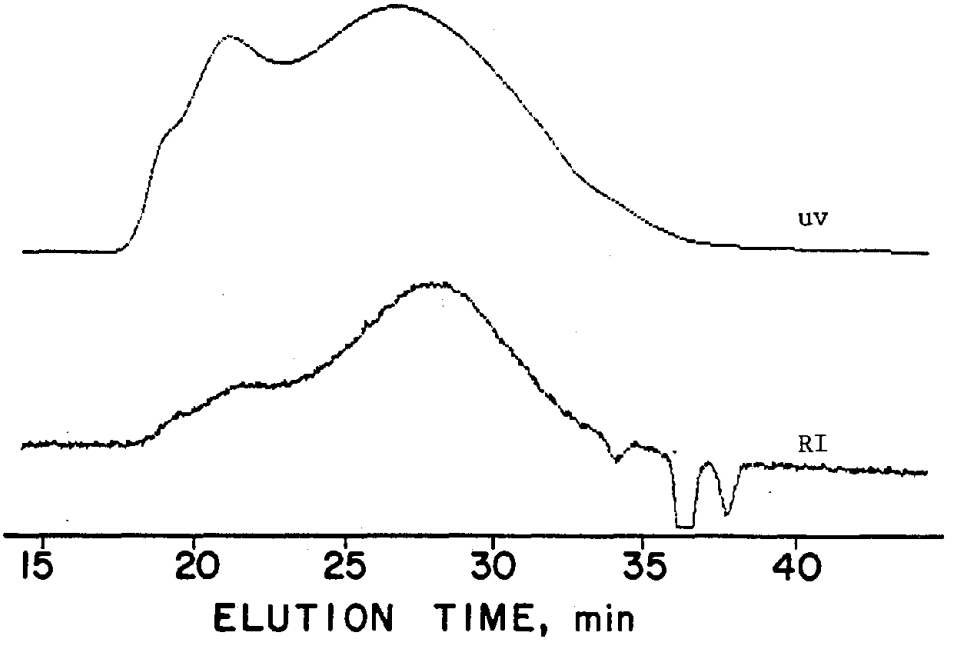

Figure 131. GPC chromatograms for asphalt No. 2m.

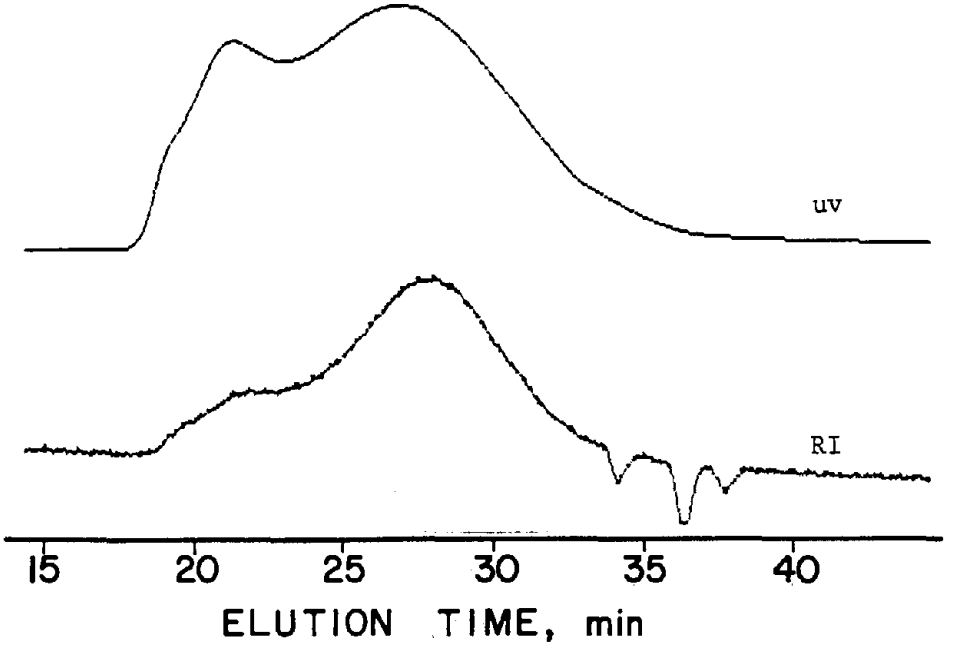

Figure 132. GPC chromatograms for asphalt No. 3m.

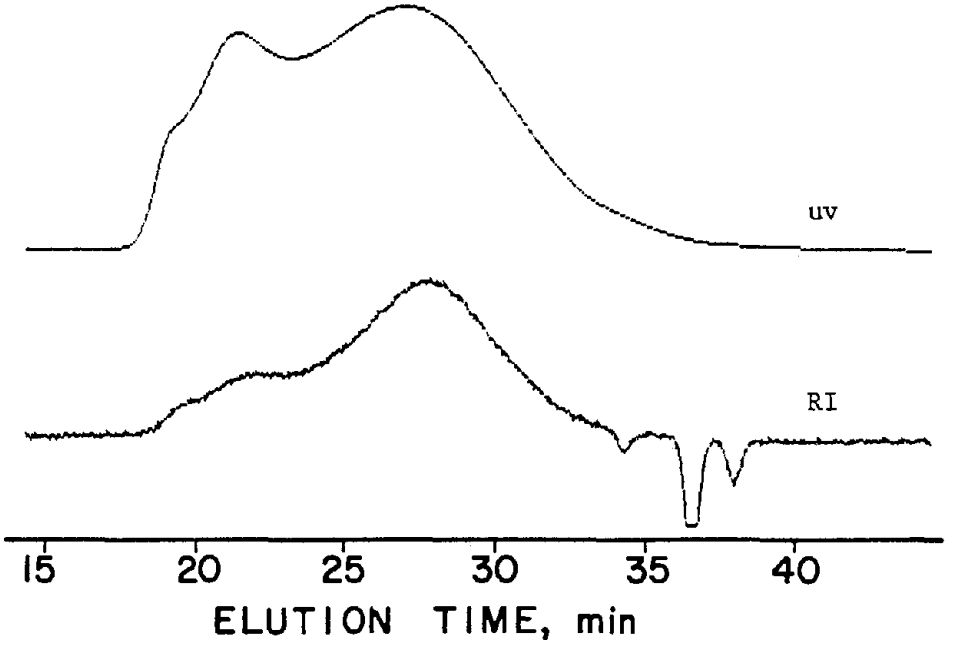

Figure 133. GPC chromatograms for asphalt No. 4m.

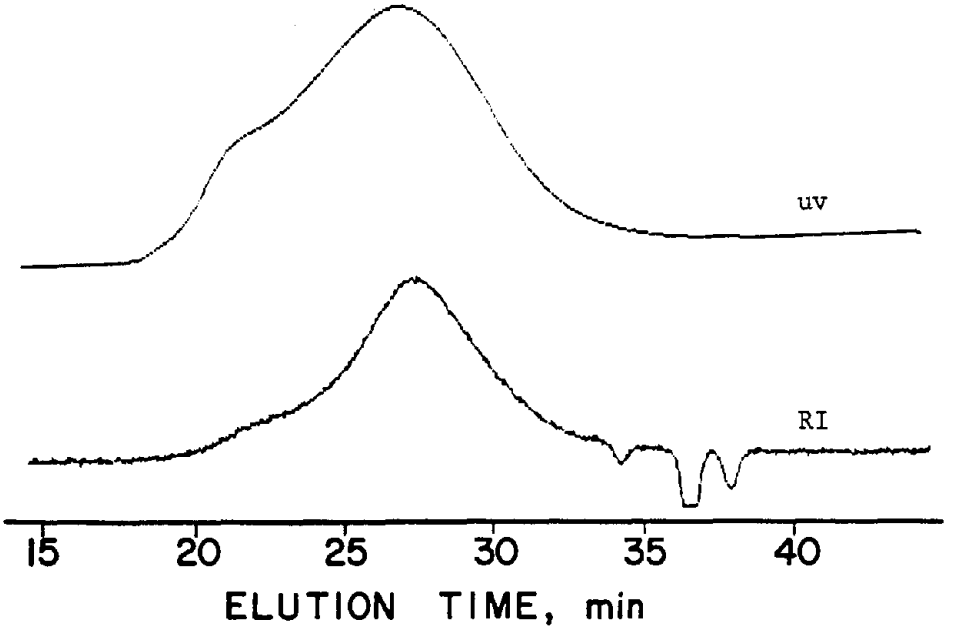

Figure 134. GPC chromatograms for asphalt No. 5m.

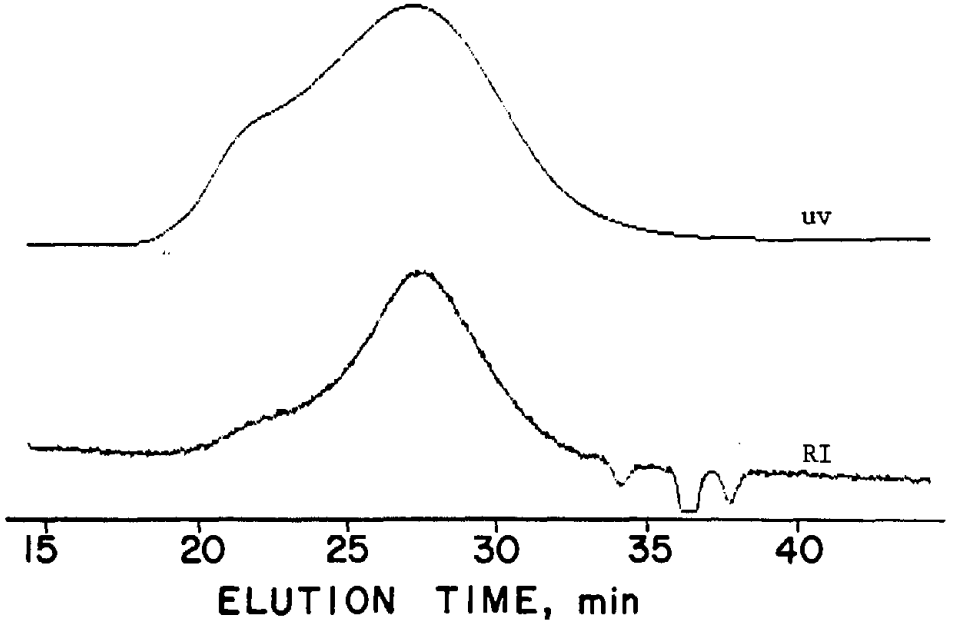

Figure 135. GPC chromatograms for asphalt No. 6m.

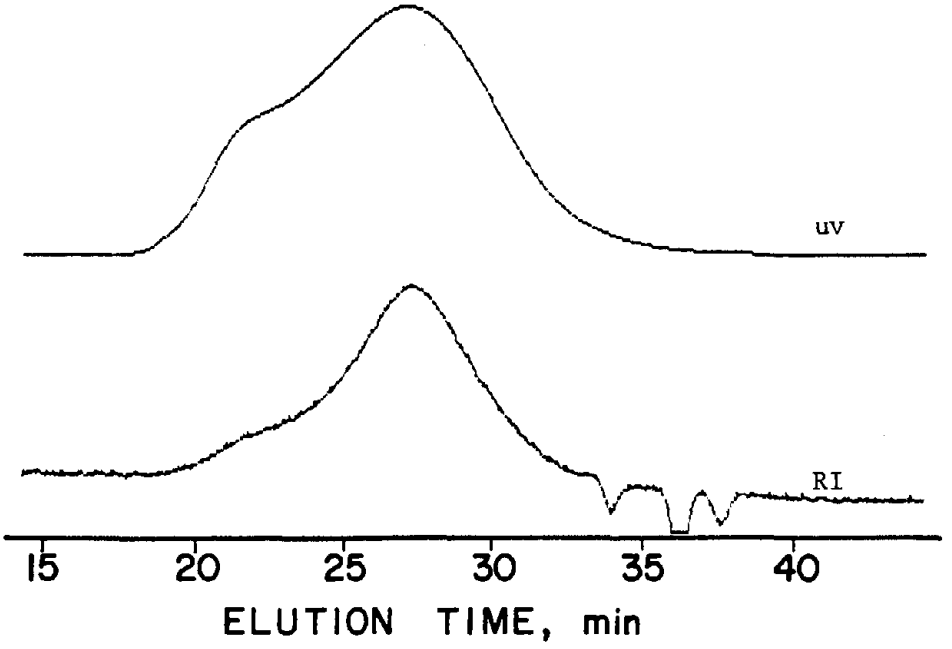

Figure 136. GPC chromatograms for asphalt No. 7m.

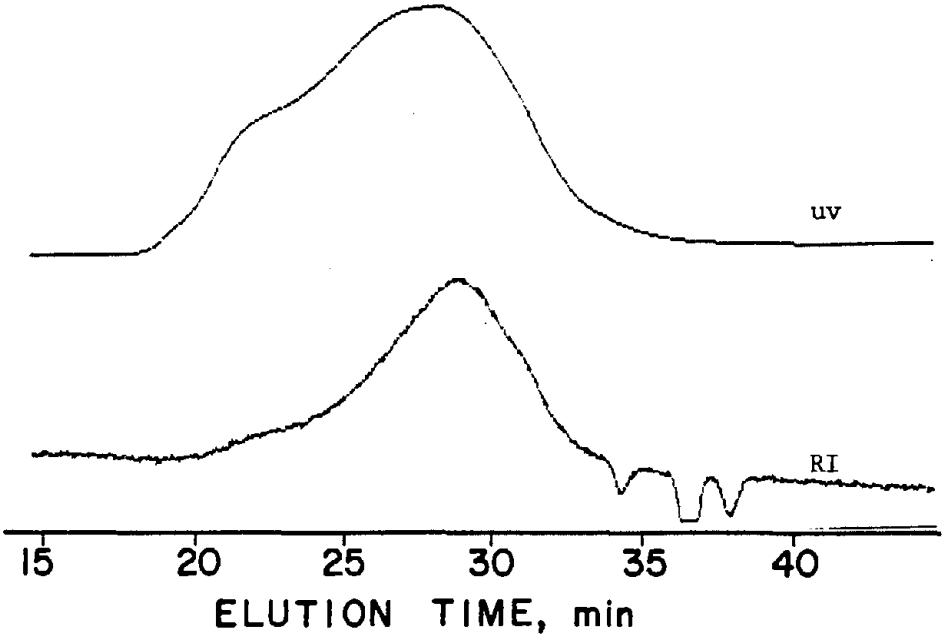

Figure 137. GPC chromatograms for asphalt No. 8m.

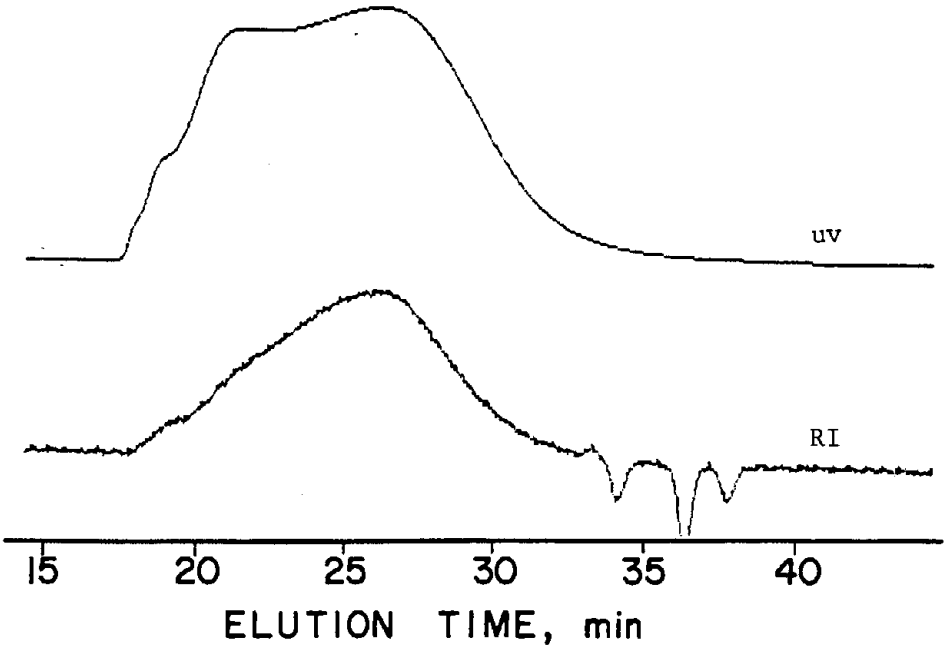

Figure 138. GPC chromatograms for asphalt No. 9m.

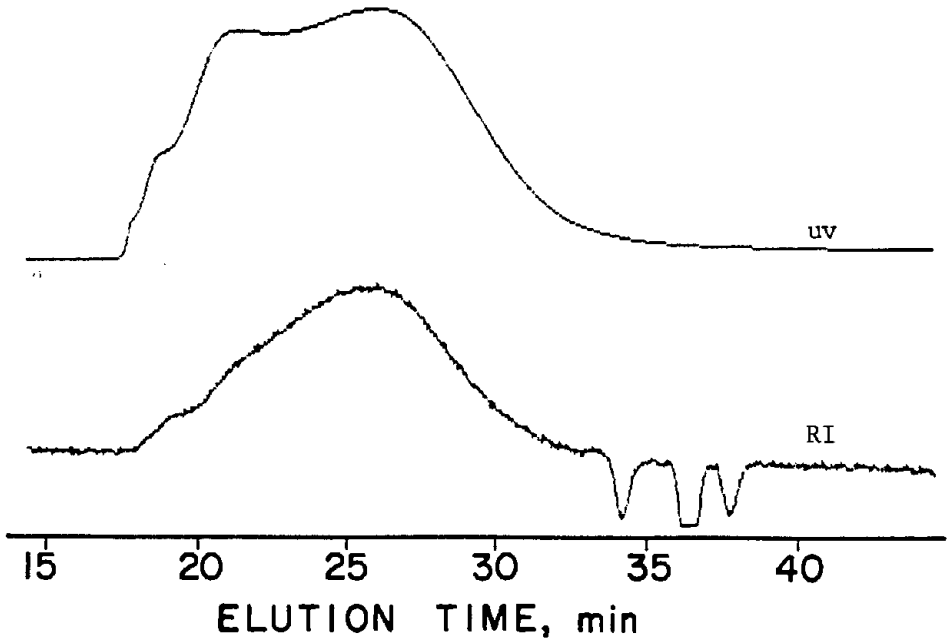

Figure 139. GPC chromatograms for asphalt No. 10m.

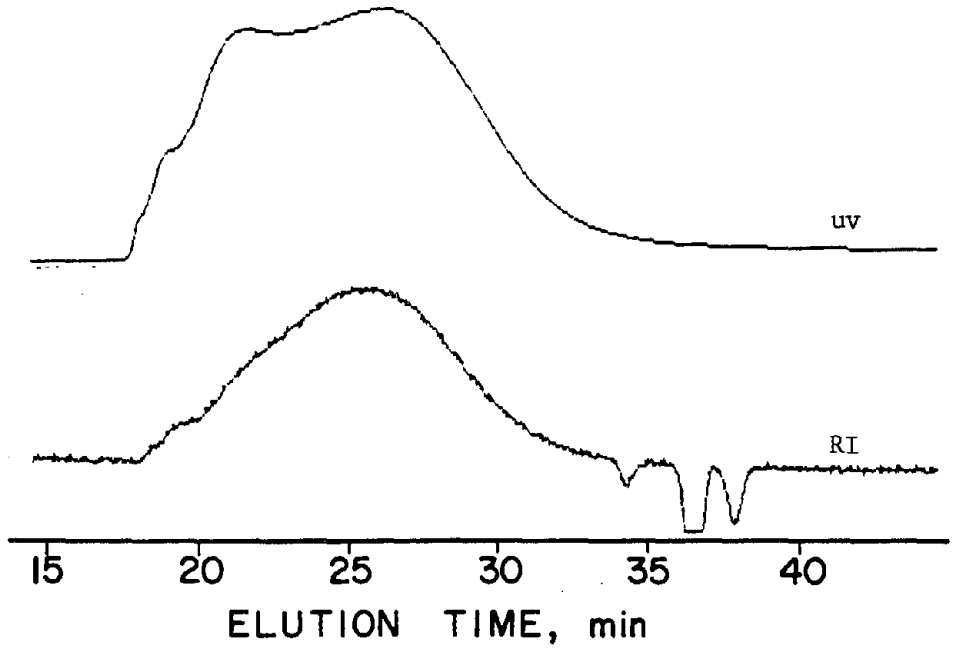

Figure 140. GPC chromatograms for asphalt No. 11m.

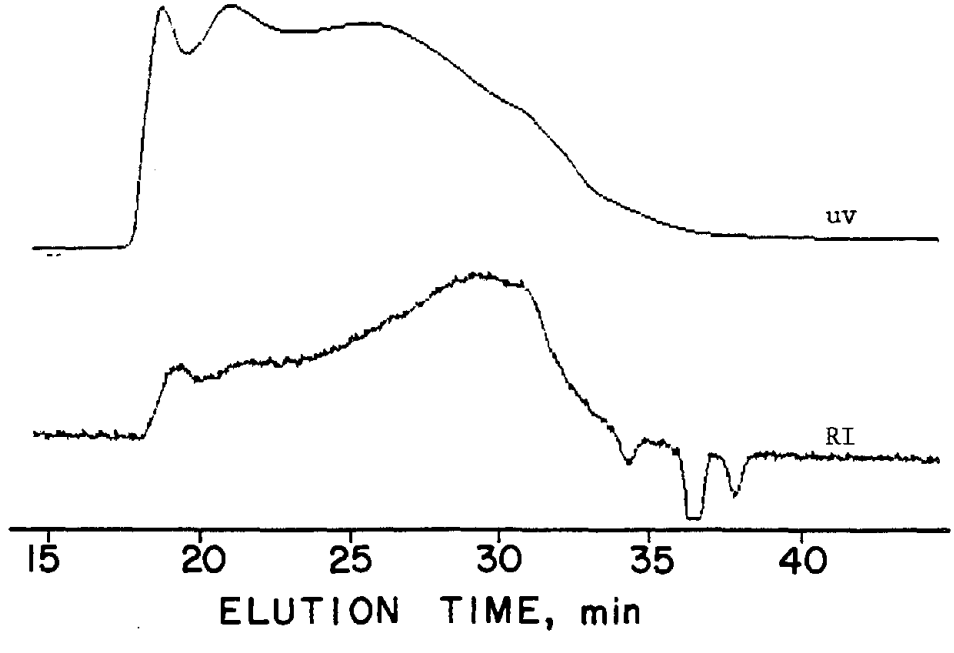

Figure 141. GPC chromatograms for asphalt No. 12m.

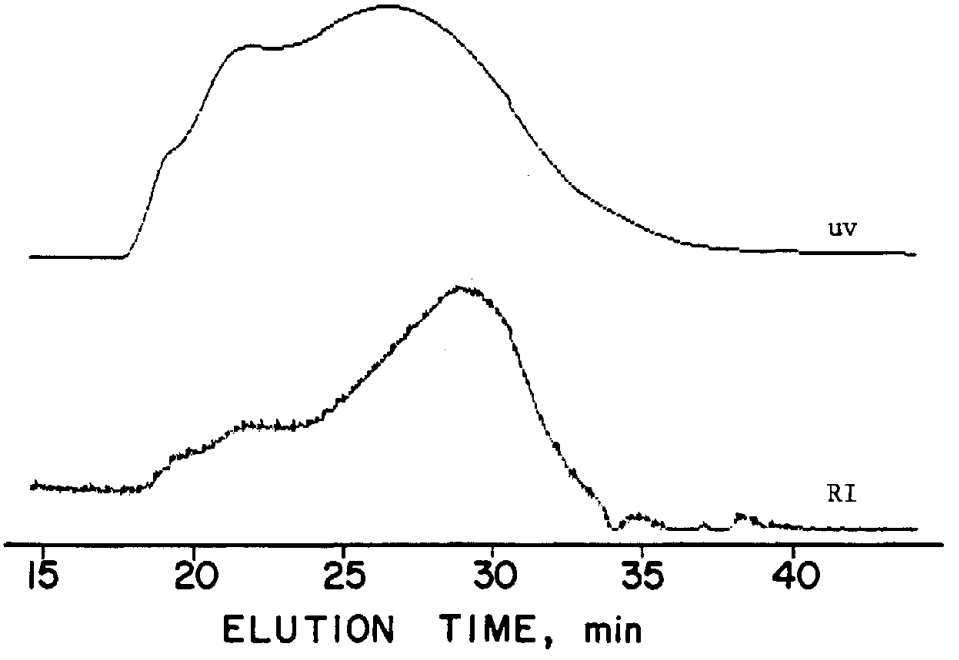

Figure 142. GPC chromatograms for asphalt No. 13m.

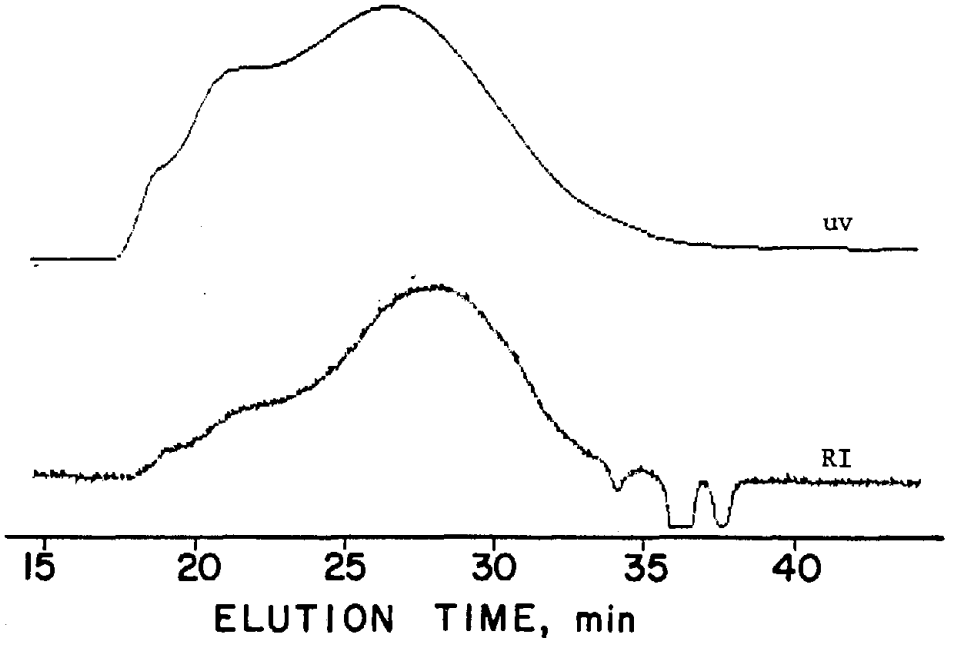

Figure 143. GPC chromatograms for asphalt No. 14m.

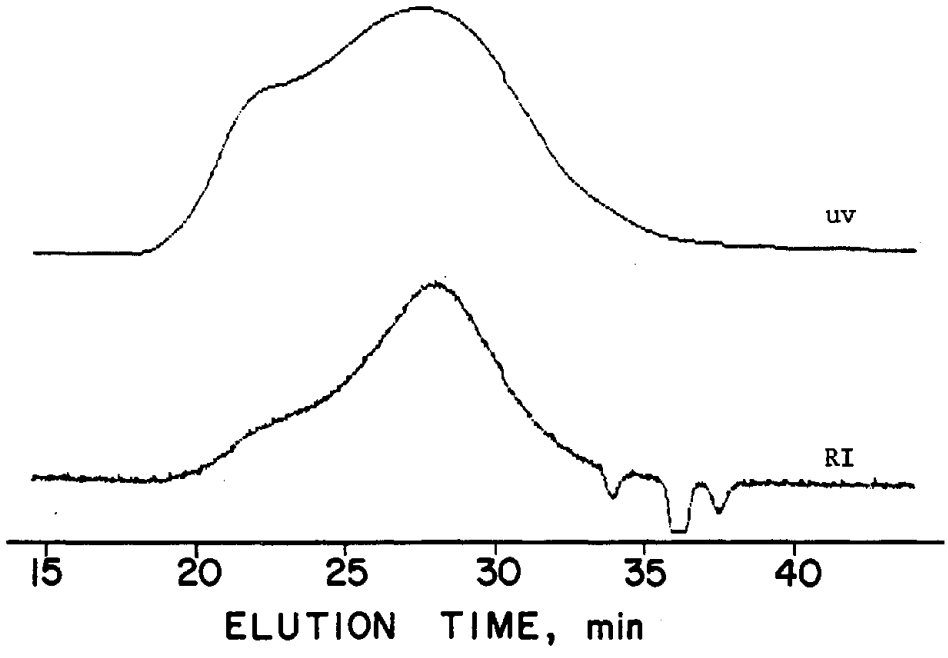

Figure 144. GPC chromatograms for asphalt No. 15m.

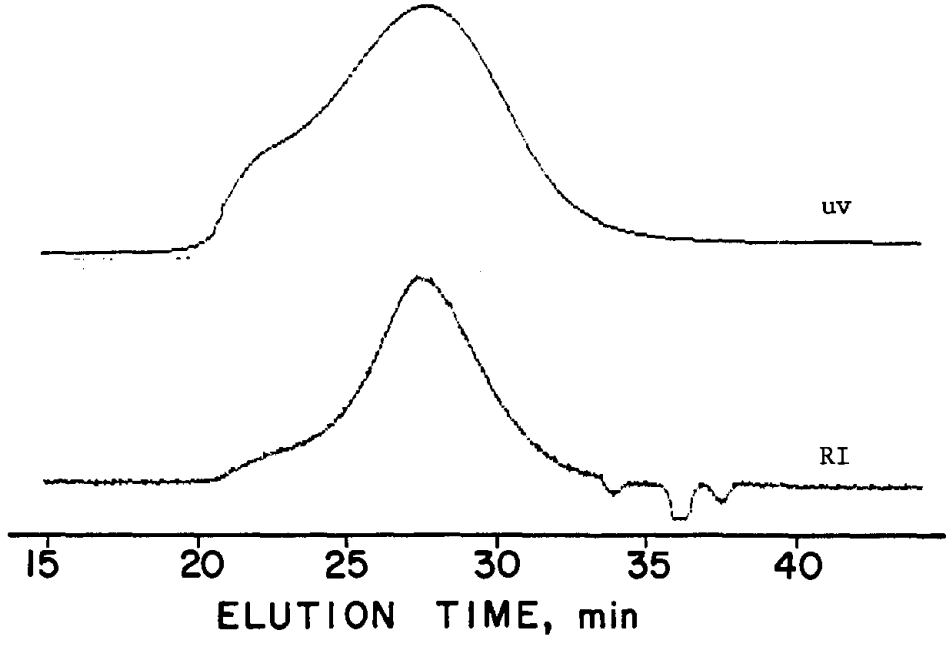

Figure 145. GPC chromatograms for asphalt No. 16m.

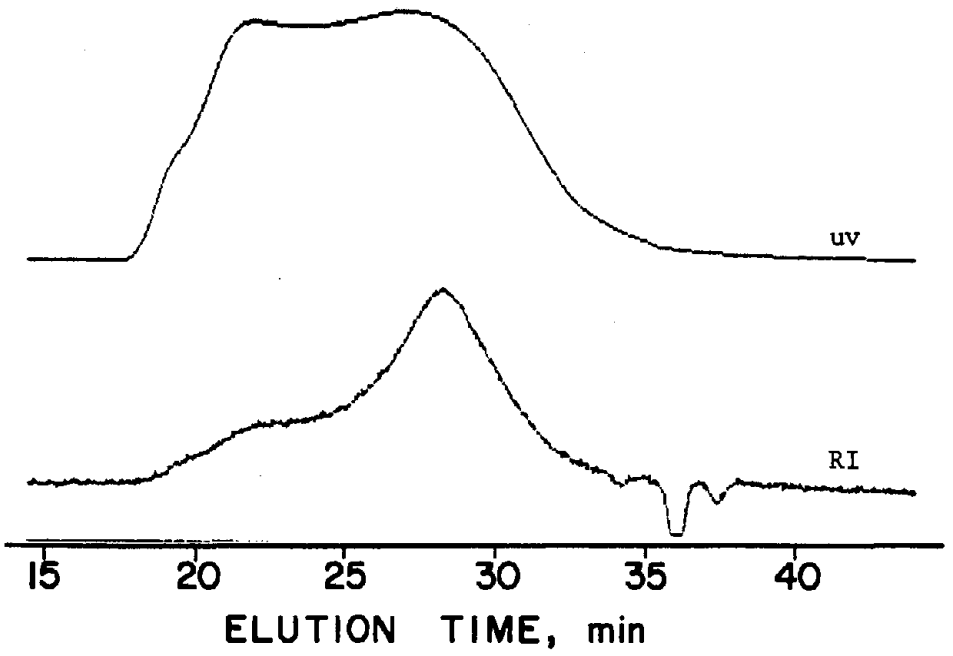

Figure 146. GPC chromatograms for asphalt No. 17m.

APPENDIX E

TEST DATA AND CALCULATED PARAMETERS

This appendix contains data that were obtained in the laboratory during the performance of the contract. In addition, a number of computed variables or parameters are presented here. The data are arranged in 62 continuous columns. Where appropriate, the columns are annotated with a description of the data and the equation used to calculate the numerical entries in the column is given.

(1)	(2)	(3)*	(4)	(5)	(6)	(7)	(8)
			Penetration, 0.1 mm, 100 g, 5 s				
Asphalt No.	Source	Grade[1]	77 °F, Unaged, 0.1 mm	77 °F, RTFOT, 0.1 mm	41 °F, RTFOT, 0.1 mm	59 °F, RTFOT, 0.1 mm	95 °F, RTFOT, 0.1 mm
1	A	1	90	50		17	152
2	B	0	189	96	12	29	
3	B	1	121	66		22	180
4	B	2	71	41		15	114
5	C	0	144	76	8	23	
6	C	1	98	51		17	163
7	C	2	60	34		11	92
8	D	2	52	36		11	110
9	E	0	182	117	12	34	
10	E	1	108	72		23	213
11	E	2	68	45		16	142
12	F	1	134	67		28	162
13	G	0	241	125	17	44	
14	G	1	155	77	9	26	
15	H	2	86	49		18	121
16	I	1	98	56		15	171
17	I	1	87	55		24	137

[1]Code for viscosity grade, or nearest viscosity grade for AR graded and penetration graded asphalts.

Note: Columns marked with an asterisk (*) contain test data or parameters that were included in the statistical analysis.

(1)	(9)	(10)	(11)	(12)	(13)	(14)
Asphalt No.	Viscosity at 140 °F, P, Unaged	Viscosity at 140 °F, P, RTFOT	Viscosity at 275 °F, cSt, Unaged	Viscosity at 275 °F, cSt, RTFOT	Softening Point Temp. °F, Unaged	Softening Point Temp. °F, RTFOT
1	1130	3170	268	393	114	124
2	650	1640	239	377	102	115
3	1370	3520	333	524	111	125
4	3100	8150	480	797	121	132
5	540	1320	204	292	108	116
6	1020	2220	264	374	114	121
7	1790	5170	336	545	120	130
8	2230	4430	267	383	119	127
9	560	917	348	452	104	112
10	1100	1940	479	623	112	120
11	1900	4400	637	894	120	128
12	1320	4350	318	589	107	124
13	610	1310	202	322	95	108
14	860	2500	267	427	104	119
15	1670	4850	331	530	114	127
16	770	1740	210	274	116	124
17	750	2350	205	294	119	127

Note: Columns marked with an asterisk (*) contain test data or variables that were included in the statistical analysis.

(1)	(15)*	(16)	(17)	(18)	(19)	(20)	(21)
Asphalt No.	Fraass Brittle Point Temp, °F, RTFOT	Mass Loss, RTFOT[2]	77 °F Pen (100 g, 5 s) Aging Index, Aged/Unaged	140 °F Vis Aging Index, Aged/Unaged	275 °F Vis Aging Index, Aged/Unaged	A_F RTFOT	A RTFOT
1	13	0.007	0.556	2.81	1.47	0.0264	0.0475
2	4	-0.745	0.508	2.52	1.58	0.0251	0.0452
3	0	-0.668	0.545	2.57	1.57	0.0254	0.0457
4	7	-0.541	0.577	2.62	1.66	0.0245	0.0441
5	0	-0.185	0.528	2.44	1.43	0.0276	0.0497
6	7	-0.086	0.520	2.18	1.42	0.0273	0.0491
7	22	-0.170	0.567	2.89	1.62	0.0256	0.0461
8	24	-0.271	0.692	1.99	1.43	0.0278	0.0500
9	-6	0.129	0.642	1.64	1.30	0.0275	0.0495
10	1	0.129	0.667	1.76	1.30	0.0269	0.0484
11	5	0.143	0.662	2.32	1.40	0.0263	0.0473
12	8	-1.502	0.500	3.30	1.85	0.0212	0.0382
13	-6	-1.280	0.519	2.15	1.59	0.0241	0.0434
14	0	-0.757	0.497	2.91	1.60	0.0259	0.0466
15	6	0.157	0.570	2.90	1.60	0.0230	0.0414
16	10	0.328	0.571	2.25	1.30	0.0294	0.0529
17	3	0.143	0.632	3.14	1.43	0.0210	0.0378

[2]A positive sign indicates mass gain during RTFOT.

Note: Columns marked with an asterisk (*) contain test data or variables that were included in the the statistical analyses.

(20) A_F, absolute value of slope of plot of log-penetration versus temperature, °F

(21) A, absolute value of slope of plot on Shell BTDC, penetration branch, °C

(1)	(22)	(23)
Asphalt No.	A' RTFOT	C.I., Class Index RTFOT
1	0.0455	1.1
2	0.0430	0.4
3	0.0430	2.5
4	0.0421	1.2
5	0.0448	1.7
6	0.0444	0.9
7	0.0441	0.0
8	0.0471	0.9
9	0.0383	4.1
10	0.0385	3.8
11	0.0386	3.5
12	0.0426	-2.5
13	0.0437	-1.2
14	0.0435	1.7
15	0.0441	-1.7
16	0.0468	3.9
17	0.0474	-3.8

(22) A', absolute value of slope of plot on Shell BTDC, viscosity branch, °C

$$A' = \left[\frac{46.07(\eta''_{275} - \eta''_{140})}{72.27 + 8.5\,(\eta''_{275} + \eta''_{140}) + \eta''_{275}\,\eta''_{140}}\right]\,[1/75]$$

where

η''_{275} = log [viscosity at 275 °F (135 °C)/13,000], viscosity in poises

η''_{140} = log [viscosity at 140 °F (60 °C)/13,000], viscosity in poises

(23) Class index, C.I.:

$$C.I. = \left[(-12.5 - \Delta T)^2 + (12.5\,A/A')^2\right]^{1/2} - 17.68$$

where

$\Delta T = T_{R\&B} - T_{Pen800}$, °C

A = absolute value of slope of plot on Shell BTDC, penetration branch, °C

A' = absolute value of slope of plot on Shell BTDC, viscosity branch, °C

(1)	(24)	(25)*	(26)*
Asphalt No.	PI Unaged	PI RTFOT	$PI_{log\text{-}pen}$ RTFOT
1	-0.93	-0.93	-1.12
2	-0.79	-0.57	-0.79
3	-0.54	-0.10	-0.86
4	-0.48	-0.36	-0.63
5	-0.51	-1.07	-1.39
6	-0.68	-1.29	-1.32
7	-1.06	-0.99	-0.93
8	-1.53	-1.24	-1.43
9	-0.46	-0.47	-1.36
10	-0.73	-0.59	-1.22
11	-0.74	-0.64	-1.10
12	-0.99	-0.20	0.32
13	-1.68	-1.02	-0.53
14	-1.11	-0.56	-0.99
15	-1.06	-0.58	-0.22
16	-0.34	-0.66	-1.76
17	-0.21	-0.30	0.38

Note: Columns marked with an asterisk (*) contain test data or variables that were used in the statistical analysis.

(24),(25) PI, penetration index calculated using penetration at 77 °F (25 °C) and ring and ball softening point temperature:

$$PI = [30/(1+90B)] - 10$$

where

$$B = [2.9031 - \log (Pen_{77})]/[T_{R\&B} - 77]$$

Pen_{77} = penetration, 0.1 mm, 77 °F (25 °C), 100 g, 5 s

$T_{R\&B}$ = ring and ball softening point temperature, °F

(26) $PI_{log\text{-}pen}$, penetration index calculated using log-penetration versus temperature data:

$$PI_{log\text{-}pen} = [20 - 500A]/[1 + 50A]$$

where

A = absolute value of slope of plot on Shell BTDC, penetration branch, °C.

(1)	(27)*	(28)	(29)*
Asphalt No.	PI_{Fraass} RTFOT	PVN_{140} Unaged	PVN_{140} RTFOT
1	-0.88	-0.80	-0.64
2	-1.06	-0.16	-0.30
3	-0.14	-0.10	-0.12
4	0.11	-0.13	-0.03
5	-0.35	-0.86	-0.90
6	-0.30	-0.78	-0.96
7	-1.08	-0.94	-0.72
8	-1.44	-0.93	-0.79
9	-0.51	-0.40	-0.61
10	-0.31	-0.54	-0.59
11	0.15	-0.69	-0.48
12	-0.84	0.04	0.12
13	-0.61	0.24	-0.10
14	-0.34	-0.19	-0.22
15	-0.11	-0.46	-0.26
16	-0.75	-1.08	-1.07
17	-0.08	-1.29	-0.80

Note: Columns marked with an asterisk (*) contain test data or variables that were included in the statistical analysis.

(27) PI_{Fraass}, penetration index calculated using penetration at 77 °F (25 °C) and Fraass brittle point temperature:

$$PI_{Fraass} = [30/(1 + 90C)] - 10$$

where

$$C = [\log (Pen_{77}) - 0.07918]/[77 - T_{Fraass}]$$

Pen_{77} = penetration, 01 mm, 77 °F (25 °C), 100 g, 5 s

T_{Fraass} = Fraass brittle point temperature, °F

(28),(29) PVN_{140}, penetration-viscosity number, calculated using penetration at 77 °F (25 °C) and viscosity at 140 °F (60 °C)

$$PVN_{140} = \left[\frac{6.489 - 1.590 \log(Pen_{77}) - \log(\eta_{140})}{1.050 - 0.2234 \log (Pen_{77})}\right] (-1.5)$$

where

Pen_{77} = penetration, 0.1 mm, 77 °F (25 °C), 100 g, 5 s

η_{140} = coefficient of viscosity at 140 °F (60 °C), P

(1)	(30)	(31)*	(32)	(33)*
Asphalt No.	PVN_{275} Unaged	PVN_{275} RTFOT	VTS Unaged	VTS RTFOT
1	-0.95	-0.97	-3.61	-3.70
2	-0.27	-0.36	-3.47	-3.47
3	-0.28	-0.29	-3.50	-3.51
4	-0.34	-0.22	-3.53	-3.50
5	-0.87	-0.99	-3.53	-3.60
6	-0.88	-1.02	-3.58	-3.60
7	-1.02	-0.89	-3.60	-3.62
8	-1.46	-1.29	-3.89	-3.85
9	0.34	0.16	-3.08	-3.08
10	0.15	0.05	-3.11	-3.14
11	0.02	0.03	-3.11	-3.19
12	-0.23	-0.11	-3.53	-3.50
13	-0.23	-0.29	-3.60	-3.51
14	-0.33	-0.42	-3.49	-3.54
15	-0.68	-0.58	-3.59	-3.62
16	-1.23	-1.36	-3.66	-3.77
17	-1.38	-1.28	-3.67	-3.83

Note: Columns marked with an asterisk (*) contain test data or variables that were used in the statistical analysis.

(30),(31) PVN_{275}, penetration-viscosity number calculated using penetration at 77 °F (25 °C) and viscosity at 275 °F (135 °C):

$$PVN_{275} = \left[\frac{4.258 - 0.7967 \log(Pen_{77}) - \log(\eta_{275})}{0.7951 - 0.1858 \log(Pen_{77})}\right] (-1.5)$$

where

Pen_{77} = penetration, 0.1 mm, 77 °F (25 °C), 100 g, 5 s

η_{275} = coefficient of viscosity at 275 °F (135 °C), cSt

(32),(33) VTS, viscosity temperature susceptibility:

$$VTS = [\log \log(\eta_{275}) - \log \log(\eta_{140})]/[\log 735 - \log 600]$$

where

η_{275} = coefficient of viscosity at 275 °F (135 °C), cSt

η_{140} = coefficient of viscosity at 140 °F (60 °C), cSt

(1)	(34)	(35)*	(36)*
	Viscosity Ratio 140 °F Vis / 275 °F Vis		
Asphalt No.	Unaged	RTFOT	$T_{Pen1.2}$, °F
1	422	807	16
2	272	435	2
3	411	672	9
4	646	1022	14
5	265	452	12
6	386	594	17
7	533	947	21
8	835	1157	24
9	161	203	5
10	230	312	11
11	298	492	17
12	415	739	-6
13	302	407	-7
14	322	585	7
15	505	915	8
16	367	635	21
17	366	799	-3

Note: Columns marked with an asterisk (*) contain test data or variables that were used in the statistical analysis.

(34),(35) R_η, viscosity ratio:

$$R_\eta = \eta_{140}/\eta_{275}$$

where

η_{140} = coefficient of viscosity at 140 °F (60 °C), P or cSt

η_{275} = coefficient of viscosity at 275 °F (135 °C), P or cSt; with η_{140} units consistent

(36) $T_{Pen1.2}$, estimated temperature, °F, where the penetration is equal to 1.2:

$$T_{Pen1.2} = [0.07918 - D_F]/A_F$$

where

D_F = intercept of plot of log-penetration versus temperature, °F

A_F = absolute value of slope of plot of log-penetration versus temperature, °F

(1)	(37)*	(38)
Asphalt No.	T_{vis4GP}, °F, RTFOT	T_{Pen800}, °F, RTFOT
1	30	122
2	17	115
3	26	120
4	35	130
5	18	114
6	24	121
7	34	131
8	38	126
9	-4	108
10	7	116
11	19	124
12	28	128
13	15	111
14	24	116
15	33	130
16	26	117
17	31	132

Note: Columns marked with an asterisk (*) contain test data or variables that were used in the statistical analysis.

(37) T_{vis4GP}, temperature, °F, at which coefficient of viscosity is 4 GP:

$$T_{vis4GP} = \exp_{10} \left[2.7782 - \frac{1.0645 - \log \log(\eta_{140})}{VTS}\right] - 460$$

where

η_{140} = coefficient of viscosity at 140 °F (60 °C), cSt

VTS = viscosity temperature susceptibility, slope of log-log viscosity versus log absolute temperature, viscosity expressed in poises and temperature expressed in °R

(38) T_{Pen800}, estimated temperature at which penetration equals 800, °F (°C):

$$T_{Pen800} = [2.903 - D_F]/A_F$$

where

D_F = intercept of plot of log-penetration versus temperature, °F

A_F = absolute value of slope of plot of log-penetration versus temperature, °F

(1)	(39)	(40)
Asphalt No.	$T_{Pen800F}$, °F	T_B, Base Temperature, °F
1	125	126
2	112	117
3	125	126
4	136	135
5	121	117
6	128	124
7	129	133
8	125	131
9	112	111
10	122	120
11	134	127
12	120	126
13	110	113
14	120	120
15	131	129
16	123	120
17	129	122

Note: Columns marked with an asterisk (*) contain test data or variables that were used in the statistical analysis.

(39) $T_{Pen800F}$, temperature, °F, at a penetration of 800, extrapolated from the plot of Fraass brittle point temperature and the pentration at 77 °F (25 °C):

$$T_{Pen800F} = [(2.9031 - \log (Pen_{77}))/C] + 77$$

where:

Pen_{77} = penetration, 0.1 mm, 77 °F (25 °C), 100 g, 5 s

$C = [\log(Pen_{77}) - 0.07918]/[Pen_{77} - T_{Fraass}]$

T_{Fraass} = Fraass brittle point temperature, °F

(40) T_B, base temperature, derived from penetration at 77 °F (25 °C) and PVN_{140}; determined using a nomograph and used in conjunction with McCleod's modification of Heukelom and Klomp's version of Van der Poel's nomograph[48]

(1)	(41)*	(42)*	(43)*
	Temperature at an estimated stiffness of 1.0 GPa, at 30 min, RTFOT, °F:		
Asphalt No.	$T_{R\&B}$ and $PI_{R\&B}$	T_{Pen800} and $PI_{log\text{-}pen}$	$T_{Pen800F}$ and PI_{Fraass}
1	-44	-36	-40
2	-58	-51	-49
3	-60	-45	-60
4	-47	-44	-54
5	-44	-36	-60
6	-35	-33	-53
7	-33	-35	-31
8	-27	-27	-27
9	-63	-45	-63
10	-53	-42	-58
11	-44	-35	-56
12	-60	-67	-47
13	-56	-63	-63
14	-54	-45	-60
15	-45	-54	-54
16	-47	-24	-47
17	-54	-63	-56

Note: Columns marked with an asterisk (*) contain test data and variables that were used in the statistical analysis.

(41)-(43) T_{1GPa}, temperature, °F (°C), at which estimated stiffness is 1.0 GPa at a loading time of 30 min; found using Van der Poel's nomograph and three different sets of nomograph entrance parameters:[21,37]

(41) $T_{R\&B}$ and PI

(42) T_{Pen800} and $PI_{log\text{-}pen}$

(43) $T_{Pen800F}$ and PI_{Fraass}

(1)	(44)*	(45)*	(46)*	(47)*	(48)*
	Temperature at an estimated stiffness of 200 MPa, at 2 h, RTFOT Residue, °F:				
Asphalt No.	$T_{R\&B}$, $PI_{R\&B}$	T_{Pen800}, $PI_{log\text{-}pen}$	$T_{Pen800F}$, PI_{Fraass}	T_B, PVN_{140}	T_H, °F RTFOT
1	-24	-20	-22	-26	-29
2	-38	-35	-29	-42	-42
3	-36	-26	-36	-36	-35
4	-26	-24	-33	-29	-26
5	-27	-22	-38	-29	-31
6	-20	-18	-29	-22	-24
7	-15	-15	-13	-18	-22
8	-13	-11	-17	-18	-15
9	-44	-29	-47	-40	-36
10	-33	-24	-36	-33	-31
11	-26	-18	-33	-27	-24
12	-38	-42	-27	-40	-47
13	-36	-44	-44	-49	-49
14	-33	-27	-38	-40	-36
15	-26	-31	-31	-33	-35
16	-27	-13	-27	-22	-18
17	-31	-38	-33	-26	-45

Note: Columns marked with an asterisk (*) contain test data or variables that were used in the statistical analysis.

(44)-(46) Temperature at an estimated stiffness of 200 MPa at a loading time of 2 h, found using Van der Poel's nomograph in conjunction with various entrance parameters:[21,37]

(44) $T_{R\&B}$ and $PI_{R\&B}$

(45) T_{Pen800} and $PI_{log\text{-}pen}$

(46) $T_{Pen800F}$ and PI_{Fraass}

(47) Temperature where stiffness is 200 MPa at 2 h, estimated from McLeod's modification of Heukelom and Klomp's version of Van der Poel's nomograph, using base temperature and penetration-viscosity number, based on penetration at 77 °F (25 °C) and viscosity at 140 °F (60 °C), as entrance parameters[48]

(48) T_H, Hill's cracking temperature, °F, found using a nomograph developed by the Asphalt Institute.[37] Entrance parameters for this nomograph are penetration at 77 °F (25 °C) and penetration at 41 °F (5 °C).

(1)	(49)*	(50)	(51)	(52)*	(53)*	(54)*
Asphalt No.	Large Molecular Size, %, RTFOT	Medium Molecular Size, %, RTFOT	Small Molecular Size, %, RTFOT	No. Avg. Molecular Weight, %, RTFOT	Wt. Avg. Molecular Weight, %, RTFOT	Polydispersity Index, PDI, RTFOT
1	20	43	36	2390	2750	2.14
2	31	40	29	1320	4590	3.47
3	30	41	29	1350	5290	3.92
4	32	42	26	1470	5200	3.54
5	20	52	28	1540	8460	5.49
6	20	52	28	1560	2700	1.73
7	22	51	27	1410	8210	5.83
8	21	48	32	1230	2850	2.31
9	37	45	19	2360	8260	3.51
10	37	44	19	1970	7840	3.99
11	37	44	19	1860	7500	4.03
12	41	36	23	1260	8530	6.77
13	36	38	27	1060	4410	4.16
14	34	40	26	1190	3800	3.19
15	26	42	33	1160	2940	2.53
16	18	49	33	1310	2430	1.85
17	37	38	25	1360	3920	2.88

Note: Columns marked with an asterisk (*) contain test data or variables that were used in statistical analysis.

(49)-(51) Molecular size fractions, determined from HP-GPC analyses using procedure developed by Jennings[83,84]

(52),(53) Average relative molecular weights, from HP-GPC analyses

(54) Polydispersity index, PDI:

$$PDI = \bar{M}_w/\bar{M}_n$$

where

$\bar{M}_w$ = number average molecular weight

$\bar{M}_n$ = weight average molecular weight

(1)	(55)*	(56)*	(57)*	(58)*
	T_g, °F		Mix Temperature Shift, °F	
Asphalt No.	from DSC RTFOT	from DMA RTFOT	Tensile Strength	Static Modulus
1	-27	55	12	14
2	-18	42	-4	-18
3	-18	47		
4	-27	46	8	8
5	-34	51	0	5
6	-30	51		
7	-25	48	15	18
8	18	68	19	14
9	-38	44		
10	-28	43		
11	-28	45	4	13
12	-27	42	0	-9
13	-17	42	-14	-26
14	-25	42	1	-4
15	-27	43		
16	-26	55	5	11
17	-40	38	-1	-3

Note: Columns marked with an asterisk (*) contain test data or variables that were used in the statistical analysis.

(55) Glass transition temperature obtained from DSC thermogram

(56) Glass transition temperature estimated as the temperature where the loss modulus reaches a peak value

(57) Mix tensile strength shift temperature; see text section 4.7

(58) Mix static modulus shift temperature; see text section 4.7

(1)	(59)*	(60)*	(61)	(62)
Asphalt No.	Predicted Cracking Index, ft/1000 ft^2		Mix J_{1c}, lb-in/in^2	Mix J_{1c} Transition Temperature, ^{o}F
	THERM	TC-1		
1	366	39	2.9	43
2	374	1	3.4	29
3	396			
4	404	15	1.6	40
5	396	6	1.8	29
6	386			
7	357	74	2.6	45
8	296	0	1.3	43
9	398			
10	382			
11	384	0		
12	358	23	1.4	26
13	262	2	1.3	9
14	346	8	3.0	31
15	354			
16	412	2	3.0	49
17	420	0	2.2	32

Note: Columns marked with an asterisk (*) contain test data or variables that were used in the statistical analysis.

(59)-(60) Predicted cracking index, linear feet of cracking per 1000 ft^2 pavement area:

(59) Prediction based on THERM program

(60) Prediction based on TC-1 program

APPENDIX F

BITUMINOUS TEST DATA CHART

This appendix contains plots of the penetration and viscosity data for the original asphalt cement and the RTFOT residue.

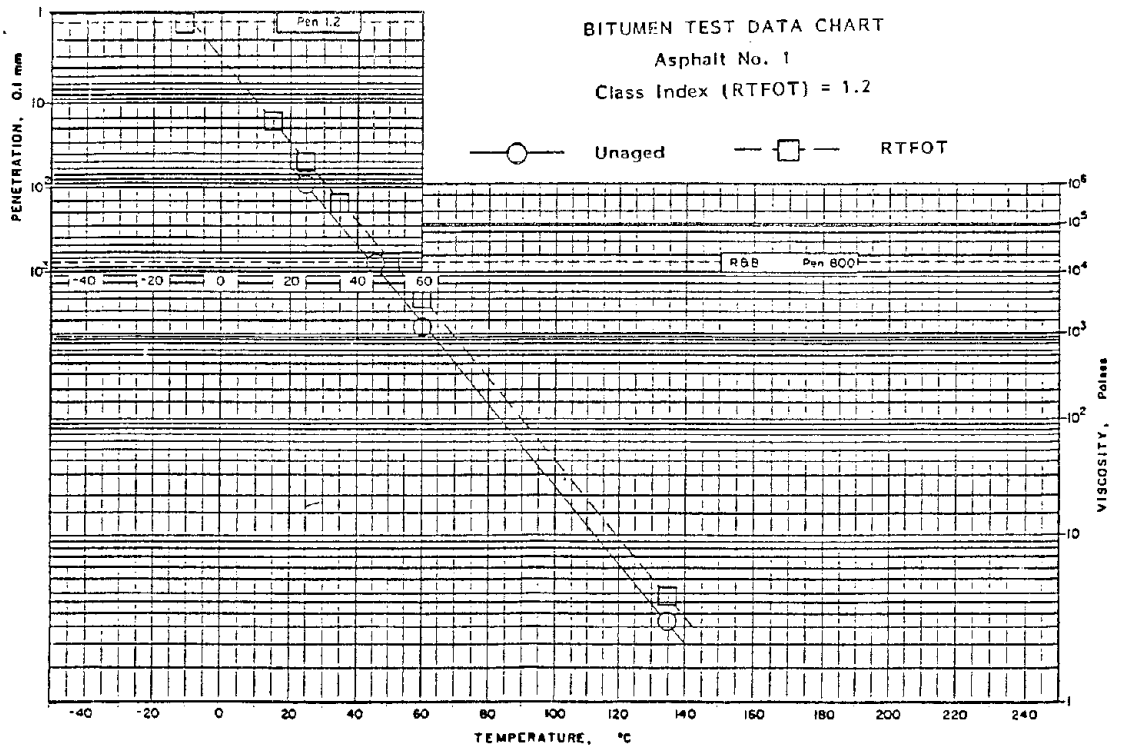

Figure 147. Bitumin test data chart, asphalt No. 1.

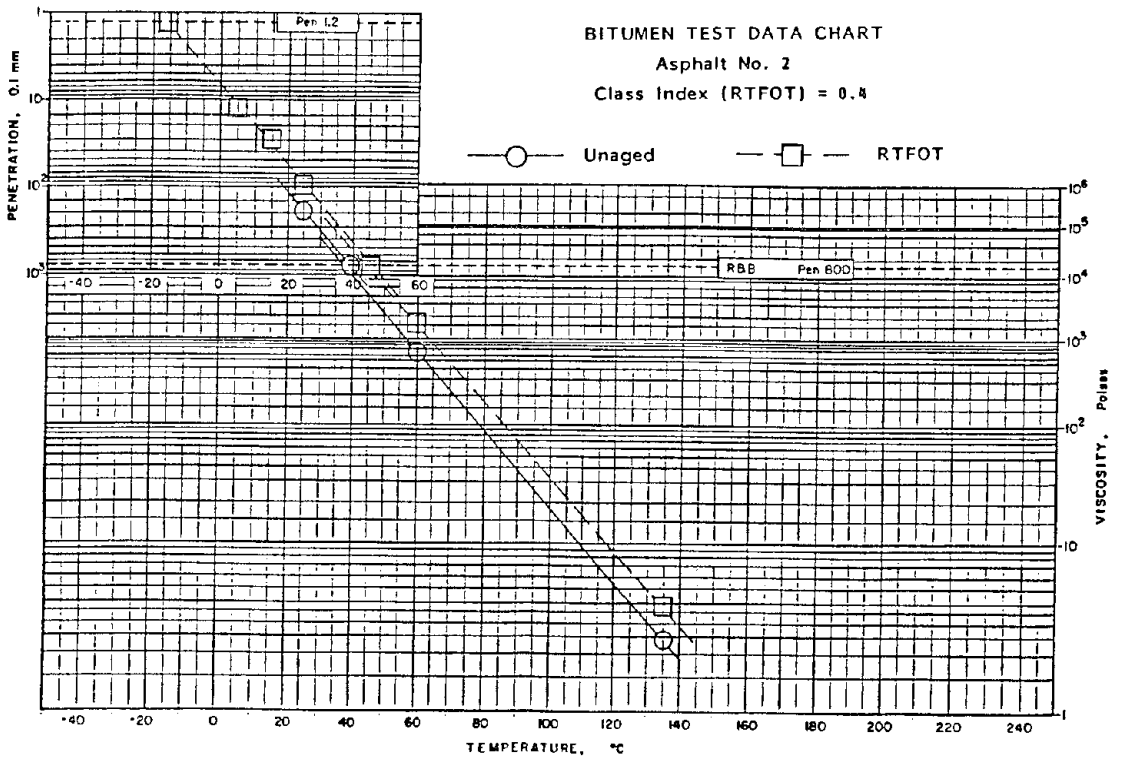

Figure 148. Bitumen test data chart, asphalt No. 2.

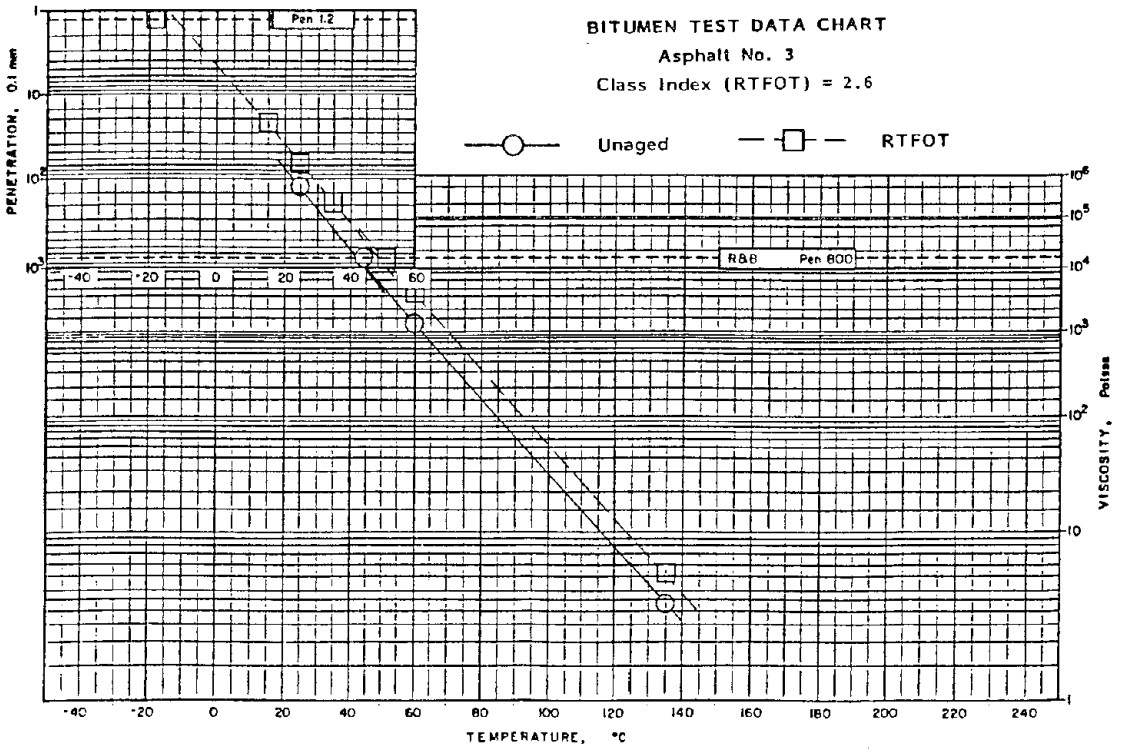

Figure 149. Bitumen test data chart, asphalt No. 3.

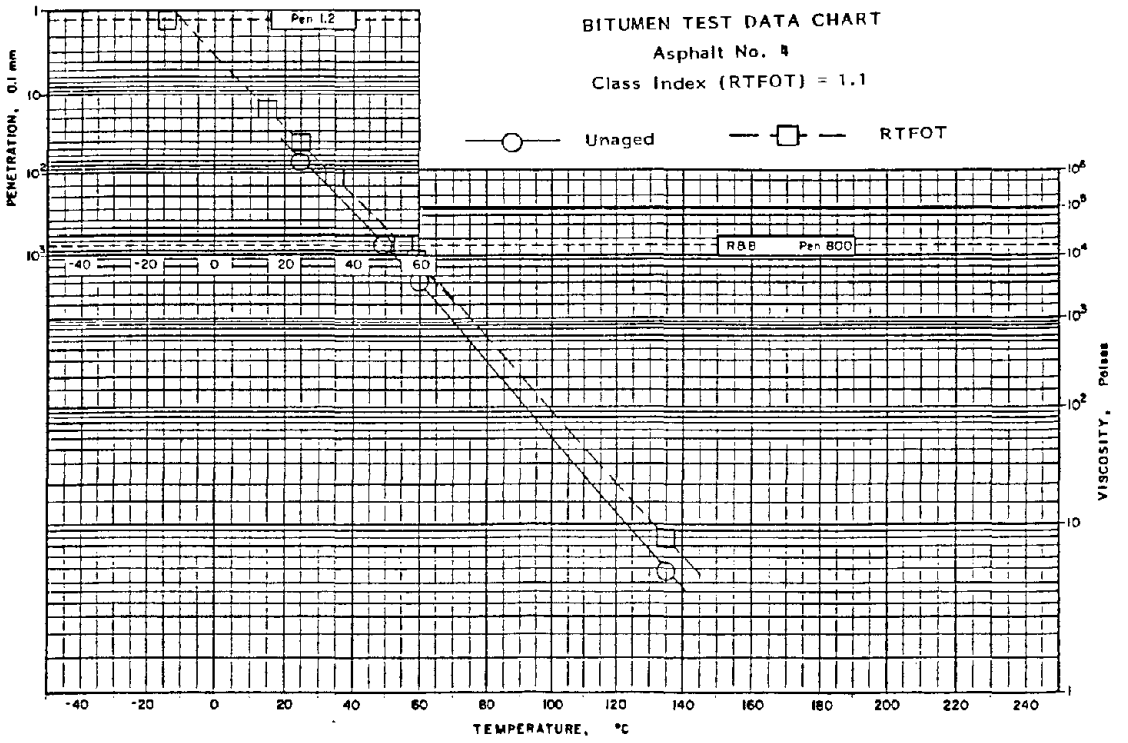

Figure 150. Bitumen test data chart, asphalt No. 4.

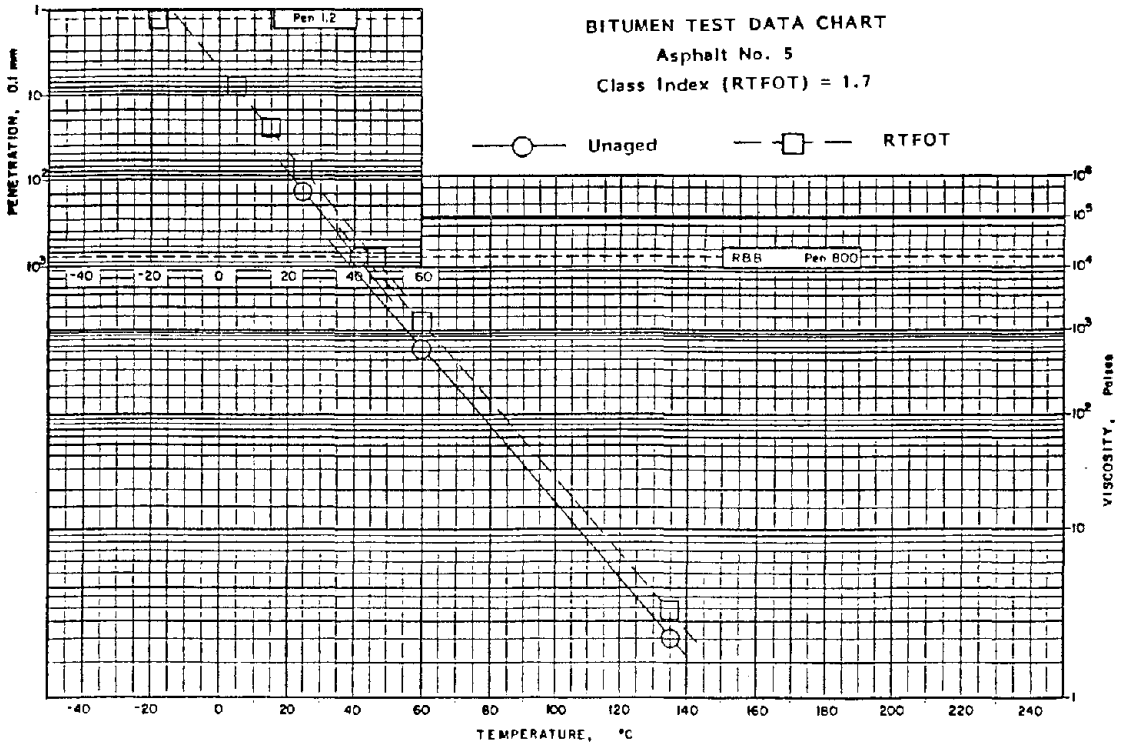

Figure 151. Bitumen test data chart, asphalt No. 5.

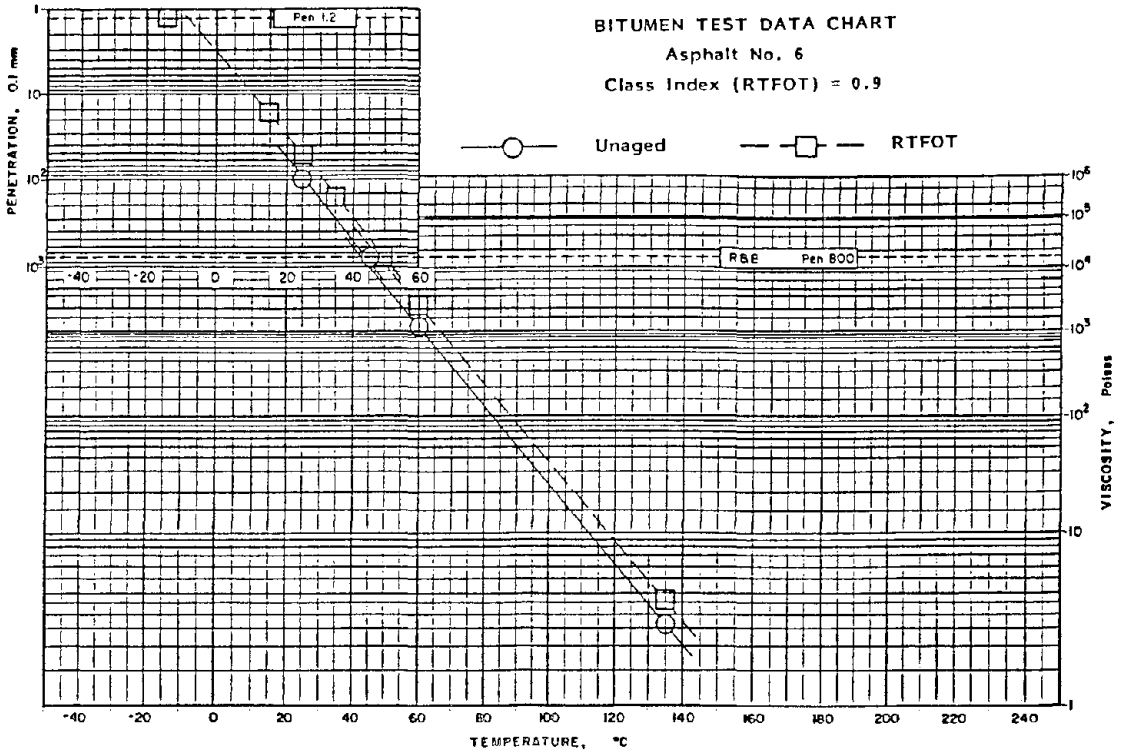

Figure 152. Bitumen test data chart, asphalt No. 6.

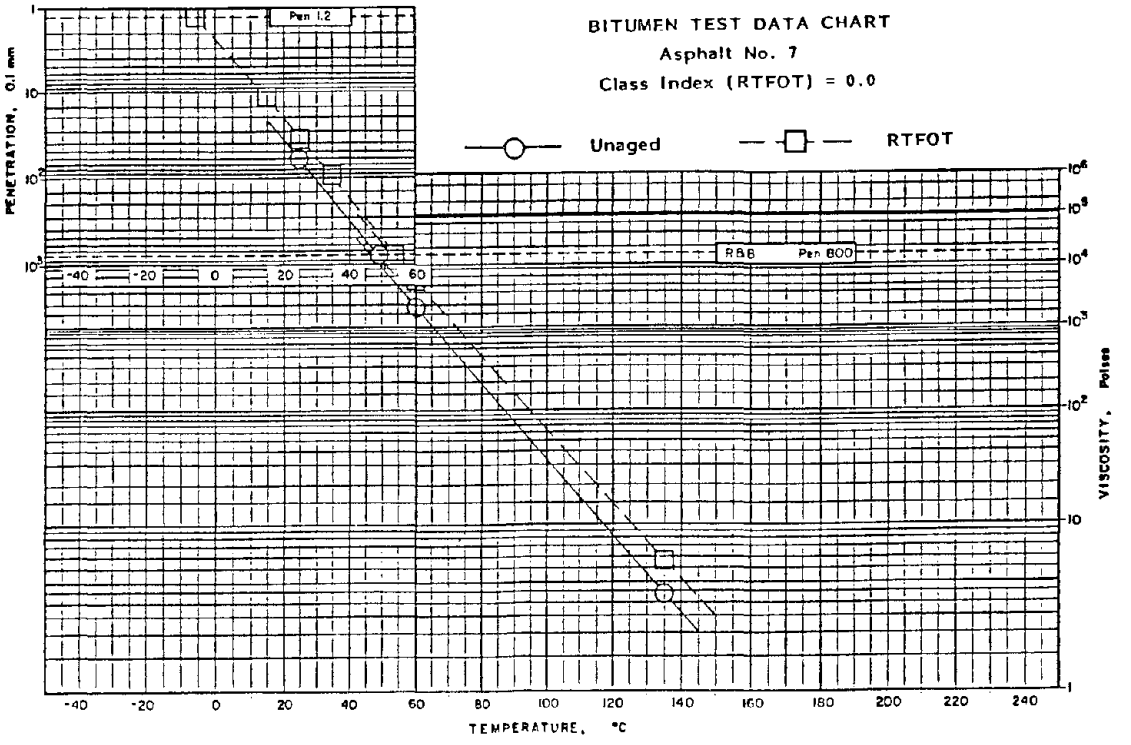

Figure 153. Bitumen test data chart, asphalt No. 7.

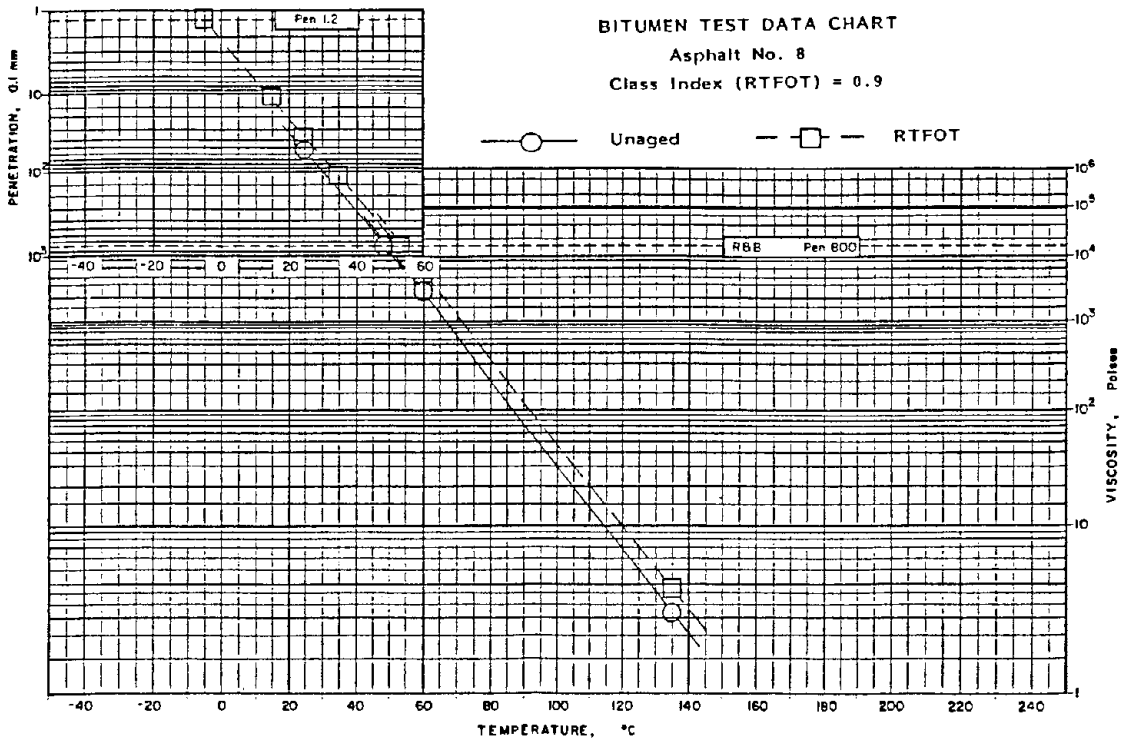

Figure 154. Bitumen test data chart, asphalt No. 8.

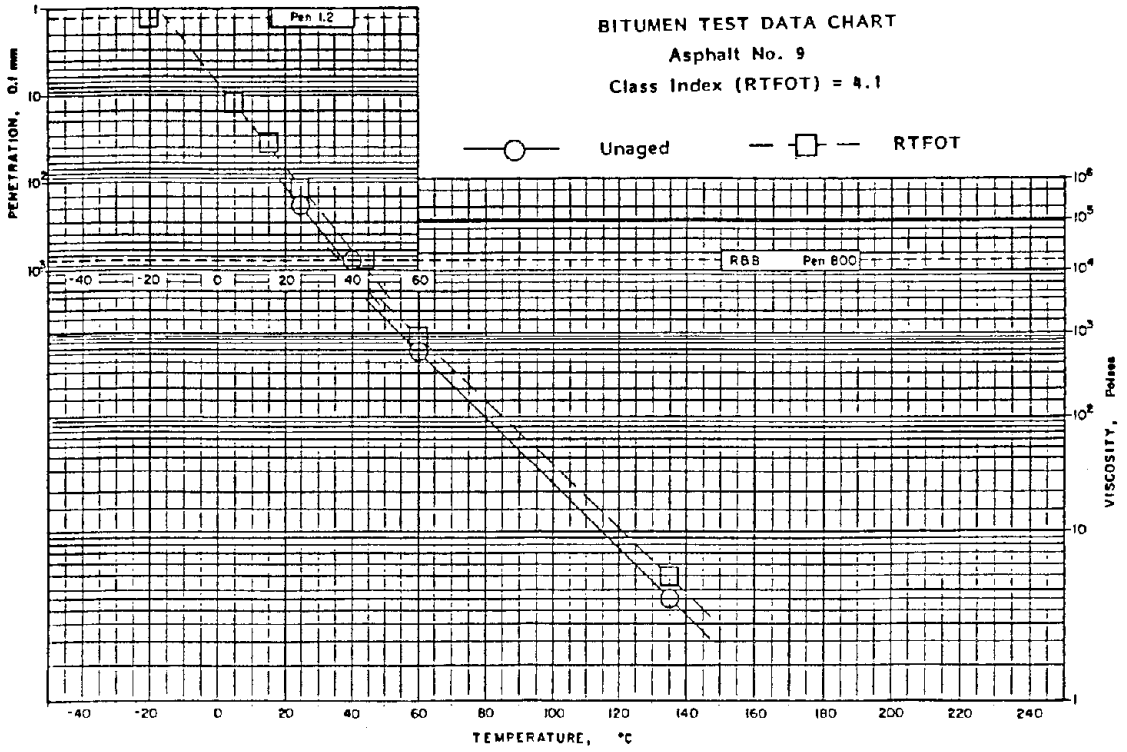

Figure 155. Bitumen test data chart, asphalt No. 9.

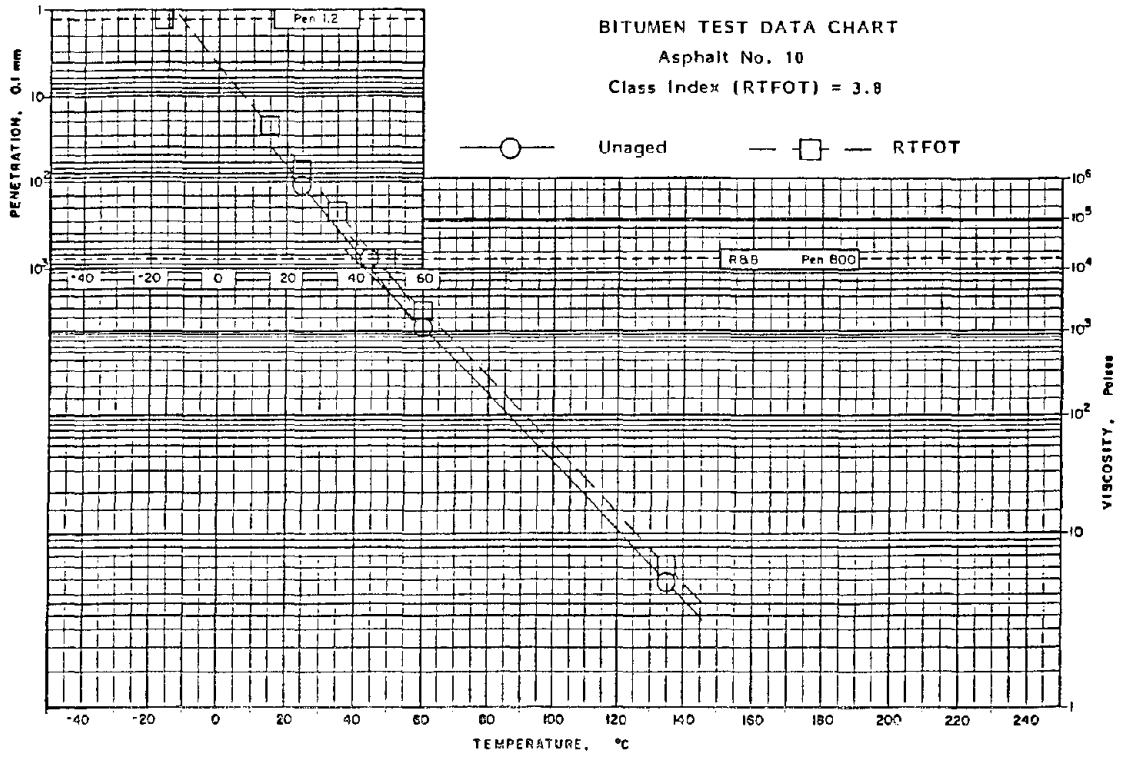

Figure 156. Bitumen test data chart, asphalt No. 10.

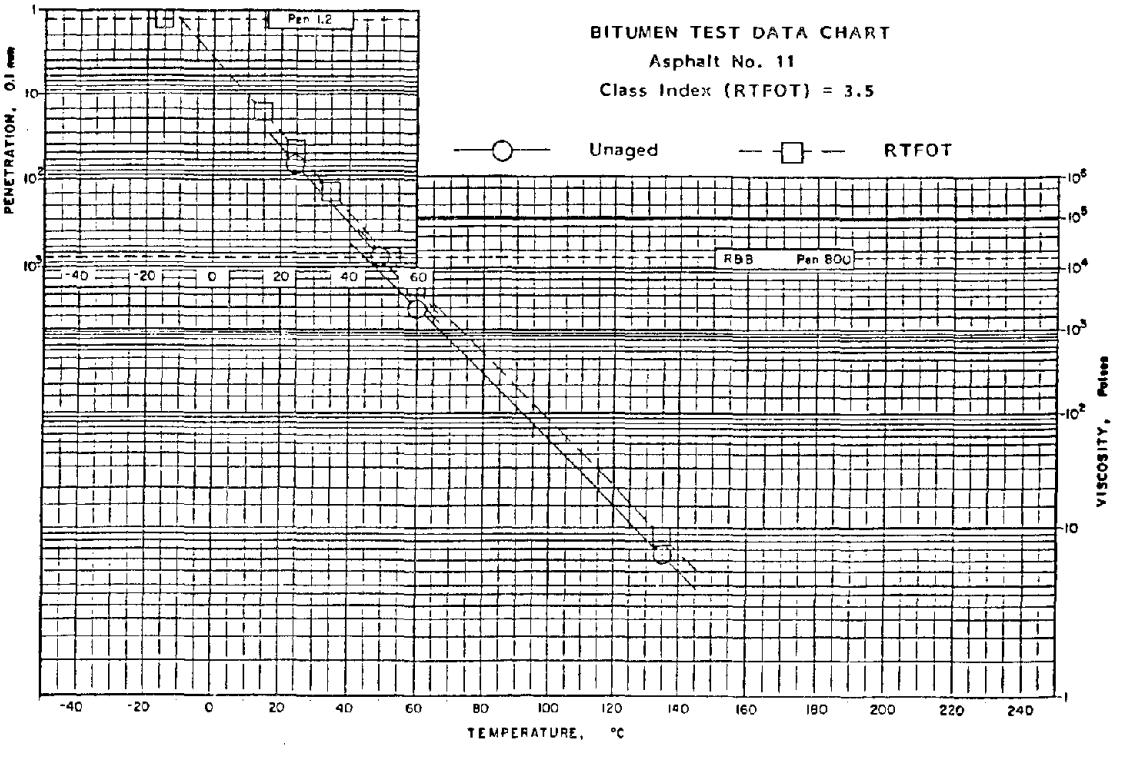

Figure 157. Bitumen test data chart, asphalt No. 11.

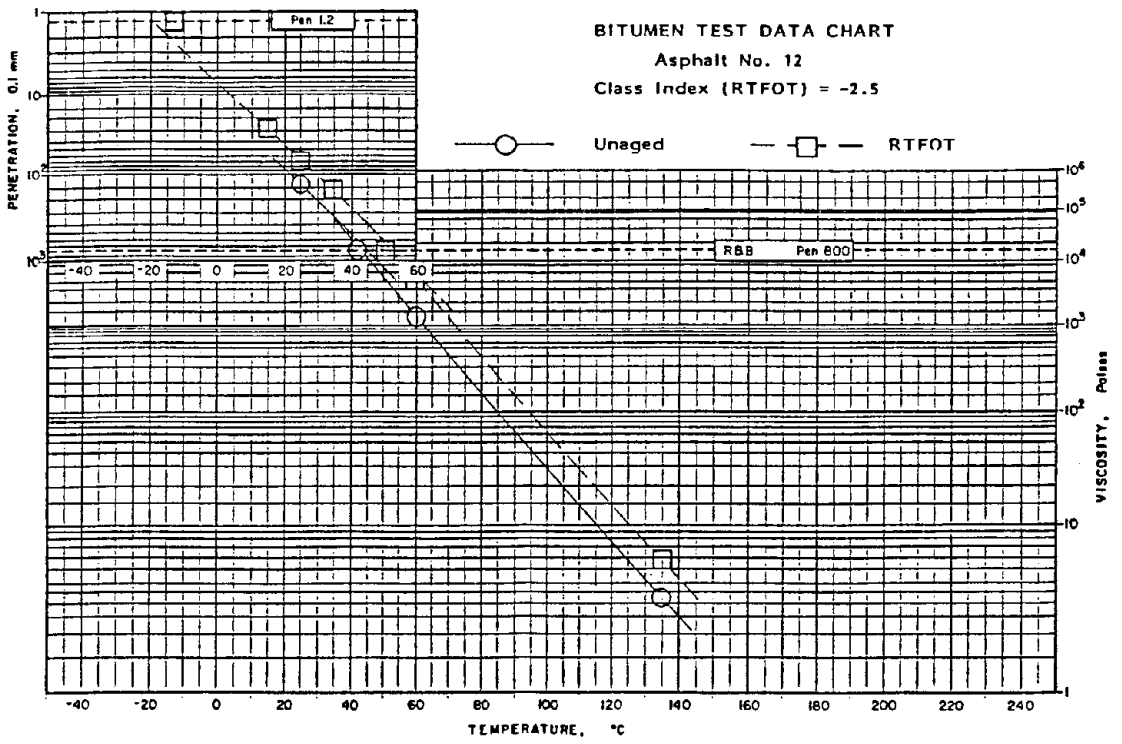

Figure 158. Bitumen test data chart, asphalt No. 12.

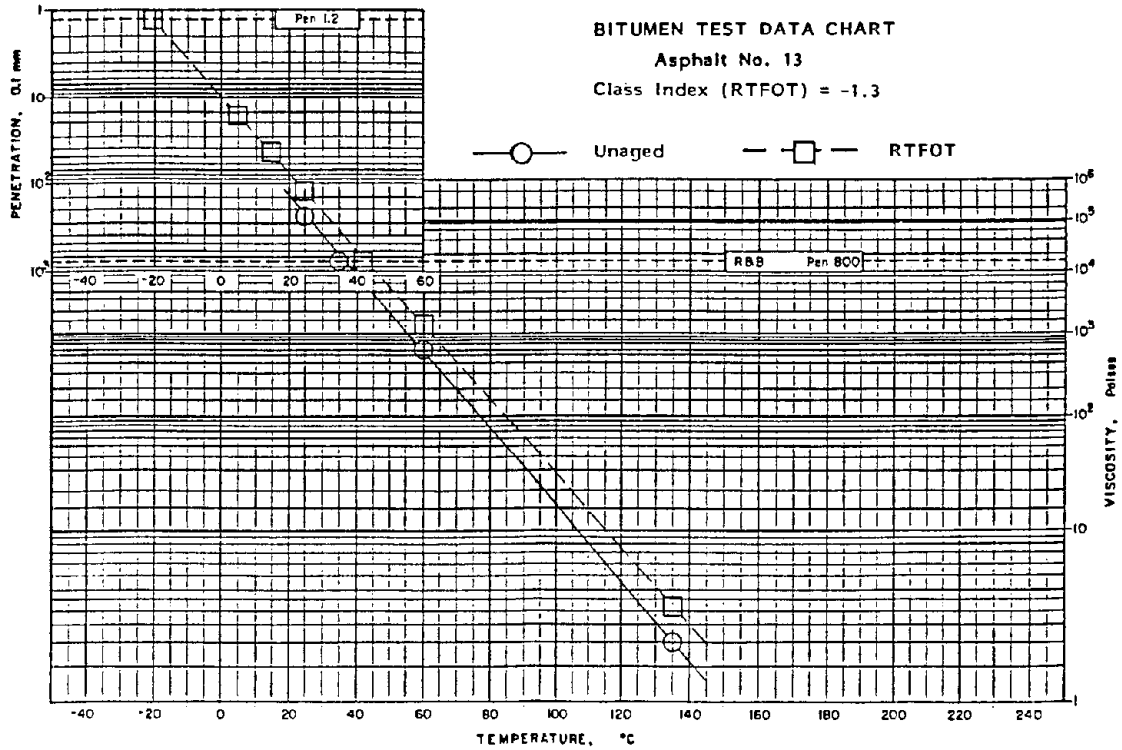

Figure 159. Bitumen test data chart, asphalt No. 13.

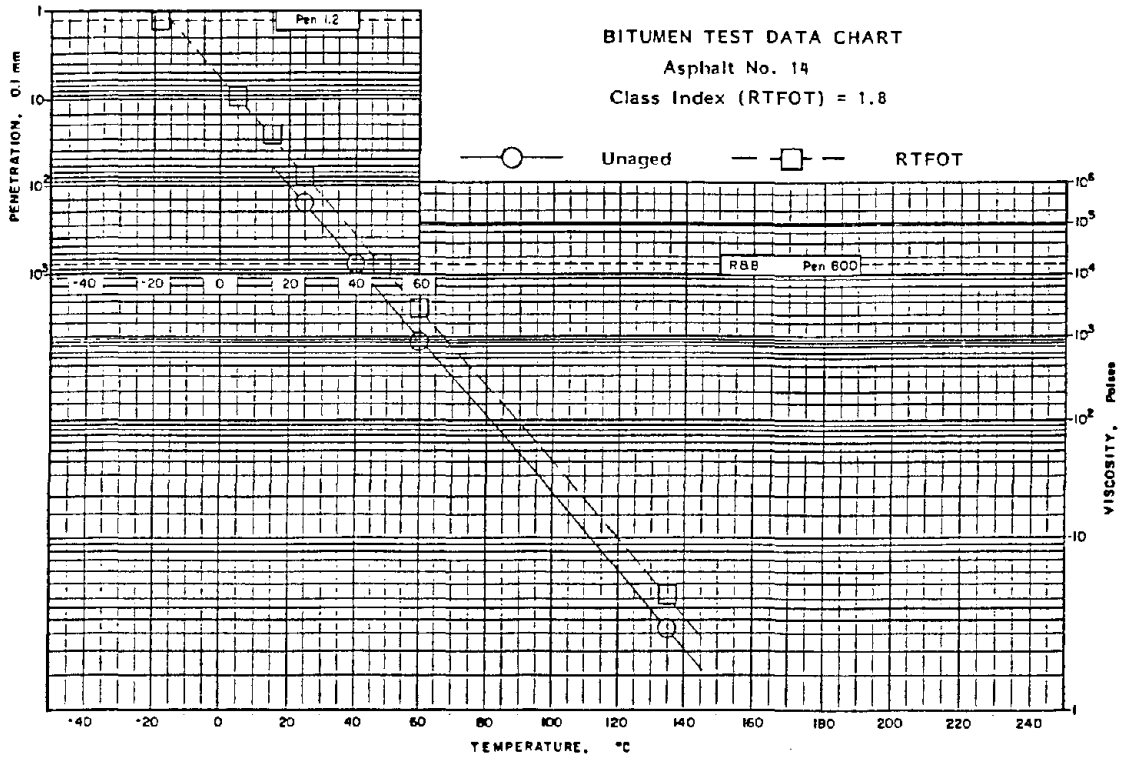

Figure 160. Bitumen test data chart, asphalt No. 14.

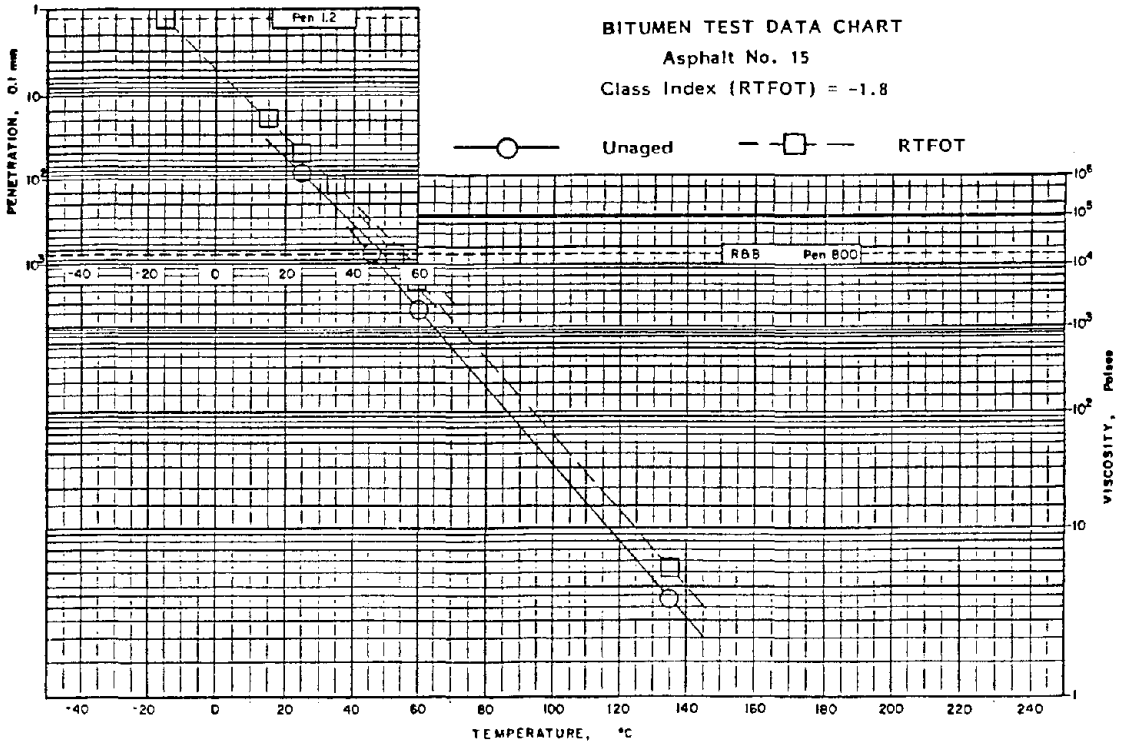

Figure 161. Bitumen test data chart, asphalt No. 15.

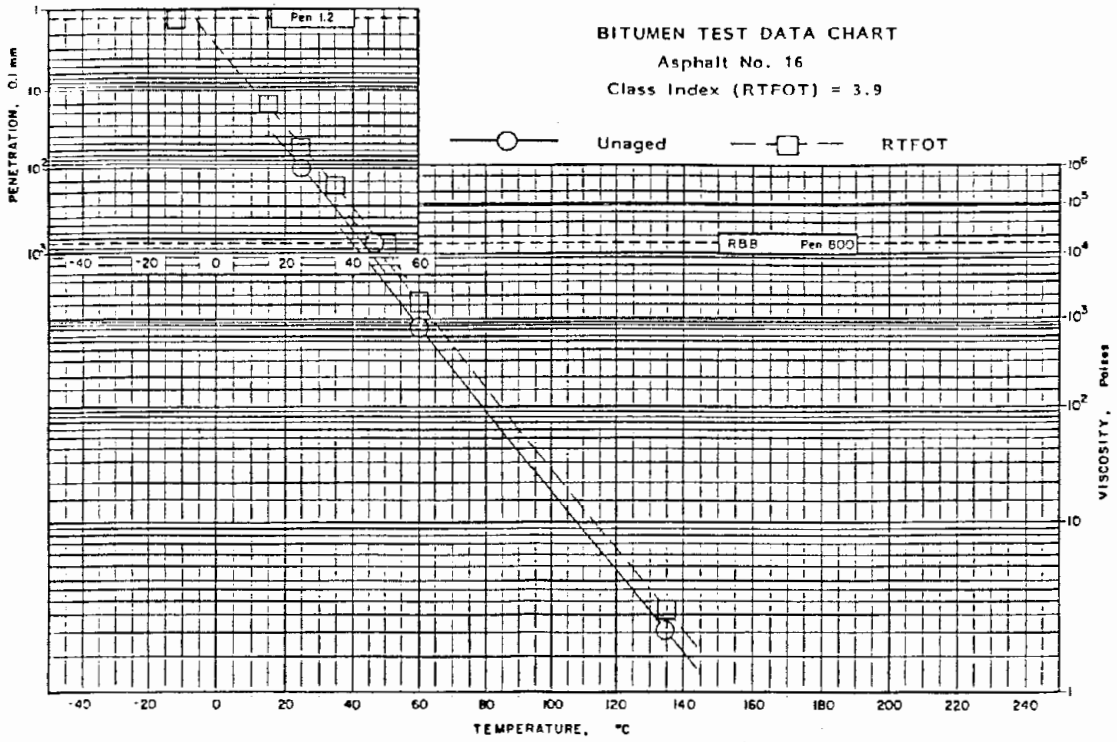

Figure 162. Bitumen test data chart, asphalt No. 16.

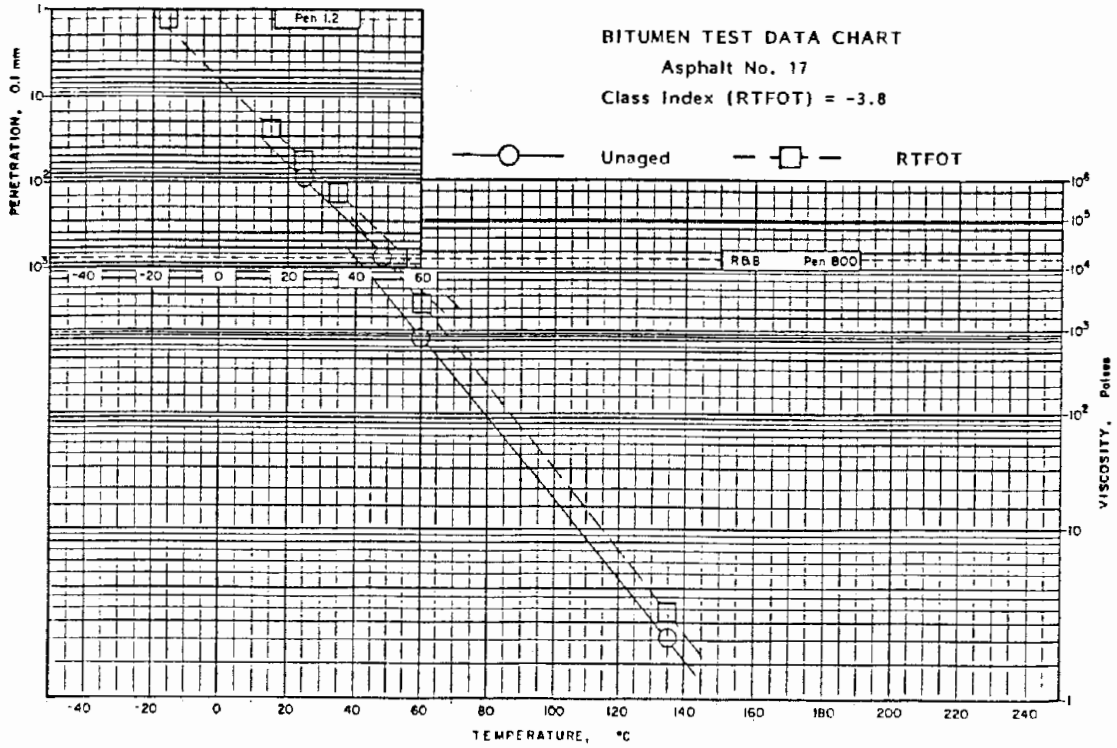

Figure 163. Bitumen test data chart, asphalt No. 17.

APPENDIX G
PROPOSED STANDARD TEST METHOD FOR FLEXURAL STIFFNESS OF ASPHALT CEMENT AT LOW TEMPERATURES BY BENDING BEAM

SCOPE

This proposed test method covers the determination of the time-dependent flexural stiffness modulus of asphalt cement at low temperatures using a three-point beam loaded at a constant stress. It is applicable to asphalts having flexural stiffnesses greater than 250 lb/in^2 (1.7 MPa) at the time and temperature of testing.

APPLICABLE DOCUMENTS

ASTM Standards:
E 1 Specifications for ASTM thermometers
D36 Softening Point of Bitumen (Ring-and-Ball Apparatus)

SUMMARY OF METHOD

A rectangular beam of asphalt cement supported at each end is subjected to a constant load applied midway between its end supports.

The deflection of the midpoint of the beam is measured as a function of time using a linear variable differential transformer (LVDT) and is recorded using a strip chart recorder or automated data acquisition systems.

The temperature of the beam specimen during testing is controlled by submerging the lower portion of the test device into a constant-temperature bath filled with a 50:50 (by volume) mixture of ethylene glycol and water.

DEFINITION

Modulus of Flexural Stiffness--the ratio formed by dividing the maximum bending stress by the maximum bending strain at a specified time of loading and temperature.

SIGNIFICANCE AND USE

The time-dependent modulus of stiffness determined by this method is particularly useful for characterization of asphalt cement at low temperatures.

Data gathered using this method are useful for research purposes and for the selection of asphalt cements according to their stiffness at low temperatures.

APPARATUS

Test Frame--The test frame, as shown in figure 164, should be constructed according to the dimensions shown in figure 165 and should be of aluminum, brass, and/or stainless steel, as specified.

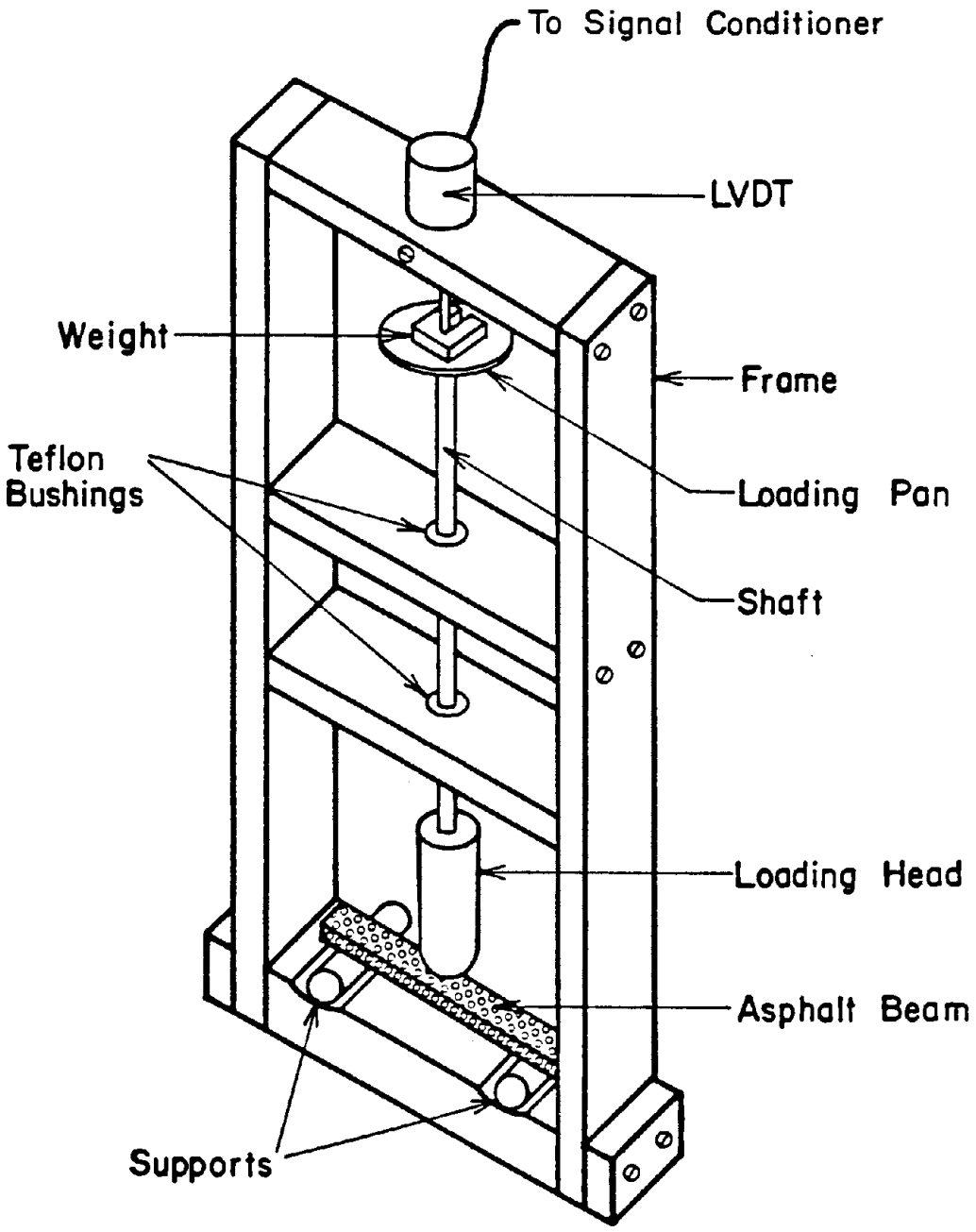

Figure 164. Schematic of bending beam creep test apparatus.

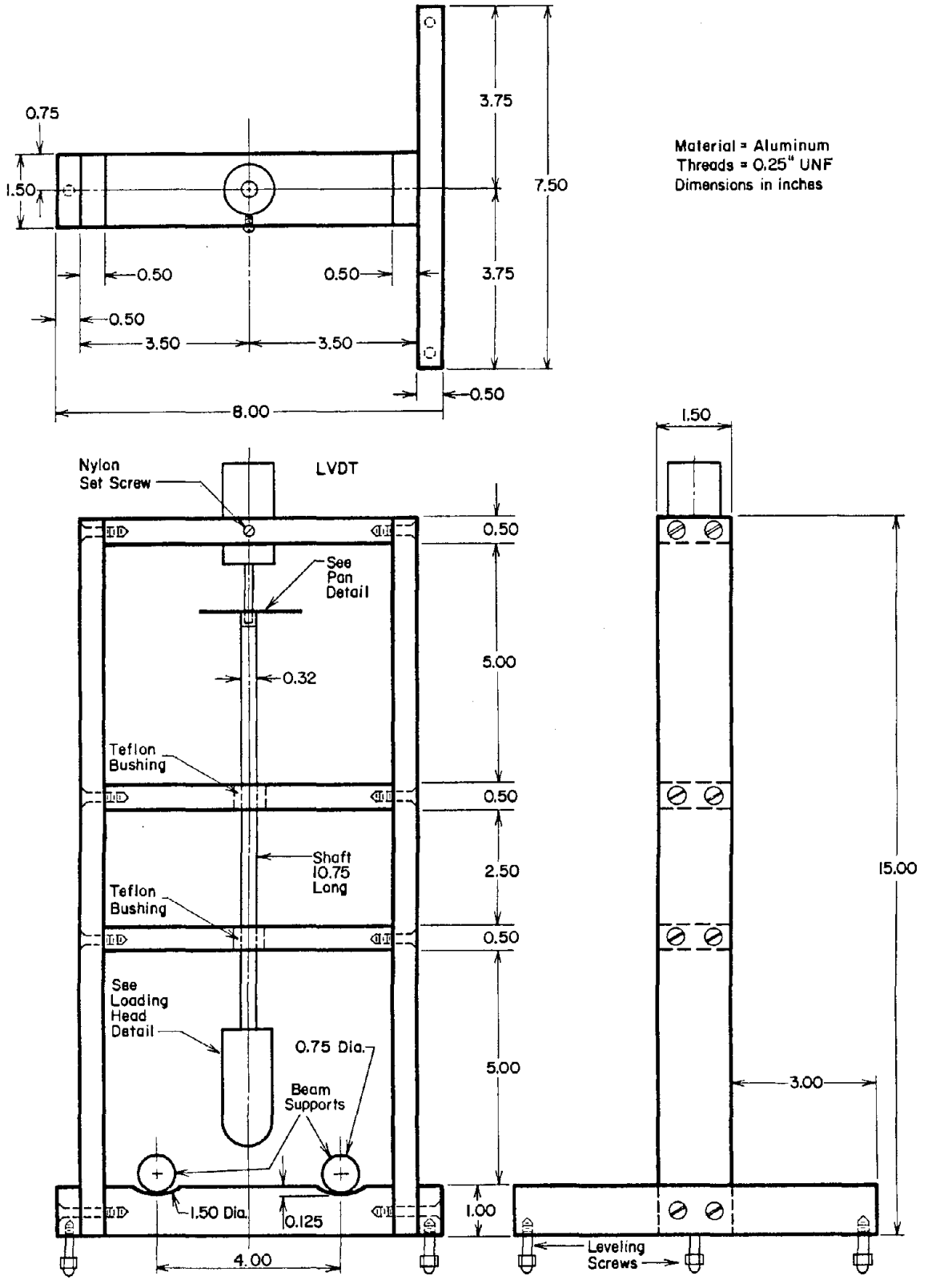

Figure 165. Drawing of loading frame; all dimensions in inches.

Loading Shaft--The loading shaft should be hollow, with high-strength aluminum alloy construction. Provisions must be made for mounting the loading plate and the LVDT shaft at the upper end of the shaft and the loading head at the lower end.

Loading Head and Beam Supports--The loading head should be 1 in (25.4 mm) in diameter and should have a nose rounded on a 0.5-in (12.7-mm) radius. The central portion of the loading nose should be bored to a 0.5-in (12.7-mm) diameter. Provisions must be made for attaching the loading shaft to the head; this connection must be water-tight (see figure 166). The loading head should be of nylon construction.

The overall construction of the loading shaft and loading head should be such that, when the frame is placed in the controlled temperature bath, the effective weight of the loading shaft, loading head, loading plate, and LVDT shaft and core are between 1 and 2 g. The hollow loading nose provides buoyancy to counteract the weight of the other moving parts.

The beam supports (figure 165) should have a radius of 3/8 in (9.5 mm). A 1 1/2-in (38-mm) diameter, 1/8-in (3.2-mm) deep recess is provided as an aid to align the beam supports. The beam supports should be of stainless steel construction.

Loading Pan, LVDT, and LVDT Shaft--The loading plate should be nylon, with sufficient size and thickness to support the loading weights without visible deflection. The LVDT should be capable of accurate measurements to 200 $\pm$ 20 μin (5 $\pm$ 0.5 μm). The LVDT shaft should be of nonmagnetic material, preferably brass, and should rigidly connect to the loading shaft and loading plate. The LVDT is mounted in a circular cutout in the upper crosspiece and is held in place by a nylon set screw. Provisions must be made for vertical adjustment of the LVDT $\pm$1/4 in ($\pm$ 6.4 mm).

Load Shaft Support--The loading shaft should be supported laterally so that it is held in a vertical alignment. If needed, a Teflon guide may be used to support the shaft to minimize friction between the shaft and its support.

Centering Jig--A jig which can be placed along the base crosspiece should be constructed with dimensions such that a test beam placed along it will be perpendicular to the supports and will be located directly under the loading head. This jig is used for rapid and accurate placement of beams prior to testing.

General Construction--The test frame should be constructed such that the LVDT, LVDT shaft, and loading shaft and bearing are coincident along a single vertical line. Improper alignment of these parts may result in binding of the loading shaft or off-center loading of the beams, causing significant errors in test results (see figure 165).

Beam Molds--Beam molds should be of flexible silicone rubber and stable to a temperature of at least 375 ^{o}F (191 ^{o}C). The exterior dimensions of the mold should be 3/4 in wide by 3/4 in high by 5 1/2 in long (19 mm wide by 19 mm high by 140 mm). These dimensions produce a mold with sufficient rigidity to assure repeatable beam dimensions and with sufficient flexibility

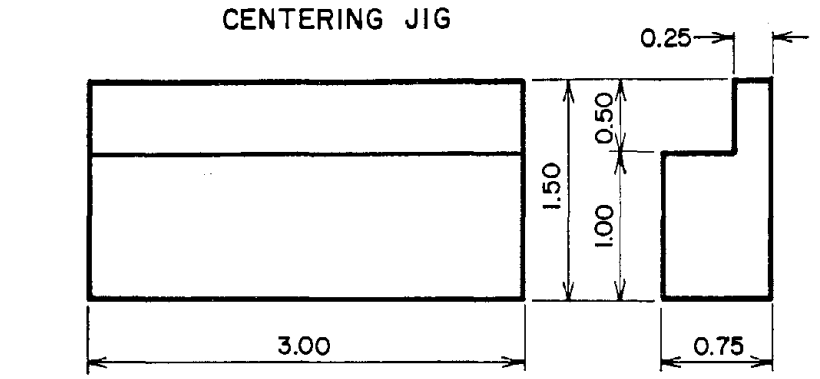

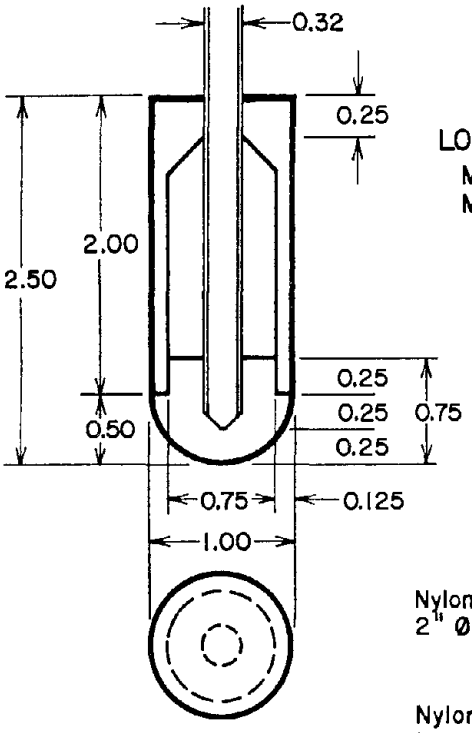

LOADING HEAD DETAIL
Material = Nylon
Must be water tight

LOADING
PAN DETAIL

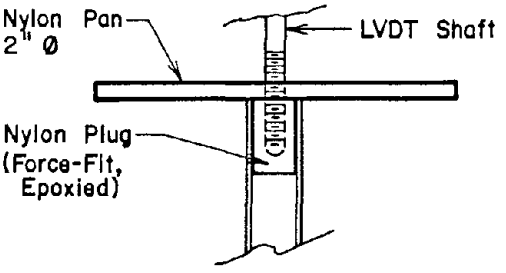

WEIGHTS
(Brass Plate)

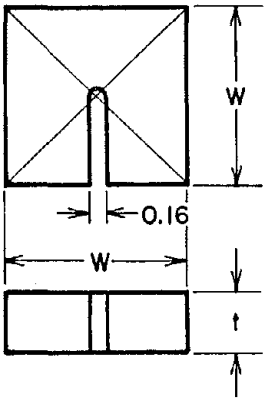

Nominal Weight	(in) W	(in) t
30	1.00	0.25
50	1.25	0.25
100	1.25	0.50
200	1.75	0.50

Figure 166. Details of loading head; all dimensions in inches.

so that the beams are readily removed from the mold. The interior dimensions of the mold should be 1/4 in wide by 1/2 in deep by 5 in long (6.4 mm wide by 12.7 mm deep by 127 mm long). The interior dimensions should be maintained to a tolerance of ± 0.005 in (± 0.13 mm) in width and thickness and ± 0.1 in (± 2.5 mm) in length.

Demolding Bath and Test Bath--The demolding bath shall be capable of maintaining a temperature of 0 °F to 10 °F (-17.7 °C to -12.2 °C). This bath is used to cool specimens prior to removing them from the molds. The test bath is used to control the temperature of the test and should be capable of maintaining the test temperature to within ± 0.5 °F (± 0.3 °C).

During demolding (see section 7.2), samples should be quite stiff but not brittle. A temperature of 0 °F to 10 °F (-17.7 °C to -12.2 °C) will generally prove to be acceptable for specimen demolding. However, for very soft asphalts, lower temperatures may be required for demolding, while for very hard asphalts, higher temperatures may be acceptable. Normal temperatures of testing range from -40 °F to 32 °F (-40 °C to 0 °C). In some cases, the testing bath may be used to cool specimens prior to demolding.

PREPARATION OF TEST SPECIMENS

Pouring--Heat the asphalt sample until it can be easily poured in an oven that has been preheated to a temperature of 325 °F (163 °C) or lower. In no case shall the sample be heated to more than 180 °F (100 °C) above its ring and ball softening point temperature. The sample should be stirred every 15 min during heating. Remove the sample from the oven and stir again. Immediately pour the asphalt into a specimen mold preheated to 275 °F to 325 °F (135 °C to 163 °C) using enough material to slightly overfill the mold. Gently stir the asphalt in the mold with a needle, running it along all edges and corners and once down the center of the mold. Permit the sample to cool for 20 to 28 h.

Trimming and Demolding--Trim excess asphalt from the top surface of the mold using a hot spatula such that the surface of the asphalt is flush with the surface of the mold. Place the mold in a bath maintained at 0 °F to 10 °F (-17.7 °C to -12.2 °C) for 20 to 30 min. Remove the mold from the bath. Loosen the specimen from the sides of the mold by running a razor blade or utility knife along both edges of the specimen. Carefully remove the specimen from the mold.

PROCEDURE

Cool the test frame to the test temperature by placing the lower portion in the test bath for a minimum of 1 h.

Remove the test frame from the test bath and raise the shaft and nose sufficiently to permit placement of the sample across the supports. Place the centering jig along one side of the base crosspiece. Remove the sample from the demolding bath and immediately place it across the supports and against the centering jig. While gently holding the sample against the supports, remove the centering jig. Immediately lower the loading nose until it barely contacts the sample. Being careful not to disturb the test specimen, place the testing frame in the test bath. The level of coolant in the bath should

be such that the central crosspiece is covered by at least 1 in (25.4 mm) of coolant. There should be at least 1.0 in (25.4 mm) of clearance between the surface of the coolant and the pan.

Zero the LVDT and allow the sample to equilibrate for 20 to 30 min. Measure and record the test bath temperature to the nearest 0.2 °F (0.1 °C). Start the recorder or data acquisition system and place the appropriate weight on the loading pan.

A 30-g weight is normally used. Larger weights may be used as long as the maximum strain in the test specimen does not exceed 0.1 percent, corresponding to a sample midpoint deflection of 0.011 in (0.28 mm). The suggested weight series is 30, 50, 100, and 200 g. Weights heavier than 200 g may result in the fracture of test specimens during testing.

The total time of testing is determined by the operator and is subject to the following limitations:

If the 30-g weight is used, the test should be terminated when the maximum sample strain reaches 5 percent, corresponding to a midpoint deflection of 0.55 in (14 mm). Deflections larger than 0.55 in (14 mm) result in large strains, and the analysis used herein is no longer valid.

If the weight used is heavier than 30 g, the test shall be terminated when the maximum strain within the sample reaches 0.1 percent, corresponding to a deflection of 0.011 in (0.28 mm). Deflections less than 0.01 in (0.28 mm) will generally produce linear behavior.

At least two previously untested specimens should be evaluated for each sample.

CALCULATIONS

Maximum Bending Stress--The maximum bending stress will occur at the midpoint of the loaded span and can be calculated by using the following equation:

$$\sigma_o = 3PL/2bd^2 \qquad (57)$$

where:

σ_o = outer fiber stress, lb/in^2 (N/m^2)
P = load, lb (N)
L = support span, in (mm); normally 4.00 in (101.6 mm)
b = beam width, in (mm); normally 0.50 in (12.7 mm)
d = beam depth, in (mm); normally 0.25 in (6.4 mm)

Equation 57 applies strictly to linear materials at small strains. The limitations on load and deflection established in the section of this specification describing the procedure are meant to ensure that specimens tested will behave in an essentially linear fashion and that the strains may in no case be greater than 5 percent. Despite these restrictions, specimen behavior may not always be linear, and slight errors will be introduced into

the calculation of stress and strain, especially as the maximum fiber strain approaches 5 percent.

Maximum Strain--The maximum strain in the outer fibers occurs at the midpoint of the support span and can be calculated by using the following equation:

$$\varepsilon(t) = 6\delta(t)d/L^2 \quad (58)$$

where:

$\varepsilon(t)$ = maximum strain at time t, in/in (mm/mm)
$\delta(t)$ = deflection at midpoint of supported span, at time t, in (mm)
d = depth of beam, in (mm); normally 0.25 in (6.4 mm)
L = support span length, mm (in); normally 4.00 in (101.6 mm)

Modulus of Flexural Stiffness--The modulus of flexural stiffness for the specimen at a specified time of loading may be calculated as follows:

$$E(t) = \sigma_o/\varepsilon(t) \quad (59)$$

where:

E(t) = modulus of flexural stiffness at time t
σ_o = maximum bending stress (equation 57)
$\varepsilon(t)$ = maximum strain at time t (equation 58).

REPORT

The report shall include the following:

- Complete identification of the specimen, including asphalt source and grade, any special treatments or additives used in preparing the sample, and specimen dimensions.
- The temperatures at which the test was performed.
- The load used during the test.
- The average and standard deviation of the modulus of flexural stiffness at the time(s) and temperature(s) of interest.

REFERENCES

1. Gaw, W. J. "The Measurement and Prediction of Asphalt Stiffnesses at Low and Intermediate Pavement Service Temperatures," Proceedings of the Association of Asphalt Paving Technologists, 47 (1978), pp. 457-494.

2. Heukelom, W. "Observations on the Rheology and Fracture of Bitumens and Asphalt Mixes," Proceedings of the Association of Asphalt Paving Technologists, 35 (1966), pp. 358-396.

3. Gaskins, F. H., Brodnyan, J. G., Philliposs, W., and Thelen, E. "The Rheology of Asphalt. II. Flow Characteristics of Asphalt," Transactions of the Society of Rheology, 4 (1960), pp. 265-278.

4. Pink, H. S., Merz, R. E., and Bosniak, D. S. "Asphalt Rheology: Experimental Determination of Dynamic Moduli at Low Temperature," Proceedings of the Association of Asphalt Paving Technologists, 49 (1980), pp. 64-88.

5. Schweyer, H. E. "A Pictorial Review of Asphalt (Bitumen) Rheology," Proceedings of the Association of Asphalt Paving Technologists: Historical Session, 43A (1974), pp. 121-157.

6. Griffin, R. L., Miles, T. K., Penther, C. J., and Simpson, W. C. "Sliding Plate Microviscometer for Rapid Measurement of Asphalt Viscosity in Absolute Units," ASTM Special Technical Publication No. 212, American Society for Testing and Materials, (1957), pp. 36-48.

7. Fenijn, J. and Krooshof, R. C. "The Sliding Plate Rheometer: A Simple Instrument for Measuring the Viscoelastic Behavior of Bitumens and Related Substances in Absolute Units," Proceedings, Canadian Technical Asphalt Association, 15 (1970), p. 123.

8. Fenijn, F. "Low Temperature Stiffness of Asphalt Binders: Measurement and Prediction," Proceedings, Canadian Technical Asphalt Association, 18 (1973), p. 31.

9. Anderson, D. A. and Goetz, W. H. "Mechanical Behavior and Reinforcement Mineral Filler-Asphalt Mixtures," Proceedings of the Association of Asphalt Paving Technologists, 42 (1973), pp. 37-61.

10. Sisko, A. W. "Determination and Treatment of Asphalt Viscosity Data," Highway Research Record, 67 (1964), pp. 27-37.

11. Anderson, D. A. and Dukatz, E. L. "Asphalt Properties and Composition: 1950-1980," Proceedings of the Association of Asphalt Paving Technologists, 49 (1980), pp. 1-22.

12. "Standard Test Method for Viscosity of Asphalt with Cone and Plate Viscometer," ASTM D 3205-77, 1986 Annual Book of ASTM Standards, Vol. 4.03, pp. 468-472.

13. Schweyer, H. E., Smith, L. L., and Fish, G. W. "A Constant Stress Rheometer for Asphalt Cements," Proceedings of the Association of Asphalt Paving Technologists, 45 (1976), pp. 53-72.

14. Schweyer, H. E. and Busot, J. C. "Experimental Studies on Viscosity of Asphalt Cements at 77 °F," Highway Research Record, 361 (1971), pp. 58-70.

15. Schweyer, H. E. and Burns, A. M. "Low Temperature Rheology of Asphalt Cements: III. Generalized Stiffness-Temperature Relations of Different Asphalts," Proceedings of the Association of Asphalt Paving Technologists, 47 (1978), pp. 1-15.

16. Pugh, H. L. D. "A Falling Co-axial Cylinder Viscometer for the Rapid Measurement of High Viscosities," J. Scientific Instruments, Vol. XXI, (1944), pp. 177-180.

17. Macosko, C. and Starita, J. M. "New Rheometer is Put to the Test," Society of Plastics Engineering Journal, 27, No. 11 (1971), pp. 38-42.

18. Macosko, C.W. and Weissert, F. C. "Applications of the Rheometrics Mechanical Spectrometer to Rubber Testing," ASTM Special Technical Publication No. 553, American Society for Testing and Materials (1974), pp. 127-141.

19. Breaking Point of Bitumen, Fraass Method, IP 80/53, The Institute of Petroleum.

20. Rigden, P. J., and Lee, A. R. "Brittle Fracture of Tars and Bitumens," Journal of Applied Chemistry, 3, No. 2 (1953), pp. 62-70.

21. Van der Poel, C. "A General System Describing the Visco-Elastic Properties of Bitumens and its Relation to Routine Test Data," Journal of Applied Chemistry, 4 (1954), p. 221.

22. Heukelom, W. "An Improved Method of Characterizing Asphaltic Bitumens with the Aid of Their Mechanical Properties," Proceedings of the Association of Asphalt Paving Technologists, 42 (1973), pp. 67-98.

23. Thenoux, G., Lees, G., and Bell, C. A. "Laboratory Investigation of the Fraass Brittle Test," Proceedings of the Association of Asphalt Paving Technologists, 54 (1985), pp. 529-548.

24. "Standard Test Procedure for Force Ductility," under development by ASTM, remarks made at Committee Meetings and results of round robin testing, ASTM Committee D-4.

25. Anderson, D. I. and Wiley, M. L. "Force Ductility: An Asphalt Performance Indication," Proceedings of the Association of Asphalt Paving Technologists, 45 (1976), pp. 25-38.

26. Epps, J., Petersen, C., Kennedy, T. W., Anderson, D. A., and Haas, R. "Chemistry, Rheology, and Engineering Properties of Manganese-Treated Asphalts and Asphalt Mixtures," Asphalt Analysis, Sulfur, Mixes and Seal Coats, Transportation Research Record 1096 (1986), pp. 106-119.

27. "Standard Test Method for Apparent Viscosity of Plastisols and Organosols at Low Shear Rates by Brookfield Viscometer," ASTM D 1824-83, 1986 Annual Book of ASTM Standards, 8.02, pp. 162-163.

28. "Standard Test Method for Apparent Viscosity of Plastisols and Organosols at High Shear Rates by Extrusion Viscometer," ASTM D 1823-82, 1986 Annual Book of ASTM Standards, 8.02, pp. 159-161.

29. "Standard Test Method for Flow Rates of Thermoplastics by Extrusion Plastometer," ASTM D 1238-85, 1986 Annual Book of ASTM Standards, 8.01, pp. 555-567.

30. "Standard Test Method for Rheological Properties of Thermoplastics with a Capillary Rheometer," ASTM D 3835-79, 1986 Annual Book of ASTM Standards, 8.03, pp. 265-272.

31. "Standard Test Method for Stiffness Properties of Plastics as a Function of Temperature by Means of a Torsion Test," ASTM D 1043-84, 1986 Annual Book of ASTM Standards, 8.01, pp. 519-533.

32. "Standard Test Method for Apparent Bending Modulus of Plastics by Means of a Cantilever Beam," ASTM D 747-84a, 1986 Annual Book of ASTM Standards, 8.01, pp. 345-350.

33. "Standard Test Method for Flexural Properties of Unreinforced and Reinforced Plastics and Electrical Insulating Materials," ASTM D 790-84a, 1986 Annual Book of ASTM Standards, 8.01, pp. 387-401.

34. Bonnaure, F., et al. "A New Method for Predicting the Stiffness of Asphalt Paving Mixtures," Proceedings of the Association of Asphalt Paving Technologists, 46 (1977), pp. 64-100.

35. Gaw, W. J., Burgess, R. A., and Young, F. D. "Road Performance after Five Years and Laboratory Predictions of Low Temperature Performance," Proceedings, Canadian Technical Asphalt Association, 19 (1974), pp. 45-98.

36. Fromm, H. J., and Phang, W. A. "Temperature-Susceptibility Control in Asphalt-Cement Specifications," Highway Research Record, No. 350 (1971), pp. 30-45.

37. Design Techniques to Minimize Low-Temperature Asphalt Pavement Transverse Cracking (College Park, MD: The Asphalt Institute, 1981), 75 pp.

38. Shahin, M. Y. and McCullough, B. F. "Prediction of Low-Temperature and Thermal-Fatigue Cracking in Flexible Pavements," Research Report 123-14 Center for Highway Research, The University of Texas at Austin, 1972.

39. Finn, F. N., Saraf, C., Kulkarni, R., Nair, K., Smith, W., and Abdullah, A. "Development of Pavement Structural Subsystems," Final Report, NCHRP Project 1-10B, National Cooperative Highway Research Program, February 1977.

40. Ruth, B. E., Bloy, L. A. K., and Avital, A. A. "Prediction of Pavement Cracking at Low Temperatures," Proceedings of the Association of Asphalt Paving Technologists, 51 (1982), pp. 53-90.

41. Hills, J. F., and Brien, D. "'The Fracture of Bitumens and Asphalt Mixes by Temperature Induced Stresses,' Discussion," Proceedings of the Association of Asphalt Paving Technologists, 35 (1966), pp. 292-309.

42. Barber, E. S. "Calculation of Maximum Pavement Temperatures from Weather Reports," HRB Bulletin 168, Highway Research Board, (1957).

43. Heukelom, W., and Klomp, A. J. G. "Road Design and Dynamic Loading," Proceedings of the Association of Asphalt Paving Technologists, 33, (1964) pp. 92-125.

44. Rauhut, J. B., Lytton, R. L., and Darter, M. I. "Pavement Damage Functions and Load Equivalence Factors," Report No. FHWA/RD-84/018, Federal Highway Administration, 1984.

45. Ruth, B. E., Bloy, L. A. K., and Avital, A. A. Low Temperature Asphalt Rheology as Related to Thermal and Dynamic Behavior of Asphalt Pavements--Phase I, Final Report Project 245-V20, Department of Civil Engineering, University of Florida, 1981, pp. 1-104.

46. Hajek, J. J., and Haas, R. C. G. "Predicting Low-Temperature Cracking Frequency of Asphalt Concrete Pavements," Highway Research Record, No. 407 (1972), pp. 39-54.

47. Haas, R. C. G. "A Method for Designing Asphalt Pavements to Minimize Low-Temperature Shrinkage Cracking," Research Report 73-1, The Asphalt Institute, 1973.

48. McLeod, N. W. "A 4-Year Survey of Low Temperature Transverse Pavement Cracking on Three Ontario Test Roads," Proceedings of the Association of Asphalt Paving Technologists, 41 (1972), pp. 424-468.

49. Fromm, H. J. and Phang, W. A. "A Study of Transverse Cracking of Bituminous Pavements," Proceedings of the Association of Asphalt Paving Technologists, 41 (1972), pp. 383-418.

50. Ewalds, H. L. and Wanhill, R. J. H. Fracture Mechanics (London: Arnold, 1984), 304 pp.

51. Irwin, G. R., Fracture, Encyclopedia of Physics, ed. S. Fluge, Springer Verlag, Berlin (1958), pp. 551-589.

52. "Standard Test Method for Plane-Strain Fracture Toughness of Metallic Materials," ASTM E399-78A, 1979 Annual Book of ASTM Standards, Part 10, pp. 540-61.

53. "Method for Crack Opening Displacement (COD) Testing," London: British Standard Institution, 1979.

54. "Standard Practice for R-Curve Determination," ASTM E 561-81, 1982 Annual Book of ASTM Standards, Part 10, pp. 680-99.

55. Moavenzadeh, F. "Asphalt Fracture," Professional paper P67-5 MIT, Cambridge, MA, 1967.

56. Herrin, M. and Bhagat, A. G. "Brittle Fracture of Asphalt Mixes," Proceedings of the Association of Asphalt Paving Technologists, 37 (1968), pp. 32-55.

57. Majidzadeh K., Ramsamooj, D. V., and Chan, A. T. "Fatigue and Fracture of Bituminous Paving Mixtures," Proceedings of the Association of Asphalt Paving Technologists, 38 (1969), pp. 495-518.

58. Majidzadeh, K., Buranarom, C., and Karakouzian, M. Application of Fracture Mechanics for Improved Design of Bituminous Concrete, Vol. I, Report No. FHWA-RD-76-91, Federal Highway Administration, 1976.

59. Lytton, R. L., Shanmugham, U., and Garrett, B. D. Design of Flexible Pavements for Thermal Fatigue Cracking, Report No. FHWA/TX-83/06+284-4, Texas Transportation Institute, Texas A & M University, 1983.

60. Paris, P. and Erdogan, F. "A Critical Analysis of Crack Propogation Laws," Transactions of the ASME Journal of Basic Engineering, Series D, 85, No. 4 (1963) pp. 528-534.

61. Chang, Hang-Sun, Lytton, R. L., and Carpenter, S. H. Prediction of Thermal Reflection Cracking in West Texas, Research Report No. 18-3, Texas Transportation Institute, Texas A & M University, 1976.

62. Barenblatt, G. I. "The Mathematical Theory of Equilibrium Cracks in Brittle Fracture," Advances in Applied Mechanics, Vol. VII, Academic Press, (1962), pp. 55-129.

63. Schapery, R. A. A Theory of Crack Growth in Viscoelastic Media, Research Report MM2764-73-1, Mechanics and Materials Research Center, Texas A & M University, 1973.

64. Germann, F. P. and Lytton, R. L. Methodology for Predicting the Reflection Cracking Life of Asphalt Concrete Overlays, Research Report 207-5, Texas Transportation Institute, Texas A & M University, 1979.

65. de Bats, F. Th., "External Report The Computer Programs PONOS and POEL," AMSR. 0008.72, 1972.

66. Goodrich, J. L. "Asphalt and Polymer Modified Asphalt Properties Related to the Performance of Asphalt Concrete Mixes," paper presented before the Annual Meeting of the Association of Asphalt Paving Technologists, 1988.

67. Anderson, D. A., Kilareski, W. P., and Bonaquist, R. F. Fourth Cycle of Pavement Research at the Pennsylvania Transportation Research Facility, Vol. 1, Construction and Operation of the Pavement Durability Research Facility, PTI Report No. 8415 (University Park, PA: The Pennsylvania Transportation Institute, 1984), 95 pp.

68. Young, R. J. Introduction to Polymers, New York: Chapman and Hall, 1981, pp. 199-206 and 238-241.

69. Schmidt, R. J. and Santucci, L. E., "A Practical Method for Determining the Glass Transition Temperature of Asphalts and Calculation of their Low Temperature Viscosities," Proceedings of the Association of Asphalt Paving Technologists, 35 (1966), pp. 61-80.

70. Anderson, D. A., and Goetz, W., Mechanical Behavior of Asphalt Mineral Powder Composites and Asphalt Mineral Interaction, Joint Highway Research Program 71-5 , Purdue University, West Lafayette, Ind., 1971.

71. Altegelt, K. H. Chromatography in Petroleum Analysis, New York: M. Dekker (1979).

72. Reerink, H. and Lijzenga, J. "Gel-Permeation Chromatography Calibration Curve for Asphaltenes and Bituminous Resins," Analytical Chemistry, 47, No. 13 (1975), pp. 2160-2167.

73. Brule, B. "Calibration Curve for GPC Analysis of Asphalts," American Chemical Society, Division of Fuel Chemistry, Preprints of Papers, 26, No. 2 (1981), pp. 28-37.

74. Jennings, P. W. and Pribanic, J. Asphalt Analytical Methodology High Pressure Gel Permeation Chromatography, Symposium on Asphalt Analytical Methodology in 1986 TRB Meeting, Gaines Hall Laboratory, Department of Chemistry, Montana State University.

75. Altgelt, K. H. "Fractionation of Asphaltenes by Gel Permeation Chromatography," Journal of Applied Polymer Science, 9 (1965), pp. 3389-3393.

76. Such, C., Brule, B., and Baluja-Santos, C. "Characterization of a Road Asphalt by Chromatographic Techniques," Journal of Liquid Chromatography 2 (1979), pp. 437-453.

77. Haley, G. A. "Molecular and Unit Sheet Weights of Asphalt Fractions Separated by Gel Permeation Chromatography," Analytical Chemistry, 43, No. 3, (1971), pp. 371-375.

78. Brule, B. "Characterization of Bituminous Compounds by Gel Permeation Chromatography," Journal of Liquid Chromatography, 2 (1979), pp. 165-192.

79. Snyder, L. R. "Determination of Asphalt Molecular Weight Distributions by Gel Permeation Chromatography," Analytical Chemistry, 41, No. 10 (1969), pp. 1223-1227.

80. Kiet, H. H., Blanchard, L. P. and Malhotta, S. L. "The Gel Permeation Chromatography of Asphalt and the Characterization of Its Fractions in Terms of Molecular and Unit Sheet Weights," Separation Science, 12 (1977), pp. 607-634.

81. Altgelt, K. H. and Hirsch E. "GPC Separation and Integrated Structural Analysis of Petroleum Heavy Ends," Separation Science, 5 (1970), pp. 855-862.

82. Garrick, N. W. and Wood, L. E. The Relationship Between HP-GPC Data and The Rheological Properties of Asphalts, Report prepared for 65th Annual Meeting of the Transportation Research Board (1986).

83. Jennings, P. W. and Pribanic, J. A. S. "The Expanded Montana Asphalt Quality Study Using High Pressure Liquid Chromatography," Report prepared for the Montana Department of Highways Research Program by Department of Chemistry, Montana State University (1985).

84. Pribanic, J., Personal communication, 1988.

85. Rice, J. R. Mathematical Analysis in Mechanics of Fracture, An Advanced Treatise, ed. H. Liebowitz, Academic Press, New York, Vol. 2 (1968), pp. 192-311.

86. Asyst: A Scientific System (New York: MacMillan Publishing Co., Inc., 1985).

87. Johrdal, P., Brent Rauhut Engineering, Internal memorandum, 1987.

88. Anderson, D. A., Dukatz, E. L., and Rosenberger, J. L. "Properties of Asphalt Cement and Asphaltic Concrete," Proceedings of the Association of Asphalt Paving Technologists, 52, (1983), pp. 291-324.

89. Kandhal, P. S., "Low Temperature Shrinkage Cracking of Pavements in Pennsylvania," Proceedings of the Association of Asphalt Paving Technologists, 47 (1982), pp. 73-98.

90. Merkle, J. G., Paris, P. C., and Rice, J. R. "Some Further Results of Integral Analysis and Estimates," Progress in Flaw Growth and Fracture Toughness Testing, ASTM Special Technical Publication No. 536, American Society for Testing and Materials (1973), pp. 231-245.

91. Sumpter, J. D. G. and Turner, C. E. "Method for Laboratory Determination of J_c," Cracks and Fracture, ASTM Special Technical Publication No. 601, American Society of Testing Materials, 1976, pp. 3-18.

92. Little, D. N., and Mahboob, K., "Engineering Properties of First Generation Plasticized Sulfur Binders and Low Temperature Fracture Evaluation of Plasticized Sulfur Paving Mixtures," Transportation Research Record 1034, TRB, Washington, D.C., 1985, pp. 103-111.

93. Ferry, J. D. "Viscoelastic Properties of Polymers, (New York: Wiley, 1961).

94. Dobson, G. R., "The Dynamic Mechanical Properties of Bitumen," Proceedings of the Association of Asphalt Paving Technologists, 38 (1969), pp. 123-139.

95. Christensen, R. M. Theory of Viscoelasticity, (New York: Academic Press, Inc., 1982).

96. Haas, R. C. G, and W. A. Phang, "Low Temperature Pavement Cracking," paper presented at 63rd Annual Meeting of the Association of Asphalt Paving Technologists, Williamsburg, Virginia, 1988, to be published in Vol. 57, Proceedings of the Association of Asphalt Paving Technologists.

☆ U.S. GOVERNMENT PRINTING OFFICE: 1990 — 717-000/27068